



Universität
Rostock



Traditio et Innovatio

Abundance, distribution, composition, and weathering resistance of microplastics in different marine systems

Cumulative Dissertation

to obtain the academic degree
Doctor rerum naturalium (Dr. rer. nat.)
of the Faculty of Mathematics and Natural Sciences
at the University of Rostock

submitted by

M. Sc. Janika Melina Reineccius

born on 08. December 1993 in Bonn-Duisdorf, Germany

Rostock, February 2023

https://doi.org/10.18453/rosdok_id00004364

The work in this thesis was carried out between November 2019 and February 2023 under the supervision of Prof. Dr. Joanna J. Waniek in the working group “Bio-physical interactions” within the Marine Chemistry department at the Leibniz Institute for Baltic Sea Research Warnemünde, Germany.

1. Reviewer: Prof. Dr. Joanna J. Waniek
Leibniz Institute for Baltic Sea Research Warnemünde

2. Reviewer: Prof. Dr. Uta Passow
Memorial University of Newfoundland, Canada

Date of submission: 08. February 2023

Date of defence: 23. May 2023

Eidesstattliche Erklärung

Ich versichere hiermit an Eides statt, dass ich die vorliegende Arbeit selbstständig angefertigt und ohne fremde Hilfe verfasst habe, keine außer den von mir angegebenen Hilfsmitteln und Quellen dazu verwendet habe und die den benutzten Werken inhaltlich und wörtlich entnommenen Stellen als solche kenntlich gemacht habe.

Janika Melina Reineccius

Table of Contents

Danksagung	iv
Abstract	v
Zusammenfassung	vi
List of Abbreviations	vii
List of Figures	viii
List of Tables	xi
1 Aims and Motivation	1
2 Introduction	3
2.1 Background Information	3
2.1.1 Application and Environmental Transport Pathways of Plastics	3
2.1.2 Toxicity	4
2.1.3 Sinking of MP	5
2.1.4 Degradation process	6
2.2 Detection Methods for MP in Environmental Samples	8
2.2.1 Sampling Method	8
2.2.2 Separation Methods	9
2.2.3 Instrumental Analysis	11
3 Materials and Methods	16
3.1 Method development and validation	16
3.2 Field samples	18
3.2.1 Sampling site and sample collection	18
3.2.2 MP extraction	21
3.2.3 Analysis	22
4 Results and Discussion	23
4.1 MP fluxes and properties	23

4.2	Correlations and transport pathways	25
4.3	Source regions	26
4.4	Seasonality of MP (mass) fluxes	27
4.5	Degradation rate of MPs	29
4.6	Extrapolation and comparison with previous studies	34
5	Summary and Outlook	39
	References	41
	Supplementary Materials	69
	Contributions to the Manuscripts	77
	Publication I: Separation of microplastics from mass-limited samples by an effective adsorption technique	78
	Publication II: First long-term evidence of microplastic pollution in the deep subtropical Northeast Atlantic	96
	Publication III: Abiotic long-term simulation of microplastic weathering pathways under different aqueous conditions.	108
	Curriculum Vitae	122

Danksagung

Bereits im Jahr 2015 erfuhr ich von der Möglichkeit, hier in Rostock die marine Umweltverschmutzung zu untersuchen und zu studieren, auch das Thema Mikroplastik in den Ozeanen kam dabei zur Sprache. Inmitten meines Bachelorstudium an der HS Bonn-Rhein-Sieg war damit klar wohin es gehen sollte, doch nur mit der Hilfe all dieser hervorragenden Menschen ist mir dieser Weg bis hierher gelungen.

Mein größter und herzlichster Dank gebührt damit Prof. Dr. Joanna J. Waniek. Sie hat mir diesen Weg geebnet und viele Dinge für die Zukunft gelehrt. Die stets offene Tür und gleichermaßen offenen Gespräche trugen immer zur neuen Motivation bei und verhinderten jegliche Stagnation. Auch die Offenheit für neue Ideen war sehr hilfreich. Nebenbei ermöglichte sie mir die Teilnahme an mehreren bedeutenden Seereisen, welche mein bereits bestehendes Interesse zur Wissenschaft in eine uneingeschränkte Liebe mit nun unbezahlbaren Erfahrungen und Erinnerungen umwandelte. Darüber hinaus möchte ich ganz herzlich Prof. Dr. Detlef E. Schulz-Bull danken, der ebenfalls zu diesen Seereisen beitrug und mich während meiner Doktorarbeit begleitete. Auch hier danke ich vielmals für die Anregungen und Gespräche, auch während des Thesis Komitees.

Auch den übrigen Mitgliedern des Thesis Komitees möchte ich herzlichst danken, insbesondere Dr. Annika Jahnke für die zahlreichen Tipps und den Input, die auch über die Meetings hinaus gingen. Dies gilt auch für Dr. Helena Osterholz und Dr. Sonja Oberbeckmann für die hilfreichen Diskussionen bezüglich meiner Arbeiten. Auch den Co-Autoren möchte ich meinen Dank aussprechen, vor allem Dr. Jonas Bresien, der mir alle notwendigen Messungen ermöglichte und mit den zahlreichen Gesprächen und Erklärungen weitere Sichtweisen offenbarte. Eine beachtliche Menge trug außerdem Dr. Mischa Schönke zu diesen Arbeiten bei. Durch ihn wurden mir besonders im Bereich des Programmierens neue Möglichkeiten und Wege eröffnet. Zudem begleitete er mich seit Beginn dieser Arbeit immer mit einem offenen Ohr und hilfreichen Ratschlägen zu jeder vorstellbaren Frage.

Weiterhin möchte ich einen riesen Dank an alle lieben und hilfsbereiten Kollegen der Arbeitsgruppen "Bio-physikalische Wechselwirkungen" und "Organische Spurenstoffe" aussprechen. Hier möchte ich besonders Paul Cwierz, Dr. Sebastian Neubert, Dr. Marisa Wirth, Arne Estelmann, Dr. Helena Frãzao und Oscar Beltran-Perez erwähnen und natürlich auch alle, die mich auf den Seereisen unterstützt haben. Dies gilt genauso für die Crew der Fahrten SO269, SO296, der EMB Terminfahrt und natürlich meiner lieben Familie.

VIELEN DANK FÜR ALLES!

Abstract

No anthropogenic pollutant is more widespread in the marine environment than microplastics (MP). Expectedly, it also entails many problems. MP can be mistaken for food by various marine animals and often causes blockages or inflammation in their digestive systems, which can even lead to death. Due to its inertness, the plastic itself is not directly toxic to animals, but a wide range of additives can affect the health of marine fauna. In addition, the respective monomers, degradation products, and sorbed pollutants are also of concern. In particular, the long residence time of plastics in the marine environment poses a problem, as the plastic particles have sufficient time to absorb pollutants and be consumed by native organisms.

Regarding the amounts of plastic in the oceans, however, there are still large uncertainties, as the determined amounts do not match the expected higher quantities. To resolve this contradiction about plastic fate, the present work deals with the investigation of the material sinking into the deep sea. These temporally resolved results provide information on the abundances, polymer composition, and particle sizes of sinking MP particles to elucidate the fate of the plastic while drawing conclusions about responsible transport mechanisms. Furthermore, an additional laboratory experiment was implemented to determine the weathering behavior of the five most common polymer types in the aqueous environment.

The results showed that MP (mass) fluxes in the 2000 m deep Northeast Atlantic were not only measurable but were up to $3146.81 \text{ items day}^{-1} \text{ m}^{-2}$ high. Furthermore, the recorded fluxes varied greatly in both amount and polymer composition. Mainly polyethylene (PE) was found in the samples, whose fluxes correlated with those of the lithogenic fraction during 2003 - 2015, indicating an atmospheric transport pathway. The heavier polymer types, consisting mainly of polyvinyl chloride (PVC), followed a seasonal dependence with higher fluxes in winter, which could indicate transport within the water column. The unexpectedly low percentage of polypropylene (PP) detected in sinking material compared to the global application could arise from this polymer type's observed low weathering resistance in the aquatic system.

Zusammenfassung

Kein anthropogener Schadstoff ist in der marinen Umwelt weiter verbreitet als Mikroplastik, was erwartungsgemäß auch viele Probleme mit sich bringt. Mikroplastik kann von verschiedenen marinen Spezies mit dessen Nahrung verwechselt werden und führt in dessen Verdauungssystemen häufig zu Blockaden oder Entzündungen bis hin zum Tod. Aufgrund der Reaktionsträgheit ist Plastik selbst nicht direkt toxisch für die Tiere, jedoch kann die weite Bandbreite an Additiven Einfluss auf die Gesundheit der marinen Fauna nehmen. Darüber hinaus sind auch die jeweiligen Monomere, Abbauprodukte, sowie sorbierte Schadstoffe bedenklich. Insbesondere die lange Verweilzeit des Kunststoffes in der marinen Umwelt stellt ein Problem dar, da die Plastikpartikel ausreichend Zeit haben, Schadstoffe aufzunehmen und von einheimischen Organismen konsumiert zu werden.

Hinsichtlich der Plastikmengen in den Ozeanen bestehen allerdings noch große Unsicherheiten, da die ermittelten nicht mit den erwarteten höheren Mengen übereinstimmen. Um die Fragen nach dem Verbleib des Plastiks zu beantworten, befasst sich die vorliegende Arbeit mit der Untersuchung des in die Tiefsee absinkenden Materials. Diese zeitlich aufgelösten Mikroplastikabundanzen sollen Auskunft über die Häufigkeiten, Polymerzusammensetzung und Partikelgrößen der sinkenden Mikroplastikpartikel geben, um damit den Verbleib des Plastiks aufzuklären und Rückschlüsse auf verantwortliche Transportmechanismen zu erlauben. Damit außerdem der Einfluss der Verwitterung berücksichtigt werden kann, wurde das Verwitterungsverhalten der fünf in der Umwelt am häufigsten vorkommenden Polymertypen in einem Laborexperiment untersucht.

Die Ergebnisse zeigten, dass die Mikroplastik-(masse)flüsse in dem 2000 m tiefen Nordost Atlantik nicht nur messbar waren, sondern bis zu $3146.81 \text{ Partikel Tag}^{-1} \text{ m}^{-2}$ betragen. Darüber hinaus wurde beobachtet, dass die Flüsse sowohl in der Menge als auch in der Polymerzusammensetzung stark variierten. Hauptsächlich wurde Polyethylen (PE) in den Proben gefunden, dessen Flüsse in den Jahren 2003 - 2015 mit denen der lithogenen Fraktion korrelierten, was auf einen atmosphärischen Transportweg hindeutet. Die schwereren Polymertypen die hauptsächlich aus Polyvinylchlorid (PVC) bestanden, folgten einer saisonalen Abhängigkeit mit höheren Flüssen im Winter, was auf einen Transport in der Wassersäule hindeuten kann. Die unerwartet geringen Anteile von Polypropylen (PP) im sinkenden Material im Vergleich zur globalen Anwendung, können die Folge der ermittelten geringen Verwitterungsresistenz des Polymers im aquatischen System sein.

List of Abbreviations

ABS	Acrylonitrile butadiene styrene
ATR	Attenuated total reflectance
BS	Baltic Sea
CTD	conductivity, temperature, depth measuring rosette with Niskin bottles
DDT	Dichlorodiphenyltrichloroethane
EO	Enzymatic-oxidative
FPA	Focal plane array
FTIR	Fourier transform infrared spectroscopy
GF	Glass fiber
HCH	Hexachlorocyclohexane
HP	polymer types heavier than seawater
LP	polymer types lighter than seawater
MP	Microplastic
MUC	Multi corer
PA	Polyamide
PAH	Polycyclic aromatic hydrocarbon
PCB	Polychlorinated biphenyl
PE	Polyethylene
PET	Polyethylene terephthalate
PMMA	Polymethyl methacrylate
POM	Polyoxymethylene
PP	Polypropylene
PS	Polystyrene
PUR	Polyurethane
PVC	Polyvinyl chloride
pyr-GC/MS	Pyrolysis gas chromatography/mass spectrometry
ROV	Remotely operated vehicle
SCS	South China Sea
SDS	Sodium dodecyl sulfate
SEM	Scanning electron microscopy
ST	Sodium polytungstate
TD-Pyr-GC/MS	Thermal desorption pyrolysis gas chromatography/mass spectrometry
TED-GC/MS	Thermal extraction desorption gas chromatography/mass spectrometry
TGA-DSC	Thermogravimetry coupled differential scanning calorimetry
UV	ultraviolet
WW	Warnow

List of Figures

Figure 2.1. Visualization of the MP fragmentation caused by weathering. With the break out of the uppermost polymer layer, an unweathered layer is exposed.	7
Figure 3.1. Entire extraction procedure of both possible MP separation methods with the syringes cascade (a) and the density separation method (b). Both methods start with a freeze-dried sample followed by the first clean-up step with the digestion. This figure was adopted and edited from Reineccius et al. (2021)	18
Figure 3.2. Location of the mooring station Kiel 276 in the Subtropical North-east Atlantic (33°N, 22°W) and sampling stations in the northern South China Sea (SCS) for MP analysis. In the SCS map, the filled black triangles symbolize the sediment sampling stations, and the red triangles represent the net sampling stations. The prevailing major winds and currents are sketched in gray and blue, respectively. For the SCS map, surface currents are given, which were adapted from Deich et al. (2021) for this area: Eastern and western Guangdong Coastal Current (EGCC, WGCC), SCS Warm Current (SCSWC) and SCS Branch of Kuroshio (SCSBK). The red areas of the upper overview map present the zoomed area for the Atlantic and SCS maps.	19
Figure 4.1. MP fluxes (a), MP mass fluxes (b), calcium carbonate fluxes (c), and aluminum fluxes (d) for all analyzed samples (n = 110). Dashed black lines in figure b represent flux ranges resulting from the mass calculation with a range of potential polymer densities. The bar width indicates the sampling interval for each sample, with gaps that illustrate mooring failure or no deployment. The vertical dashed gray lines mirror the intervals for the respective sampling series. Note the different scales of the y-axis between the figures (adopted from Reineccius & Waniek (2022)).	23

Figure 4.2.	Mean sizes of detected MP particles in sediment trap samples for all samples (a) and the size distribution for each sampling series, as well as for the sum of all detected MPs (b) (adopted and edited from Reineccius & Waniek (2022)). The gray areas represent the standard deviation range (\pm s.d.) and the dashed black line in (b) marks the mean from the sampling series, calculated for the respective particle number (n). The dashed gray lines in (a) separate the sampling series.	24
Figure 4.3.	Monthly calcium (Ca) and aluminum (Al) fluxes in $\text{mg day}^{-1} \text{m}^{-2}$ (a) (adopted from Pullwer & Waniek (2020)), monthly MP (mass) fluxes (b) (adopted from Reineccius & Waniek (2022)), (mass) fluxes of the sum of all polymer types lighter than seawater (LP) (c) , and heavier than seawater (HP) (d)	28
Figure 4.4.	Carbonyl (C=O), hydroxyl (O-H), and C=C (vinyl for polyethylene (PE), polypropylene (PP), and polyvinyl chloride (PVC) and aromatic for polystyrene (PS) and polyethylene terephthalate (PET)) bond indices for the five different polymer types (PE, PP, PS, PET, and PVC) and the three water types Warnow River (WW) water, Baltic Sea (BS) water, and South China Sea (SCS) water. The vertical lines represent the standard deviation (\pm s.d.) resulting from triplicates (adopted from Reineccius et al. (2022)).	31
Figure 4.5.	Surface roughness expressed as the power spectral density (PSD) for all weathered polymer types PE, PP, PS, PET, and PVC as colored lines and the respective root-mean-square roughness (S_q) over the exposure time in black for the three different water media (Warnow, Baltic Sea, and South China Sea water). Error bars represent the standard deviation (\pm s.d.) resulting from triplicates.	32
Figure 4.6.	MP abundances in sediments (a) extracted from the literature listed in (b) and Table S1 (Supplementary Materials) with the mean MP abundance for each reference and potential abundances calculated from the uncertainties of the respective detection method (b)	37

Figure 4.7. MP abundances in water (**a**) extracted from the literature listed in (**b**) and in Table S2 (Supplementary Materials) with the mean MP abundance for each reference and potential abundances calculated from the uncertainties of the respective detection method (**b**). . . . 38

List of Tables

Table 2.1.	General data of the six most produced polymer types. Density and application data were adapted from Coyle et al. (2020), PlasticEurope (2021) and Hidalgo-Ruz et al. (2012). The data on global plastic production are from 2015 (Geyer et al., 2017).	10
Table 2.2.	Overview of MP collection and detection methods for different marine sediment sample types, including the sampling procedures, used digestion agents (if applied), density separation solutions (if applied), and analysis methods used in various studies.	14
Table 2.3.	Overview of MP collection and detection methods for different marine water sample types, including the sampling procedures, used digestion agents (if applied), density separation solutions (if applied), and analysis methods used in various studies.	15
Table 4.1.	Correlation coefficients (r) for PE and PVC with element fluxes adopted from previous works (Pullwer & Waniek, 2020). $ r = 0.10$ are defined as a weak correlation, $ r = 0.30$ moderate and $ r > 0.50$ strong. Correlation coefficients ≥ 0.5 with statistical significance ($p < 0.05$) are given in bold (Pearson correlation test, $n = 219$, $\alpha = 0.05$).	26

1. Aims and Motivation

The use of plastic in our modern society is fraught with considerable conflicts, as plastic has greatly improved our quality of life and promoted economic development. However, its disposal is not always adequately managed, making the pollution of the environment clearly visible. This pollution is not without consequences from an economic and environmental point of view. Due to the unsightly appearance of the polluted beaches, tourism suffers losses, but the ecology is also severely affected. Furthermore, the large visible pieces of plastic are just the tip of the iceberg.

The smaller MP particles are even more widespread, and their effects are not yet fully understood. Moreover, according to initial experimental studies, MP has been found to have a significant impact on marine species, and it can also enter the human diet via seafood. To better understand the potential risks to humans and marine species, studies are essential to clarify the distribution and fate of MP in the ocean. Due to the low weight, first expectations assumed that MP accumulates at the ocean surface. However, more recent studies have shown that the MP amounts determined in the marine environment do not correspond to expectations. Consequently, there must be other unexplored processes influencing the fate of MP. The fate of MP is expected to be mainly affected by two mechanisms: I) High MP amounts that sink through the water column are preserved for the next hundreds or thousands of years in the seabed; II) Fragmentation and mineralization of plastic are caused by weathering processes.

This thesis will focus on both mechanisms to clarify the actual MP fate in marine waters. In this context, the aims of this thesis were:

- (a) Develop a suitable method to extract and analyze MP particles in sediment trap samples (**Reineccius et al., 2021**).
- (b) Determine MP abundances sinking into the deep sea using sediment trap samples to prove that MP sinks through the water column (also for light MP) and to determine the MP flux rate for time-resolved abundances (**Reineccius & Waniek, 2022**).
- (c) Investigate the influence of weathering to improve our understanding of the remaining MP in the aquatic system, which does not immediately sink through the water column (**Reineccius et al., 2022**).

The first aim (a) was realized by laboratory experiments focusing on the extraction and determination of MP particles in mass-limited samples from sediment traps (≤ 100 mg).

The determination method should be as accurate as possible, which includes the lowest possible contamination of the samples, effective removal of natural materials, and a high recovery rate of MP particles. At the same time, the method should be fast and easy to manage. A method that fulfills these two criteria was developed in the first stage of this thesis (**Reineccius et al., 2021**).

This method was established to analyze MP particles in sediment traps, which are useful to obtain timely resolved MP abundances from the water column. These analyses were implemented in the second step (b) (**Reineccius & Waniek, 2022**). The considered traps were deployed at the edge of the North Atlantic Subtropical Gyre, which is known to accumulate large amounts of plastic. This location enables the observation of MP abundances at a remote place, with limited direct local plastic inputs by humans. In this work, time-resolved MP fluxes in the deep ocean were determined for the first time. These data can also be used to reveal correlations with previously examined data that can provide information, e.g., about transport pathways. However, determining the residence time of MP in the ocean is still doubtful. Furthermore, previous studies do not provide accurate information about tracing the plastic age back, leading to the need for further investigations in this field.

To get a rough overview of the retention time of MP in the aquatic environment, monitoring MP changes during exposure under environmental conditions is necessary. However, the wide variety of plastic properties and local climate conditions is a big challenge for the research. In addition, it is assumed that plastic is transported mainly via rivers, which leads to a change in the salinity of the surrounding water in the rivers compared to the ocean. Consequently, different polymer types should be chosen to observe changes over the exposure time under aquatic environmental conditions (including sunlight, oxygen availability, and water movements) at different water salinity. Such experiments were implemented in the laboratory for 18 months in three different water types with different salinity (Warnow, Baltic Sea, and South China Sea water) for aim (c) (**Reineccius et al., 2022**).

2. Introduction

2.1. Background Information

2.1.1. Application and Environmental Transport Pathways of Plastics

It is almost impossible to imagine our everyday life without plastic. Plastic is light, strong, inexpensive, durable, and corrosion-resistant and can be used in a wide range of fields. The range of applications can be further expanded by adding various additives such as fillers, plasticizers, flame-retardants, thermal stabilizers, antimicrobial agents, or colors. Finally, manufacturable plastic products range from flexible to rigid objects, adhesives, foams, and fibers (Napper & Thompson, 2020). Plastic makes everyone's everyday life easier, offers many advantages for industry, e.g., in the food, construction, or automotive sectors, and is an important contributor to medical progress (PlasticsEurope, 2021). The first manufactured synthetic plastic, known as "Bakelite," which was already produced in the early 20th century, was used only in household products. However, with the discovery of its versatility, plastic production increased rapidly, with mass production starting in the 1950s (Napper & Thompson, 2020). Meanwhile, the plastics industry is the eighth most important in Europe, with a turnover of 330 billion Euros in 2020 (PlasticsEurope, 2021). However, Europe is far from the continent with the highest plastic production. In 2020, 367 million tons of plastic were manufactured worldwide, of which 50% was produced in Asia alone, 19% in North America, and 15% in Europe. The shares of Africa (7%) and South America (4%) are lower (PlasticsEurope, 2021).

Most of the plastic today is used for commercial or industrial packaging and is therefore intended for single use. Polymer types such as polyethylene (PE) and polypropylene (PP), but also polyethylene terephthalate (PET), meet the corresponding requirements for packaging materials, such as low weight and high elasticity. These three polymer types account for 58.4% of European plastics production (PlasticsEurope, 2021). Considering polyvinyl chloride (PVC), which is mainly used in the construction industry, polystyrene (PS) and polyurethane (PUR), in addition to the plastics mentioned above, these are the six most commonly produced polymers in Europe, which account for more than 80% of total plastics production in 2020.

This young single-use culture of plastic for packaging materials has far-reaching consequences. Careless handling and poor waste management, with global recycling rates of only 9% in 2015, result in millions of tons of plastic entering the environment every year

(Geyer et al., 2017). The mobilization of plastic by rivers, winds, or other environmental factors, or direct input by shipping, fishing, or aquaculture, leads to the plastic eventually ending up in the open ocean (Auta et al., 2017; Blumenröder et al., 2017; Rochman, 2018). Supported by its long durability and ongoing entry, plastic accumulates in the ocean, which is already reflected in the high plastic amounts within the large oceanic gyres called the "Ocean Garbage Patches" (Egger et al., 2020; Lebreton et al., 2018; Van Sebille et al., 2012).

Between 1.15 and 2.41 million metric tons of plastic were estimated to reach the oceans yearly by rivers alone, steadily increasing the availability of plastic to marine species (Lebreton et al., 2017). In addition to the numerous dangers for marine animals that get entangled in large pieces of plastic and receive injuries or die, the tiny plastic particles pose an even greater threat to marine species. Depending on their size, plastic is mistaken for food by numerous marine species, leading to digestive tract blockages and injuries, followed by increased morbidity and mortality (Alimba & Faggio, 2019). Filter-feeding species such as mussels are one of the most affected marine species, consuming high amounts of plastic by filtering polluted seawater (Setälä et al., 2016). However, the digestive tracts of many other benthic, demersal, benthopelagic, or pelagic species were also found to contain high MP amounts (Avio et al., 2020). MP, defined in a size range 1 - 5000 μm , is the most frequently detected plastic size in the marine environment (Napper & Thompson, 2020; Hidalgo-Ruz et al., 2012) and was already found to accumulate in the marine food web (Avio et al., 2020; Nelms et al., 2018). Via seafood, MP also reaches the human diet, but the effects on the human organism have not yet been fully researched (Yuan et al., 2022).

2.1.2. Toxicity

Besides the direct and indirect physical damages, MPs can also have toxic effects due to the release of monomer or oligomer residues from incomplete polymerization reactions or additives added during manufacture (Conti et al., 2021; Gewert et al., 2018; Sørensen et al., 2021). For example, bisphenol A and phthalates are the most common additives used as plasticizers to make synthetic plastic materials more malleable and flexible. However, they are also known as "Endocrine Disrupting Chemicals" (Conti et al., 2021).

Supported by the large surface-to-volume ratio in combination with the lipophilic polymer nature, MP offers many attachment sides for surrounding environmental pollutants. Persistent organic pollutants such as polychlorinated biphenyls (PCBs), polycyclic aromatic hydrocarbons (PAHs), dichlorodiphenyltrichloroethanes (DDTs), or hexachlorocyc-

clohexanes (HCHs) (Antunes et al., 2013; Frias et al., 2010; Ogata et al., 2009; Rios et al., 2007) but also harmful metals (Brennecke et al., 2016; Graca et al., 2014) or pathogens (Zettler et al., 2013) can accumulate at the polymer surface in higher concentration than that of the surrounding seawater (Guo & Wang, 2019). Attached to the MP surface, these harmful pollutants can be transported across the globe or into the digestive tract of feeding organisms. Once in the digestive tract, pollutants can be leached with an enhanced toxic effect due to the high pollutant concentrations adsorbed at the contaminated MP particles (Yu et al., 2019). For PCB and PAH, an increased uptake by a factor of 1.3 to 2.4 was determined, caused by the transfer via MP (Rochman et al., 2013). Due to the tendency of biomagnification, these organic pollutants accumulate within the food chain with the highest concentrations reaching the top predators, including humans (Yuan et al., 2022).

2.1.3. Sinking of MP

Due to the low weight of MPs and the lower density of the two most common polymer types PE ($0.92 - 0.97 \text{ g cm}^{-3}$) and PP ($0.90 - 0.91 \text{ g cm}^{-3}$) compared to seawater ($\sim 1.02 \text{ g cm}^{-3}$), MP is assumed to float at the ocean surface (Bergmann et al., 2015; Hidalgo-Ruz et al., 2012). However, today only a few studies have indicated a discrepancy between the detected amounts of MP at the ocean surface and the expected amounts according to the globally increasing plastic production (Cózar et al., 2014; Woodall et al., 2014). Considerably lower MP abundances were recovered at the sea surface. Instead, low-density MPs have been detected in numerous field studies in the water column and deep-sea sediments in even higher abundances than at the water surface (Choy et al., 2019; Zhou et al., 2021). This phenomenon indicates that even light MP particles travel through the water column and enter the deep sea.

The reason why lightweight MP particles begin to sink is not yet fully understood. Initial models have shown that weight increase due to biological processes such as biofouling or aggregation is a major contributor to increased MP sinking rates (Kaiser et al., 2017; Kooi et al., 2017). These processes can also be regressive due to grazing of the surface fouling, leading to float-sink cycles of such MP items, which thus dwell in the water column over a long time (Andrady, 2017). However, the time MP generally takes to reach the seabed and the associated input rate is still unknown. In addition to the biofouling processes, the formation of aggregates can vary strongly in their attached weight depending on the involved organisms. Excellent candidates to facilitate aggregation are, e.g., diatoms (Passow, 2002), which sink faster than cryptophyte caused by the biogenic silica content, heavier than the

organic matter (Long et al., 2015). Besides these biological processes, physical processes such as currents, waves, and winds, as well as the MP size, density, and shape, can play a significant role in affecting the sinking velocity of MP (Kooi et al., 2017; Kowalski et al., 2016). This wealth of possible influencing factors hinders predicting models about the retention time of MP within the water column (Akdogan & Guven, 2019) and increases the necessity for insightful field studies.

2.1.4. Degradation process

The degradation rate of MPs is important for a large number of research fields. For example, it can significantly affect the concentration of adsorbed contaminants, the release of additives, the sinking velocity through the water column or the horizontal transport pathway, and generally, the residence time in the environment until the total degradation. Caused by irregular MP surfaces and ongoing fragmentation (visualized in Fig. 2.1) to smaller particles due to degradation, the surface-to-volume ratio further increases, offering more attachment sides for pollutants, more leaching areas for additives, and a higher particle surface more prone to water movements (Alimba & Faggio, 2019; Jahnke et al., 2017; Luo et al., 2020a). In addition to visible surface changes and fragmentation, changes also occur at the molecular level. However, the research into these changes, especially regarding the chemical degradation products, is still largely unexplored (Andrady, 2011; Gewert et al., 2015, 2018; Song et al., 2017).

The mechanisms responsible for the degradation of MPs include, in particular, physical and chemical weathering processes, such as photo-oxidation, photo-thermal oxidation, mechanical abrasion, or hydrolysis (Alimi et al., 2022). In addition, there is also evidence of microorganisms capable of degrading plastics, resulting in mineralization of the polymer structure to CO_2 , N_2 , CH_4 , H_2O , or H_2S (Du et al., 2021; Paço et al., 2017; Syranidou et al., 2017). The most rapid degradation is expected to occur under conditions like those found on beaches due to the combination of high ultraviolet (UV) radiation, mechanical abrasion by waves and sand, and high temperature variations at most locations (Song et al., 2017). In contrast, due to the lack of UV radiation, stable and low temperatures, no wave actions, and slow biological processes, sunken MP is expected to last in the deep sea for hundreds to thousands of years or even longer (Barnes et al., 2009).

Besides environmental conditions, the MP composition, shape, and size also influence the degradation rate (Alimi et al., 2022; Jahnke et al., 2017; Min et al., 2020; Ter Halle et al., 2016). Depending on the polymer type and structure of the polymer backbone, the

polymer may be more or less resistant to external influences, such as PE compared to PP. The additional tertiary carbon in the PP backbone is more prone to abiotic attack, leading to a faster chain scissoring of PP (Gewert et al., 2015). Added additives such as antioxidants, UV stabilizers, or heat stabilizers influence the MP residence time likewise (Hahladakis et al., 2018). Some possible influencing factors, such as the water salinity, have not yet been sufficiently investigated (Alimi et al., 2022; Sun et al., 2020).

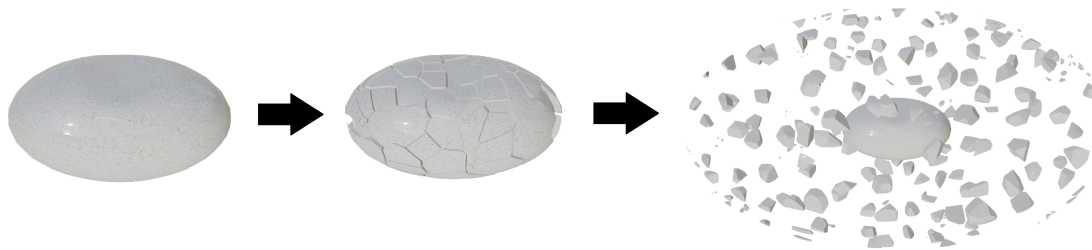


Figure 2.1. Visualization of the MP fragmentation caused by weathering. With the break out of the uppermost polymer layer, an unweathered layer is exposed.

Due to the high importance of knowing the degradation rate of MPs in the environment, several laboratory and outdoor experiments were conducted in which potential changes in the surface morphology and chemical composition were monitored (Julienne et al., 2019; Liu et al., 2019; Luo et al., 2020a; Song et al., 2017; Ter Halle et al., 2016; Zvekic et al., 2022). However, a major challenge in determining the degradation rate is the high number of influencing factors and the long duration of MPs in the environment. To accelerate the experiment time, unnatural intense UV radiation was commonly used, generating high temperatures (Alimi et al., 2022; Andrade et al., 2019; Müller et al., 2018). However, this intense radiation can lead to distortions of the weathering pathway and cannot be directly extrapolated for MPs weathered under environmental conditions (Alimi et al., 2022; Andrade et al., 2019; Zvekic et al., 2022).

Given the enormous amounts of plastics already accumulating in the oceans, it is mandatory to be able to make better statements about the transport routes, the actual residence time of MP in the environment, their morphological and chemical changes, as well as their weathering products, to understand the damage already done and the dangers the human beings and the environment will be exposed to in the future.

2.2. Detection Methods for MP in Environmental Samples

In order to determine the amounts of MPs in the marine environment, a wide variety of sample types are available for sampling and analysis. In general, a distinction is made primarily between sediment and water samples. In addition, biota samples are also examined to determine the amounts of MPs ingested by various marine animals. Depending on the sample type, the detection methods must be adjusted. However, due to the absence of a standardized method, a large number of different detection methods exist even for the same sample types (Way et al., 2022) (visualized in Supplementary Materials Fig. S3).

In this large research field, this work focuses on the procedures for marine sediment and water samples and does not include biota samples. As MP pollution is a huge modern problem, numerous studies have already dealt with this topic, including marine samples. In order to obtain an accurate description, despite the diversity of studies and their different methods, all studies focusing on detecting MPs in marine sediments and waters were reviewed. Studies were only selected when results, sampling sites, and methods were described accurately and when results were presented per volume or weight unit. All remaining selected references used for the overview ($n = 192$) in this section are listed in the Supplementary Materials (Table S1 and S2).

2.2.1. Sampling Method

Marine sediment samples can be further divided into offshore and onshore samples, which require different sampling procedures. Examples of applied sampling procedures and related separation and analysis methods are given in Table 2.2. The most commonly used sampling procedure, described in 44% out of 67 MP studies focused on offshore sediment sampling (Supplementary Materials Table S2), is the coring method, with the Box corer as the most frequently used coring system followed by the Gravity corer. With 34%, the grab sampling method is the second most frequently applied sampling procedure in which the Van Veen grab sampler was used in particular. Further sampling methods include sediment collection by divers (15%) or dredges (4%). For onshore sampling at beaches, mangroves, or other coastal areas, stainless steel shovels, spatulas, spoons, or a direct scoop by glass jars or cups were applied. The area to collect the samples was chosen systematically by specific distances between sampling locations and the tide mark. For every sample, a fixed area of mostly 0.25 m^2 (e.g., Dekiff et al. (2014); Baztan et al. (2014); Rios-Mendoza et al. (2021); Sathish et al. (2020)) was sampled, varying in size and sampling depth between studies.

Marine water samples were collected with nets in most studies (56% out of 82 references). Surface water sampling was conducted by nets for 60%, especially the Manta and Neuston nets but also pumping systems (13%) or different containers were used (Table 2.3). The water column was most frequently sampled via a pumping system (50%) or CTD (conductivity, temperature, depth) device connected to a rosette with Niskin bottles. However, some studies also used the net sampling method (19%).

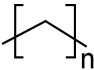
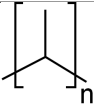
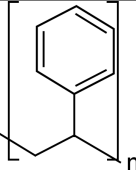
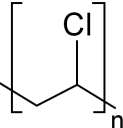
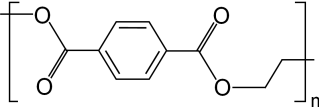
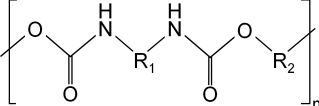
There is another option to collect marine MP samples from the water column, which specializes in settling particles descending through the water column. This device is called a "sediment trap" but is rarely used in MP research. Sediment traps can collect sinking particles over a selected period, ranging between a few days to several months (Waniek et al., 2000), enabling time-resolved monitoring of MPs. Only two studies have considered MPs in marine sediment trap samples. One is Enders et al. (2019) in which sediment traps were deployed in the Baltic Sea in the Arkona and Gotland basin, and the other was mounted in the Southeast Gulf of California in Mexico (Rios-Mendoza et al., 2021). The sediment trap used by Enders et al. (2019) is described very differently in its construction compared to the device used by Rios-Mendoza et al. (2021). While the first mentioned device was a round and funnel-shaped construction, covering an area of 0.50 m², the second sediment trap consists of PVC tubes with 1 m length and 10 cm diameter (~ 0.01 m²).

2.2.2. Separation Methods

The particulate matrix of marine samples is very complex due to its diverse composition. Large matrix amounts interfere with spectroscopic analysis methods, so numerous methods have been developed to reduce the matrix before instrumental analysis. Besides sediments, samples can contain a huge amount of biogenic materials, which depending on regional native species, can differ in their composition, leading to high amounts of cellulose, proteins, chitin, biogenic silica, calcium carbonate, or other contents. A density separation step is commonly used to remove sediments, while a digestion step is performed to dissolve biogenic materials. As no standardized MP extraction method exists, the order in which the two steps are performed can vary, as well as the used agents and filtration procedures.

For the density separation, salt is dissolved in water to achieve a high-density solution. This solution is then used to separate the heavy sediments in the samples from the buoyant MP particles by decanting the supernatant. The most frequently used type of a high-density solution is the saturated sodium chloride (NaCl) solution which is applied in 43% out of 109 considered field studies detecting MP in sediment samples. The second most

Table 2.1. General data of the six most produced polymer types. Density and application data were adapted from Coyle et al. (2020), PlasticsEurope (2021) and Hidalgo-Ruz et al. (2012). The data on global plastic production are from 2015 (Geyer et al., 2017).

type	density (g cm^{-3})	structural formula	global production	application
PE	0.92–0.97		116 MT	bags, toys, bottles, pipes, trays, containers, packaging, microbeads in personal care products, etc.
PP	0.90–0.91		68 MT	ropes, bottles, pipes, caps, packaging, microbeads in personal care products, etc.
PS	1.04–1.10		25 MT	insulating boxes, building insulation, floats, cups, packaging, medical devices, microbeads in personal care products, etc.
PVC	1.16–1.58		38 MT	pipes, containers, window frames, flooring, shower curtains, cable insulation, etc.
PET	1.37–1.45		33 MT	bottles, strapping, packaging, thermal insulation, microbeads, etc.
PUR	1.2		27 MT	building insulation, pillows, mattresses, insulating foams, etc.

commonly used salt is sodium iodide (NaI) (20%), which can reach a significantly higher density (1.6 g cm^{-3}) compared to the saturated NaCl solution (1.2 g cm^{-3}) resulting in a broader range of considerable MP types (Table 2.1, Qiu et al. (2016)). Further used salts are zinc chloride (ZnCl_2) (e.g., Martin et al. (2020); Uddin et al. (2021)), sodium polytungstate ($\text{H}_2\text{Na}_6\text{O}_{40}\text{W}_{12}$) (e.g., Enders et al. (2019)), calcium chloride (CaCl_2) (e.g., Li et al. (2020); Stolte et al. (2015)), potassium formate (CHKO_2) (e.g., Xue et al. (2020)), potassium iodide (KI) (Phuong et al. (2018); Aslam et al. (2019)) and very rarely used salts such as sodium tungstate dihydrate (Kanhai et al. (2019); Pagter et al. (2018)), magnesium chloride MgCl_2 (Cutroneo et al. (2022)), or cesium chloride (CsCl) (Dodson et al. (2020)).

In some cases, non-saline substances such as canola oil were used for separation, in which MP accumulates due to its hydrophobic properties (Crichton et al., 2017; Ross et al., 2021; Courtene-Jones et al., 2020).

If a digestion step was needed (applied in 52% out of 192 field studies listed in Table S1 and S2), usually hydrogen peroxide (H_2O_2) was used for sediment samples (60%), as well as for water samples (51%). The Fenton reagent is also a frequently used digestion agent (18%), in which H_2O_2 in combination with Iron II (Fe(II)) is added to the sample to accelerate the oxidation reaction (Bergmann et al., 2017). Additionally, enzymes were used frequently to remove specific sample matrix ingredients, such as proteinase K or protease to remove proteins, lipase for lipids, or cellulase for cellulose (e.g., Rist et al. (2020); Roscher et al. (2021); McEachern et al. (2019)). To further increase the digestion efficiency, H_2O_2 is used in some studies as well (Lorenz et al., 2019; Tekman et al., 2020). Bases such as potassium hydroxide (KOH) and sodium hydroxide (NaOH), acids like nitric acid (HNO_3), hydrochloric acid (HCl), sulfuric acid, or sodium hypochlorite solution and also sodium dodecyl sulfate (SDS) were also used to digest biogenic matrix fractions (Table S1 and S2, as well as Enders et al. (2017); Imhof et al. (2016)).

2.2.3. Instrumental Analysis

The analysis of MPs can generally be divided into three groups, visual, spectroscopic, and thermo-analytical identification. The visual identification is based on particle classification into typical morphological characteristics of MP particles. Based on typical colors and shapes of MP, it was assumed that the particles under investigation were of synthetic origin. Some typical shapes are fibers, lines, filaments, spheres, films, sheets, pellets, fragments, and foamed MPs (Shim et al., 2018). This identification method is the cheapest and finds much application in numerous studies (21% out of 192 references). For a higher resolution, scanning electron microscopy (SEM) is applied to support the visual identification (e.g., Retama et al. (2016)). In addition to the visual identification method, Nile Red can be used to assist. The Nile Red is a fluorescing dye adhering to common MP species, making microscopic counting easier and reducing the subjectivity of human sorting (Erni-Cassola et al., 2017). However, the use of Nile Red is limited by the fact that it was originally utilized as a stain for lipids in biological cells, which consequently requires a high degree of sample purity before staining MPs (Prata et al., 2021). Another disadvantage of visual identification methods is the need for a reliable specification of polymer types, resulting in the failure to distinguish them from natural residues, leading to large detection errors

(Huppertsberg & Knepper, 2018; Prata et al., 2021; Lenz et al., 2015; Hidalgo-Ruz et al., 2012). Only 68% of visually identified MPs were spectroscopically confirmed for their synthetic origin with increasing uncertainties with decreasing MP particle sizes (Lenz et al., 2015).

With spectroscopic identification methods, chemical properties of single particles can be detected by interactions of sample molecules or atoms with specific radiation enabling the differentiation between polymer types and natural particles. The Fourier-transform infrared (FTIR) spectroscopy, used in 68% out of 192 MP studies, is the most commonly used instrumentation in MP research. Micro-FTIR analysis instruments equipped with focal plane array (FPA) detectors in transmission mode allows recording an entire filter containing MP particles with several thousand spectra recorded simultaneously up to a smaller particle size of 10 μm (Huppertsberg & Knepper, 2018). However, this equipment requires large financial support, unattainable for smaller scientific institutions, which consequently tend to use less expensive equipment.

A common method for analyzing MP is to visually identify MP items based on characteristic features with the subsequent measurement of some visually identified MPs with FTIR in attenuated total reflectance (ATR) mode (e.g., Lin et al. (2020); Li et al. (2020); Lin et al. (2021); Patterson et al. (2019); Mistri et al. (2020); Falahudin et al. (2020)). However, this method is subject to many inaccuracies. First, for FTIR measurements in ATR mode, contact between the microplastic items with the instrument crystal is necessary, which requires a particle size of a minimum of 500 μm , rejecting the analysis of smaller items (Huppertsberg & Knepper, 2018). Furthermore, visual sorting is subject to many errors (Lenz et al., 2015). The second most commonly used spectroscopic identification method is Raman spectroscopy (12% out of 192 MP studies). With Raman, a spectroscopic resolution of 1 μm can be achieved. Furthermore, due to the analysis of backscattered light, no background interferences are expected in contrast to the FTIR analysis (Huppertsberg & Knepper, 2018). However, this method is strongly limited by the high cost and time required to use the device. Furthermore, dyes can impede the detection of the polymer types by spectral overlay, which is also problematic for FTIR in transmission mode (Huppertsberg & Knepper, 2018).

Examples of thermo-analytical methods used to identify MPs are pyrolysis gas chromatography-mass spectrometry (pyr-GC/MS), thermogravimetry coupled to differential scanning calorimetry (TGA-DSC), and thermal extraction desorption gas chromatography-mass spectrometry (TED-GC/MS) (Huppertsberg & Knepper, 2018). Out of these three

methods, the pyr-GC/MS is the most frequently applied instrumentation in MP surveys, becoming more popular recently (Fischer & Scholz-Böttcher, 2017). This method is based on the combustion of the sample resulting in many individual fragmentation substances characteristic of specific polymer types. These substances are trapped in the gas chromatography column and measured with mass spectrometry. Limitations for this application are the small amounts of sample masses and particle sizes that must be transferred into thermal desorption tubes (1.5 mm) and the need for highly effective sample cleanup to avoid misinterpretations (Fischer & Scholz-Böttcher, 2017; Strungaru et al., 2019). Without sample cleanup, natural fractions in the sample, such as chitin, can release e.g. styrene within the measuring process as a decomposition product. This is the same decomposition product as for polystyrene and can therefore lead to an overestimation of this polymer type (Fischer & Scholz-Böttcher, 2017). Another disadvantage is the lack of individual particle information about the MP number, size, and shape. Instead, the quantification of one polymer type can be evaluated by their specific peak areas as a whole, which on the other side, also includes nanoplastic or small MP items not able to consider with spectroscopic methods. Furthermore, this method enables organic plastic additives to be measured simultaneously with the polymers themselves with less time expenditure (Dekiff et al., 2014; Fries et al., 2013; Strungaru et al., 2019; Fischer & Scholz-Böttcher, 2017).

Table 2.2. Overview of MP collection and detection methods for different marine sediment sample types, including the sampling procedures, used digestion agents (if applied), density separation solutions (if applied), and analysis methods used in various studies.

type	sampling	digestion	density sep.	analysis	reference
seabed	PVC Core (by divers)	enzymes	NaI	μ FTIR	Dahl et al. (2021)
seabed	Gravity Corer	Fenton	NaI	μ FTIR	Lin et al. (2020)
seabed	Gravity Corer	H ₂ O ₂	HCO ₂ K	μ Raman	Xue et al. (2020)
seabed	Van Veen grab	–	NaCl	μ FTIR	Claessens et al. (2011)
seabed	Gravity Corer	H ₂ O ₂	CaCl ₂	μ FTIRn	Li et al. (2020)
seabed	Gravity Corer	H ₂ O ₂	NaI	ATR-FTIR	Matsuguma et al. (2017)
seabed	Box Corer	–	–	ATR-FTIR	Brandon et al. (2019)
seabed	Gravity Corer	–	ZnCl ₂	ATR-FTIR	Uddin et al. (2021)
seabed	Box Corer/Push-Corer	–	NaCl & NaI	μ Raman	Chen et al. (2020)
seabed	Box Corer	–	H ₂ Na ₆ O ₄₀ W ₁₂	FTIR	Martin et al. (2017)
seabed	Core tubes (by divers)	–	–	visually	Alomar et al. (2016)
seabed	Box Corer	–	NaCl	μ FTIR	Filgueiras et al. (2019)
seabed	Eckman Dredge	H ₂ O ₂	NaCl	FTIR	Tsang et al. (2017)
seabed	Multiple Corer (MUC)	Fenton	ZnCl ₂	FPA-FTIR	Tekman et al. (2020)
mangroves	spatula	–	NaCl	FTIR	Nor & Obbard (2014)
mangroves	shovel	–	NaCl & NaI	FTIR	Zhou et al. (2020)
beach	spoon	–	NaCl & NaI	TD-Pyr-GC/MS ¹	Dekiff et al. (2014)
beach	spatula	H ₂ O ₂	ZnCl ₂	visually	Esiukova (2017)
beach	spoon	–	water	visually	Baztan et al. (2014)
beach	glass jar	H ₂ O ₂	CaCl ₂	Raman	Hamilton et al. (2021)
beach	spoon	–	NaCl	FTIR	Carlsson et al. (2021)
beach	spatula	KOH/HNO ₃	KI	μ FTIR	Phuong et al. (2018)
beach	shovel	H ₂ O ₂	NaCl & ZnCl ₂	ATR-FTIR	Kor et al. (2020)
beach	shovel	–	NaCl	FTIR	Chen & Chen (2020)
beach	cup	–	ZnCl ₂	FTIR	Coppock et al. (2017)

¹ TD-Pyr-GC/MS = thermal desorption pyrolysis gas chromatography/mass spectrometry

Table 2.3. Overview of MP collection and detection methods for different marine water sample types, including the sampling procedures, used digestion agents (if applied), density separation solutions (if applied), and analysis methods used in various studies.

type	sampling	digestion	density sep.	analysis	reference
surface	Neuston Net	EO ¹	ZnCl ₂	FPA- μ FTIR ²	Lorenz et al. (2019)
surface	Manta Net	-	NaCl	μ FTIR	Stolte et al. (2015)
surface	canisters	H ₂ O ₂	CaCl ₂	visually	Rios-Mendoza et al. (2021)
surface	intake pump	H ₂ O ₂	-	ATR-FTIR	Wu et al. (2019)
surface	Neuston Net	-	-	ATR-FTIR	Yakushev et al. (2021)
surface	intake pump	EO ¹	ZnCl ₂	FTIR	Roscher et al. (2021)
surface	WP2 Net	-	-	visually	Aytan et al. (2016)
surface	Manta Net	H ₂ O ₂	water	visually	Gewert et al. (2017)
surface	glas bottles	H ₂ O ₂	-	ATR-FTIR	Sathish et al. (2020)
surface	steel bucket	H ₂ O ₂	-	μ FTIR	Dai et al. (2018)
surface	Manta Net	Fenton	NaCl	FTIR	Mu et al. (2019)
surface	Manta Net	SCS & H ₂ O ₂	NaCl	FTIR	Carlsson et al. (2021)
column	Bongo Net & pump	H ₂ O ₂	NaCl	μ FTIR	Cai et al. (2018)
column	ROV ³	-	-	Raman	Choy et al. (2019)
column	intake pump	-	-	FPA-FTIR	Cincinelli et al. (2017)
column	CTD	-	-	ATR-FTIR	Courtene-Jones et al. (2017)
column	intake pump	HCl	-	Nile Red	DesForges et al. (2014)
column	Bongo Net & CTD	HF	-	FTIR	Di Mauro et al. (2017)
column	intake pump	SDS	-	Raman	Enders et al. (2015)
column	intake pump	KOH	-	FTIR	Pabortsava & Lampitt (2020)
column	submersible pump	Fenton	NaCl	μ FTIR	Song et al. (2018)
column	steel sieve	SDS & EO ¹	-	FTIR	Tekman et al. (2020)
column	submersible pump	Fenton & HCl	-	Raman	Zobkov et al. (2019)
column	CTD	-	-	μ FTIR	Zhou et al. (2021)

¹ EO = enzymatic-oxidative digestion, including different enzymes and H₂O₂.

² for case of uncertain spectra, Raman spectroscopy was used additionally.

³ ROV = remotely operated vehicle equipped with a filtration device.

3. Materials and Methods

3.1. Method development and validation

Because there is still no standard method for extracting MPs, a proper method for analyzing environmental samples must be chosen. The method chosen has to be as accurate as possible, with the lowest risks of losses and contamination while keeping the effort low. For the first tries to analyze MP in sediment trap samples, an easy-to-handle method was applied, which was also used in numerous previous studies (Blašković et al., 2016; Fastelli et al., 2016; Cannas et al., 2017; Ronda et al., 2019; Romeo et al., 2015). This method includes a density separation step with a saturated NaCl solution and a visual inspection using a microscope and was previously utilized for microfibers in sediment trap samples by Reineccius et al. (2020). However, the challenge in using this method for sediment trap samples occurred in the high amount of biogenic materials contained in the samples, especially in sampling periods of high primary production rates. Distinguishing between natural and synthetic particles was difficult or impossible due to material overlaying. Furthermore, polymers with higher densities compared to the NaCl solution, such as PET or PVC, cannot be considered. Sediment trap samples with highly complex matrices but limited sample masses are difficult to analyze with the most commonly applied methods leading to the need for a fitted extraction process [Publication 1: **Reineccius et al. (2021)**].

To remove biogenic materials within the scope of the present work, digestion agents were introduced in the first step of the MP extraction protocol. As some strong acids and alkaline agents were verified to affect MPs in their shape or weight, or even dissolve them entirely (Hurley et al., 2018; Karami et al., 2017; Olsen et al., 2020), a less aggressive wet peroxide digestion step (Prata et al., 2019) was chosen to digest biogenic fractions with some enhancements. To examine the effectiveness of digestion agents, a dried and chopped algae mix was used. For potential influences on MP particles, powder of nine different polymer types (PE, PP, PET, PS, PVC, polyamide (PA), polymethyl methacrylate (PMMA), polyoxymethylene (POM), acrylonitrile butadiene styrene (ABS)) were used to monitor weight, size, and color changes after the respective digestion treatment. After testing digestion solutions such as the Fenton reagent, KOH, combinations with ethanol, SDS, acetic acid, ammonia, detergent solution, or the H₂O₂ activation via UV radiation at various temperatures and exposure times, the application of H₂O₂ with acetic acid has proven to be the best combination of effectiveness and handling with no significant effects

on MP particles **Reineccius et al. (2021)**.

Despite the high efficiency of H_2O_2 in combination with acetic acid, biogenic residues were still left, prone to be confused with MPs in visual analysis. To further enhance the sample cleanup and be able to remove sediments or lithogenic fractions, two different apertures were compared (Fig. 3.1). In one application, a commonly used density separation step was introduced using sodium tungstate dihydrate ($\text{Na}_2\text{WO}_4 \cdot 2\text{H}_2\text{O}$), with a final density of 1.6 g cm^{-3} in the saturated state. The next application was a syringe cascade coated with lubricant oil at the inner syringe walls. This coating constitutes a lipophilic layer that retains lipophilic MP polymers and lets non-lipophilic matrix residues pass (**Reineccius et al., 2021**). The density separation was conducted in a custom-made separation device consisting of an Erlenmeyer flask connected to a bearing valve with a small glass tube extension at the top (Fig. 3.1b). For recovery rates, MP particles ($n = 100$) of the respective polymer types (PE, PP, PET, PS, PVC, PA) were filled into the flask. Then, the valve with glass tube extension was screwed onto the flask and filled with the density solution until the half height of the glass tube. To avoid contamination, the upper tube end was covered with aluminum foil. After stirring this solution for 1 h, the mixture was left to rest for 23 h until the valve was closed. After the resting time, the supernatant containing floating MP particles was filtered on glass microfiber (GF) filters, and the recovered MPs were counted under the microscope. This procedure was repeated three times for each polymer type (**Reineccius et al., 2021**).

To determine recovery rates of the syringe cascade application, 100 MP particles (PE, PP, PET, PS, PVC, PA) in 20 mL ultra-pure water were filled into the cascade consisting of three vertically stacked syringes. The passed suspension was collected in a glass beaker and filled into the syringe cascade again. This procedure was repeated three times in total and conducted in triplicates for each polymer type, respectively. The loaded syringes were then rinsed with ultra-pure water and infused with a warm detergent solution (50°C) to recover the MP particles. The received detergent solution was then filtered with GF filters to count the recovered MPs under the microscope as described in **Reineccius et al. (2021)**.

An average recovery rate of 98.1% was obtained with the density separation technique. The lowest rate was achieved for PVC due to the high density of PVC (1.56 g cm^{-3}), which caused some of the observed particles to accumulate at the bottom. However, the solution with a density of 1.60 g cm^{-3} should include this type of PVC, suggesting density differences within a polymer type. Using the syringe cascade, a mean recovery rate of 98.0% was achieved (**Reineccius et al., 2021**). The lowest rates were found for less lipophilic

polymer types such as PA (88.7%) but very high and stable (low standard deviation) rates for PE, PP, and PS. Besides that, this application is easier to handle than the density separation, it can be performed quickly, and large quantities of a salt solution are not required. Due to these advantages, separation using the syringe cascade combined with the previous digestion step using H_2O_2 and acetic acid, was chosen for further application for environmental samples.

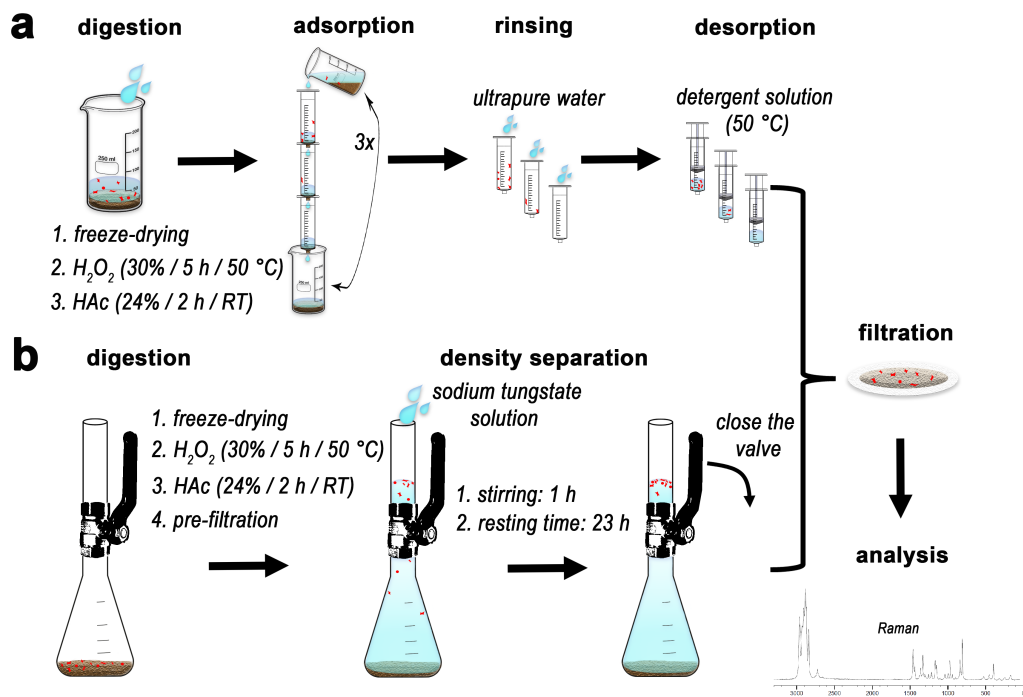


Figure 3.1. Entire extraction procedure of both possible MP separation methods with the syringes cascade (a) and the density separation method (b). Both methods start with a freeze-dried sample followed by the first clean-up step with the digestion. This figure was adopted and edited from Reineccius et al. (2021).

3.2. Field samples

3.2.1. Sampling site and sample collection

The focus of this study is based on sediment trap samples collected at the mooring station Kiel 276 [Publication 2: Reineccius & Waniek (2022)]. This station is located at 33°N, 22°W within the deep Madeira Basin of 5300 m depth halfway between the Azores and the

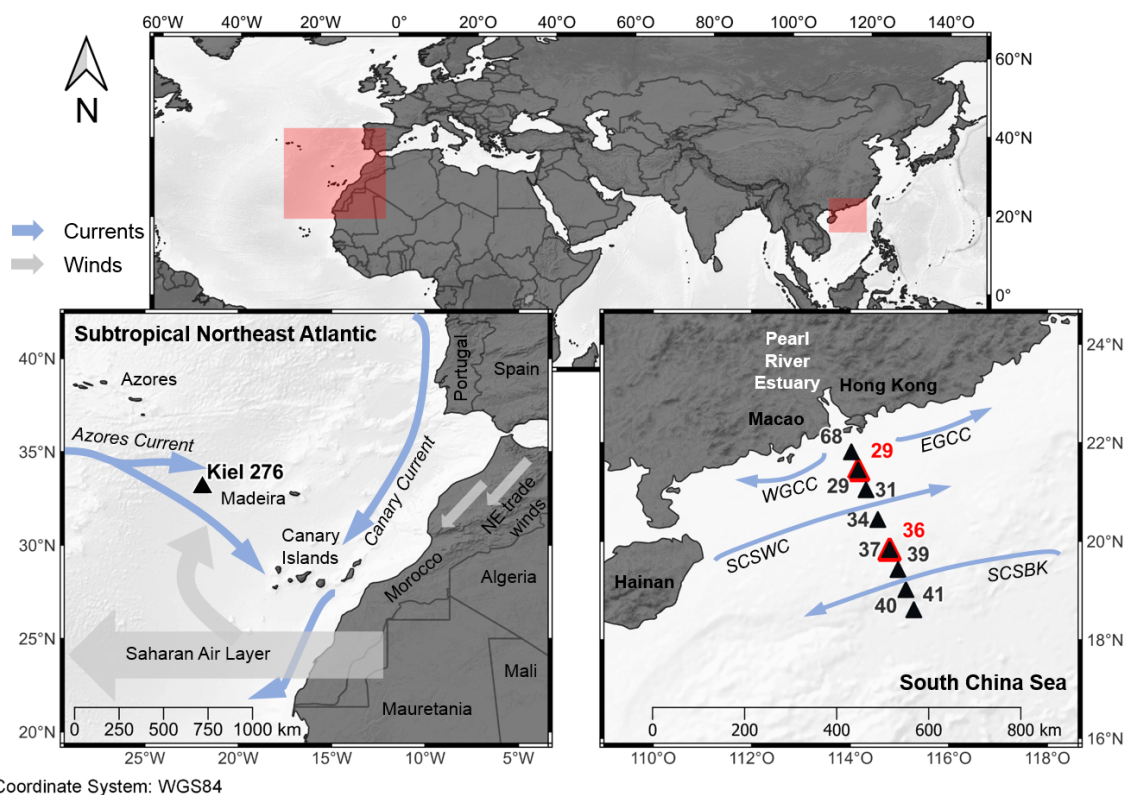


Figure 3.2. Location of the mooring station Kiel 276 in the Subtropical Northeast Atlantic (33°N, 22°W) and sampling stations in the northern South China Sea (SCS) for MP analysis. In the SCS map, the filled black triangles symbolize the sediment sampling stations, and the red triangles represent the net sampling stations. The prevailing major winds and currents are sketched in gray and blue, respectively. For the SCS map, surface currents are given, which were adapted from Deich et al. (2021) for this area: Eastern and western Guangdong Coastal Current (EGCC, WGCC), SCS Warm Current (SCSWC) and SCS Branch of Kuroshio (SCSBK). The red areas of the upper overview map present the zoomed area for the Atlantic and SCS maps.

Canary Islands. The sampling site is influenced by current velocities between 20 - 25 cm s^{-1} in the thermocline (270 m depth) and the Mediterranean outflow (1000 m depth) and lower velocities of 5 cm s^{-1} in the deeper water column (1000 - 2600 m depth). The sediment trap considered for MP analysis was deployed at 2000 m depth. This results in a catchment area of about 100 km^2 , which is influenced by interannual and seasonal propagation of the Azores Front (Fründt & Waniek, 2012; Waniek et al., 2004, 2005). Depending on the Azores Front position, the mixed layer depth and the related primary production in this area are also affected. The primary production rate combined with the lithogenic input via

atmospheric transport are the main influencing processes of the total particle flux in 2000 m depth (Waniek et al., 2005; Pullwer & Waniek, 2020). The largest representative of the total particle flux is the biogenic content, containing up to 80% calcium carbonate in this part of the subtropical Northeast Atlantic (Waniek et al., 2005). This proportion is strongly influenced by calcium carbonate forming planktonic species such as coccolithophorids and foraminifera (Waniek et al., 2005). The lithogenic input is coupled with Saharan dust outbreaks transporting large amounts of dust into the North Atlantic, which sink to the deep sea supported by biogenic ballast effects (Brust & Waniek, 2010; Pullwer & Waniek, 2020).

For the MP detection in this work, the sediment trap sampling series 23 - 29 were analyzed, including 110 samples in total, which were collected between April 2003 and June 2015 (**Reineccius & Waniek, 2022**). The deployed sediment traps used for the sample collection are fiberglass reinforced plastic funnels (slope of 34° , opening of 0.5 m^2), sealed with epoxide resin and equipped with a revolver holding 21 PP sample bottles (type S/MT 234, K.U.M., Germany). The rotating revolver enables specific sampling in intervals, which range between 11 and 62 days for the analyzed samples. The shorter intervals were applied during high particle flux rates after high primary production in the upper water column. The funnel is covered with a hexagonal lattice grid baffle made of resin-sealed special paper to avoid losses of sample material by movements of the surrounding water. Before deployment, the sediment trap and sample bottles are cleaned. These clean bottles holding a volume of 400 cm^3 are filled with a mixture of in-situ seawater and sodium azide (4:1) (NaN_3 5% stock solution in high purity water) to preserve sinking materials immediately. To fit the salt content in the sample bottles to the surrounding seawater (38 g L^{-1}), NaCl was added.

After recovery of the sediment traps two years after deployment, the sample bottles were closed with caps immediately and stored in the dark at $4 - 6^\circ\text{C}$ until laboratory analysis. In the laboratory, large zooplankton "swimmers" were removed manually, and the samples were split into four equal aliquots. One of these four splits was freeze-dried, and 100 mg (if available) were weighed into a glass beaker for MP analysis (**Reineccius & Waniek, 2022**).

In addition to the sediment trap samples, eight sediment samples and two plankton net samples were selected from the South China Sea (SCS) to investigate the applicability of this method for environmental samples (**Reineccius et al., 2021**). The samples were collected from the Pearl River estuary to the deep SCS perpendicular to the coast of China

during the Sonne 269 cruise (SO269) (Fig. 3.2). This sampling location was chosen due to the proximity to the Pearl River, characterized by its large water volume transport into the SCS and the high population density around the river delta. The Pearl River passes large Chinese cities and is consequently expected to transport high amounts of MP into the SCS. The sediment samples were gathered by a Multi-core vessel with Plexiglas (PMMA) core pipes, with 60 cm height and 10 cm inner diameter. About 10 g from the uppermost 3 cm of each core was used for the MP analysis, which was freeze-dried before extraction. The plankton net samples were taken by a Multi-closing net (100 μm mesh size, 50 \times 50 cm square opening) from 50 m water depth to the surface at station SCS 29 and with an Apstein plankton net (500 μm mesh size, ring diameter of 50 cm) from 100 m water depth to the surface at station SCS 36. A half split was taken from both net samples to analyze MPs, which were also freeze-dried before further treatment procedures. The detailed procedure is described in **Reineccius et al. (2021)**.

3.2.2. MP extraction

To remove biogenic material in the sample, the validated method described above (section 3.1, **(Reineccius et al., 2021)**) was applied. In brief, 20 mL H_2O_2 (30% w/w, for synthesis, Merck KGaA, Germany) were added to the sample and left to react for 5 h at 50 $^\circ\text{C}$. After this time, 20 mL acetic acid (24% w/w, VWR International, Germany) was added and left to react another 2 h at room temperature to remove biogenic calcium carbonate. After the reaction time, the samples were filled into the coated syringe cascade, holding the lipophilic MP particles and letting non-lipophilic particles pass through the cascade. Each sample was passed through the cascade three times and rinsed with ultra-pure water subsequently to remove non-lipophilic residues. A warm detergent solution (50 $^\circ\text{C}$) was used to detach the MPs. The obtained suspension containing MPs was finally filtered onto an AnodiscTM filter (WhatmanTM, 25 mm diameter, 0.2 μm nominal pore size, CatNo. 6809–6022) **(Reineccius & Waniek, 2022)**.

After filtration, the filters were directly transferred to a glass slide and covered with a coverslip to avoid contamination. Additional contamination precautions have been taken by the previous filtration of all used solutions over glass fiber filters (WhatmanTM, 47 mm diameter, 0.7 μm nominal pore size, CatNo. 1825–047). Besides that, the samples were covered with aluminum foil between all steps. Every step in which the sample came into contact with the air was implemented under the fume cupboard (average airborne contamination < 1 fiber within 0.75 – 4.75 h (Wesch et al., 2017)). Furthermore, a white cotton lab coat was

worn, and the laboratory was just used by the conducting person during the MP extraction steps. In addition, the samples were handled carefully to reduce contamination, and blank samples were prepared. One of the 21 sample bottles mounted at the trap was not exposed to the marine environment and was not collecting sinking material. These blank samples reflect the whole sample processing and were called "sampling blanks". Sampling blanks were available for the sampling series 24, 25, 26, and 29 and were treated the same way as the samples containing sinking material. Additionally, one blank sample was prepared for each sample set (5-10 samples), which were applied for SCS net and sediment samples as well as sediment trap samples. These blanks were prepared within the same day as the sample treatment in the lab to trace contamination sources back. For these, an empty beaker was filled with the digestion solution instead of a beaker filled with sample material in the first treatment step. After this step, the whole treatment and analysis process was conducted the same way as for the samples. Therefore, these blank samples were called "method blanks". The entire sample treatment and handling are described in **Reineccius & Waniek (2022)** in detail.

3.2.3. Analysis

Raman spectroscopy (LabRAM HR 800 Horiba Jobin YVON) with integrated NGS Lab-Spec software was applied to identify MP on the prepared filters (**Reineccius & Waniek, 2022**). This instrument is equipped with a microscope (Olympus BX41 microscope with variable lenses) and a camera to visualize and digitally display small particles. In the case of a few visible MP particles on the filter, the entire filter was manually scanned for potential MPs. When particle numbers were too high, a quarter or 100 random window positions (about 15%) of the filter were scanned and extrapolated for the entire filter. For searching for suspect MP particles, a magnification of $10 \times$ (window size 0.7×0.9 mm) with transmitted light was used. For measurements, $50 \times$ magnification and a red laser were applied (633 nm, 17 mW, air-cooled HeNe laser) at 10 s integration time and ten accumulation scans in the wavenumber range $50 - 3800 \text{ cm}^{-1}$. The measured spectra were evaluated with the KnowItAll Information System 2020 software (WILEY) and compared against the included spectral library to identify the polymer type. Those spectra with a matching degree $< 80\%$ were rejected as a synthetic polymer. For particle size measurements, every positively identified MP particle was photographed. To additionally determine the particle volumes and masses, the method described in **Reineccius et al. (2021)** (Publication 1) and **Reineccius & Waniek (2022)** (Publication 2) was applied.

4. Results and Discussion

4.1. MP fluxes and properties

In each sediment trap sample collected in 2000 m depth, MP particles were found in quantities between 35 and 31,080 per sample. On the blank filters, particle numbers between 0 and 7 (average of 1.8 items) were identified as MPs. This results in a blank-corrected MP flux of $1.13 - 3146.81 \text{ items day}^{-1} \text{ m}^{-2}$, sinking into the 2000 m deep Subtropical Northeast Atlantic. More detailed results are given in **Reineccius & Waniek (2022)**. All calculated MP (mass) fluxes, determined between April 2003 and June 2015, are illustrated in Fig. 4.1a and b, together with the calcium (Fig. 4.1c) and aluminum (Fig. 4.1d) fluxes, representing biogenic and lithogenic fractions, respectively.

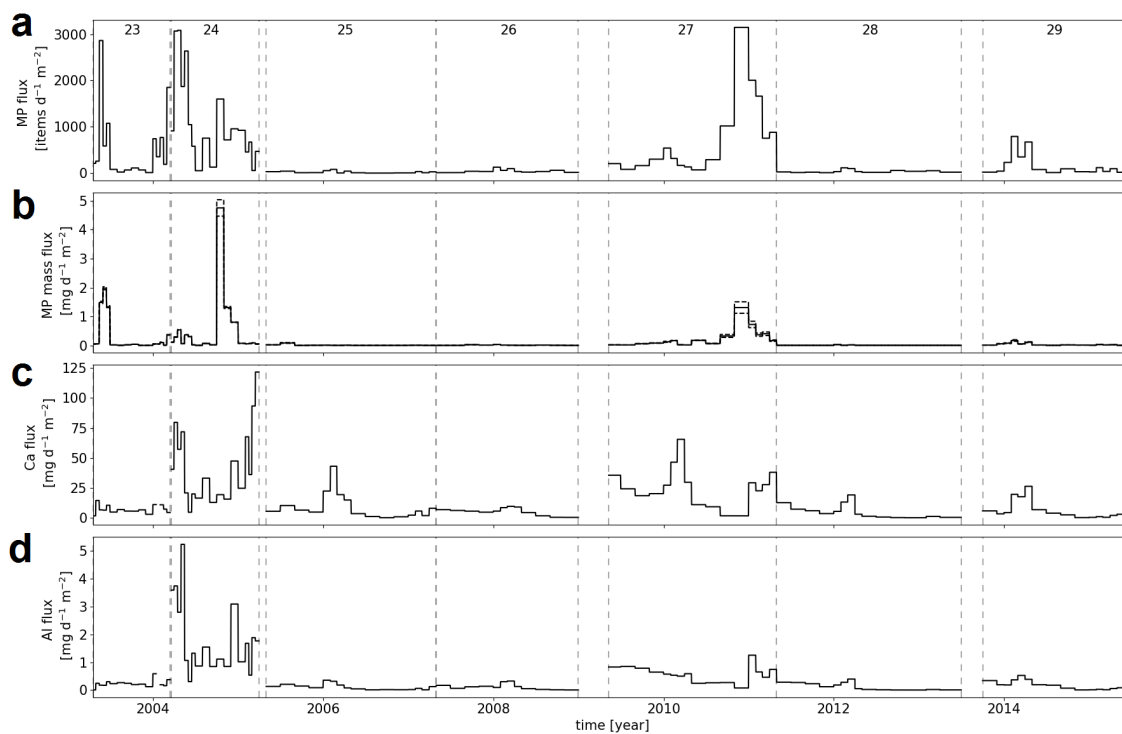


Figure 4.1. MP fluxes (**a**), MP mass fluxes (**b**), calcium carbonate fluxes (**c**), and aluminum fluxes (**d**) for all analyzed samples ($n = 110$). Dashed black lines in figure **b** represent flux ranges resulting from the mass calculation with a range of potential polymer densities. The bar width indicates the sampling interval for each sample, with gaps that illustrate mooring failure or no deployment. The vertical dashed gray lines mirror the intervals for the respective sampling series. Note the different scales of the y-axis between the figures (adopted from **Reineccius & Waniek (2022)**).

The highest fluxes were recorded during May and June 2003 (series 23), between March and June 2004 (series 24), and from September 2010 until April 2011 (series 27) (Fig. 4.1a and b). Depending on the MP particle sizes, the calculated MP mass fluxes can highly differ compared to the MP fluxes. The highest MP mass flux was detected during October 2004 (series 24), suggesting the combination of large MP items and high quantities. In total, however, the MP sizes within the sample series were not differing greatly (Fig. 4.2). The mean size of all detected MP particles in all samples was $88.44 \pm 113.46 \mu\text{m}$, with the most abundant particle sizes below $100 \mu\text{m}$. Comparing the various polymer types, no significant differences in particle sizes were recognized as well.

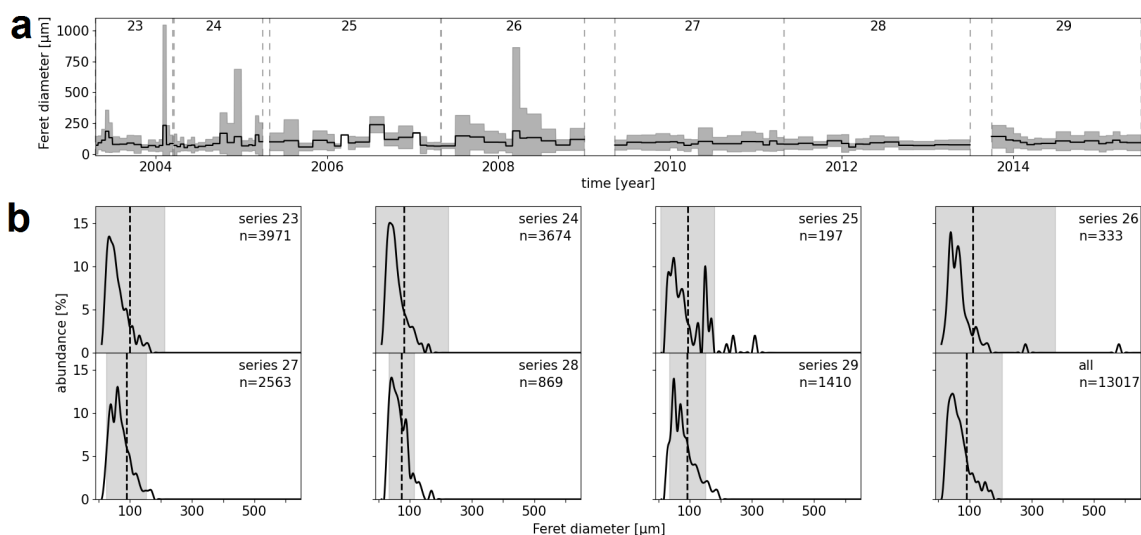


Figure 4.2. Mean sizes of detected MP particles in sediment trap samples for all samples (a) and the size distribution for each sampling series, as well as for the sum of all detected MPs (b) (adopted and edited from **Reineccius & Waniek (2022)**). The gray areas represent the standard deviation range (\pm s.d.) and the dashed black line in (b) marks the mean from the sampling series, calculated for the respective particle number (n). The dashed gray lines in (a) separate the sampling series.

The two most frequently detected polymer types were PE and PVC (**Reineccius & Waniek, 2022**). PE accounts for 68.3% of the total MP flux and 73.4% of the MP mass flux. This high occurrence fits well with global production, with PE as the most produced polymer type worldwide (Andrady, 2011; Geyer et al., 2017). The fraction of PVC was 29.7% and 22.0% in the MP flux and MP mass flux, respectively. The remaining fractions were PP, PS, PMMA, and PET. The most rarely detected polymer types were PA, polytetrafluoroethylene (Teflon), and a polymer mixture of PE and PP.

The first high occurrence of MP within the years 2004 and 2005 (Fig. 4.1) is mainly attributed to PE fluxes. The second high MP occurrence in 2010 - 2011 contains high amounts of PVC, indicating a high variability of polymer types between the years.

4.2. Correlations and transport pathways

Between the individual polymer (mass) fluxes, no correlation was found for the four most abundant polymers (PE, PVC, PP, PS). However, correlations between fluxes of PVC and PA, PVC and PMMA, as well as PA and PMMA were found (**Reineccius & Waniek, 2022**). Possibly, this is connected to similar transport pathways for polymer types lighter than seawater (PE, PP) and those heavier than seawater (PVC, PS, PA, PET, PMMA). PS were excluded for this hypothesis, as it is very frequently produced in foam shapes. Consequently, it can be lighter as well as heavier than seawater. However, correlations were also not found between PE and PP with densities both lighter than seawater ($0.92 - 0.97$ and $0.90 - 0.91 \text{ g cm}^{-3}$, respectively) (Tab. 2.1).

Another reason for these different occurrences can be attributed to various source regions combined with different transport pathways. In more northern regions of the Atlantic Ocean towards the Arctic Ocean, PET or PA were the most reported polymer types (Tekman et al., 2020; Courtene-Jones et al., 2020, 2017). In more southern regions of the Atlantic, PE was the main contributor of the entire MP content (Enders et al., 2015; Pabortsava & Lampitt, 2020; Law et al., 2010). Combined with the fluctuating current velocities and directions at the investigated mooring station Kiel 276 (Frãzao et al., 2021), the different polymer types can be transported and mixed from varying sites. Furthermore, the transport pathway can be an important contributor to the MP particle composition, which can occur via winds or currents at this site. Comparing the PE fluxes with the lithogenic flux, a strong correlation was observed ($r = 0.603$, $p < 0.05$) (**Reineccius & Waniek, 2022**), indicating a similar transport pathway. The lithogenic flux at the mooring station Kiel 276 mainly contains dust originating from North African sources and contains a high amount of aluminum. Mobilized by strong winds, desert or city dust was transported into higher air layers reaching the Saharan air layer. This air layer can transport large amounts of dust over long distances until the western Atlantic Ocean (Brust & Waniek, 2010). Via the northeast trade winds blowing from the north of Africa with higher population densities to the southwestern part with lower inhabitants, the city dust proportion can increase in the transported dust. The MP content in city dust can be high, as investigated by previous studies (Allen et al., 2019; Truong et al., 2021). Especially the PE content has been shown

to be high in the dust even at remote places (Parolini et al., 2021). Combined with the correlation, which was found between PE and the lithogenic fraction (mainly Al), supported by correlations of PE with further typical lithogenic elements such as Fe, Mg, and Ti (Table 4.1), this strongly suggests an atmospheric transport pathway of PE originating from land-based sources (**Reineccius & Waniek, 2022**).

Table 4.1. Correlation coefficients (r) for PE and PVC with element fluxes adopted from previous works (Pullwer & Waniek, 2020). $|r| = 0.10$ are defined as a weak correlation, $|r| = 0.30$ moderate and $|r| > 0.50$ strong. Correlation coefficients ≥ 0.5 with statistical significance ($p < 0.05$) are given in bold (Pearson correlation test, $n = 219$, $\alpha = 0.05$).

	Ca	Al	Fe	Mg	Ti	S	As	Zr	Sb	PE	PVC
Ca		0.742	0.689	0.751	0.670	0.719	0.448	0.712	0.212	0.371	0.020
Al			0.977	0.994	0.984	0.525	0.491	0.990	0.246	0.603	-0.009
Fe				0.961	0.961	0.562	0.595	0.976	0.378	0.577	0.061
Mg					0.980	0.492	0.440	0.980	0.198	0.618	-0.053
Ti						0.403	0.380	0.986	0.143	0.590	-0.088
S							0.829	0.519	0.663	0.138	0.505
As								0.482	0.930	0.188	0.511
Zr									0.237	0.570	-0.009
Sb										0.063	0.534
PE											-0.102
PVC											

For PVC, no correlations with lithogenic elements were observed. Instead, strong correlations were recognized between PVC and S, As, as well as Sb (Table 4.1). These fluxes are potentially attributed to PVC additives or substances used in the manufacturing processes of PVC, such as sulfur (S). Antimony (Sb) is known as a commonly used additive of PVC, as well as arsenic (As) which is used as a bio-stabilizer (BMU, 2020).

4.3. Source regions

By investigating the composition of the lithogenic content in sediment trap samples carried out in previous studies (e.g., Brust & Waniek (2010); Pullwer & Waniek (2020)), the source region of this lithogenic material can be traced back. This procedure was also applied for the sediment trap samples selected for microplastic analysis (**Reineccius & Waniek, 2022**). As the study site Kiel 276 is influenced by recurrent Sahara dust outbreaks, an African origin can be assumed for the major lithogenic fraction. Therefore, the mineral composition of the lithogenic flux material was compared to the characteristic regional compositions of African soils. For this, clay minerals such as illite, kaolinite, smectite, palygorskite, and

chlorite are commonly used (Brust & Waniek, 2010).

In sample series 23 and 24, the highest PE fluxes were detected, making the lithogenic origin for these series the most interesting (**Reineccius & Waniek, 2022**). In series 23, the illite and kaolinite fraction (I/K) varied greatly (between 0.5 and >2 for some samples), combined with large amounts of palygorskite contained in the samples. Additionally, chlorite is present, suggesting source regions in Morocco and the Atlas Mountains (Brust & Waniek, 2010; Bout-Roumazelles et al., 2007; Scheuven et al., 2013). The lithogenic fraction contained in series 24 suggests a source region far away from the mooring position. Higher amounts of quartz, low I/K values, and low palygorskite and chlorite fractions are characteristic of southern Algeria and northern Mali (Brust & Waniek, 2010; Bout-Roumazelles et al., 2007; Scheuven et al., 2013). For the following sample series 25, 26, and 27, in which the PE fluxes were much lower (**Reineccius & Waniek, 2022**), the source region is inconclusive. The I/K content is higher, the smectite content is low, and no palygorskite was detected. As palygorskite is characteristic of the northwestern Sahara soil compositions (Morocco, central Algeria, western Mauritania) (Bout-Roumazelles et al., 2007; Brust & Waniek, 2010; Reiff et al., 1986) and higher smectite contents were characteristic for Mauritania and western Chad, these regions can be excluded for potential source regions. Instead, these compositions fit well with Gran Canaria soil (Menéndez et al., 2020) but can also be a strong mixture of different source regions.

4.4. Seasonality of MP (mass) fluxes

To investigate seasonal relations of MP fluxes, the daily flux values were monthly averaged for the available data between the years 2003 and 2015 (**Reineccius & Waniek, 2022**). The resulting monthly MP (mass) fluxes are illustrated in Fig. 4.3. As the most frequently detected polymer type (PE) is lighter than seawater and was detected at 2000 m depth, a ballast effect as described in section 2.1.3 has to be considered. Consequently, the seasonal pattern for the biogenic content (Ca) is expected to be similar to the seasonal pattern of the polymer fraction that is lighter than seawater (LP). Actually, this assumption was confirmed by the occurrence of a summer slump for the MP (mass) fluxes of LP in July - September, which is characteristic of lower biogenic fluxes at the same time. Besides that, higher LP fluxes were also found in April and May, corresponding to the spring bloom, which leads to a maximum biogenic flux between February and April at 2000 m depth.

For the MP (mass) fluxes for polymer types heavier than seawater (HP), the summer slump can also be observed with the lowest fluxes between May and August. However, the

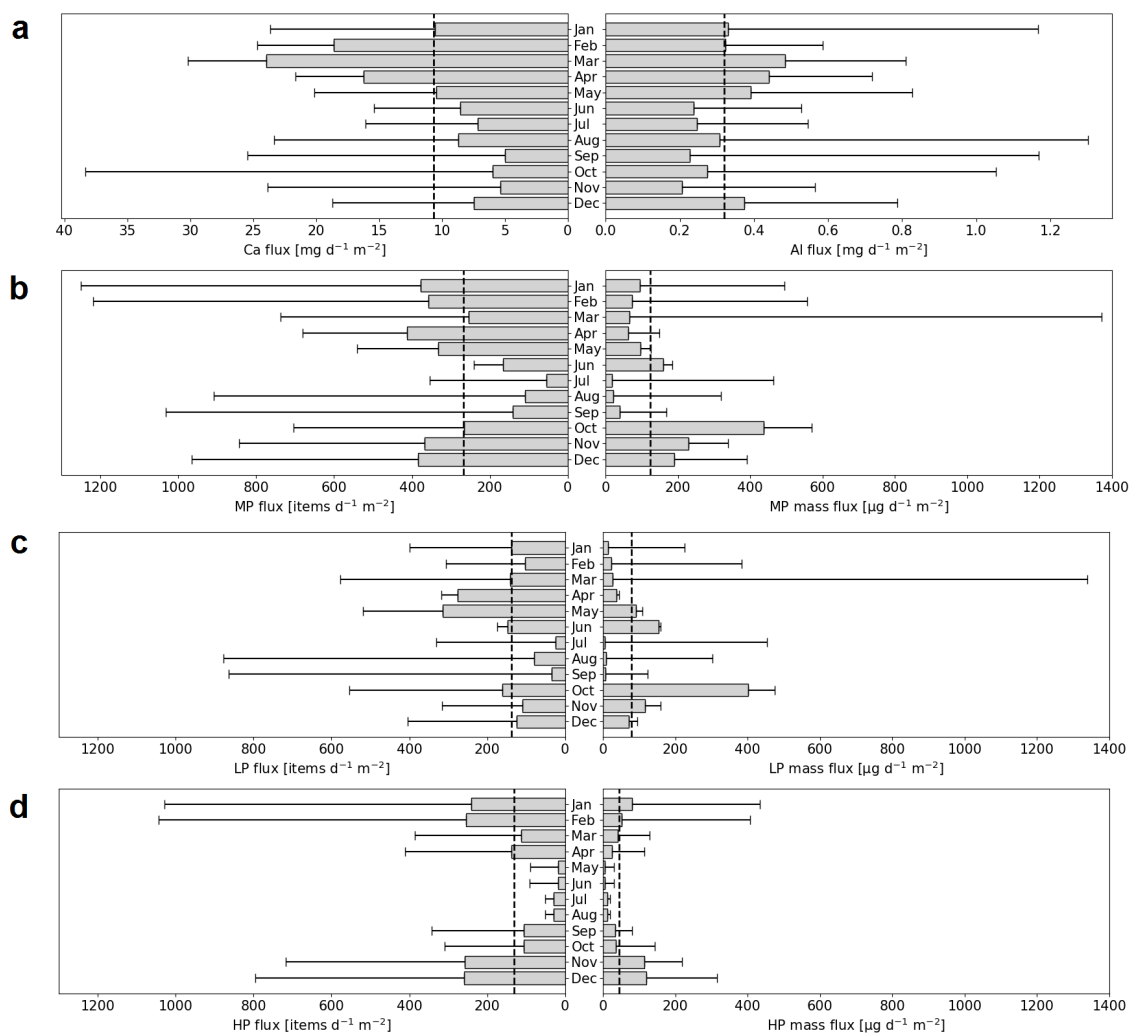


Figure 4.3. Monthly calcium (Ca) and aluminum (Al) fluxes in $\text{mg day}^{-1} \text{m}^{-2}$ (a) (adopted from Pullwer & Waniek (2020)), monthly MP (mass) fluxes (b) (adopted from Reineccius & Waniek (2022)), (mass) fluxes of the sum of all polymer types lighter than seawater (LP) (c), and heavier than seawater (HP) (d).

highest fluxes were found for the entire winter between November and February instead of spring months with potential biogenic ballasting (Reineccius & Waniek, 2022). This suggests a different dominant sinking and transport mechanism for heavier polymers compared to light polymer types. This assumption is supported by the fact that heavier polymer types with a mean size of $88.44 \pm 113.46 \mu\text{m}$ are more likely to be transported

in the water column than via winds due to their weight and larger sizes compared to the smaller atmospheric transported clay materials ($\sim 1 - 2 \mu\text{m}$ (Brust & Waniek, 2010)). In the case of the distribution of HPs in the whole water column and its higher density than seawater, HPs are very likely to sink by their own weight. The only obstacle in the vertical sinking pathway is the strong stratification within the upper water column during summertime, hindering those particles to sink. A deeper mixed layer depth in autumn and winter can drive the sinking of HPs in November and December contrastingly.

4.5. Degradation rate of MPs

Besides the input rates of plastic into the marine environment and the flux rates of MP sinking into the deep sea, the degradation rates are needed to assess the fate and total marine plastic load. These MP particles detected in sediment trap samples (**Reineccius & Waniek, 2022**) were strongly fragmented and rough in their surface shape, which can suggest an advanced degradation. However, the degradation rate is dependent on a wide variety of influencing processes as described in section 2.1.4. This variability hinders the assessment of the retention time of MP in the marine environment. Additionally, as mentioned in section 4.4, heavier polymer types are not buoyant at the water surface but can be distributed within the water column. These conditions can further affect the degradation rate with lower photo-oxidation in deeper water layers (Lechthaler et al., 2020). Due to these unpredictable factors, a location in which the different polymer types are exposed to similar conditions is considered for the first estimation of the degradation rate. For a marine location, the beach or coast is the only location in which the particles cannot sink to deeper water layers and are exposed to solar radiation and mechanical stress. In addition, temperature fluctuations prevail and oxygen is available for oxidation processes. Respective experiments were implemented in [Publication 3: **Reineccius et al. (2022)**]. In this experiment, the polymer types PE, PP, PS, PET, and PVC were weathered under simulated beach conditions for 18 months. Besides different polymer types, various water media were chosen to investigate the potential effects of salinity.

When polymers are exposed to UV radiation and oxygen, the first effect that was noticed is the degradation of hydroxyl (-OH) groups (Fig. 4.4), which are visible at about $3300 - 3450 \text{ cm}^{-1}$. This is also explained in previous theoretical descriptions (Gewert et al., 2015) for polymers with C-H backbones only (PE, PP, PS). However, as visible in Figure 4.4, PVC was also observed to generate -OH groups in the first days of the experiment. These groups weakened fast after one to two weeks until they reached the starting level

after eight weeks of exposure time again. Besides -OH generation, PVC was also observed to release its chlorine compounds at the same time and its additive (CaCO_3) within the first week. With ATR-FTIR measurements, which are commonly used in MP detection studies, PVC was hard to identify already after the first week. Even the characteristic methyl peaks at wavelengths between 2900 and 3000 cm^{-1} changed over time and are more similar to PE methyl peaks after the experiment time (18 months). This phenomenon was also observed by a previous study implemented by Hendrickson et al. (2018), in which PE was identified for some environmental collected MP particles with ATR-FTIR while PVC was identified with pyr-GC/MS for the same items. With Raman measurements, PVC was also detected successfully after all exposure times in this work (**Reineccius et al., 2022**). This observation suggests that PVC may have been underestimated in studies using ATR-FTIR as an analytical method. Furthermore, this observation may explain the large amounts of PVC found in the sediment trap samples for which Raman spectroscopy was applied (**Reineccius & Waniek, 2022**). The reason for these different results by using different analysis methods is the penetration depth, which differs between the methods. ATR-FTIR probes the near-surface region of the sample only, which in the case of PVC can provide misleading information after weathering.

The advantage of using ATR-FTIR, on the other hand, is the possibility of detecting molecular surface changes with high sensitivity for oxygen components. Introduced by weathering processes, oxygen compounds such as carbonyl groups are expected at the polymer surface, which can be found between 1700 and 1800 cm^{-1} in the FTIR spectra. The strongest carbonyl peak, which appears at about 1717 cm^{-1} (ketone peak), is commonly used to calculate the carbonyl index (CI) (Liu et al., 2019; Miranda et al., 2021; Luo et al., 2020b; Rouillon et al., 2016) as an indication of the weathering degree of plastic. In case of linearity or another predictable progression of the CI, the weathering degree can be defined for environmentally collected plastics. However, this application is connected to various inaccuracies. As visible in Figure 4.4, the CI (C=O bonds) is not following a predictable progression for most polymer types (**Reineccius et al., 2022**). Instead, it fluctuated strongly for PS and PET, showing an increase followed by a plateau and a decrease for PVC and is also decreasing after a linear increase for PP. Solely for PE, a linear increase in CI within the 18 months of weathering time in Baltic Sea (BS) and SCS water was found, but also these developments contain fluctuations within the first eight months (Fig. 4.4).

The fluctuation in the CI can be attributed to an ongoing reaction for the -OH groups.

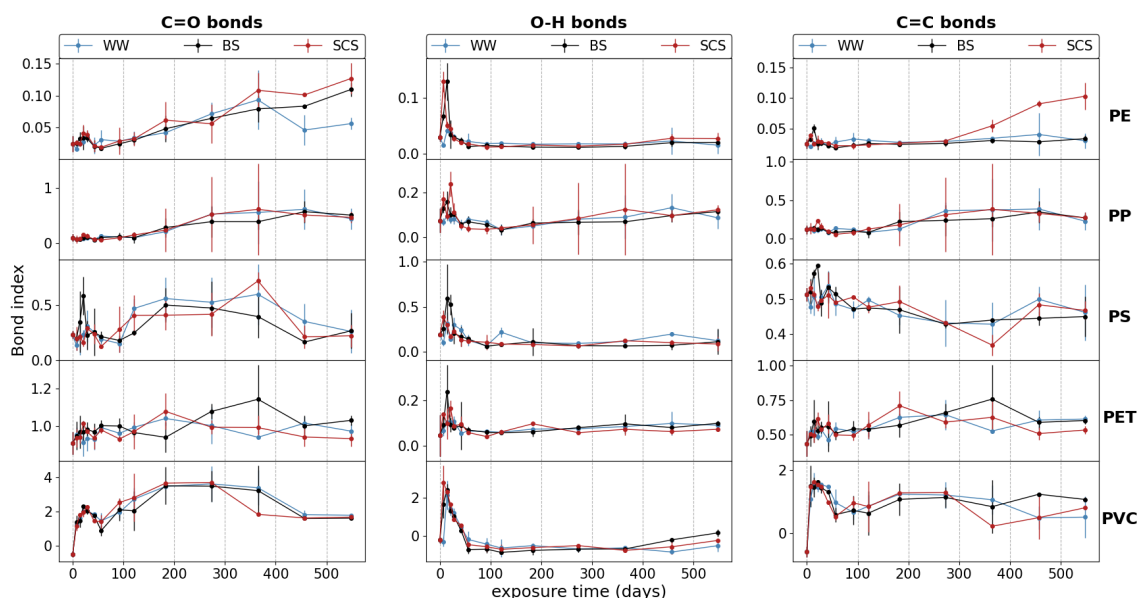


Figure 4.4. Carbonyl (C=O), hydroxyl (O-H), and C=C (vinyl for PE, PP, and PVC and aromatic for PS and PET) bond indices for the five different polymer types (PE, PP, PS, PET, and PVC) and the three water types Warnow River (WW) water, Baltic Sea (BS) water, and South China Sea (SCS) water. The vertical lines represent the standard deviation (\pm s.d.) resulting from triplicates (adopted from **Reineccius et al. (2022)**).

Potentially smaller soluble or volatile substances can finally be produced, which were released and could change the FTIR spectra as also hypothesized previously (Fernández-González et al., 2021). Another reason is the abrasion or fragmentation of the plastic surface, releasing new unweathered polymer sub-layers for which the fragmentation process starts again. This would result in an FTIR spectrum similar to less or unweathered equivalent polymers.

In the 18 months long experiment, PP was found to be the most unstable polymer type, lowering the pH of all tested water types (WW, BS, and SCS water) and showing the fastest fragmentation starting after nine months of exposure (see publication 3: **Reineccius et al. (2022)**). As large PP items are expected to float at the water surface, due to their low weight, photo-oxidation and fragmentation are expected to occur comparable fast for marine accumulating plastics. Another important finding for PP was the new property of those broken-out secondary PP fragments that are not exclusively buoyant at the water surface but sink to the vessel's bottom as well. Furthermore, the generated PP fragments, which were released, are very small, with the majority below $2\ \mu\text{m}$. The

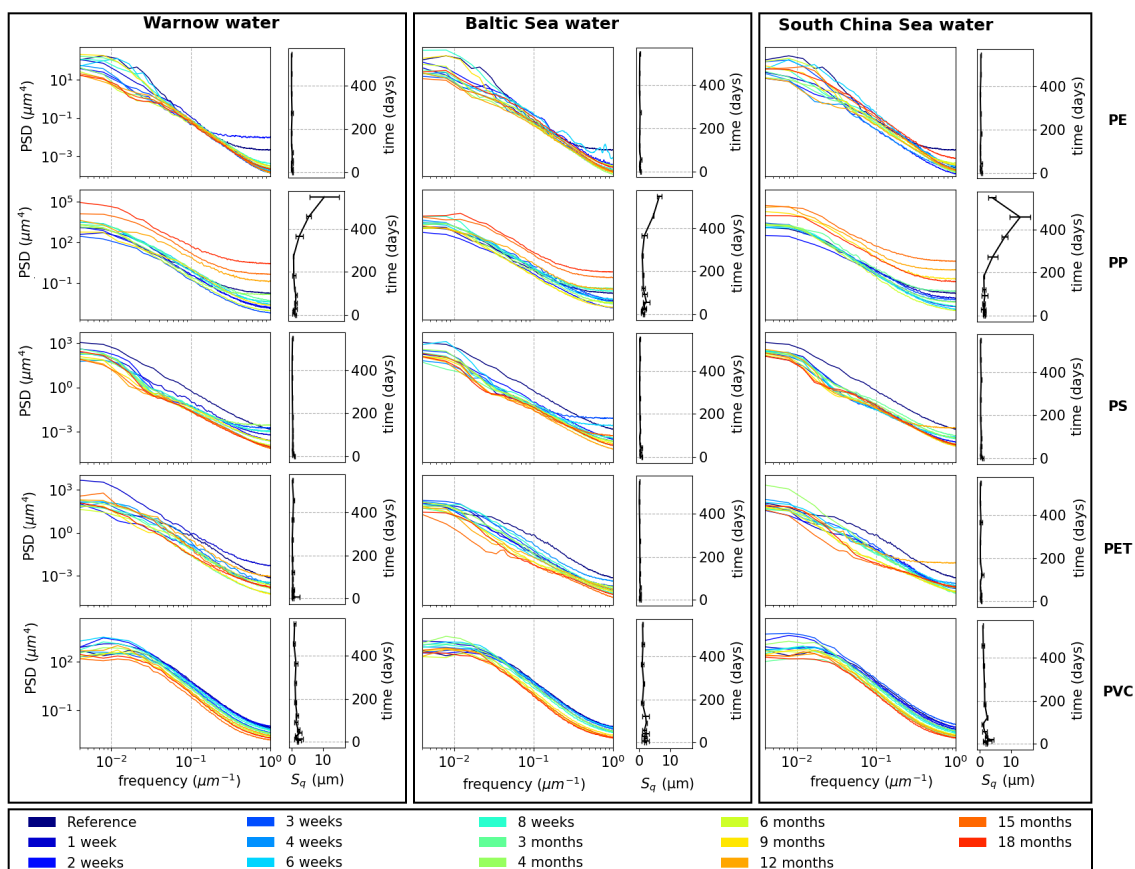


Figure 4.5. Surface roughness expressed as the power spectral density (PSD) for all weathered polymer types PE, PP, PS, PET, and PVC as colored lines and the respective root-mean-square roughness (S_q) over the exposure time in black for the three different water media (Warnow, Baltic Sea, and South China Sea water). Error bars represent the standard deviation (\pm s.d.) resulting from triplicates.

instrumental detection limit of the FTIR and Raman spectroscopes are generally at $10\ \mu\text{m}$, making the consideration of these PP fragments in field studies difficult, with potential large underestimations of PP abundances. The generation of such small fragments was also observed in other weathering experiments, e.g., for low-density PE (Menzel et al., 2022).

In this work, the polymer types PE, PS, PET, and PVC are not fragmented over time (Reineccius et al., 2022). Instead, the polymer surface was visibly ablated for the polymer types PS, PET, and PVC, resulting in a smoother surface compared to the pristine state. This process is visible in the surface roughness of these polymer types (Fig. 4.5),

which decreases with progressing weathering time. This abrasion of the uppermost surface layer can also lead to changing FTIR spectra but less than in case of fragmentation. By monitoring the weight loss of fragmented PP and abraded PS, PET, and PVC, significant weight losses were observed for PP exposed to Warnow (WW) and SCS water with also significant higher weight losses for SCS water compared to BS and WW water. For the abraded polymer types, a significant weight loss was only observed for PVC exposed to WW water, with no differences between the water media. The amounts of secondary MPs detected in the water were also highest for PP compared to the other polymer types.

Considering the sum of influencing factors of fragmentation, abrasion, ongoing reaction, and the generation of volatile or soluble compounds, the CI is not able to define the weathering degree of marine plastic sufficiently. Besides that, additives added during manufacturing and varying environmental conditions further distort the defined predictions of the CI developments. Regarding these influencing processes, the generation of the C=C bonds is also not following a predictable development (Fig. 4.4). Due to unknown initial states, the crystallinity can also not be used to determine the weathering degree (**Reineccius et al., 2022**). Consequently, there is no reliable method to determine the age or degree of weathering of plastics that accumulate in the marine environment until now. Nevertheless, to determine the residence time of plastic in the oceans, longer experiments are needed in which plastic is exposed to environmental conditions until its disappearance. This process, however, can take several years or even decades.

With the previous findings made by **Reineccius et al. (2022)**, PP was the first polymer type getting undetectable in the marine environment. Its fast fragmentation leads to weight losses between 5 and 21% after 12,960 sunshine hours, depending on the water media. Considering the annual sunshine hours in Germany of 1665 h, this corresponds to 7.78 years, with half of this time in which no fragmentation occurred. Assuming a stable fragmentation rate of 5%, which was determined for Baltic Sea water for the last nine months of the experiment and the German sunshine hours, PP would be fully fragmented after 82 years. In saltier water, such as the SCS water with a fragmentation rate of 21% and annual sunshine hours of 1908 h, the total fragmentation of PP would only need about 20 years. For the other polymer types, this means an even longer fragmentation or degradation time under marine conditions, especially for polymer types sinking to the seabed.

The sunshine hours in the Canary Islands are much higher, with 4800 h and about 2200 h in Madeira. This more extended radiation would lead to a faster plastic degradation, with an estimated complete fragmentation in only 8 - 17 years for PP close to the mooring site

Kiel 276. Considering an aquatic transport pathway via rivers, PP items can rest for a long time at the land-based source before exposure to the river. Combined with a long traveling time between 1 - 10 years until floating items can reach the mooring station at 33°N and 22°W (Van Sebille et al., 2012), PP is expected to be low at such remote places. Indeed, PP was rarely detected at this mooring station with only 0.6% of the total MP flux (**Reineccius & Waniek, 2022**). This is significantly less than the European PP demand of 19.7%. Even at the North Atlantic surface, PP amounts are lower than expected, with 6% found by Enders et al. (2015). Consequently, these dominating polymer types arriving at the mooring station Kiel 276 at 2000 m depth can be expected to be both the most durable and the most produced polymer types.

4.6. Extrapolation and comparison with previous studies

The total amount of mismanaged plastic waste between 1950 and 2015 was estimated to be 4977 million tons (Mt) worldwide and ended up in landfills or the natural environment (Geyer et al., 2017). For the same period, a total plastic mass between 17 and 47 Mt was calculated for the Atlantic Ocean alone, which accumulates in the water and sediments (Pabortsava & Lampitt, 2020). This corresponds to less than 1% of the estimated mismanaged plastic waste accumulating in the Atlantic Ocean. Assuming an equal distribution of MP in the oceans, this is still only 1 - 4% of all mismanaged plastic waste which is assumed to accumulate in the oceans worldwide. This agrees well with the annual plastic input into the oceans via rivers of 1.15 - 2.41 Mt year⁻¹ (Lebreton et al., 2017), which is also about 1% of the annual waste generation estimated by Geyer et al. (2017). However, the amount of plastic disposed of in the environment was estimated to be higher with 80 Mt in 2015 (Lebreton & Andrady, 2019). Jambeck et al. (2015) have also calculated much higher plastic masses with 4.8 - 12.7 Mt entered the marine environment in 2010, and a progressing increase is expected (one order of magnitude by 2025).

The flux data calculated for the sediment trap samples analyzed by **Reineccius & Waniek (2022)** suggest an annual MP input of 5.4 Mt year⁻¹ into the Atlantic Ocean alone (area of 81.2×10^6 km² (Pabortsava & Lampitt, 2020)). Assuming an equal distribution of plastic in the oceans, this corresponds to 24.0 Mt year⁻¹, which is in good agreement with the calculations conducted by Jambeck et al. (2015). As described by Geyer et al. (2017) and Jambeck et al. (2015), plastic pollution in the oceans is expected to increase due to the ongoing increase of plastic production and waste generation. However, the sinking materials collected between 2003 and 2015 do not reveal a significant elevation in MP abundances

(Fig. 4.1). Instead, the MP fluxes seem to be coupled to single events, leading to high fluxes followed by years with low MP abundances (**Reineccius & Waniek, 2022**). Therefore, longer time series are essential to detect potentially increasing MP (mass) flux rates reliably. In the literature, there are various studies in which increasing plastic pollution has also not been found (e.g., Law et al. (2010)). On the other hand, over longer time scales between 30 and 60 years, plastic pollution has elevated, even in the Atlantic Ocean (Ostle et al., 2019; Wilcox et al., 2019).

Another approach for investigating global plastic pollution development is comparing samples from previous studies taken in different years. However, due to differing environmental factors and methodologies, the abundances of MP vary widely between these studies, even for the same years or similar locations (Fig. 4.7 and 4.6). Allowing for some variation among the different methods, the calculated potential MP abundance increased for most consistent studies, except for ten sediment and four surface water studies, where slight decreases were observed (Fig. 4.6b and 4.7b). An overestimation can explain the decreasing abundance due to visual detection, which is estimated to have an average success rate of 68% (Lenz et al., 2015). Additionally, the used density solutions were considered with the potentially rejected polymer types, which are not floating in the respective solution. In the case of a saturated NaCl solution, 26% (PS, PET, PVC, polyurethane) of the total MP amount was potentially rejected in this method, which was calculated from the total European production rate. In the case of the use of water as a flotation agent, only 50% (PE, PP) were expected to be recovered in the samples. Besides that, also the size was considered. To obtain a reference size distribution, all detected MP particles found in sediment trap samples ($n = 13017$) were used.

If a net with a mesh size of $300\ \mu\text{m}$ was used to sample water for MP analysis, it can be assumed that smaller particles were not included. As MPs $> 300\ \mu\text{m}$ in size are very rare in the analyzed sediment trap samples (2%) but also in previous water and sediment samples with less than 1% (Bergmann et al., 2017; Tekman et al., 2020) a large underestimation can be assumed. This assumed underestimation leads to an increase in potential MP abundance by more than one order of magnitude. Another considered factor was the analysis method. In the case of the application of the ATR-FTIR mode, a high loss of PVC fractions was assumed, as explained in the previous section. PVC account for 9.6% of the total European demand, leading to an equivalent potential underestimation. Some factors, such as the fragmentation progress or particles smaller than $10\ \mu\text{m}$ and degradation due to digestion solutions, were not included in this calculation due to high uncertainties or

unknown effects. However, those factors can additionally lead to a current underestimation of MP abundances in the environment.

For the presented overview, only those studies that focused on marine surface water samples reported as MP items per m^3 were considered (Fig. 4.7). In addition, only studies that provided the necessary details, such as sampling locations and methodical approaches, were selected. The same approach was used for studies on marine sediment samples, but the results were expressed in items per kg (Fig. 4.6).

The presented MP detection assessment revealed a high level of uncertainty, with abundances in some cases being up to three orders of magnitude higher (Fig. 4.6 and 4.7). Based on the findings of this work, it must be assumed that especially studies conducted in the Asian region based on samples taken along the Chinese coast, as well as along the US and Mexican coasts, show much higher MP abundances in marine waters than previously assumed (Fig. 4.6 and S2). Due to the high accuracy of Arctic and Antarctic MP studies, calculated abundances are changing less. In Europe, the MP abundance increased predominantly for the Mediterranean Sea, resulting in similar results as those for the Baltic and North Seas. A similar trend was observed for sediment studies, with higher abundances along the Chinese coast, the Mediterranean Sea, and the US coastline. Fewer differences were verified for Australia, and the most northern studies in north Canada, North Atlantic, as well as the Baltic and North Sea.

The exorbitantly high MP abundances calculated for the Chinese coastline are in good agreement with previously estimated regional plastic inputs by Lebreton et al. (2017). Interestingly, also the Indonesian environment is expected to be loaded with plastic waste, but MP abundances are comparably low at the water surface of these areas. Instead, sediments contained higher MP loads. In contrast, European plastic quantity was expected to be lower compared to the Chinese marine environment (Lebreton et al., 2017), especially for the semi-enclosed Baltic Sea. However, detected MP abundances are in the same order of magnitude after the methodical correction as the MP findings at the Chinese coastlines (Fig. S1 and S2). Even in the Arctic region, MP loads are higher than expected. A potential explanation for this observation is the MP "dilution" in the open oceans. In the open ocean, currents are suspected to play an important role in plastic recovery. The transportation of high plastic amounts accumulating in the subtropical North Atlantic Gyre is enabled by the northwards North Atlantic Current and the Norwegian Current. Antarctica is less affected by currents that pass highly populated regions leading to low plastic accumulations (Fig. 4.7 and 4.6).

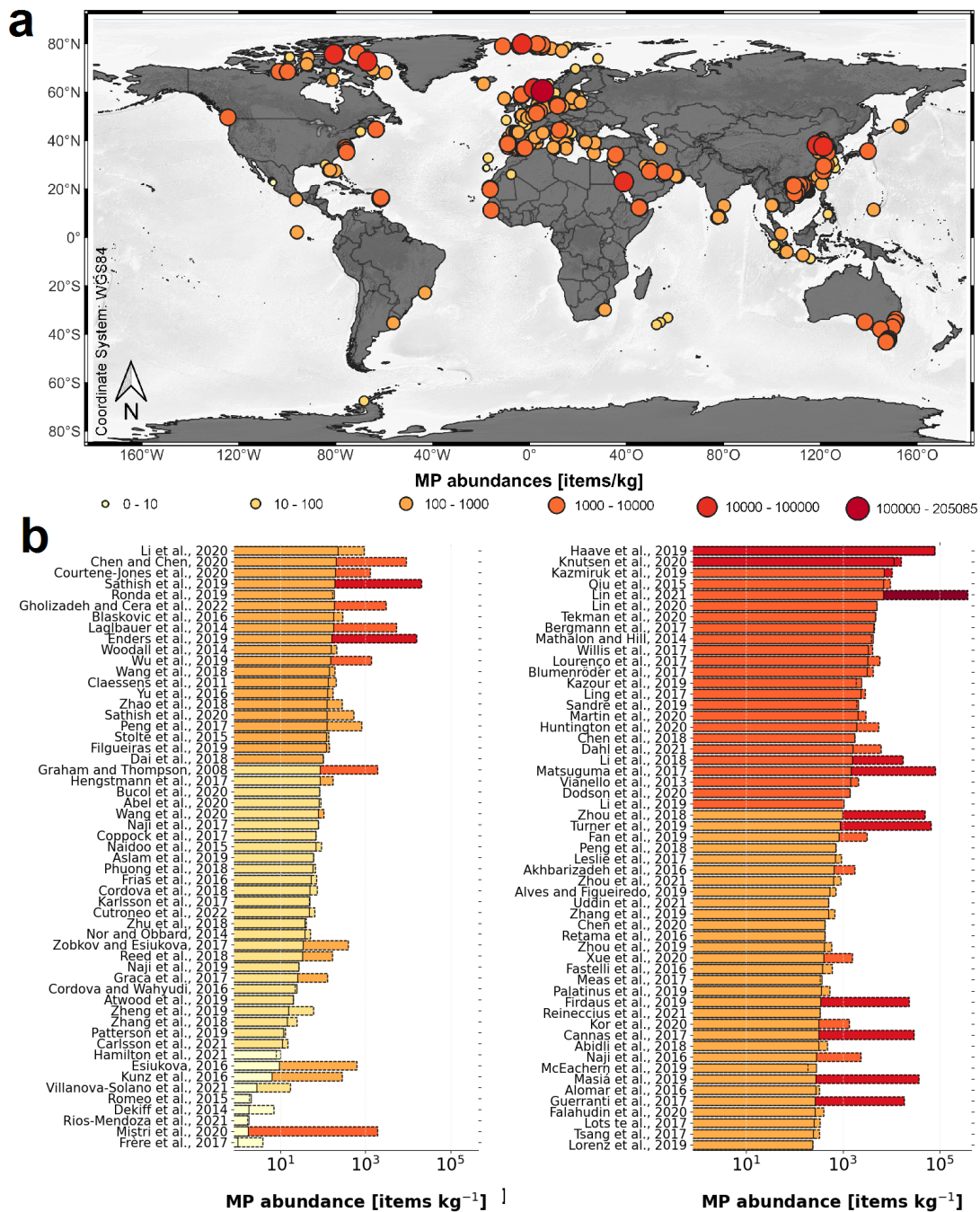


Figure 4.6. MP abundances in sediments (a) extracted from the literature listed in (b) and Table S1 (Supplementary Materials) with the mean MP abundance for each reference and potential abundances calculated from the uncertainties of the respective detection method (b).

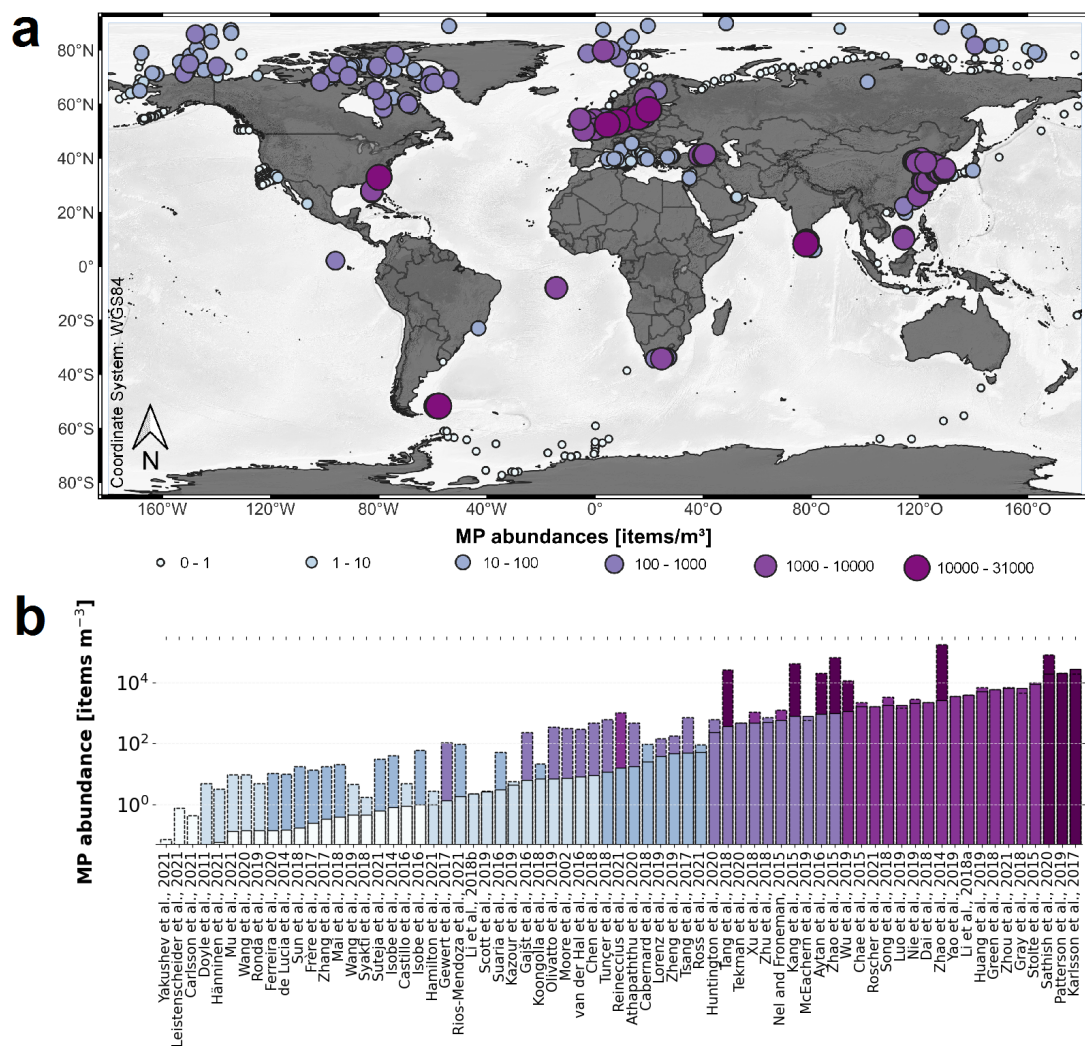


Figure 4.7. MP abundances in water (a) extracted from the literature listed in (b) and in Table S2 (Supplementary Materials) with the mean MP abundance for each reference and potential abundances calculated from the uncertainties of the respective detection method (b).

5. Summary and Outlook

The present thesis focuses on the fate of MP in marine systems for which two hypotheses were considered. The first hypothesis was that plastic floats on the water's surface, but some proportions also sink through the water column to the seabed (I). The second hypothesis was that MP weathered at the water surface, leading to fragmentation and the formation of smaller and more fragile MP items (II). In order to investigate hypothesis I, sediment trap samples were used to estimate potentially sinking MP amounts in specific time intervals (**Reineccius & Waniek, 2022**). As these samples are mass-limited and potentially contain small and fragile MPs, a gentle but effective extraction method is needed. Because no standardized method for MP extraction exists, a new method for mass-limited samples was established and validated with artificial and natural samples collected from a highly MP-polluted area (**Reineccius et al., 2021**). This newly developed method enables MP recovery rates of 98%, similar to highly effective density separation methods combined with a gentle digestion step.

In this work, sediment trap samples from 2000 m depth between April 2003 and June 2015 were selected from the subtropical Northeast Atlantic, providing the opportunity to investigate MP abundances at a remote place (**Reineccius & Waniek, 2022**). The detected MP flux rates were highly variable over time, with a strongly differing polymer composition. The main contributors were PE and PVC, with smaller abundances of PP, PS, and other polymer types. The MP particles were strongly fragmented and small, dominated by particles $< 100 \mu\text{m}$. No significant size differences were observed between the seasons, sampling series, or polymer types. Instead, a correlation of PE fluxes with the lithogenic fluxes was revealed, indicating a similar transport pathway via the air. For PVC, a seasonality was found with higher flux rates during winter compared to summer. This observation is likely attributed to marine seasonal conditions such as stratification.

A weathering experiment was conducted with conditions similar to the onshore aquatic environment to examine hypothesis II (**Reineccius et al., 2022**). In this experiment, the weathering progress of five different polymer types (PE, PP, PS, PET, and PVC) was monitored in three different water media (Warnow (WW), Baltic Sea (BS), and South China Sea (SCS) water). In the frame of this experiment, changes were observed for all polymer types resulting in different fragmentation speeds, as well as molecular and morphological surface changes. These results indicate rapid molecular changes within the polymer surfaces, potentially releasing various degradation products into the surrounding water.

For PP, the fastest degradation progress was found with strong fragmentation into small (mainly $< 2 \mu\text{m}$) sinking PP fragments and a lowering of the pH value over the exposure time. PVC was also observed to degrade fast but with more remarkable changes in the molecular surface instead of fragmentation.

Concerning the global plastic fate, these findings reveal that those previously "missing" plastic fractions are factual sinking into the deep sea, continuously accumulating in the seabed. Besides that, the fragmentation of plastic caused by weathering can lead to MP particle sizes smaller than the detection limits of current spectroscopic methods. The resulting underestimation further justifies the low amounts of detected plastic in the environment compared to the higher predictions of marine plastic pollution. This work suggests that the mineralization of plastic in the marine environment contributes to a minor proportion. The main reasons for the unexpected lower global plastic detection are the distribution of particles into hidden or difficult-to-reach locations, such as the deep sea, as well as limited detection techniques. Due to the limited spectroscopic opportunities in detecting MP items $< 10 \mu\text{m}$, a mass-based detection method such as the pyr-GC/MS is proposed for future investigations for more precise results of the total plastic amount. Additionally, a standardized extraction and sampling method is needed to enable reliable comparisons between previous studies, which should consider the sum of all MP sizes (1 - 5000 μm). The use of sampling methods rejecting a wide size range, e.g., by using mesh sizes of 300 μm or more, can lead to significant misleading results in MP abundances (more than 99%).

More reliable and comparable results could be achieved if the detection methods for MP were standardized in marine environmental samples. This achievement will enable comparisons between different sediment trap samples representing the MP flux rates of different locations. Combined with additional data about MP abundances in the water surface and the sea bottom, those sediment trap data could be used to resolve the global plastic fate in the marine systems and give an overview of the distribution, transport pathway, and sources. With increased knowledge about the global distribution and fate of MPs in the oceans, hot spots with high pollution levels can be revealed. Further research is also needed to discover all potential threats concerning the degradation products of plastic.

References

- Abel, S. M., Primpke, S., Int-Veen, I., Brandt, A., & Gerdt, G. (2020). Systematic identification of microplastics in abyssal and hadal sediments of the Kuril Kamchatka trench. *Environmental Pollution*, *269*, 116095. doi:10.1016/j.envpol.2020.116095.
- Abidli, S., Antunes, J. C., Ferreira, J. L., Lahbib, Y., Sobral, P., & El Menif, N. T. (2018). Microplastics in sediments from the littoral zone of the north Tunisian coast (Mediterranean Sea). *Estuarine, Coastal and Shelf Science*, *205*, 1–9. doi:10.1016/j.ecss.2018.03.006.
- Akdogan, Z., & Guven, B. (2019). Microplastics in the environment: A critical review of current understanding and identification of future research needs. *Environmental Pollution*, *254*, 113011. doi:10.1016/j.envpol.2019.113011.
- Akhbarizadeh, R., Moore, F., Keshavarzi, B., & Moeinpour, A. (2017). Microplastics and potentially toxic elements in coastal sediments of Iran's main oil terminal (Khark Island). *Environmental Pollution*, *220*, 720–731. doi:10.1016/j.envpol.2016.10.038.
- Alimba, C. G., & Faggio, C. (2019). Microplastics in the marine environment: current trends in environmental pollution and mechanisms of toxicological profile. *Environmental Toxicology and Pharmacology*, *68*, 61–74. doi:10.1016/j.etap.2019.03.001.
- Alimi, O. S., Claveau-Mallet, D., Kurusu, R. S., Lapointe, M., Bayen, S., & Tufenkji, N. (2022). Weathering pathways and protocols for environmentally relevant microplastics and nanoplastics: What are we missing? *Journal of Hazardous Materials*, *423*, 126955. doi:10.1016/j.jhazmat.2021.126955.
- Allen, S., Allen, D., Phoenix, V. R., Le Roux, G., Durántez Jiménez, P., Simonneau, A., Binet, S., & Galop, D. (2019). Atmospheric transport and deposition of microplastics in a remote mountain catchment. *Nature Geoscience*, *12*, 339–344. doi:10.1038/s41561-019-0335-5.
- Alomar, C., Estarellas, F., & Deudero, S. (2016). Microplastics in the Mediterranean Sea: deposition in coastal shallow sediments, spatial variation and preferential grain size. *Marine Environmental Research*, *115*, 1–10. doi:10.1016/j.marenvres.2016.01.005.
- Alves, V. E., & Figueiredo, G. M. (2019). Microplastic in the sediments of a highly eutrophic tropical estuary. *Marine Pollution Bulletin*, *146*, 326–335. doi:10.1016/j.marpolbul.2019.06.042.
- Andrade, J., Fernández-González, V., López-Mahía, P., & Muniategui, S. (2019). A low-cost system to simulate environmental microplastic weathering. *Marine Pollution Bulletin*, *149*, 110663. doi:10.1016/j.marpolbul.2019.110663.

- Andrady, A. L. (2011). Microplastics in the marine environment. *Marine Pollution Bulletin*, *62*, 1596–1605. doi:10.1016/j.marpolbul.2011.05.030.
- Andrady, A. L. (2017). The plastic in microplastics: A review. *Marine Pollution Bulletin*, *119*, 12–22. doi:10.1016/j.marpolbul.2017.01.082.
- Antunes, J., Frias, J., Micaelo, A., & Sobral, P. (2013). Resin pellets from beaches of the Portuguese coast and adsorbed persistent organic pollutants. *Estuarine, Coastal and Shelf Science*, *130*, 62–69. doi:10.1016/j.ecss.2013.06.016.
- Aslam, H., Ali, T., Mortula, M. M., & Attaelmanan, A. G. (2019). Evaluation of microplastics in beach sediments along the coast of Dubai, UAE. *Marine Pollution Bulletin*, *150*, 110739. doi:10.1016/j.marpolbul.2019.110739.
- Athapaththu, A., Thushari, G., Dias, P., Abeygunawardena, A., Egodaunya, K., Liyanage, N., Pitawala, H., & Senevirathna, J. (2020). Plastics in surface water of southern coastal belt of Sri Lanka (Northern Indian Ocean): Distribution and characterization by FTIR. *Marine Pollution Bulletin*, *161*, 111750. doi:10.1016/j.marpolbul.2020.111750.
- Atwood, E. C., Falcieri, F. M., Piehl, S., Bochow, M., Matthies, M., Franke, J., Carniel, S., Sclavo, M., Laforsch, C., & Siegert, F. (2019). Coastal accumulation of microplastic particles emitted from the Po River, Northern Italy: comparing remote sensing and hydrodynamic modelling with in situ sample collections. *Marine Pollution Bulletin*, *138*, 561–574. doi:10.1016/j.marpolbul.2018.11.045.
- Auta, H. S., Emenike, C., & Fauziah, S. (2017). Distribution and importance of microplastics in the marine environment: a review of the sources, fate, effects, and potential solutions. *Environment International*, *102*, 165–176. doi:10.1016/j.envint.2017.02.013.
- Avio, C. G., Pittura, L., d’Errico, G., Abel, S., Amorello, S., Marino, G., Gorbi, S., & Regoli, F. (2020). Distribution and characterization of microplastic particles and textile microfibers in Adriatic food webs: General insights for biomonitoring strategies. *Environmental Pollution*, *258*, 113766. doi:10.1016/j.envpol.2019.113766.
- Aytan, U., Valente, A., Senturk, Y., Usta, R., Sahin, F. B. E., Mazlum, R. E., & Agirbas, E. (2016). First evaluation of neustonic microplastics in Black Sea waters. *Marine Environmental Research*, *119*, 22–30. doi:10.1016/j.marenvres.2016.05.009.
- Ballent, A., Corcoran, P. L., Madden, O., Helm, P. A., & Longstaffe, F. J. (2016). Sources and sinks of microplastics in Canadian Lake Ontario nearshore, tributary and beach sediments. *Marine Pollution Bulletin*, *110*, 383–395. doi:10.1016/j.marpolbul.2016.06.037.

- Barnes, D. K., Galgani, F., Thompson, R. C., & Barlaz, M. (2009). Accumulation and fragmentation of plastic debris in global environments. *Philosophical Transactions of the Royal Society B: Biological Sciences*, *364*, 1985–1998. doi:10.1098/rstb.2008.0205.
- Baztan, J., Carrasco, A., Chouinard, O., Cleaud, M., Gabaldon, J. E., Huck, T., Jaffrès, L., Jorgensen, B., Miguelez, A., Paillard, C. et al. (2014). Protected areas in the Atlantic facing the hazards of micro-plastic pollution: first diagnosis of three islands in the Canary Current. *Marine Pollution Bulletin*, *80*, 302–311. doi:10.1016/j.marpolbul.2013.12.052.
- Bergmann, M., Gutow, L., & Klages, M. (2015). *Marine Anthropogenic Litter*. Springer Nature. doi:10.1007/978-3-319-16510-3.
- Bergmann, M., Wirzberger, V., Krumpfen, T., Lorenz, C., Primpke, S., Tekman, M. B., & Gerdts, G. (2017). High quantities of microplastic in Arctic deep-sea sediments from the HAUSGARTEN observatory. *Environmental Science & Technology*, *51*, 11000–11010. doi:10.1021/acs.est.7b03331.
- Blašković, A., Fastelli, P., Čižmek, H., Guerranti, C., & Renzi, M. (2016). Plastic litter in sediments from the Croatian marine protected area of the natural park of Telašćica bay (Adriatic Sea). *Marine Pollution Bulletin*, *114*, 583–586. doi:10.1016/j.marpolbul.2016.09.018.
- Blumenröder, J., Sechet, P., Kakkonen, J. E., & Hartl, M. G. (2017). Microplastic contamination of intertidal sediments of Scapa Flow, Orkney: a first assessment. *Marine Pollution Bulletin*, *124*, 112–120. doi:10.1016/j.marpolbul.2017.07.009.
- BMU (2020). Sachstand über die Schadstoffe in Kunststoffen und ihre Auswirkungen auf die Entsorgung (UM19 34 5080). Bundesministerium für Umwelt, Naturschutz und nukleare Sicherheit.
- Bout-Roumazielles, V., Nebout, N. C., Peyron, O., Cortijo, E., Landais, A., & Masson-Delmotte, V. (2007). Connection between South Mediterranean climate and North African atmospheric circulation during the last 50,000 yr BP North Atlantic cold events. *Quaternary Science Reviews*, *26*, 3197–3215. doi:10.1016/j.quascirev.2007.07.015.
- Brandon, J. A., Jones, W., & Ohman, M. D. (2019). Multidecadal increase in plastic particles in coastal ocean sediments. *Science advances*, *5*, eaax0587. doi:10.1126/sciadv.aax0587.
- Brennecke, D., Duarte, B., Paiva, F., Caçador, I., & Canning-Clode, J. (2016). Microplastics as vector for heavy metal contamination from the marine environment. *Estuarine, Coastal and Shelf Science*, *178*, 189–195. doi:10.1016/j.ecss.2015.12.003.

- Brust, J., & Waniek, J. J. (2010). Atmospheric dust contribution to deep-sea particle fluxes in the subtropical Northeast Atlantic. *Deep Sea Research Part I: Oceanographic Research Papers*, 57, 988–998. doi:10.1016/j.dsr.2010.04.011.
- Bucol, L. A., Romano, E. F., Cabcaban, S. M., Siplon, L. M. D., Madrid, G. C., Bucol, A. A., & Polidoro, B. (2020). Microplastics in marine sediments and rabbitfish (*Siganus fuscescens*) from selected coastal areas of Negros Oriental, Philippines. *Marine Pollution Bulletin*, 150, 110685. doi:10.1016/j.marpolbul.2019.110685.
- Cabernard, L., Roscher, L., Lorenz, C., Gerdt, G., & Primpke, S. (2018). Comparison of Raman and Fourier transform infrared spectroscopy for the quantification of microplastics in the aquatic environment. *Environmental Science & Technology*, 52, 13279–13288. doi:10.1021/acs.est.8b03438.
- Cai, M., He, H., Liu, M., Li, S., Tang, G., Wang, W., Huang, P., Wei, G., Lin, Y., Chen, B. et al. (2018). Lost but can't be neglected: huge quantities of small microplastics hide in the South China Sea. *Science of the Total Environment*, 633, 1206–1216. doi:10.1016/j.scitotenv.2018.03.197.
- Cannas, S., Fastelli, P., Guerranti, C., & Renzi, M. (2017). Plastic litter in sediments from the coasts of south Tuscany (Tyrrhenian Sea). *Marine Pollution Bulletin*, 119, 372–375. doi:10.1016/j.marpolbul.2017.04.008.
- Carlsson, P., Singdahl-Larsen, C., & Lusher, A. L. (2021). Understanding the occurrence and fate of microplastics in coastal Arctic ecosystems: The case of surface waters, sediments and walrus (*Odobenus rosmarus*). *Science of The Total Environment*, 792, 148308. doi:10.1016/j.scitotenv.2021.148308.
- Castillo, A. B., Al-Maslmani, I., & Obbard, J. P. (2016). Prevalence of microplastics in the marine waters of Qatar. *Marine Pollution Bulletin*, 111, 260–267. doi:10.1016/j.marpolbul.2016.06.108.
- Chae, D.-H., Kim, I.-S., Kim, S.-K., Song, Y. K., & Shim, W. J. (2015). Abundance and distribution characteristics of microplastics in surface seawaters of the Incheon/Kyeonggi coastal region. *Archives of Environmental Contamination and Toxicology*, 69, 269–278. doi:10.1007/s00244-015-0173-4.
- Cheang, C. C., Ma, Y., & Fok, L. (2018). Occurrence and composition of microplastics in the seabed sediments of the coral communities in proximity of a metropolitan area. *International Journal of Environmental Research and Public Health*, 15, 2270. doi:10.3390/ijerph15102270.
- Chen, M., Jin, M., Tao, P., Wang, Z., Xie, W., Yu, X., & Wang, K. (2018). Assessment of microplastics derived from mariculture in Xiangshan Bay, China. *Environmental Pollution*, 242, 1146–1156. doi:10.1016/j.envpol.2018.07.133.

- Chen, M.-C., & Chen, T.-H. (2020). Spatial and seasonal distribution of microplastics on sandy beaches along the coast of the Hengchun Peninsula, Taiwan. *Marine Pollution Bulletin*, *151*, 110861. doi:10.1016/j.marpolbul.2019.110861.
- Chen, S., Wu, R., & Chen, W. (2020). Strengthened connection between springtime North Atlantic Oscillation and North Atlantic tripole SST pattern since the late 1980s. *Journal of Climate*, *33*, 2007–2022. doi:10.1175/JCLI-D-19-0628.1.
- Choy, C. A., Robison, B. H., Gagne, T. O., Erwin, B., Firl, E., Halden, R. U., Hamilton, J. A., Katija, K., Lisin, S. E., Rolsky, C. et al. (2019). The vertical distribution and biological transport of marine microplastics across the epipelagic and mesopelagic water column. *Scientific Reports*, *9*, 1–9. doi:10.1038/s41598-019-44117-2.
- Cincinelli, A., Scopetani, C., Chelazzi, D., Lombardini, E., Martellini, T., Katsoyiannis, A., Fossi, M. C., & Corsolini, S. (2017). Microplastic in the surface waters of the Ross Sea (Antarctica): occurrence, distribution and characterization by FTIR. *Chemosphere*, *175*, 391–400. doi:10.1016/j.chemosphere.2017.02.024.
- Claessens, M., De Meester, S., Van Landuyt, L., De Clerck, K., & Janssen, C. R. (2011). Occurrence and distribution of microplastics in marine sediments along the Belgian coast. *Marine Pollution Bulletin*, *62*, 2199–2204. doi:10.1016/j.marpolbul.2011.06.030.
- Conti, I., Simioni, C., Varano, G., Brenna, C., Costanzi, E., & Neri, L. M. (2021). Legislation to limit the environmental plastic and microplastic pollution and their influence on human exposure. *Environmental Pollution*, *288*, 117708. doi:10.1016/j.envpol.2021.117708.
- Coppock, R. L., Cole, M., Lindeque, P. K., Queirós, A. M., & Galloway, T. S. (2017). A small-scale, portable method for extracting microplastics from marine sediments. *Environmental Pollution*, *230*, 829–837. doi:10.1016/j.envpol.2017.07.017.
- Cordova, M. R., & Wahyudi, A. J. (2016). Microplastic in the deep-sea sediment of Southwestern Sumatran Waters. *Marine Research in Indonesia*, *41*, 27–35. doi:10.14203/mri.v41i1.99.
- Courtene-Jones, W., Quinn, B., Ewins, C., Gary, S. F., & Narayanaswamy, B. E. (2020). Microplastic accumulation in deep-sea sediments from the Rockall Trough. *Marine Pollution Bulletin*, *154*, 111092. doi:10.1016/j.marpolbul.2020.111092.
- Courtene-Jones, W., Quinn, B., Gary, S. F., Mogg, A. O., & Narayanaswamy, B. E. (2017). Microplastic pollution identified in deep-sea water and ingested by benthic invertebrates in the Rockall Trough, North Atlantic Ocean. *Environmental Pollution*, *231*, 271–280. doi:10.1016/j.envpol.2017.08.026.

- Coyle, R., Hardiman, G., & O'Driscoll, K. (2020). Microplastics in the marine environment: A review of their sources, distribution processes, uptake and exchange in ecosystems. *Case Studies in Chemical and Environmental Engineering*, *2*, 100010. doi:10.1016/j.cscee.2020.100010.
- Cózar, A., Echevarría, F., González-Gordillo, J. I., Irigoien, X., Úbeda, B., Hernández-León, S., Palma, Á. T., Navarro, S., García-de Lomas, J., Ruiz, A. et al. (2014). Plastic debris in the open ocean. *Proceedings of the National Academy of Sciences*, *111*, 10239–10244. doi:10.1073/pnas.1314705111.
- Crichton, E. M., Noël, M., Gies, E. A., & Ross, P. S. (2017). A novel, density-independent and FTIR-compatible approach for the rapid extraction of microplastics from aquatic sediments. *Analytical Methods*, *9*, 1419–1428. doi:10.1039/c6ay02733d.
- Cutroneo, L., Capello, M., Domi, A., Consani, S., Lamare, P., Coyle, P., Bertin, V., Dornic, D., Reboa, A., Geneselli, I. et al. (2022). Microplastics in the abyss: a first investigation into sediments at 2443-m depth (Toulon, France). *Environmental Science and Pollution Research*, *29*, 9375–9385. doi:10.1007/s11356-021-17997-z.
- Dahl, M., Bergman, S., Björk, M., Diaz-Almela, E., Granberg, M., Gullström, M., Leiva-Dueñas, C., Magnusson, K., Marco-Méndez, C., Piñeiro-Juncal, N. et al. (2021). A temporal record of microplastic pollution in Mediterranean seagrass soils. *Environmental Pollution*, *273*, 116451. doi:10.1016/j.envpol.2021.116451.
- Dai, Z., Zhang, H., Zhou, Q., Tian, Y., Chen, T., Tu, C., Fu, C., & Luo, Y. (2018). Occurrence of microplastics in the water column and sediment in an inland sea affected by intensive anthropogenic activities. *Environmental Pollution*, *242*, 1557–1565. doi:10.1016/j.envpol.2018.07.131.
- Deich, C., Frazão, H. C., Appelt, J.-S., Li, W., Pohlmann, T., & Waniek, J. J. (2021). Occurrence and distribution of estrogenic substances in the northern South China Sea. *Science of the Total Environment*, *770*, 145239. doi:10.1016/j.scitotenv.2021.145239.
- Dekiff, J. H., Remy, D., Klasmeier, J., & Fries, E. (2014). Occurrence and spatial distribution of microplastics in sediments from Norderney. *Environmental Pollution*, *186*, 248–256. doi:10.1016/j.envpol.2013.11.019.
- Desforges, J.-P. W., Galbraith, M., Dangerfield, N., & Ross, P. S. (2014). Widespread distribution of microplastics in subsurface seawater in the NE Pacific Ocean. *Marine Pollution Bulletin*, *79*, 94–99. doi:10.1016/j.marpolbul.2013.12.035.
- Di Mauro, R., Kupchik, M. J., & Benfield, M. C. (2017). Abundant plankton-sized microplastic particles in shelf waters of the northern Gulf of Mexico. *Environmental Pollution*, *230*, 798–809. doi:10.1016/j.envpol.2017.07.030.

- Dodson, G. Z., Shotorban, A. K., Hatcher, P. G., Waggoner, D. C., Ghosal, S., & Noffke, N. (2020). Microplastic fragment and fiber contamination of beach sediments from selected sites in Virginia and North Carolina, USA. *Marine Pollution Bulletin*, *151*, 110869. doi:10.1016/j.marpolbul.2019.110869.
- Doyle, M. J., Watson, W., Bowlin, N. M., & Sheavly, S. B. (2011). Plastic particles in coastal pelagic ecosystems of the Northeast Pacific ocean. *Marine Environmental Research*, *71*, 41–52. doi:10.1016/j.marenvres.2010.10.001.
- Du, H., Xie, Y., & Wang, J. (2021). Microplastic degradation methods and corresponding degradation mechanism: Research status and future perspectives. *Journal of Hazardous Materials*, *418*, 126377. doi:10.1016/j.jhazmat.2021.126377.
- Egger, M., Sulu-Gambari, F., & Lebreton, L. (2020). First evidence of plastic fallout from the North Pacific Garbage Patch. *Scientific Reports*, *10*, 1–10. doi:10.1038/s41598-020-64465-8.
- Enders, K., K  ppler, A., Biniash, O., Feldens, P., Stollberg, N., Lange, X., Fischer, D., Eichhorn, K.-J., Pollehne, F., Oberbeckmann, S. et al. (2019). Tracing microplastics in aquatic environments based on sediment analogies. *Scientific Reports*, *9*, 1–15. doi:10.1038/s41598-019-50508-2.
- Enders, K., Lenz, R., Beer, S., & Stedmon, C. A. (2017). Extraction of microplastic from biota: recommended acidic digestion destroys common plastic polymers. *ICES Journal of Marine Science*, *74*, 326–331. doi:10.1093/icesjms/fsw173.
- Enders, K., Lenz, R., Stedmon, C. A., & Nielsen, T. G. (2015). Abundance, size and polymer composition of marine microplastics $\geq 10 \mu\text{m}$ in the Atlantic Ocean and their modelled vertical distribution. *Marine Pollution Bulletin*, *100*, 70–81. doi:10.1016/j.marpolbul.2015.09.027.
- Erni-Cassola, G., Gibson, M. I., Thompson, R. C., & Christie-Oleza, J. A. (2017). Lost, but found with Nile red: a novel method for detecting and quantifying small microplastics (1 mm to 20 μm) in environmental samples. *Environmental Science & Technology*, *51*, 13641–13648. doi:10.1021/acs.est.7b04512.
- Esiukova, E. (2017). Plastic pollution on the Baltic beaches of Kaliningrad region, Russia. *Marine Pollution Bulletin*, *114*, 1072–1080. doi:10.1016/j.marpolbul.2016.10.001.
- Falahudin, D., Cordova, M. R., Sun, X., Yogaswara, D., Wulandari, I., Hindarti, D., & Arifin, Z. (2020). The first occurrence, spatial distribution and characteristics of microplastic particles in sediments from Banten Bay, Indonesia. *Science of the Total Environment*, *705*, 135304. doi:10.1016/j.scitotenv.2019.135304.

- Fastelli, P., Blašković, A., Bernardi, G., Romeo, T., Čížmek, H., Andaloro, F., Russo, G. F., Guerranti, C., & Renzi, M. (2016). Plastic litter in sediments from a marine area likely to become protected (Aeolian Archipelago's islands, Tyrrhenian sea). *Marine Pollution Bulletin*, *113*, 526–529. doi:10.1016/j.marpolbul.2016.08.054.
- Fernández-González, V., Andrade-Garda, J., López-Mahía, P., & Muniategui-Lorenzo, S. (2021). Impact of weathering on the chemical identification of microplastics from usual packaging polymers in the marine environment. *Analytica Chimica Acta*, *1142*, 179–188. doi:10.1016/j.aca.2020.11.002.
- Ferreira, M., Thompson, J., Paris, A., Rohindra, D., & Rico, C. (2020). Presence of microplastics in water, sediments and fish species in an urban coastal environment of Fiji, a Pacific small island developing state. *Marine Pollution Bulletin*, *153*, 110991. doi:10.1016/j.marpolbul.2020.110991.
- Filgueiras, A. V., Gago, J., Campillo, J. A., & León, V. M. (2019). Microplastic distribution in surface sediments along the Spanish Mediterranean continental shelf. *Environmental Science and Pollution Research*, *26*, 21264–21273. doi:10.1007/s11356-019-05341-5.
- Firdaus, M., Trihadiningrum, Y., & Lestari, P. (2020). Microplastic pollution in the sediment of Jagir estuary, Surabaya City, Indonesia. *Marine Pollution Bulletin*, *150*, 110790. doi:10.1016/j.marpolbul.2019.110790.
- Fischer, M., & Scholz-Böttcher, B. M. (2017). Simultaneous Trace Identification and Quantification of Common Types of Microplastics in Environmental Samples by Pyrolysis-Gas Chromatography-Mass Spectrometry. *Environmental Science and Technology*, *51*, 5052–5060. doi:10.1021/acs.est.6b06362.
- Frãzao, H. C., Prien, R., Müller, T. J., Schulz-Bull, D. E., & Waniek, J. (2021). 30 years of temporal variability of temperature and currents below the main thermocline between 1980–2009 in the subtropical Northeast Atlantic (Kiel 276, 33°N, 22°W). *Journal of Marine Systems*, *217*, 103517. doi:10.1016/j.jmarsys.2021.103517.
- Frere, L., Paul-Pont, I., Rinnert, E., Petton, S., Jaffré, J., Bihannic, I., Soudant, P., Lambert, C., & Huvet, A. (2017). Influence of environmental and anthropogenic factors on the composition, concentration and spatial distribution of microplastics: a case study of the Bay of Brest (Brittany, France). *Environmental Pollution*, *225*, 211–222. doi:10.1016/j.envpol.2017.03.023.
- Frias, J., Sobral, P., & Ferreira, A. M. (2010). Organic pollutants in microplastics from two beaches of the Portuguese coast. *Marine Pollution Bulletin*, *60*, 1988–1992. doi:10.1016/j.marpolbul.2010.07.030.

- Frias, J. P., Gago, J., Otero, V., & Sobral, P. (2016). Microplastics in coastal sediments from Southern Portuguese shelf waters. *Marine Environmental Research*, *114*, 24–30. doi:10.1016/j.marenvres.2015.12.006.
- Fries, E., Dekiff, J. H., Willmeyer, J., Nuelle, M.-T., Ebert, M., & Remy, D. (2013). Identification of polymer types and additives in marine microplastic particles using pyrolysis-GC/MS and scanning electron microscopy. *Environmental Science: Processes & Impacts*, *15*, 1949–1956. doi:10.1039/c3em00214d.
- Fründt, B., & Waniek, J. J. (2012). Impact of the Azores Front propagation on deep ocean particle flux. *Central European Journal of Geosciences*, *4*, 531–544. doi:10.2478/s13533-012-0102-2.
- Gajšt, T., Bizjak, T., Palatinus, A., Liubartseva, S., & Kržan, A. (2016). Sea surface microplastics in Slovenian part of the Northern Adriatic. *Marine Pollution Bulletin*, *113*, 392–399. doi:10.1016/j.marpolbul.2016.10.031.
- Gewert, B., Ogonowski, M., Barth, A., & MacLeod, M. (2017). Abundance and composition of near surface microplastics and plastic debris in the Stockholm Archipelago, Baltic Sea. *Marine Pollution Bulletin*, *120*, 292–302. doi:10.1016/j.marpolbul.2017.04.062.
- Gewert, B., Plassmann, M., Sandblom, O., & MacLeod, M. (2018). Identification of chain scission products released to water by plastic exposed to ultraviolet light. *Environmental Science & Technology Letters*, *5*, 272–276. doi:10.1021/acs.estlett.8b00119.
- Gewert, B., Plassmann, M. M., & MacLeod, M. (2015). Pathways for degradation of plastic polymers floating in the marine environment. *Environmental Science: Processes & Impacts*, *17*, 1513–1521. doi:10.1039/c5em00207a.
- Geyer, R., Jambeck, J. R., & Law, K. L. (2017). Production, use, and fate of all plastics ever made. *Science Advances*, *3*, 25–29. doi:10.1126/sciadv.1700782.
- Gholizadeh, M., & Cera, A. (2022). Microplastic contamination in the sediments of Qarasu estuary in Gorgan Bay, south-east of Caspian Sea, Iran. *Science of The Total Environment*, *838*, 155913. doi:10.1016/j.scitotenv.2022.155913.
- Graca, B., Beldowska, M., Wrzesień, P., & Zgrundo, A. (2014). Styrofoam debris as a potential carrier of mercury within ecosystems. *Environmental Science and Pollution Research*, *21*, 2263–2271. doi:10.1007/s11356-013-2153-4.
- Graham, E. R., & Thompson, J. T. (2009). Deposit- and suspension-feeding sea cucumbers (Echinodermata) ingest plastic fragments. *Journal of Experimental Marine Biology and Ecology*, *368*, 22–29. doi:10.1016/j.jembe.2008.09.007.

- Gray, A. D., Wertz, H., Leads, R. R., & Weinstein, J. E. (2018). Microplastic in two South Carolina Estuaries: Occurrence, distribution, and composition. *Marine Pollution Bulletin*, *128*, 223–233. doi:10.1016/j.marpolbul.2018.01.030.
- Green, D. S., Kregting, L., Boots, B., Blockley, D. J., Brickle, P., Da Costa, M., & Crowley, Q. (2018). A comparison of sampling methods for seawater microplastics and a first report of the microplastic litter in coastal waters of Ascension and Falkland Islands. *Marine Pollution Bulletin*, *137*, 695–701. doi:10.1016/j.marpolbul.2018.11.004.
- Guerranti, C., Cannas, S., Scopetani, C., Fastelli, P., Cincinelli, A., & Renzi, M. (2017). Plastic litter in aquatic environments of Maremma Regional Park (Tyrrhenian Sea, Italy): Contribution by the Ombrone river and levels in marine sediments. *Marine Pollution Bulletin*, *117*, 366–370. doi:10.1016/j.marpolbul.2017.02.021.
- Guo, X., & Wang, J. (2019). The chemical behaviors of microplastics in marine environment: A review. *Marine Pollution Bulletin*, *142*, 1–14. doi:10.1016/j.marpolbul.2019.03.019.
- Haave, M., Lorenz, C., Primpke, S., & Gerdt, G. (2019). Different stories told by small and large microplastics in sediment—first report of microplastic concentrations in an urban recipient in Norway. *Marine Pollution Bulletin*, *141*, 501–513. doi:10.1016/j.marpolbul.2019.02.015.
- Hahladakis, J. N., Velis, C. A., Weber, R., Iacovidou, E., & Purnell, P. (2018). An overview of chemical additives present in plastics: Migration, release, fate and environmental impact during their use, disposal and recycling. *Journal of Hazardous Materials*, *344*, 179–199. doi:10.1016/j.jhazmat.2017.10.014.
- van der Hal, N., Ariel, A., & Angel, D. L. (2016). Exceptionally high abundances of microplastics in the oligotrophic Israeli Mediterranean coastal waters. *Marine Pollution Bulletin*, *116*, 151–155. doi:10.1016/j.marpolbul.2016.12.052.
- Hamilton, B. M., Bourdages, M. P., Geoffroy, C., Vermaire, J. C., Mallory, M. L., Rochman, C. M., & Provencher, J. F. (2021). Microplastics around an Arctic seabird colony: Particle community composition varies across environmental matrices. *Science of the Total Environment*, *773*, 145536. doi:10.1016/j.scitotenv.2021.145536.
- Hänninen, J., Weckström, M., Pawłowska, J., Szymańska, N., Uurasjärvi, E., Zajaczkowski, M., Hartikainen, S., & Vuorinen, I. (2021). Plastic debris composition and concentration in the Arctic Ocean, the North Sea and the Baltic Sea. *Marine Pollution Bulletin*, *165*, 112150. doi:10.1016/j.marpolbul.2021.112150.
- Hendrickson, E., Minor, E. C., & Schreiner, K. (2018). Microplastic abundance and composition in western Lake Superior as determined via microscopy, Pyr-GC/MS, and FTIR. *Environmental Science & Technology*, *52*, 1787–1796. doi:10.1021/acs.est.7b05829.

- Hengstmann, E., Tamminga, M., vom Bruch, C., & Fischer, E. K. (2017). Microplastic in beach sediments of the Isle of Rügen (Baltic Sea) - Implementing a novel glass elutriation column. *Marine Pollution Bulletin*, *126*, 263–274. doi:10.1016/j.marpolbul.2017.11.010.
- Hidalgo-Ruz, V., Gutow, L., Thompson, R. C., & Thiel, M. (2012). Microplastics in the marine environment: a review of the methods used for identification and quantification. *Environmental Science & Technology*, *46*, 3060–3075. doi:10.1021/es2031505.
- Huang, Y., Yan, M., Xu, K., Nie, H., Gong, H., & Wang, J. (2019). Distribution characteristics of microplastics in Zhubi reef from South China Sea. *Environmental Pollution*, *255*, 113133. doi:10.1016/j.envpol.2019.113133.
- Huntington, A., Corcoran, P. L., Jantunen, L., Thaysen, C., Bernstein, S., Stern, G. A., & Rochman, C. M. (2020). A first assessment of microplastics and other anthropogenic particles in Hudson Bay and the surrounding eastern Canadian Arctic waters of Nunavut. *Facets*, *5*, 432–454. doi:10.1139/FACETS-2019-0042.
- Huppertsberg, S., & Knepper, T. P. (2018). Instrumental analysis of microplastics—benefits and challenges. *Analytical and Bioanalytical Chemistry*, *410*, 6343–6352. doi:10.1007/s00216-018-1210-8.
- Hurley, R. R., Lusher, A. L., Olsen, M., & Nizzetto, L. (2018). Validation of a method for extracting microplastics from complex, organic-rich, environmental matrices. *Environmental Science & Technology*, *52*, 7409–7417. doi:10.1021/acs.est.8b01517.
- Imhof, H. K., Laforsch, C., Wiesheu, A. C., Schmid, J., Anger, P. M., Niessner, R., & Ivleva, N. P. (2016). Pigments and plastic in limnetic ecosystems: A qualitative and quantitative study on microparticles of different size classes. *Water Research*, *98*, 64–74. doi:10.1016/j.watres.2016.03.015.
- Isobe, A., Kubo, K., Tamura, Y., Nakashima, E., Fujii, N. et al. (2014). Selective transport of microplastics and mesoplastics by drifting in coastal waters. *Marine Pollution Bulletin*, *89*, 324–330. doi:10.1016/j.marpolbul.2014.09.041.
- Isobe, A., Uchiyama-Matsumoto, K., Uchida, K., & Tokai, T. (2016). Microplastics in the southern ocean. *Marine Pollution Bulletin*, *114*, 623–626. doi:10.1016/j.marpolbul.2016.09.037.
- Jahnke, A., Arp, H. P. H., Escher, B. I., Gewert, B., Gorokhova, E., Kühnel, D., Ogonowski, M., Potthoff, A., Rummel, C., Schmitt-Jansen, M. et al. (2017). Reducing uncertainty and confronting ignorance about the possible impacts of weathering plastic in the marine environment. *Environmental Science & Technology Letters*, *4*, 85–90. doi:10.1021/acs.estlett.7b00008.

- Jambeck, J. R., Geyer, R., Wilcox, C., Siegler, T. R., Perryman, M., Andrady, A., Narayan, R., & Law, K. L. (2015). Plastic waste inputs from land into the ocean. *Science*, *347*, 768–771. doi:10.1126/science.1260352.
- Julienne, F., Delorme, N., & Lagarde, F. (2019). From macroplastics to microplastics: Role of water in the fragmentation of polyethylene. *Chemosphere*, *236*, 124409. doi:10.1016/j.chemosphere.2019.124409.
- Kaiser, D., Kowalski, N., & Waniek, J. J. (2017). Effects of biofouling on the sinking behavior of microplastics. *Environmental Research Letters*, *12*, 124003. doi:10.1088/1748-9326/aa8e8b.
- Kang, J.-H., Kwon, O.-Y., & Shim, W. J. (2015). Potential threat of microplastics to zooplanktivores in the surface waters of the Southern Sea of Korea. *Archives of Environmental Contamination and Toxicology*, *69*, 340–351. doi:10.1007/s00244-015-0210-3.
- Kanhai, L. D. K., Johansson, C., Frias, J., Gardfeldt, K., Thompson, R. C., & O'Connor, I. (2019). Deep sea sediments of the Arctic Central Basin: a potential sink for microplastics. *Deep Sea Research Part I: Oceanographic Research Papers*, *145*, 137–142. doi:10.1016/j.dsr.2019.03.003.
- Karami, A., Golieskardi, A., Choo, C. K., Romano, N., Ho, Y. B., & Salamatnia, B. (2017). A high-performance protocol for extraction of microplastics in fish. *Science of the Total Environment*, *578*, 485–494. doi:10.1016/j.scitotenv.2016.10.213.
- Karlsson, T. M., Vethaak, A. D., Almroth, B. C., Ariese, F., van Velzen, M., Hassellöv, M., & Leslie, H. A. (2017). Screening for microplastics in sediment, water, marine invertebrates and fish: method development and microplastic accumulation. *Marine Pollution Bulletin*, *122*, 403–408. doi:10.1016/j.marpolbul.2017.06.081.
- Kazmiruk, T. N., Kazmiruk, V. D., & Bendell, L. (2018). Abundance and distribution of microplastics within surface sediments of a key shellfish growing region of Canada. *PLoS One*, *14*, 1–16. doi:10.1371/journal.pone.0225945.
- Kazour, M., Jemaa, S., Issa, C., Khalaf, G., & Amara, R. (2019). Microplastics pollution along the Lebanese coast (Eastern Mediterranean Basin): Occurrence in surface water, sediments and biota samples. *Science of the Total Environment*, *696*, 133933. doi:10.1016/j.scitotenv.2019.133933.
- Khalik, W. M. A. W. M., Ibrahim, Y. S., Anuar, S. T., Govindasamy, S., & Baharuddin, N. F. (2018). Microplastics analysis in Malaysian marine waters: a field study of Kuala Nerus and Kuantan. *Marine Pollution Bulletin*, *135*, 451–457. doi:10.1016/j.marpolbul.2018.07.052.

- Knutsen, H., Cyvin, J. B., Totland, C., Lilleeng, Ø., Wade, E. J., Castro, V., Pettersen, A., Laugesen, J., Møskeland, T., & Arp, H. P. H. (2020). Microplastic accumulation by tube-dwelling, suspension feeding polychaetes from the sediment surface: A case study from the Norwegian Continental Shelf. *Marine Environmental Research*, *161*, 105073. doi:10.1016/j.marenvres.2020.105073.
- Kooi, M., Nes, E. H. v., Scheffer, M., & Koelmans, A. A. (2017). Ups and downs in the ocean: effects of biofouling on vertical transport of microplastics. *Environmental Science & Technology*, *51*, 7963–7971. doi:10.1021/acs.est.6b04702.
- Koongolla, J. B., Andrady, A., Kumara, P. T. P., & Gangabadage, C. (2018). Evidence of microplastics pollution in coastal beaches and waters in southern Sri Lanka. *Marine Pollution Bulletin*, *137*, 277–284. doi:10.1016/j.marpolbul.2018.10.031.
- Kor, K., Ghazilou, A., & Ershadifar, H. (2020). Microplastic pollution in the littoral sediments of the northern part of the Oman Sea. *Marine Pollution Bulletin*, *155*, 111166. doi:10.1016/j.marpolbul.2020.111166.
- Kowalski, N., Reichardt, A. M., & Waniek, J. J. (2016). Sinking rates of microplastics and potential implications of their alteration by physical, biological, and chemical factors. *Marine Pollution Bulletin*, *109*, 310–319. doi:10.1016/j.marpolbul.2016.05.064.
- Kunz, A., Walther, B. A., Löwemark, L., & Lee, Y. C. (2016). Distribution and quantity of microplastic on sandy beaches along the northern coast of Taiwan. *Marine Pollution Bulletin*, *111*, 126–135. doi:10.1016/j.marpolbul.2016.07.022.
- Laglbauer, B. J., Franco-Santos, R. M., Andreu-Cazenave, M., Brunelli, L., Papadatou, M., Palatinus, A., Grego, M., & Deprez, T. (2014). Macrodebris and microplastics from beaches in Slovenia. *Marine Pollution Bulletin*, *89*, 356–366. doi:10.1016/j.marpolbul.2014.09.036.
- Law, K. L., Morét-Ferguson, S., Maximenko, N. A., Proskurowski, G., Peacock, E. E., Hafner, J., & Reddy, C. M. (2010). Plastic accumulation in the North Atlantic subtropical gyre. *Science*, *329*, 1185–1188. doi:10.1126/science.1192321.
- Lebreton, L., & Andrady, A. (2019). Future scenarios of global plastic waste generation and disposal. *Palgrave Communications*, *5*, 1–11. doi:10.1057/s41599-018-0212-7.
- Lebreton, L., Slat, B., Ferrari, F., Sainte-Rose, B., Aitken, J., Marthouse, R., Hajbane, S., Cunsolo, S., Schwarz, A., Levivier, A. et al. (2018). Evidence that the Great Pacific Garbage Patch is rapidly accumulating plastic. *Scientific Reports*, *8*, 1–15. doi:10.1038/s41598-018-22939-w.

- Lebreton, L., Van Der Zwet, J., Damsteeg, J.-W., Slat, B., Andrady, A., & Reisser, J. (2017). River plastic emissions to the world's oceans. *Nature Communications*, *8*, 1–10. doi:10.1038/ncomms15611.
- Lechthaler, S., Schwarzbauer, J., Reicherter, K., Stauch, G., & Schüttrumpf, H. (2020). Regional study of microplastics in surface waters and deep sea sediments south of the Algarve Coast. *Regional Studies in Marine Science*, *40*, 101488. doi:10.1016/j.rsma.2020.101488.
- Lefebvre, C., Saraux, C., Heitz, O., Nowaczyk, A., & Bonnet, D. (2019). Microplastics FTIR characterisation and distribution in the water column and digestive tracts of small pelagic fish in the Gulf of Lions. *Marine Pollution Bulletin*, *142*, 510–519. doi:10.1016/j.marpolbul.2019.03.025.
- Leistenschneider, C., Burkhardt-Holm, P., Mani, T., Primpke, S., Taubner, H., & Gerdt, G. (2021). Microplastics in the Weddell Sea (Antarctica): a forensic approach for discrimination between environmental and vessel-induced microplastics. *Environmental Science & Technology*, *55*, 15900–15911. doi:10.1021/acs.est.1c05207.
- Lenz, R., Enders, K., Stedmon, C. A., Mackenzie, D. M., & Nielsen, T. G. (2015). A critical assessment of visual identification of marine microplastic using Raman spectroscopy for analysis improvement. *Marine Pollution Bulletin*, *100*, 82–91. doi:10.1016/j.marpolbul.2015.09.026.
- Leslie, H., Brandsma, S., Van Velzen, M., & Vethaak, A. (2017). Microplastics en route: Field measurements in the Dutch river delta and Amsterdam canals, wastewater treatment plants, North Sea sediments and biota. *Environment International*, *101*, 133–142. doi:10.1016/j.envint.2017.01.018.
- Li, J., Green, C., Reynolds, A., Shi, H., & Rotchell, J. M. (2018a). Microplastics in mussels sampled from coastal waters and supermarkets in the United Kingdom. *Environmental Pollution*, *241*, 35–44. doi:10.1016/j.envpol.2018.05.038.
- Li, J., Huang, W., Xu, Y., Jin, A., Zhang, D., & Zhang, C. (2020). Microplastics in sediment cores as indicators of temporal trends in microplastic pollution in Andong salt marsh, Hangzhou Bay, China. *Regional Studies in Marine Science*, *35*, 101149. doi:10.1016/j.rsma.2020.101149.
- Li, J., Zhang, H., Zhang, K., Yang, R., & Li, Y., Ruize and Li (2018b). Characterization, source, and retention of microplastic in sandy beaches and mangrove wetlands of the Qinzhou Bay, China. *Marine Pollution Bulletin*, *136*, 401–406. doi:10.1016/j.marpolbul.2018.09.025.

- Li, R., Zhang, L., Xue, B., & Wang, Y. (2018c). Abundance and characteristics of microplastics in the mangrove sediment of the semi-enclosed Maowei Sea of the south China sea: New implications for location, rhizosphere, and sediment compositions. *Environmental Pollution*, *244*, 685–692. doi:10.1016/j.envpol.2018.10.089.
- Li, Y., Wolanski, E., Dai, Z., Lambrechts, J., Tang, C., & Zhang, H. (2018d). Trapping of plastics in semi-enclosed seas: Insights from the Bohai Sea, China. *Marine Pollution Bulletin*, *137*, 509–517. doi:10.1016/j.marpolbul.2018.10.038.
- Lin, J., Xu, X.-M., Yue, B.-Y., Xu, X.-P., Liu, J.-Z., Zhu, Q., & Wang, J.-H. (2020). Multidecadal records of microplastic accumulation in the coastal sediments of the East China Sea. *Chemosphere*, *270*, 128658. doi:10.1016/j.chemosphere.2020.128658.
- Lin, J., Xu, X.-P., Yue, B.-Y., Li, Y., Zhou, Q.-Z., Xu, X.-M., Liu, J.-Z., Wang, Q.-Q., & Wang, J.-H. (2021). A novel thermoanalytical method for quantifying microplastics in marine sediments. *Science of the Total Environment*, *760*, 144316. doi:10.1016/j.scitotenv.2020.144316.
- Ling, S., Sinclair, M., Levi, C., Reeves, S., & Edgar, G. (2017). Ubiquity of microplastics in coastal seafloor sediments. *Marine Pollution Bulletin*, *121*, 104–110. doi:10.1016/j.marpolbul.2017.05.038.
- Liu, P., Qian, L., Wang, H., Zhan, X., Lu, K., Gu, C., & Gao, S. (2019). New insights into the aging behavior of microplastics accelerated by advanced oxidation processes. *Environmental Science & Technology*, *53*, 3579–3588. doi:10.1021/acs.est.9b00493.
- Long, M., Moriceau, B., Gallinari, M., Lambert, C., Huvet, A., Raffray, J., & Soudant, P. (2015). Interactions between microplastics and phytoplankton aggregates: impact on their respective fates. *Marine Chemistry*, *175*, 39–46. doi:10.1016/j.marchem.2015.04.003.
- Lorenz, C., Roscher, L., Meyer, M. S., Hildebrandt, L., Prume, J., Löder, M. G., Primpke, S., & Gerdt, G. (2019). Spatial distribution of microplastics in sediments and surface waters of the southern North Sea. *Environmental Pollution*, *252*, 1719–1729. doi:10.1016/j.envpol.2019.06.093.
- Lots, F. A., Behrens, P., Vijver, M. G., Horton, A. A., & Bosker, T. (2017). A large-scale investigation of microplastic contamination: Abundance and characteristics of microplastics in European beach sediment. *Marine Pollution Bulletin*, *123*, 219–226. doi:10.1016/j.marpolbul.2017.08.057.
- Lourenço, P. M., Serra-Gonçalves, C., Ferreira, J. L., Catry, T., & Granadeiro, J. P. (2017). Plastic and other microfibers in sediments, macroinvertebrates and shorebirds from three intertidal wetlands of southern Europe and west Africa. *Environmental Pollution*, *231*, 123–133. doi:10.1016/j.envpol.2017.07.103.

- de Lucia, G. A., Caliani, I., Marra, S., Camedda, A., Coppa, S., Alcaro, L., Campani, T., Giannetti, M., Coppola, D., Cicero, A. M. et al. (2014). Amount and distribution of neustonic micro-plastic off the western Sardinian coast (Central-Western Mediterranean Sea). *Marine Environmental Research*, *100*, 10–16. doi:10.1016/j.marenvres.2014.03.017.
- Luo, H., Li, Y., Zhao, Y., Xiang, Y., He, D., & Pan, X. (2020a). Effects of accelerated aging on characteristics, leaching, and toxicity of commercial lead chromate pigmented microplastics. *Environmental Pollution*, *257*, 113475. doi:10.1016/j.envpol.2019.113475.
- Luo, H., Zhao, Y., Li, Y., Xiang, Y., He, D., & Pan, X. (2020b). Aging of microplastics affects their surface properties, thermal decomposition, additives leaching and interactions in simulated fluids. *Science of The Total Environment*, *714*, 136862. doi:10.1016/j.scitotenv.2020.136862.
- Luo, W., Su, L., Craig, N. J., Du, F., Wu, C., & Shi, H. (2019). Comparison of microplastic pollution in different water bodies from urban creeks to coastal waters. *Environmental Pollution*, *246*, 174–182. doi:10.1016/j.envpol.2018.11.081.
- Maes, T., Van der Meulen, M. D., Devriese, L. I., Leslie, H. A., Huvet, A., Frère, L., Robbens, J., & Vethaak, A. D. (2017). Microplastics baseline surveys at the water surface and in sediments of the North-East Atlantic. *Frontiers in Marine Science*, *4*, 1–13. doi:10.3389/fmars.2017.00135.
- Mai, L., Bao, L.-J., Shi, L., Liu, L.-Y., & Zeng, E. Y. (2018). Polycyclic aromatic hydrocarbons affiliated with microplastics in surface waters of Bohai and Huanghai Seas, China. *Environmental Pollution*, *241*, 834–840. doi:10.1016/j.envpol.2018.06.012.
- Martin, C., Baalkhuyur, F., Valluzzi, L., Saderne, V., Cusack, M., Almahasheer, H., Krishnakumar, P., Rabaoui, L., Qurban, M., Arias-Ortiz, A. et al. (2020). Exponential increase of plastic burial in mangrove sediments as a major plastic sink. *Science Advances*, *6*, 1–8. doi:10.1126/sciadv.aaz5593.
- Martin, J., Lusher, A., Thompson, R. C., & Morley, A. (2017). The deposition and accumulation of microplastics in marine sediments and bottom water from the Irish continental shelf. *Scientific Reports*, *7*, 1–9. doi:10.1038/s41598-017-11079-2.
- Masiá, P., Ardura, A., & Garcia-Vazquez, E. (2019). Microplastics in special protected areas for migratory birds in the Bay of Biscay. *Marine Pollution Bulletin*, *146*, 993–1001. doi:10.1016/j.marpolbul.2019.07.065.
- Mathalon, A., & Hill, P. (2014). Microplastic fibers in the intertidal ecosystem surrounding Halifax Harbor, Nova Scotia. *Marine Pollution Bulletin*, *81*, 69–79. doi:10.1016/j.marpolbul.2014.02.018.

- Matsuguma, Y., Takada, H., Kumata, H., Kanke, H., Sakurai, S., Suzuki, T., Itoh, M., Okazaki, Y., Boonyatumanond, R., Zakaria, M. P. et al. (2017). Microplastics in sediment cores from Asia and Africa as indicators of temporal trends in plastic pollution. *Archives of Environmental Contamination and Toxicology*, *73*, 230–239. doi:10.1007/s00244-017-0414-9.
- McEachern, K., Alegria, H., Kalagher, A. L., Hansen, C., Morrison, S., & Hastings, D. (2019). Microplastics in Tampa Bay, Florida: abundance and variability in estuarine waters and sediments. *Marine Pollution Bulletin*, *148*, 97–106. doi:10.1016/j.marpolbul.2019.07.068.
- Menéndez, I., Herrera-Holguín, C., & Mangas, J. (2020). Upper Quaternary coastal palaeoenvironments and palaeosea levels in Las Canteras beach, Gran Canaria (Canary Islands, Spain). *Marine Geology*, *429*, 106322. doi:10.1016/j.margeo.2020.106322.
- Menzel, T., Meides, N., Mauel, A., Mansfeld, U., Kretschmer, W., Kuhn, M., Herzig, E. M., Altstädt, V., Strohmriegl, P., Senker, J. et al. (2022). Degradation of low-density polyethylene to nanoplastic particles by accelerated weathering. *Science of the Total Environment*, *826*, 154035. doi:10.1016/j.scitotenv.2022.154035.
- Min, K., Cuiffi, J. D., & Mathers, R. T. (2020). Ranking environmental degradation trends of plastic marine debris based on physical properties and molecular structure. *Nature Communications*, *11*, 1–11. doi:10.1038/s41467-020-14538-z.
- Miranda, M. N., Sampaio, M. J., Tavares, P. B., Silva, A. M., & Pereira, M. F. R. (2021). Aging assessment of microplastics (LDPE, PET and uPVC) under urban environment stressors. *Science of The Total Environment*, *796*, 148914. doi:10.1016/j.scitotenv.2021.148914.
- Mistri, M., Scoponi, M., Granata, T., Moruzzi, L., Massara, F., & Munari, C. (2020). Types, occurrence and distribution of microplastics in sediments from the northern Tyrrhenian Sea. *Marine Pollution Bulletin*, *153*, 111016. doi:10.1016/j.marpolbul.2020.111016.
- Moore, C. J., Moore, S. L., Weisberg, S. B., Lattin, G. L., & Zellers, A. F. (2002). A comparison of neustonic plastic and zooplankton abundance in southern California's coastal waters. *Marine Pollution Bulletin*, *44*, 1035–1038. doi:10.1016/S0025-326X(02)00150-9.
- Morgana, S., Ghigliotti, L., Estévez-Calvar, N., Stifanese, R., Wieckzorek, A., Doyle, T., Christiansen, J. S., Faimali, M., & Garaventa, F. (2018). Microplastics in the Arctic: a case study with sub-surface water and fish samples off Northeast Greenland. *Environmental Pollution*, *242*, 1078–1086. doi:10.1016/j.envpol.2018.08.001.

- Mu, J., Zhang, S., Qu, L., Jin, F., Fang, C., Ma, X., Zhang, W., & Wang, J. (2019). Microplastics abundance and characteristics in surface waters from the Northwest Pacific, the Bering Sea, and the Chukchi Sea. *Marine Pollution Bulletin*, *143*, 58–65. doi:10.1016/j.marpolbul.2019.04.023.
- Müller, A., Becker, R., Dorgerloh, U., Simon, F.-G., & Braun, U. (2018). The effect of polymer aging on the uptake of fuel aromatics and ethers by microplastics. *Environmental Pollution*, *240*, 639–646. doi:10.1016/j.envpol.2018.04.127.
- Naidoo, T., Glassom, D., & Smit, A. J. (2015). Plastic pollution in five urban estuaries of KwaZulu-Natal, South Africa. *Marine Pollution Bulletin*, *101*, 473–480. doi:10.1016/j.marpolbul.2015.09.044.
- Naji, A., Esmaili, Z., & Khan, F. R. (2016). Plastic debris and microplastics along the beaches of the Strait of Hormuz, Persian Gulf. *Marine Pollution Bulletin*, *114*, 1057–1062. doi:10.1016/j.marpolbul.2016.11.032.
- Naji, A., Esmaili, Z., Mason, S. A., & Dick Vethaak, A. (2017). The occurrence of microplastic contamination in littoral sediments of the Persian Gulf, Iran. *Environmental Science and Pollution Research*, *24*, 20459–20468. doi:10.1007/s11356-017-9587-z.
- Naji, A., Nuri, M., Amiri, P., & Niyogi, S. (2019). Small microplastic particles (S-MPPs) in sediments of mangrove ecosystem on the northern coast of the Persian Gulf. *Marine Pollution Bulletin*, *146*, 305–311. doi:10.1016/j.marpolbul.2019.06.033.
- Napper, I. E., & Thompson, R. C. (2020). Plastic debris in the marine environment: history and future challenges. *Global Challenges*, *4*, 1900081. doi:10.1002/gch2.201900081.
- Nel, H. A., & Froneman, P. W. (2015). A quantitative analysis of microplastic pollution along the south-eastern coastline of South Africa. *Marine Pollution Bulletin*, *101*, 274–279. doi:10.1016/j.marpolbul.2015.09.043.
- Nelms, S. E., Galloway, T. S., Godley, B. J., Jarvis, D. S., & Lindeque, P. K. (2018). Investigating microplastic trophic transfer in marine top predators. *Environmental Pollution*, *238*, 999–1007. doi:10.1016/j.envpol.2018.02.016.
- Nie, H., Wang, J., Xu, K., Huang, Y., & Yan, M. (2019). Microplastic pollution in water and fish samples around Nanxun Reef in Nansha Islands, South China Sea. *Science of the Total Environment*, *696*, 134022. doi:10.1016/j.scitotenv.2019.134022.
- Nor, N. H. M., & Obbard, J. P. (2014). Microplastics in Singapore’s coastal mangrove ecosystems. *Marine Pollution Bulletin*, *79*, 278–283. doi:10.1016/j.marpolbul.2013.11.025.

- Ogata, Y., Takada, H., Mizukawa, K., Hirai, H., Iwasa, S., Endo, S., Mato, Y., Saha, M., Okuda, K., Nakashima, A. et al. (2009). International Pellet Watch: Global monitoring of persistent organic pollutants (POPs) in coastal waters. 1. Initial phase data on PCBs, DDTs, and HCHs. *Marine Pollution Bulletin*, *58*, 1437–1446. doi:10.1016/j.marpolbul.2009.06.014.
- Olivatto, G. P., Martins, M. C. T., Montagner, C. C., Henry, T. B., & Carreira, R. S. (2019). Microplastic contamination in surface waters in Guanabara Bay, Rio de Janeiro, Brazil. *Marine Pollution Bulletin*, *139*, 157–162. doi:10.1016/j.marpolbul.2018.12.042.
- Olsen, L. M. B., Knutsen, H., Mahat, S., Wade, E. J., & Arp, H. P. H. (2020). Facilitating microplastic quantification through the introduction of a cellulose dissolution step prior to oxidation: Proof-of-concept and demonstration using diverse samples from the Inner Oslofjord, Norway. *Marine Environmental Research*, *161*, 105080. doi:10.1016/j.marenvres.2020.105080.
- Ostle, C., Thompson, R. C., Broughton, D., Gregory, L., Wootton, M., & Johns, D. G. (2019). The rise in ocean plastics evidenced from a 60-year time series. *Nature Communications*, *10*, 1–6. doi:10.1038/s41467-019-09506-1.
- Pabortsava, K., & Lampitt, R. S. (2020). High concentrations of plastic hidden beneath the surface of the Atlantic Ocean. *Nature Communications*, *11*, 1–11. doi:10.1038/s41467-020-17932-9.
- Paço, A., Duarte, K., da Costa, J. P., Santos, P. S., Pereira, R., Pereira, M., Freitas, A. C., Duarte, A. C., & Rocha-Santos, T. A. (2017). Biodegradation of polyethylene microplastics by the marine fungus *Zalerion maritimum*. *Science of the Total Environment*, *586*, 10–15. doi:10.1016/j.scitotenv.2017.02.017.
- Pagter, E., Frias, J., & Nash, R. (2018). Microplastics in Galway Bay: A comparison of sampling and separation methods. *Marine Pollution Bulletin*, *135*, 932–940. doi:10.1016/j.marpolbul.2018.08.013.
- Palatinus, A., Viršek, M. K., Robič, U., Grego, M., Bajt, O., Šiljić, J., Suaria, G., Liubartseva, S., Coppini, G., & Peterlin, M. (2019). Marine litter in the Croatian part of the middle Adriatic Sea: Simultaneous assessment of floating and seabed macro and micro litter abundance and composition. *Marine Pollution Bulletin*, *139*, 427–439. doi:10.1016/j.marpolbul.2018.12.038.
- Parolini, M., Antonioli, D., Borgogno, F., Gibellino, M. C., Fresta, J., Albonico, C., De Felice, B., Canuto, S., Concedi, D., Romani, A. et al. (2021). Microplastic contamination in snow from Western Italian alps. *International Journal of Environmental Research and Public Health*, *18*, 1–10. doi:10.3390/ijerph18020768.

- Passow, U. (2002). Transparent exopolymer particles (TEP) in aquatic environments. *Progress in Oceanography*, *55*, 287–333. doi:10.1016/S0079-6611(02)00138-6.
- Patterson, J., Jeyasanta, K. I., Sathish, N., Booth, A. M., & Edward, J. P. (2019). Profiling microplastics in the Indian edible oyster, *Magallana bilineata* collected from the Tuticorin coast, Gulf of Mannar, Southeastern India. *Science of the Total Environment*, *691*, 727–735. doi:10.1016/j.scitotenv.2019.07.063.
- Peng, G., Zhu, B., Yang, D., Su, L., Shi, H., & Li, D. (2017). Microplastics in sediments of the Changjiang Estuary, China. *Environmental Pollution*, *225*, 283–290. doi:10.1016/j.envpol.2016.12.064.
- Peng, X., Chen, M., Chen, S., Dasgupta, S., Xu, H., Ta, K., Du, M., Li, J., Guo, Z., Bai, S. et al. (2018). Microplastics contaminate the deepest part of the world's ocean. *Geochemical Perspectives Letters*, *9*, 1–5. doi:10.7185/geochemlet.1829.
- Phuong, N. N., Poirier, L., Lagarde, F., Kamari, A., & Zalouk-Vergnoux, A. (2018). Microplastic abundance and characteristics in French Atlantic coastal sediments using a new extraction method. *Environmental Pollution*, *243*, 228–237. doi:10.1016/j.envpol.2018.08.032.
- PlasticsEurope (2021). Plastics - the Facts 2021: An analysis of European plastics production, demand and waste data. *PlasticsEurope*, *33*.
- Prata, J. C., da Costa, J. P., Duarte, A. C., & Rocha-Santos, T. (2019). Methods for sampling and detection of microplastics in water and sediment: a critical review. *TrAC Trends in Analytical Chemistry*, *110*, 150–159. doi:10.1016/j.trac.2018.10.029.
- Prata, J. C., Sequeira, I. F., Monteiro, S. S., Silva, A. L. P., da Costa, J. P., Dias-Pereira, P., Fernandes, A. J. S., da Costa, F. M., Duarte, A. C., & Rocha-Santos, T. (2021). Preparation of biological samples for microplastic identification by Nile Red. *Science of the Total Environment*, *783*, 147065. doi:10.1016/j.scitotenv.2021.147065.
- Pullwer, J., & Waniek, J. J. (2020). Particulate trace metal fluxes in the center of an oceanic desert: Northeast Atlantic subtropical gyre. *Journal of Marine Systems*, *212*, 103447. doi:10.1016/j.jmarsys.2020.103447.
- Qiu, Q., Peng, J., Yu, X., Chen, F., Wang, J., & Dong, F. (2015). Occurrence of microplastics in the coastal marine environment: First observation on sediment of China. *Marine Pollution Bulletin*, *98*, 274–280. doi:10.1016/j.marpolbul.2015.07.028.
- Qiu, Q., Tan, Z., Wang, J., Peng, J., Li, M., & Zhan, Z. (2016). Extraction, enumeration and identification methods for monitoring microplastics in the environment. *Estuarine, Coastal and Shelf Science*, *176*, 102–109.

- Reed, S., Clark, M., Thompson, R., & Hughes, K. A. (2018). Microplastics in marine sediments near Rothera research station, Antarctica. *Marine Pollution Bulletin*, *133*, 460–463. doi:10.1016/j.marpolbul.2018.05.068.
- Reiff, J., Forbes, G. S., Spiexsma, F. T. M., & Reynders, J. (1986). African dust reaching northwestern Europe: A case study to verify trajectory calculations. *Journal of Applied Meteorology and Climatology*, *25*, 1543–1567.
- Reineccius, J., Appelt, J.-S., Hinrichs, T., Kaiser, D., Stern, J., Prien, R. D., & Waniek, J. J. (2020). Abundance and characteristics of microfibers detected in sediment trap material from the deep subtropical North Atlantic Ocean. *Science of The Total Environment*, *738*, 140354. doi:10.1016/j.scitotenv.2020.140354.
- Reineccius, J., Bresien, J., & Waniek, J. J. (2021). Separation of microplastics from mass-limited samples by an effective adsorption technique. *Science of The Total Environment*, *788*, 147881. doi:10.1016/j.scitotenv.2021.147881.
- Reineccius, J., Schönke, M., & Waniek, J. J. (2022). Abiotic Long-Term Simulation of Microplastic Weathering Pathways under Different Aqueous Conditions. *Environmental Science & Technology*, (accepted). doi:10.1021/acs.est.2c05746.
- Reineccius, J., & Waniek, J. J. (2022). First long-term evidence of microplastic pollution in the deep subtropical Northeast Atlantic. *Environmental Pollution*, *305*, 119302. doi:10.1016/j.envpol.2022.119302.
- Retama, I., Jonathan, M., Shruti, V., Velumani, S., Sarkar, S., Roy, P. D., & Rodríguez-Espinosa, P. (2016). Microplastics in tourist beaches of Huatulco Bay, Pacific coast of southern Mexico. *Marine Pollution Bulletin*, *113*, 530–535. doi:10.1016/j.marpolbul.2016.08.053.
- Rios, L. M., Moore, C., & Jones, P. R. (2007). Persistent organic pollutants carried by synthetic polymers in the ocean environment. *Marine Pollution Bulletin*, *54*, 1230–1237. doi:10.1016/j.marpolbul.2007.03.022.
- Rios-Mendoza, L. M., Ontiveros-Cuadras, J. F., Leon-Vargas, D., Ruiz-Fernández, A. C., Rangel-García, M., Pérez-Bernal, L. H., & Sanchez-Cabeza, J.-A. (2021). Microplastic contamination and fluxes in a touristic area at the SE Gulf of California. *Marine Pollution Bulletin*, *170*, 112638. doi:10.1016/j.marpolbul.2021.112638.
- Rist, S., Vianello, A., Winding, M. H. S., Nielsen, T. G., Almeda, R., Torres, R. R., & Vollertsen, J. (2020). Quantification of plankton-sized microplastics in a productive coastal Arctic marine ecosystem. *Environmental Pollution*, *266*, 115248. doi:10.1016/j.envpol.2020.115248.

- Rochman, C. M. (2018). Microplastics research—from sink to source. *Science*, *360*, 28–29. doi:10.1126/science.aar7734.
- Rochman, C. M., Hoh, E., Kurobe, T., & Teh, S. J. (2013). Ingested plastic transfers hazardous chemicals to fish and induces hepatic stress. *Scientific Reports*, *3*, 1–7. doi:10.1038/srep03263.
- Romeo, T., D’Alessandro, M., Esposito, V., Scotti, G., Berto, D., Formalewicz, M., Noventa, S., Giuliani, S., Macchia, S., Sartori, D. et al. (2015). Environmental quality assessment of Grand Harbour (Valletta, Maltese Islands): a case study of a busy harbour in the Central Mediterranean Sea. *Environmental Monitoring and Assessment*, *187*, 1–21. doi:10.1007/s10661-015-4950-3.
- Ronda, A. C., Arias, A. H., Oliva, A. L., & Marcovecchio, J. E. (2019). Synthetic microfibers in marine sediments and surface seawater from the Argentinean continental shelf and a Marine Protected Area. *Marine Pollution Bulletin*, *149*, 110618. doi:10.1016/j.marpolbul.2019.110618.
- Roscher, L., Fehres, A., Reisel, L., Halbach, M., Scholz-Böttcher, B., Gerriets, M., Badewien, T. H., Shiravani, G., Wurpts, A., Primpke, S. et al. (2021). Microplastic pollution in the Weser estuary and the German North Sea. *Environmental Pollution*, *288*, 117681. doi:10.1016/j.envpol.2021.117681.
- Ross, P. S., Chastain, S., Vassilenko, E., Etemadifar, A., Zimmermann, S., Quesnel, S.-A., Eert, J., Solomon, E., Patankar, S., Posacka, A. M. et al. (2021). Pervasive distribution of polyester fibres in the Arctic Ocean is driven by Atlantic inputs. *Nature Communications*, *12*, 1–9. doi:10.1038/s41467-020-20347-1.
- Rouillon, C., Bussiere, P.-O., Desnoux, E., Collin, S., Vial, C., Therias, S., & Gardette, J.-L. (2016). Is carbonyl index a quantitative probe to monitor polypropylene photodegradation? *Polymer Degradation and Stability*, *128*, 200–208. doi:10.1016/j.polymdegradstab.2015.12.011.
- Sandre, F., Dromard, C. R., Le Menach, K., Bouchon-Navaro, Y., Cordonnier, S., Tapie, N., Budzinski, H., & Bouchon, C. (2019). Detection of adsorbed chlordecone on microplastics in marine sediments in Guadeloupe: a preliminary study. *Gulf and Caribbean Research*, *30*, GCFI8–GCFI14. doi:10.18785/GCR.3001.14.
- Sathish, M. N., Jeyasanta, K. I., & Patterson, J. (2020). Monitoring of microplastics in the clam *Donax cuneatus* and its habitat in Tuticorin coast of Gulf of Mannar (GoM), India. *Environmental Pollution*, *266*, 115219. doi:10.1016/j.envpol.2020.115219.
- Sathish, N., Jeyasanta, K. I., & Patterson, J. (2019). Abundance, characteristics and surface degradation features of microplastics in beach sediments of five coastal areas in Tamil

- Nadu, India. *Marine Pollution Bulletin*, 142, 112–118. doi:10.1016/j.marpolbul.2019.03.037.
- Scheuvens, D., Schütz, L., Kandler, K., Ebert, M., & Weinbruch, S. (2013). Bulk composition of northern African dust and its source sediments—A compilation. *Earth-Science Reviews*, 116, 170–194. doi:10.1016/j.earscirev.2012.08.005.
- Scott, N., Porter, A., Santillo, D., Simpson, H., Lloyd-Williams, S., & Lewis, C. (2019). Particle characteristics of microplastics contaminating the mussel *Mytilus edulis* and their surrounding environments. *Marine Pollution Bulletin*, 146, 125–133. doi:10.1016/j.marpolbul.2019.05.041.
- Setälä, O., Norkko, J., & Lehtiniemi, M. (2016). Feeding type affects microplastic ingestion in a coastal invertebrate community. *Marine Pollution Bulletin*, 102, 95–101. doi:10.1016/j.marpolbul.2015.11.053.
- Shim, W. J., Hong, S. H., & Eo, S. (2018). Marine microplastics: Abundance, distribution, and composition. In *Microplastic Contamination in Aquatic Environments* (pp. 1–26). Elsevier. doi:10.1016/B978-0-12-813747-5.00001-1.
- Song, Y. K., Hong, S. H., Eo, S., Jang, M., Han, G. M., Isobe, A., & Shim, W. J. (2018). Horizontal and vertical distribution of microplastics in Korean coastal waters. *Environmental Science & Technology*, 52, 12188–12197. doi:10.1021/acs.est.8b04032.
- Song, Y. K., Hong, S. H., Jang, M., Han, G. M., Jung, S. W., & Shim, W. J. (2017). Combined effects of UV exposure duration and mechanical abrasion on microplastic fragmentation by polymer type. *Environmental Science & Technology*, 51, 4368–4376. doi:10.1021/acs.est.6b06155.
- Sørensen, L., Groven, A. S., Hovsbakken, I. A., Del Puerto, O., Krause, D. F., Sarno, A., & Booth, A. M. (2021). UV degradation of natural and synthetic microfibers causes fragmentation and release of polymer degradation products and chemical additives. *Science of the Total Environment*, 755, 143170. doi:10.1016/j.scitotenv.2020.143170.
- Stolte, A., Forster, S., Gerdts, G., & Schubert, H. (2015). Microplastic concentrations in beach sediments along the German Baltic coast. *Marine Pollution Bulletin*, 99, 216–229. doi:10.1016/j.marpolbul.2015.07.022.
- Strungaru, S.-A., Jijie, R., Nicoara, M., Plavan, G., & Faggio, C. (2019). Micro-(nano) plastics in freshwater ecosystems: abundance, toxicological impact and quantification methodology. *Trends in Analytical Chemistry*, 110, 116–128. doi:10.1016/j.trac.2018.10.025.

- Sun, X., Liang, J., Zhu, M., Zhao, Y., & Zhang, B. (2018). Microplastics in seawater and zooplankton from the Yellow Sea. *Environmental Pollution*, *242*, 585–595. doi:10.1016/j.envpol.2018.07.014.
- Sun, Y., Yuan, J., Zhou, T., Zhao, Y., Yu, F., & Ma, J. (2020). Laboratory simulation of microplastics weathering and its adsorption behaviors in an aqueous environment: a systematic review. *Environmental Pollution*, *265*, 114864. doi:10.1016/j.envpol.2020.114864.
- Suteja, Y., Atmadipoera, A. S., Riani, E., Nurjaya, I. W., Nugroho, D., & Cordova, M. R. (2021). Spatial and temporal distribution of microplastic in surface water of tropical estuary: Case study in Benoa Bay, Bali, Indonesia. *Marine Pollution Bulletin*, *163*, 111979. doi:10.1016/j.marpolbul.2021.111979.
- Syakti, A. D., Hidayati, N. V., Jaya, Y. V., Siregar, S. H., Yude, R., Asia, L., Wong-Wah-Chung, P., Doumenq, P. et al. (2018). Simultaneous grading of microplastic size sampling in the Small Islands of Bintan water, Indonesia. *Marine Pollution Bulletin*, *137*, 593–600. doi:10.1016/j.marpolbul.2018.11.005.
- Syranidou, E., Karkanorachaki, K., Amorotti, F., Franchini, M., Repouskou, E., Kaliva, M., Vamvakaki, M., Kolvenbach, B., Fava, F., Corvini, P. F.-X. et al. (2017). Biodegradation of weathered polystyrene films in seawater microcosms. *Scientific Reports*, *7*, 1–12. doi:10.1038/s41598-017-18366-y.
- Tang, G., Liu, M., Zhou, Q., He, H., Chen, K., Zhang, H., Hu, J., Huang, Q., Luo, Y., Ke, H. et al. (2018). Microplastics and polycyclic aromatic hydrocarbons (PAHs) in Xiamen coastal areas: implications for anthropogenic impacts. *Science of the Total Environment*, *634*, 811–820. doi:10.1016/j.scitotenv.2018.03.336.
- Tekman, M. B., Wekerle, C., Lorenz, C., Primpke, S., Hasemann, C., Gerdt, G., & Bergmann, M. (2020). Tying up loose ends of microplastic pollution in the Arctic: distribution from the sea surface through the water column to deep-sea sediments at the HAUSGARTEN observatory. *Environmental Science & Technology*, *54*, 4079–4090. doi:10.1021/acs.est.9b06981.
- Ter Halle, A., Ladirat, L., Gendre, X., Goudouneche, D., Pusineri, C., Routaboul, C., Tenailleau, C., Duployer, B., & Perez, E. (2016). Understanding the fragmentation pattern of marine plastic debris. *Environmental Science & Technology*, *50*, 5668–5675. doi:10.1021/acs.est.6b00594.
- Truong, T. N. S., Strady, E., Kieu-Le, T. C., Tran, Q. V., Le, T. M. T., & Thuong, Q. T. (2021). Microplastic in atmospheric fallouts of a developing Southeast Asian megacity under tropical climate. *Chemosphere*, *272*, 129874. doi:10.1016/j.chemosphere.2021.129874.

- Tsang, Y., Mak, C., Liebich, C., Lam, S., Sze, E. T., & Chan, K. (2017). Microplastic pollution in the marine waters and sediments of Hong Kong. *Marine Pollution Bulletin*, *115*, 20–28. doi:10.1016/j.marpolbul.2016.11.003.
- Uddin, S., Fowler, S. W., Uddin, M. F., Behbehani, M., & Naji, A. (2021). A review of microplastic distribution in sediment profiles. *Marine Pollution Bulletin*, *163*, 111973. doi:10.1016/j.marpolbul.2021.111973.
- Van Sebille, E., England, M. H., & Froyland, G. (2012). Origin, dynamics and evolution of ocean garbage patches from observed surface drifters. *Environmental Research Letters*, *7*, 1–6. doi:10.1088/1748-9326/7/4/044040.
- Vianello, A., Boldrin, A., Guerriero, P., Moschino, V., Rella, R., Sturaro, A., & Da Ros, L. (2013). Microplastic particles in sediments of Lagoon of Venice, Italy: First observations on occurrence, spatial patterns and identification. *Estuarine, Coastal and Shelf Science*, *130*, 54–61. doi:10.1016/j.ecss.2013.03.022.
- Villanova-Solano, C., Díaz-Peña, F. J., Hernández-Sánchez, C., González-Sálamo, J., González-Pleiter, M., Vega-Moreno, D., Fernández-Piñas, F., Fraile-Nuez, E., Machín, F., & Hernández-Borges, J. (2022). Microplastic pollution in sublittoral coastal sediments of a North Atlantic island: The case of La Palma (Canary Islands, Spain). *Chemosphere*, *288*, 132530. doi:10.1016/j.chemosphere.2021.132530.
- Wang, F., Nian, X., Wang, J., Zhang, W., Peng, G., Ge, C., Dong, C., Qu, J., & Li, D. (2018a). Multiple dating approaches applied to the recent sediments in the Yangtze River (Changjiang) subaqueous delta. *The Holocene*, *28*, 858–866. doi:10.1177/0959683617752847.
- Wang, T., Hu, M., Song, L., Yu, J., Liu, R., Wang, S., Wang, Z., Sokolova, I. M., Huang, W., & Wang, Y. (2020). Coastal zone use influences the spatial distribution of microplastics in Hangzhou Bay, China. *Environmental Pollution*, *266*, 115137. doi:10.1016/j.envpol.2020.115137.
- Wang, T., Zou, X., Li, B., Yao, Y., Zang, Z., Li, Y., Yu, W., & Wang, W. (2018b). Preliminary study of the source apportionment and diversity of microplastics: taking floating microplastics in the South China Sea as an example. *Environmental Pollution*, *245*, 965–974. doi:10.1016/j.envpol.2018.10.110.
- Waniek, J., Koeve, W., & Prien, R. D. (2000). Trajectories of sinking particles and the catchment areas above sediment traps in the northeast Atlantic. *Journal of Marine Research*, *58*, 983–1006. doi:10.1357/002224000763485773.
- Waniek, J. J., Schulz-Bull, D. E., Blanz, T., Prien, R. D., Oschlies, A., & Müller, T. J. (2004). Interannual variability of deep water particle flux in relation to production

- and lateral sources in the northeast Atlantic. *Deep Sea Research Part I: Oceanographic Research Papers*, *52*, 33–50. doi:10.1016/j.dsr.2004.08.008.
- Waniek, J. J., Schulz-Bull, D. E., Kuss, J., & Blanz, T. (2005). Long time series of deep water particle flux in three biogeochemical provinces of the northeast Atlantic. *Journal of Marine Systems*, *56*, 391–415. doi:10.1016/j.jmarsys.2005.03.001.
- Way, C., Hudson, M. D., Williams, I. D., & Langley, G. J. (2022). Evidence of underestimation in microplastic research: A meta-analysis of recovery rate studies. *Science of The Total Environment*, *805*, 150227. doi:10.1016/j.scitotenv.2021.150227.
- Wesch, C., Elert, A. M., Wörner, M., Braun, U., Klein, R., & Paulus, M. (2017). Assuring quality in microplastic monitoring: About the value of clean-air devices as essentials for verified data. *Scientific Reports*, *7*, 1–8. doi:10.1038/s41598-017-05838-4.
- Wilcox, C., Hardesty, B. D., & Law, K. L. (2019). Abundance of floating plastic particles is increasing in the Western North Atlantic Ocean. *Environmental Science & Technology*, *54*, 790–796. doi:10.1021/acs.est.9b04812.
- Willis, K. A., Eriksen, R., Wilcox, C., & Hardesty, B. D. (2017). Microplastic distribution at different sediment depths in an urban estuary. *Frontiers in Marine Science*, *4*, 1–8. doi:10.3389/fmars.2017.00419.
- Woodall, L. C., Sanchez-Vidal, A., Canals, M., Paterson, G. L., Coppock, R., Sleight, V., Calafat, A., Rogers, A. D., Narayanaswamy, B. E., & Thompson, R. C. (2014). The deep sea is a major sink for microplastic debris. *Royal Society Open Science*, *1*, 140317. doi:10.1098/rsos.140317.
- Wu, N., Zhang, Y., Zhang, X., Zhao, Z., He, J., Li, W., Ma, Y., & Niu, Z. (2019). Occurrence and distribution of microplastics in the surface water and sediment of two typical estuaries in Bohai Bay, China. *Environmental Science: Processes & Impacts*, *21*, 1143–1152. doi:10.1039/c9em00148d.
- Xu, P., Peng, G., Su, L., Gao, Y., Gao, L., & Li, D. (2018). Microplastic risk assessment in surface waters: A case study in the Changjiang Estuary, China. *Marine Pollution Bulletin*, *133*, 647–654. doi:10.1016/j.marpolbul.2018.06.020.
- Xue, B., Zhang, L., Li, R., Wang, Y., Guo, J., Yu, K., & Wang, S. (2020). Underestimated microplastic pollution derived from fishery activities and “hidden” in deep sediment. *Environmental Science & Technology*, *54*, 2210–2217. doi:10.1021/acs.est.9b04850.
- Yakushev, E., Gebruk, A., Osadchiev, A., Pakhomova, S., Lusher, A., Berezina, A., van Bavel, B., Vorozheikina, E., Chernykh, D., Kolbasova, G. et al. (2021). Microplastics distribution in the Eurasian Arctic is affected by Atlantic waters and Siberian rivers. *Communications Earth & Environment*, *2*, 1–10. doi:10.1038/s43247-021-00091-0.

- Yao, W., Di, D., Wang, Z., Liao, Z., Huang, H., Mei, K., Dahlgren, R. A., Zhang, M., & Shang, X. (2019). Micro-and macroplastic accumulation in a newly formed *Spartina alterniflora* colonized estuarine saltmarsh in southeast China. *Marine Pollution Bulletin*, *149*, 110636. doi:10.1016/j.marpolbul.2019.110636.
- Yu, F., Yang, C., Zhu, Z., Bai, X., & Ma, J. (2019). Adsorption behavior of organic pollutants and metals on micro/nanoplastics in the aquatic environment. *Science of the Total Environment*, *694*, 133643. doi:10.1016/j.scitotenv.2019.133643.
- Yuan, Z., Nag, R., & Cummins, E. (2022). Human health concerns regarding microplastics in the aquatic environment-From marine to food systems. *Science of The Total Environment*, *823*, 153730. doi:10.1016/j.scitotenv.2022.153730.
- Zettler, E. R., Mincer, T. J., & Amaral-Zettler, L. A. (2013). Life in the “plastisphere”: microbial communities on plastic marine debris. *Environmental Science & Technology*, *47*, 7137–7146. doi:10.1021/es401288x.
- Zhang, B., Wu, D., Yang, X., Teng, J., Liu, Y., Zhang, C., Zhao, J., Yin, X., You, L., Liu, Y. et al. (2019a). Microplastic pollution in the surface sediments collected from Sishili Bay, North Yellow Sea, China. *Marine Pollution Bulletin*, *141*, 9–15. doi:10.1016/j.marpolbul.2019.02.021.
- Zhang, C., Zhou, H., Cui, Y., Wang, C., Li, Y., & Zhang, D. (2019b). Microplastics in offshore sediment in the yellow Sea and east China Sea, China. *Environmental Pollution*, *244*, 827–833. doi:10.1016/j.envpol.2018.10.102.
- Zhang, W., Zhang, S., Wang, J., Wang, Y., Mu, J., Wang, P., Lin, X., & Ma, D. (2017). Microplastic pollution in the surface waters of the Bohai Sea, China. *Environmental Pollution*, *231*, 541–548. doi:10.1016/j.envpol.2017.08.058.
- Zhao, J., Ran, W., Teng, J., Liu, Y., Liu, H., Yin, X., Cao, R., & Wang, Q. (2018). Microplastic pollution in sediments from the Bohai Sea and the Yellow Sea, China. *Science of the Total Environment*, *640*, 637–645. doi:10.1016/j.scitotenv.2018.05.346.
- Zhao, S., Zhu, L., & Li, D. (2015). Microplastic in three urban estuaries, China. *Environmental Pollution*, *206*, 597–604. doi:10.1016/j.envpol.2015.08.027.
- Zhao, S., Zhu, L., Wang, T., & Li, D. (2014). Suspended microplastics in the surface water of the Yangtze Estuary System, China: first observations on occurrence, distribution. *Marine Pollution Bulletin*, *86*, 562–568. doi:10.1016/j.marpolbul.2014.06.032.
- Zheng, Y., Li, J., Cao, W., Liu, X., Jiang, F., Ding, J., Yin, X., & Sun, C. (2019). Distribution characteristics of microplastics in the seawater and sediment: a case study in

-
- Jiaozhou Bay, China. *Science of the Total Environment*, 674, 27–35. doi:10.1016/j.scitotenv.2019.04.008.
- Zhou, Q., Tu, C., Fu, C., Li, Y., Zhang, H., Xiong, K., Zhao, X., Li, L., Waniek, J. J., & Luo, Y. (2020). Characteristics and distribution of microplastics in the coastal mangrove sediments of China. *Science of the Total Environment*, 703, 134807. doi:10.1016/j.scitotenv.2019.134807.
- Zhou, Q., Tu, C., Yang, J., Fu, C., Li, Y., & Waniek, J. J. (2021). Trapping of Microplastics in Halocline and Turbidity Layers of the Semi-enclosed Baltic Sea. *Frontiers in Marine Science*, 8, 761566. doi:10.3389/fmars.2021.761566.
- Zhou, Q., Zhang, H., Fu, C., Zhou, Y., Dai, Z., Li, Y., Tu, C., & Luo, Y. (2018). The distribution and morphology of microplastics in coastal soils adjacent to the Bohai Sea and the Yellow Sea. *Geoderma*, 322, 201–208. doi:10.1016/j.geoderma.2018.02.015.
- Zhu, L., Bai, H., Chen, B., Sun, X., Qu, K., & Xia, B. (2018). Microplastic pollution in North Yellow Sea, China: Observations on occurrence, distribution and identification. *Science of the Total Environment*, 636, 20–29. doi:10.1016/j.scitotenv.2018.04.182.
- Zobkov, M., & Esiukova, E. (2017). Microplastics in Baltic bottom sediments: quantification procedures and first results. *Marine Pollution Bulletin*, 114, 724–732. doi:10.1016/j.marpolbul.2016.10.060.
- Zobkov, M., Esiukova, E., Zyubin, A., & Samusev, I. (2019). Microplastic content variation in water column: The observations employing a novel sampling tool in stratified Baltic Sea. *Marine Pollution Bulletin*, 138, 193–205. doi:10.1016/j.marpolbul.2018.11.047.
- Zvekcic, M., Richards, L. C., Tong, C. C., & Krogh, E. T. (2022). Characterizing photochemical ageing processes of microplastic materials using multivariate analysis of infrared spectra. *Environmental Science: Processes & Impacts*, 24, 52–61. doi:10.1039/d1em00392e.

Supplementary Materials

Table S1.	Selected references for the literature review used in sections 2.2 and 4.6 including field studies focused on marine seabed, mangroves, and beach sediments.	70
Table S2.	Selected references for sections 2.2 including field studies focused on marine waters. Figure 4.7 also bases on these references, with the exclusion of water column studies (Cai et al., 2018; Choy et al., 2019; Cincinelli et al., 2017; Courtene-Jones et al., 2017; Desforges et al., 2014; Di Mauro et al., 2017; Enders et al., 2015; Pabortsava & Lampitt, 2020; Song et al., 2018; Tekman et al., 2020; Zobkov et al., 2019; Zhou et al., 2021).	72
Figure S1.	Potential MP abundances in marine sediments extracted from the literature listed in Table S1. The calculation of those potential abundances is explained in section 4.6.	75
Figure S2.	Potential MP abundances in marine surface waters extracted from the literature listed in Table S2. The calculation of those potential abundances is explained in section 4.6.	76
Figure S3.	Overview of commonly applied sampling procedures, extraction methods, and analysis techniques for the respective sampling types. Depending on the water content, respective samples were freeze-dried or filtered before applying chemicals. No water reduction step is also possible. The listed extraction steps (density separation and digestion) were used depending on the sample characteristics and can also be skipped. The used chemicals were chosen based on availability, price, toxicity, handling, reaction speed, efficiency, and/or effects on the MPs. The listed analysis techniques can be applied for every sample type and can not be ignored.	76

Table S1. Selected references for the literature review used in sections 2.2 and 4.6 including field studies focused on marine seabed, mangroves, and beach sediments.

sampling	digestion	salt	analysis	reference
seabed				
divers	enzymatic	NaI	FTIR	Dahl et al. (2021)
corer	Fenton	NaI	FTIR	Lin et al. (2020)
divers	–	ZnCl ₂	FTIR	Martin et al. (2020)
corer	H ₂ O ₂	NaCl	FTIR	Wang et al. (2018a)
corer	H ₂ O ₂	CHKO ₂	Raman	Xue et al. (2020)
grab	–	NaCl	FTIR	Claessens et al. (2011)
corer	–	oil	FTIR	Courtene-Jones et al. (2020)
corer	H ₂ O ₂	CaCl ₂	FTIR	Li et al. (2020)
corer	Fenton	NaI	FTIR	Lin et al. (2021)
corer	H ₂ O ₂	ZnCl ₂	FTIR	Uddin et al. (2021)
corer	–	NaCl & NaI	Raman	Chen et al. (2020)
divers	–	–	visual	Alomar et al. (2016)
divers	–	NaCl	visual	Blašković et al. (2016)
divers	–	NaCl	visual	Fastelli et al. (2016)
corer	–	NaCl	FTIR	Filgueiras et al. (2019)
grab	–	NaCl & ST ¹	Raman	Frere et al. (2017)
divers	–	NaCl	FTIR	Frias et al. (2016)
grab	–	NaCl	FTIR	Graca et al. (2014)
corer	H ₂ O ₂	NaCl	FTIR	Peng et al. (2017)
corer	–	NaCl	FTIR	Reed et al. (2018)
dredge	H ₂ O ₂	NaCl	FTIR	Tsang et al. (2017)
corer	H ₂ O ₂	NaI	FTIR	Zhang et al. (2019b)
corer	H ₂ O ₂	NaCl	FTIR	Zhao et al. (2018)
corer	H ₂ O ₂	NaI	FTIR	Zhu et al. (2018)
divers	H ₂ O ₂	NaCl	FTIR	Villanova-Solano et al. (2022)
corer	–	NaCl & NaI	FTIR	Dai et al. (2018)
corer	Fenton	ZnCl ₂	FTIR	Tekman et al. (2020)
grab & corer	mixture ²	ST ¹	FTIR	Enders et al. (2019)
grab	Fenton	ZnCl ₂	FTIR	Gholizadeh & Cera (2022)
corer	–	NaCl	FTIR	Vianello et al. (2013)
grab	–	NaCl	FTIR	Leslie et al. (2017)
grab	Fenton	NaCl	FTIR	Firdaus et al. (2020)
grab	–	NaCl	FTIR	Alves & Figueiredo (2019)
corer	Fenton	NaI	visually	Willis et al. (2017)
grab	EO ³	ZnCl ₂	FTIR	Lorenz et al. (2019)
grab	H ₂ O ₂	NaCl	visually	Maes et al. (2017)

sampling	digestion	salt	analysis	reference
grab	–	ZnCl ₂	FTIR	Zheng et al. (2019)
corer	–	NaCl	FTIR	Zhou et al. (2021)
dredge	Fenton	ZnCl ₂	visually	Zobkov & Esiukova (2017)
corer	–	NaCl	visually	Cannas et al. (2017)
corer	–	NaCl	FTIR	Woodall et al. (2014)
corer	–	NaCl	FTIR	Naidoo et al. (2015)
grab	mixture ⁴	ZnCl ₂ /CaCl ₂	FTIR	Knutsen et al. (2020)
grab	H ₂ O ₂	MgCl ₂	Raman	Cutroneo et al. (2022)
corer	Fenton	ZnCl ₂	FTIR	Bergmann et al. (2017)
corer	–	NaCl & NaI	Raman	Peng et al. (2018)
corer	Fenton	ZnCl ₂	FTIR	Abel et al. (2020)
grab	H ₂ O ₂	NaI	FTIR	Patterson et al. (2019)
grab	H ₂ O ₂	NaCl	FTIR	Wang et al. (2020)
grab	–	ZnCl ₂	FTIR	Chen et al. (2018)
corer	–	ST ¹	FTIR	Huntington et al. (2020)
divers	–	NaI	visually	Graham & Thompson (2009)
grab	Fenton	NaI	visually	Ling et al. (2017)
corer	H ₂ O ₂	NaCl	visually	Cordova & Wahyudi (2016)
divers	NaOH	NaCl	visually	Sandre et al. (2019)
grab	–	NaI	visually	McEachern et al. (2019)
grab	enzymatic	ZnCl ₂	FTIR	Haave et al. (2019)
dredge	–	NaCl	visually	Ronda et al. (2019)
grab	–	–	FTIR	Mistri et al. (2020)
grab	–	NaCl	FTIR	Palatinus et al. (2019)
grab	–	NaCl	visually	Romeo et al. (2015)
corer	–	ST ¹	Raman	Ballent et al. (2016)
grab	–	NaCl	FTIR	Falahudin et al. (2020)
divers	H ₂ O ₂	ZnCl ₂	FTIR	Cheang et al. (2018)
corer	H ₂ O ₂	NaCl	FTIR	Zhang et al. (2019a)
steel plate	–	ZnCl ₂	Raman	Kazour et al. (2019)
metal cylinder	KOH	ZnCl ₂	FTIR	Bucol et al. (2020)
mangroves				
not specified	H ₂ O ₂	CaCl ₂	FTIR	Li et al. (2018b)
not specified	H ₂ O ₂	CHKO ₂	Raman	Li et al. (2018c)
spatula	–	NaCl	FTIR	Nor & Obbard (2014)
shovel	–	NaCl & NaI	FTIR	Zhou et al. (2020)
shovel	–	NaCl & NaI	FTIR	Naji et al. (2019)
spatula	–	–	FTIR	Lourenço et al. (2017)
beaches				
glass jar	–	NaCl	FTIR	Blumenröder et al. (2017)

sampling	digestion	salt	analysis	reference
spoon	–	NaCl & NaI	TD-Pyr-GC/MS ⁴	Dekiff et al. (2014)
spatula	H ₂ O ₂	ZnCl ₂	visually	Esiukova (2017)
spoon	H ₂ O ₂	elutriation	Nile Red	Hengstmann et al. (2017)
not specified	–	water	visually	Baztan et al. (2014)
not specified	–	NaCl	FTIR	Kunz et al. (2016)
spoon	–	NaCl	Raman	Lots et al. (2017)
spatula	–	NaCl	visually	Laglbauer et al. (2014)
spoon	–	NaCl & NaI	FTIR	Naji et al. (2016)
spoon	–	NaCl & NaI	FTIR	Naji et al. (2017)
watch glass	–	NaCl	FTIR	Qiu et al. (2015)
spatula	–	NaCl	FTIR	Rios-Mendoza et al. (2021)
spoon	H ₂ O ₂	CaCl ₂	visually	Stolte et al. (2015)
shovel	H ₂ O ₂	NaI	FTIR	Wu et al. (2019)
shovel	–	NaCl	FTIR	Yu et al. (2019)
shovel	–	NaCl & NaI	FTIR	Zhou et al. (2018)
tweezers	H ₂ O ₂	ZnCl ₂	FTIR	Sathish et al. (2019)
spoon	H ₂ O ₂	NaI	FTIR	Sathish et al. (2020)
spoon	–	ZnCl ₂	FTIR	Chen et al. (2018)
glass jar	H ₂ O ₂	CaCl ₂	Raman	Hamilton et al. (2021)
spoon	–	NaCl	FTIR	Carlsson et al. (2021)
trowel	H ₂ O ₂	NaCl	visually	Mathalon & Hill (2014)
corer	–	CsCl	Raman	Dodson et al. (2020)
corer or spatula	KOH or HNO ₃	KI	FTIR	Phuong et al. (2018)
spoon	KOH	KI	FTIR	Aslam et al. (2019)
shovel	H ₂ O ₂	NaCl & ZnCl ₂	FTIR	Kor et al. (2020)
not specified	–	NaCl	FTIR	Masiá et al. (2019)
shovel	–	NaCl	FTIR	Chen & Chen (2020)
steel quadrat	–	ZnCl ₂	FTIR	Atwood et al. (2019)
spatula	–	NaCl	FTIR	Abidli et al. (2018)
spatula	–	NaCl	visually	Kazmiruk et al. (2018)
steel cup	–	ZnCl ₂	FTIR	Coppock et al. (2017)
spoon	H ₂ O ₂	NaCl	visually	Karlsson et al. (2017)
not specified	H ₂ O ₂	ZnCl ₂	SEM	Retama et al. (2016)
bucket	–	NaCl	visually	Guerranti et al. (2017)
spade	–	NaCl & NaI	visually	Akhbarizadeh et al. (2017)

¹ ST = sodium polytungstate.

² mixture = SDS, enzymes, NaOH, and HCl were used.

³ EO = enzymatic-oxidative digestion.

⁴ TD-Pyr-GC/MS = thermal desorption pyrolysis gas chromatography/mass spectrometry.

Table S2. Selected references for sections 2.2 including field studies focused on marine waters. Figure 4.7 also bases on these references, with the exclusion of water column studies (Cai et al., 2018; Choy et al., 2019; Cincinelli et al., 2017; Courtene-Jones et al., 2017; Desforges et al., 2014; Di Mauro et al., 2017; Enders et al., 2015; Pabortsava & Lampitt, 2020; Song et al., 2018; Tekman et al., 2020; Zobkov et al., 2019; Zhou et al., 2021).

sampling	digestion	salt	analysis	reference
surface				
net	–	NaCl	FTIR	Rios-Mendoza et al. (2021)
canisters	H ₂ O ₂	CaCl ₂	visually	Stolte et al. (2015)
pump	H ₂ O ₂	–	FTIR	Wu et al. (2019)
net	EO ¹	ZnCl ₂	FTIR	Lorenz et al. (2019)
pump	–	–	FTIR	Zheng et al. (2019)
CTD	–	–	FTIR	Zhou et al. (2021)
net	–	–	FTIR	Yakushev et al. (2021)
net	–	–	visually	Moore et al. (2002)
pump	EO ¹	ZnCl ₂	FTIR	Roscher et al. (2021)
net	H ₂ O ₂	–	FTIR	Suteja et al. (2021)
tray	Fenton	NaCl	FTIR	Song et al. (2018)
net	–	–	visually	Aytan et al. (2016)
net	NaOH & HNO ₃	–	FTIR	Castillo et al. (2016)
net & sieve	–	–	FTIR	Chae et al. (2015)
net	–	–	visually	de Lucia et al. (2014)
net	–	–	Raman	Frere et al. (2017)
net	H ₂ O ₂	water	visually	Gewert et al. (2017)
net	–	–	FTIR	Isobe et al. (2016)
net	H ₂ O ₂	–	FTIR	Kang et al. (2015)
pump	KOH	–	FTIR	Luo et al. (2019)
net	–	–	visually	Nel & Froneman (2015)
net	–	NaCl	FTIR	Tsang et al. (2017)
net	–	–	visually	van der Hal et al. (2016)
net	–	–	visually	Wang et al. (2018b)
net	Fenton	–	FTIR	Zhang et al. (2017)
net & pump	H ₂ O ₂	ZnCl ₂	visually	Zhao et al. (2014)
pump	enzymatic	–	visually	Zhao et al. (2015)
net	–	–	FTIR	Leistenschneider et al. (2021)
not specified	H ₂ O ₂	ZnCl ₂	FTIR	Yao et al. (2019)
net	H ₂ O ₂	NaCl	FTIR	Tang et al. (2018)
CTD	EO ¹	–	FTIR	Tekman et al. (2020)
not specified	H ₂ O ₂	–	FTIR	Li et al. (2018a)
net	EO ¹	ZnCl ₂	Raman	Cabernard et al. (2018)
net	–	ZnCl ₂	FTIR	Scott et al. (2019)
net & glass bottles	–	–	FTIR	Green et al. (2018)

sampling	digestion	salt	analysis	reference
net	–	–	NIR ²	Gajst et al. (2016)
net	H ₂ O ₂	–	FTIR	Olivatto et al. (2019)
net	H ₂ O ₂	NaI	FTIR	Patterson et al. (2019)
glass bottle	H ₂ O ₂	–	FTIR	Sathish et al. (2020)
net	–	NaCl	Raman	Koongolla et al. (2018)
net	Fenton	digestion solution	FTIR	Athapaththu et al. (2020)
steel sampler	–	–	FTIR	Khalik et al. (2018)
net	H ₂ O ₂	ZnCl ₂	FTIR	Syakti et al. (2018)
container	H ₂ O ₂	–	Raman	Huang et al. (2019)
container	H ₂ O ₂	–	Raman	Nie et al. (2019)
bucket	H ₂ O ₂	–	FTIR	Dai et al. (2018)
net	–	–	FTIR	Sun et al. (2018)
net	KOH	NaCl	FTIR	Wang et al. (2020)
net	–	–	FTIR	Chen et al. (2018)
pump	H ₂ O ₂	–	FTIR	Xu et al. (2018)
CTD	Fenton	NaCl	FTIR	Zhu et al. (2018)
steel bucket	H ₂ O ₂	–	FTIR	Li et al. (2018d)
net	H ₂ O ₂	–	FTIR	Mai et al. (2018)
net	–	–	FTIR	Isobe et al. (2014)
net	Fenton	NaCl	FTIR	Mu et al. (2019)
pump	–	oil	FTIR	Ross et al. (2021)
net	–	–	FTIR	Doyle et al. (2011)
bucket	–	–	Raman	Huntington et al. (2020)
pump	mixture ³	ST	FTIR	Rist et al. (2020)
net	H ₂ O ₂	–	Raman	Hamilton et al. (2021)
sieve	–	–	FTIR	Morgana et al. (2018)
net	KOH	NaCl	FTIR	Carlsson et al. (2021)
net	SDS & H ₂ O ₂	–	FTIR	Hänninen et al. (2021)
steel apparatus	–	–	visually	Gray et al. (2018)
net	Fenton	NaCl	FTIR	Ferreira et al. (2020)
Van Dorn sampler	mixture ⁴	–	visually	McEachern et al. (2019)
net	H ₂ O ₂	–	visually	Ronda et al. (2019)
glass jar	H ₂ O ₂	–	visually	Karlsson et al. (2017)
net	–	–	Raman	Kazour et al. (2019)
column				
net & pump	H ₂ O ₂	NaCl	FTIR	Cai et al. (2018)
net & pump	H ₂ O ₂	NaCl	FTIR	Cai et al. (2018)
grab	–	–	Raman	Choy et al. (2019)
pump	–	–	FTIR	Cincinelli et al. (2017)
CTD	–	–	FTIR	Courtene-Jones et al. (2017)
pump	HCl	–	Nile Red	Desforges et al. (2014)

sampling	digestion	salt	analysis	reference
net & CTD	HF	–	FTIR	Di Mauro et al. (2017)
pump	SDS	–	Raman	Enders et al. (2015)
net	–	–	FTIR	Lefebvre et al. (2019)
pump	KOH	–	FTIR	Pabortsava & Lampitt (2020)
pump	Fenton	NaCl	FTIR	Song et al. (2018)
CTD	SDS & EO ¹	–	FTIR	Tekman et al. (2020)
pump	Fenton & HCl	–	Raman	Zobkov et al. (2019)
CTD	–	–	FTIR	Zhou et al. (2021)

¹ EO = enzymatic-oxidative digestion.

² NIR = near-infrared spectroscopy.

³ mixture = SDS, various enzymes, Fenton and NaOH.

⁴ mixture = Tris HCl, EDTA, NaCl, SDS, proteinase K and NaClO₄.

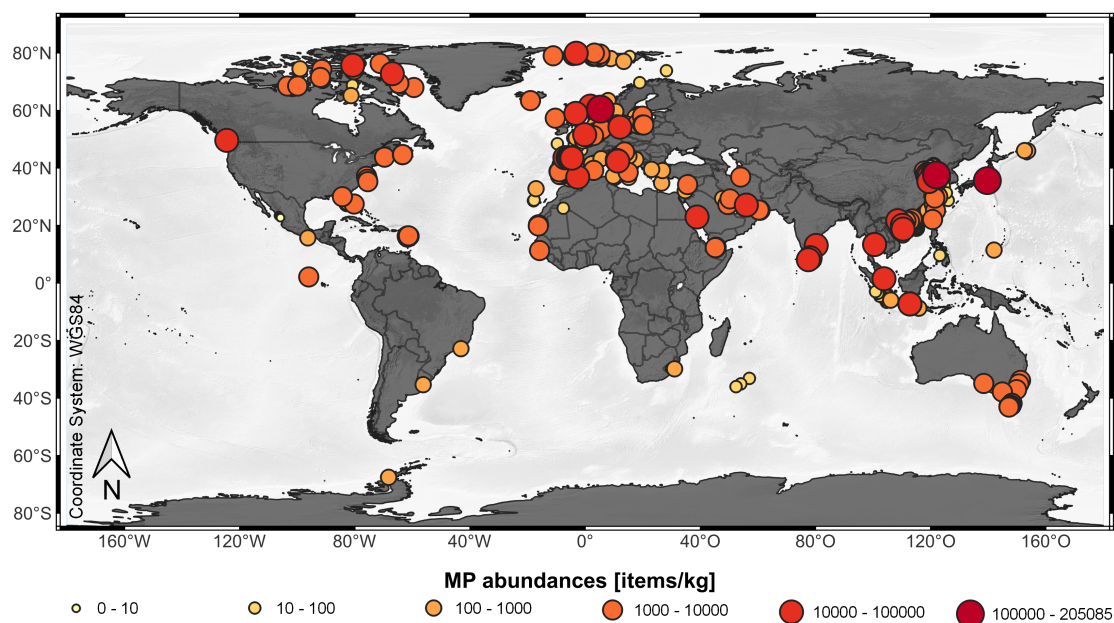


Figure S1. Potential MP abundances in marine sediments extracted from the literature listed in Table S1. The calculation of those potential abundances is explained in section 4.6.

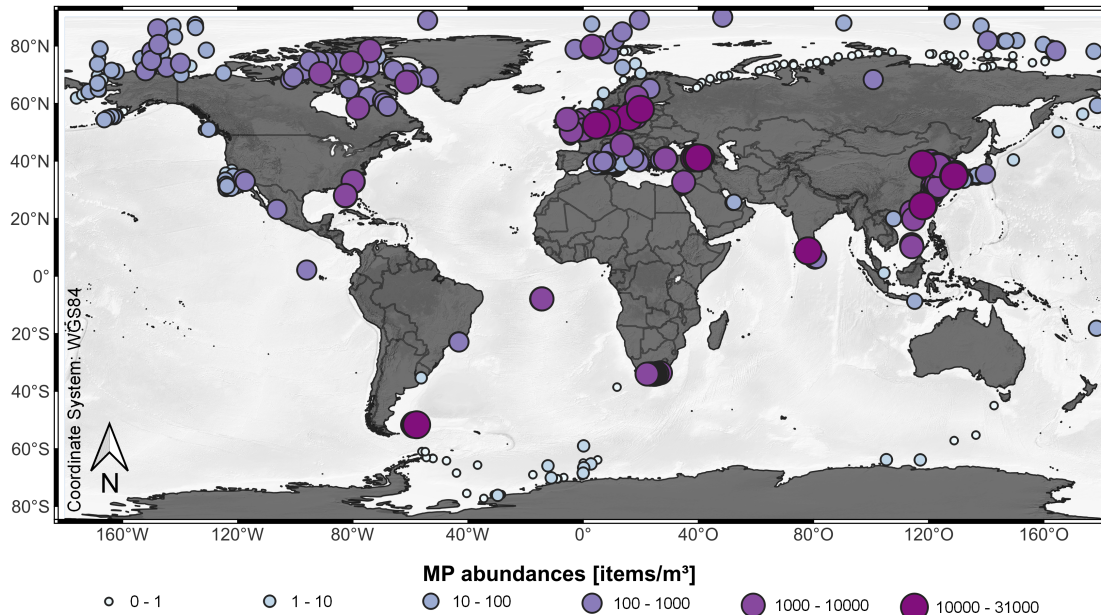


Figure S2. Potential MP abundances in marine surface waters extracted from the literature listed in Table S2. The calculation of those potential abundances is explained in section 4.6.

Sampling type	Sampling procedure	Extraction method	Analysis	
Sediment sample	Offshore: <ul style="list-style-type: none"> Box corer Gravity corer Grab Divers Dredge Onshore: <ul style="list-style-type: none"> Spatula Spoon Shovel Glass jar 	Contains sediments Density separation: <ul style="list-style-type: none"> NaCl NaI ZnCl₂ CaCl₂ MgCl₂ ST HCO₂K KI CsCl Water Mixtures Contains biota Digestion: <ul style="list-style-type: none"> H₂O₂ Fenton Enzymatic KOH NaOH HNO₃ SDS HF HCl Mixtures 	<ul style="list-style-type: none"> Visually FTIR Raman 	
Sediment trap sample	<ul style="list-style-type: none"> Funnel PVC tube 			Freeze-drying
Water sample	<ul style="list-style-type: none"> Nets (Neuston, Manta) Pumping system CTD Canister Sieve 			Filtration

Figure S3. Overview of commonly applied sampling procedures, extraction methods, and analysis techniques for the respective sampling types. Depending on the water content, respective samples were freeze-dried or filtered before applying chemicals. No water reduction step is also possible. The listed extraction steps (density separation and digestion) were used depending on the sample characteristics and can also be skipped. The used chemicals were chosen based on availability, price, toxicity, handling, reaction speed, efficiency, and/or effects on the MPs. The listed analysis techniques can be applied for every sample type and can not be ignored.

Contributions to the Manuscripts

Publication I

Reineccius, J., Bresien, J., Waniek, J.J. (2021). Separation of microplastics from mass-limited samples by an effective adsorption technique. *Science of the Total Environment*. 788, 147881. doi: 10.1016/j.scitotenv.2021.147881

This manuscript was conceptualized by J.J. Waniek and J. Reineccius. Experimental laboratory work, data analysis, and writing of the manuscript were performed by J. Reineccius. Measurement instruments and handling were provided by J. Bresien. The manuscript was reviewed by all authors. The contribution of J. Reineccius to this manuscript was approximately 90%.

Publication II

Reineccius, J. & Waniek, J.J. (2022). First long-term evidence of microplastic pollution in the deep subtropical Northeast Atlantic. *Environmental Pollution*. 305, 119302. doi: 10.1016/j.envpol.2022.119302

For this study, J. Reineccius performed laboratory work, including microplastic extraction and analysis for every sample. The samples and necessary foundations were provided by J.J. Waniek. Data evaluation and writing of all manuscript versions were implemented by J. Reineccius. J.J. Waniek reviewed all versions and supervised the evaluation approaches. Approximate contribution to this work by J. Reineccius of 80%.

Publication III

Reineccius, J., Schönke, M., Waniek, J.J. (2022). Abiotic long-term simulation of microplastic weathering pathways under different aqueous conditions. *Environmental Science and Technology*. (accepted). doi: 10.1021/acs.est.2c05746

This work was conceptualized by J. Reineccius and J.J. Waniek. J. Reineccius introduces the idea and first experimental setups. Under supervision and foundation by J.J. Waniek, the experimental procedure was enabled and refined. All laboratory works, analysis, and data evaluation was conducted by J. Reineccius. The evaluation of roughness measurements was supported by the specific experience of M. Schönke. All manuscript versions were drafted by J. Reineccius. J.J. Waniek and M. Schönke reviewed all versions. Approximate contribution to this work by J. Reineccius of 85%.

Publication I

Full Research Paper, *Science of the Total Environment journal*, 2021

Separation of microplastics from mass-limited samples by an effective adsorption technique

Janika Reineccius, Jonas Bresien, Joanna J. Waniek

Submitted: 3 March 2021; Accepted: 13 May 2021

doi: 10.1016/j.scitotenv.2021.147881

Abstract Microplastic in the environment hides visible and invisible dangers for the ecosystems and domiciled organisms. Due to the large quantities of microplastics already distributed worldwide, comparative studies to investigate the associated hazards, distribution patterns, and abundances are becoming increasingly important. Due to varying efforts and budgets, there is still no homogenized detection method for microplastics in the environment, which severely compromises the comparability and reliability of results between previous studies. In this study, we compare the efficacy, degradative effect on microplastics, and microplastic recovery rates of different digestion and separation methods for isolating microplastics from mass-limited environmental samples with high biogenic content. Our results show that the most gentle and effective isolation method is an adsorption-based technique that exploits the lipophilic properties of plastic for separation. This technique achieves an average microplastic recovery rate of $98.0 \pm 3.8\%$ and a matrix removal of $96.3 \pm 0.3\%$ at low cost and minimum effort. To examine the applicability of this technique to natural environmental samples, eight sediments and two plankton net samples from the South China Sea were selected to determine microplastic abundances. In the analyzed sediment samples, 0–9 microplastic items per 10 g sediment d.w. were found, while 17–25 items per m^3 were detected in net samples. Considering the respective mean plastic density, this corresponds to a calculated microplastic mass of $0\text{--}39 \mu\text{g} (10 \text{ g d.w.})^{-1}$ and $3.7\text{--}7.1 \mu\text{g m}^{-3}$ in sediment and water samples, respectively. This study represents a new way of microplastic extraction from matrix-rich mass-limited samples with high accuracy and easy feasibility at low costs, which would be useful as a worldwide homogenized method in future microplastic research projects and related data comparability.



Separation of microplastics from mass-limited samples by an effective adsorption technique

Janika Reineccius^{a,*}, Jonas Bresien^b, Joanna J. Waniek^a

^a Leibniz Institute of Baltic Sea Research, Warnemünde, Seestraße 15, 18119 Rostock, Germany

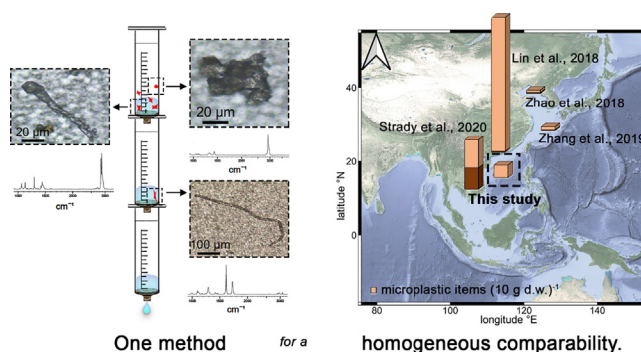
^b Institute of Chemistry, University of Rostock, Albert-Einstein-Straße 3a, 18059, Germany



HIGHLIGHTS

- New efficacy technique to separate microplastic from matrix-rich mass-limited samples.
- Adsorption separation method separated small-sized microplastics with high accuracy.
- Combined adsorption separation technique reaches a matrix removal of >96%.
- Commonly used digestion agents degrade microplastics.
- The new combined adsorption separation technique allows microplastic extraction from the particulate phase of marine samples.

GRAPHICAL ABSTRACT



ARTICLE INFO

Article history:

Received 3 March 2021

Received in revised form 22 April 2021

Accepted 13 May 2021

Available online 19 May 2021

Editor: Thomas Kevin V

Keywords:

Marine pollution
Adsorption separation
Plastic extraction
Microplastics
Matrix-rich samples
South China Sea

ABSTRACT

Microplastic in the environment hides visible and invisible dangers for the ecosystems and domiciled organisms. Due to the large quantities of microplastics already distributed worldwide, comparative studies to investigate the associated hazards, distribution patterns, and abundances are becoming increasingly important. Due to varying efforts and budgets, there is still no homogenized detection method for microplastics in the environment, which severely compromises the comparability and reliability of results between previous studies. In this study, we compare the efficacy, degradative effect on microplastics, and microplastic recovery rates of different digestion and separation methods for isolating microplastics from mass-limited environmental samples with high biogenic content. Our results show that the most gentle and effective isolation method is an adsorption-based technique that exploits the lipophilic properties of plastic for separation. This technique achieves an average microplastic recovery rate of $98.0 \pm 3.8\%$ and a matrix removal of $96.3 \pm 0.3\%$ at low cost and minimum effort. To examine the applicability of this technique to natural environmental samples, eight sediments and two plankton net samples from the South China Sea were selected to determine microplastic abundances. In the analyzed sediment samples, 0–9 microplastic items per 10 g sediment d. w. were found, while 17–25 items per m^3 were detected in net samples. Considering the respective mean plastic density, this corresponds to a calculated microplastic mass of $0\text{--}39 \mu\text{g} (10 \text{ g d.w.})^{-1}$ and $3.7\text{--}7.1 \mu\text{g m}^{-3}$ in sediment and water samples, respectively. This study represents a new way of microplastic extraction from matrix-rich mass-limited samples with high accuracy and easy feasibility at low costs, which would be useful as a worldwide homogenized method in future microplastic research projects and related data comparability.

© 2021 The Authors. Published by Elsevier B.V. This is an open access article under the CC BY license (<http://creativecommons.org/licenses/by/4.0/>).

* Corresponding author.

E-mail address: janika.reineccius@io-warnemuende.de (J. Reineccius).

1. Introduction

Plastic is one of the most common anthropogenic litter in the environment today (Derraik, 2002). It has been detected in terrestrial soils (Liu et al., 2018; Zhang et al., 2018b), in the air (Dris et al., 2017), in every ocean (Barnes et al., 2009; C  zar et al., 2014; Kanhai et al., 2017), and even in Arctic deep-sea sediments (Bergmann et al., 2017). Due to the permanently increasing production, consumption, and recycling mismanagement (Gourmelon, 2015), the environmental abundances are rising inexorably. By 2050, it is estimated that 12,000 million metric tons of plastic waste will be deposited in landfills or natural environments (Geyer et al., 2017), distributed across the globe by natural physical forces, and finally ending up in the marine environment (Alimba and Faggio, 2019; Mishra et al., 2019). Based on these global occurrences, the current era is already termed "Plasticene" (Alimi et al., 2018; Reed, 2015). Microplastics are the most frequently detected plastics worldwide, defined in the size range of 1–5000 μm (Hidalgo-Ruz et al., 2012). Due to their durability, ubiquity, lightweight, and wide range of colors and sizes, microplastic particles are often mistaken for prey by marine species (Di Mauro et al., 2017), accumulating in the food web (Avio et al., 2020; Nelms et al., 2018), and finally reaching the human diet (Auta et al., 2017; Carbery et al., 2018).

Plastic polymers themselves are considered chemically inert, but pollutants added during the manufacture, such as monomer residues or various additives like phthalates, Bisphenol A, or organophosphorus esters, can pose a threat to the environment and organisms (Suhrhoff and Scholz-B  ttcher, 2016; Teuten et al., 2009; H. Zhang et al., 2018a). Additionally, lipophilic persistent organic pollutants (Frias et al., 2010; Ogata et al., 2009; Rios et al., 2007), harmful metals (Brennecke et al., 2016; Graca et al., 2014), or pathogens (Zettler et al., 2013) originating from the surrounding water can sorb on the microplastic surface and thus be transported over long distances across the globe. To monitor the current and future hazards, it is necessary to investigate extensively the distribution patterns of microplastic abundances on a larger spatial scale. However, environmental samples offer a great natural matrix diversity, which requires different extraction steps to separate microplastic. Marine environmental sample types can be generally categorized as sedimentary, organic-rich, or aqueous matrices, which can be obtained from the seafloor (Bergmann et al., 2017; Coppock et al., 2017; Nuelle et al., 2014), on the beach (Lots et al., 2017; Yu et al., 2016), from marine organisms (Karlsson et al., 2017; Sun et al., 2017), or the water column using plankton nets, pumps (Di Mauro et al., 2017; Wang and Wang, 2018), or sediment traps (Ballent et al., 2016; Reineccius et al., 2020).

The first necessary step for the microplastic determination in marine samples is the removal of the sample matrix, whose preparation method is strongly dependent on the sample type and available resources. For samples with large amounts of sand or sediment, performing a density separation is most effective, while a digestion step is used to remove organic-rich interfering matrix (Karlsson et al., 2017). In recent studies, a range of different salt solutions was utilized for density separation, such as sodium chloride (NaCl) (Lots et al., 2017; Tsang et al., 2017), zinc chloride (ZnCl_2) (Bergmann et al., 2017; Coppock et al., 2017), sodium iodide (NaI) (Claessens et al., 2013), potassium iodide (KI) (Phuong et al., 2018), zinc bromide (ZnBr_2), sodium bromide (NaBr) (Quinn et al., 2017), calcium chloride (CaCl_2) (Stolte et al., 2015), sodium polytungstate (K  ppler et al., 2016), sodium tungstate dihydrate (Kanhai et al., 2019; Pagter et al., 2018), lithium metatungstate (Masura et al., 2015), or potassium formate solution (Zhang et al., 2016). Additionally, non-saline substances like canola oil or ethanol were used for sediment removal (Crichton et al., 2017; Herrera et al., 2018). The digestion step is often carried out with single or combined acids such as hydrochloric acid (HCl), nitric acid (HNO_3) (Desforges et al., 2015; Van Cauwenberghe et al., 2015; Van Cauwenberghe and Janssen, 2014), sulfuric acid (Imhof et al., 2016), sodium hypochlorite solution (Enders et al., 2017) or with alkaline agents

such as potassium hydroxide (KOH) (Lin et al., 2018; Luo et al., 2019) or sodium hydroxide (NaOH) (Bellas et al., 2016; Budimir et al., 2018). However, the acid, as well as the alkaline digestion agents, have been ascertained to prejudice various types of microplastic (Hurley et al., 2018; Karami et al., 2017; Olsen et al., 2020). Therefore, oxidizing agents such as hydrogen peroxide (H_2O_2) or perchloric acid (Devriese et al., 2015) were introduced, which showed less influence on polymer types in previous studies (Prata et al., 2019). Another new procedure is the use of a urea solution combined with thiourea and NaOH to remove cellulosic-rich sample components (Olsen et al., 2020), however, for this method, the application of the microplastic degrading NaOH is required. A more gentle and effective plastic separation was achieved by using enzymes (Karlsson et al., 2017), but these methods are expensive, time-consuming, and require various intermediate steps which are prone to be contamination sources.

Summarized, an effective and gentle sample matrix removal, especially for organic-rich sediment samples, is complex and can lead to analyte losses or sample contamination due to the diverse intermediary steps and chemicals (Dehaut et al., 2019). In addition, for some institutions, the high financial and time investment for an effective and gentle separation method is not affordable, leading to the utilization of simpler and less precise methods instead (Strady et al., 2020). However, using such a variety of different separation microplastic methods impeded the result comparisons between different field studies (Dehaut et al., 2019). An effective and inexpensive method to remove inorganic and natural organic particles in combination with the microplastic detection by Nile red, Raman, or Fourier transform infrared spectroscopy (FT-IR) would lead to higher accuracy and contribute majorly to the global comparability of microplastic abundances.

In this study, we present a uniform efficient microplastics extraction technique by removing matrices from several mass-limited marine sample types. Towards this aim, we compared the results of different implemented treatment protocols with the newly developed adsorption technique and tested this method on selected natural marine samples. With this study, we provide a new effective and inexpensive microplastic isolation method for different sample types that guarantees quick and unequivocal detection.

2. Materials & methods

2.1. Matrix removal efficacy

One of the biggest challenges in microplastic detection is the reliable differentiation between plastic and naturally occurring particles. Similar looking remains of shells, zooplankton, phytoplankton, or sediments are still present in the sample even after commonly used isolation methods and increase the effort for microplastic particle detection by visual or spectral analysis methods. To minimize effort and error in microplastic analysis, biogenic and non-biogenic components of the sample must be removed without degrading microplastics.

To meet these requirements, the first step of this study was to optimize the removal efficacy of digestion chemicals. For this purpose, the effectiveness of 15 different treatment protocols was tested on a biogenic-rich sample without microplastics. Based on the resulting most effective procedures, the second step was to investigate the chemical resistance of microplastic on nine different types of virgin microplastics. In the third step, two different methods for separating non-biogenic components of the sample were compared. The most effective and gentle combination of digestion and separation step with the least degrading impact on microplastics was applied in the remainder of this study.

2.1.1. Digestion protocols for the removal of biogenic materials

To investigate the effectiveness of biogenic matrix removal, a total of 15 different digestion protocols were performed on a uniform, biogenic-rich sample. The protocol with the highest digestion efficacy will

subsequently be used for further investigation within this study. The biogenic-rich sample used for each protocol was collected from the wash margin on the Baltic Sea coast (Warnemünde, Germany) and

consisted predominantly of various algae, mussels, and plankton. The biogenic material was rid of sediments, rinsed with ultrapure water, pre-shredded in a mixer, and left to dry under the fume hood. For

Protocol No.	step	chemicals	volume [mL]	exposure time [h]	temp. [°C]
1	1	H ₂ O ₂ (30%)	5	24	50
2	1	Fenton-HCl	9	24	50
3	1	Fenton-HAc	9	24	50
4	1	KOH (224 g L ⁻¹)	5	48	50
5	1	H ₂ O ₂ (30%)	5	7	50
6	1	Fenton-HAc	9	7	50
7	1	HAc (24%)	5	2	RT
	2	Ethanol (96%)	5	2	50
	3	H ₂ O ₂ (30%)	5	24	50
8	1	HAc (24%)	5	2	RT
	2	detergent solution	0.5	2	50
	3	H ₂ O ₂ (30%)	5	24	50
9	1	SDS (5 g L ⁻¹)	5	24	50
	2	HAc (24%)	5	2	RT
	3	H ₂ O ₂ (30%)	5	24	50
10	1	NH ₃ (25%)	5	3	RT
	2	HAc (24%)	5	2	RT
	3	H ₂ O ₂ (30%)	5	24	50
11	1	H ₂ O ₂ (30%)	5	24	50
	2	HAc (24%)	5	2	RT
	3	NH ₃ (25%)	5	3	RT
12	1	UV-H ₂ O ₂ (30%)	5	24	RT
	2	HAc (24%)	5	2	RT
	3	NH ₃ (25%)	5	3	RT
13	1	H ₂ O ₂ (30%)	5	24	50
	2	HAc (24%)	5	2	RT
14	1	H ₂ O ₂ (30%)	5	24	50
	2	HAc (24%)	5	2	RT
	3	saturated urea solution	10	0.7 + 24	-20 + RT
15	1	H ₂ O ₂ (30%)	5	24	50
	2	HAc (24%)	5	2	RT
	3	Schweizer reagent	5	2	RT

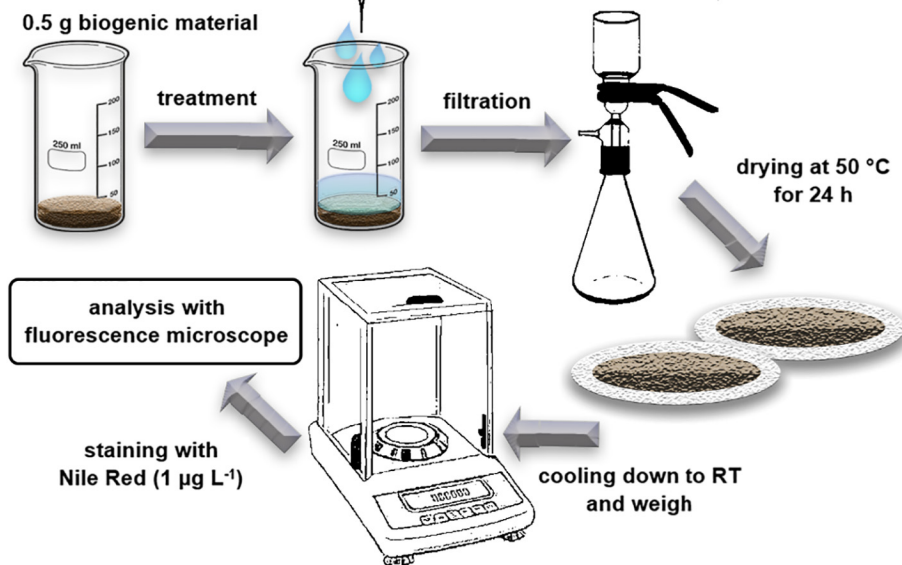


Fig. 1. The general treatment procedure of the biogenic material by the 15 digestion protocols. The digestion chemicals, volumes, exposure times, and temperatures used are described for each protocol in the framed table. After the treatment, the samples were filtrated and dried to determine the residual biogenic weight and fluorescence. HAc = acetic acid, RT = room temperature.

each protocol, 0.5 g of the dry biogenic material were weighed in a beaker in triplicates and covered with aluminum foil between the processing steps.

The following paragraph gives an overview of the 15 conducted experiments for the digestion of the biogenic material, summarized in the protocols listed in Fig. 1. The protocols 1 through 4 were conducted according to published methods (Avio et al., 2015; Dehaut et al., 2016; Hurley et al., 2018; Karami et al., 2017; Tagg et al., 2017). The authors utilized effective and gentle digestion agents to dissolve biogenic material, such as H₂O₂ (30%), Fenton reagent, and KOH. The Fenton reagent in the current study was prepared according to the instructions of Bergmann et al. (2017) by mixing acid, ultrapure water, and ferrous sulfate heptahydrate (VWR International, Germany), with H₂O₂ (30% for synthesis, Merck KGaA, Germany) in a 1:2 ratio. The acid used for Fenton acidification varies between protocol 2 acetic acid (96%, VWR International, Germany) and protocol 3 HCl (32%, Merck KGaA, Germany) (Fig. 1). For the first four protocols, the digestion agents were added to the biogenic material and allowed to react at 50 °C for 24 h. The samples, to which KOH (224 g L⁻¹, KOH pellets from Labsolute, Germany) was added, were treated for additional 24 h due to the low material removal after the first 24 h. Protocols 5 and 6 were conducted to compare the biogenic removal efficacy between the H₂O₂ and the Fenton reagent at a reduced chemical exposure time of 7 h. The more effective oxidizing agent H₂O₂ was used for the remaining protocols. For protocols 7–10, a combination of three different chemicals was applied. Before adding the oxidizing H₂O₂, acetic acid (24%) was added to the four protocols 7–10 as a weak, gentle acid and was allowed to react for 2 h at room temperature to dissolve calcareous materials. Further, the fat dissolving agent's ethanol (96%, Merck KGaA, Germany) (protocol 7), detergent (Fit GmbH, Germany) (protocol 8), SDS (5 g L⁻¹, salt from Merck KGaA, Germany) (protocol 9), and ammonia (NH₃, 25%, Otto Fischer GmbH & Co. KG, Germany) (protocol 10) were added to support the subsequent reaction of the lipophobic H₂O₂. The batch-specific volumes, exposure time, and reaction temperature used for protocols 7–10 are listed in Fig. 1. The most effective method of these four protocols is further applied in protocols 11 and 12. Protocol 11 was conducted with an inverse chemical sequence to protocol 10 to investigate the effect of different treatment sequences. In protocol 12, instead of iron ions or high temperatures, samples were illuminated with ultraviolet radiation (UV) for H₂O₂ activation. In the presence of UV radiation, free hydroxyl radicals of H₂O₂ were generated, increasing the reactive state of the solution, which is classified as the most reactive oxidant in the water treatment (Koivunen and Heinonen-Tanski, 2005). The treatment procedure remains as in protocol 11, with 5 mL of H₂O₂ added to the sample and illuminated for 24 h under UV radiation. After radiation, 5 mL of acetic acid and 5 mL ammonia were added for 2 and 3 h reaction time, respectively. The entire treatment procedure is carried out at room temperature.

Protocols 13, 14, and 15 were performed to examine the removal of poorly soluble cellulose fractions that remained after the sample treatment of protocols 1–12. In the first step, 5 mL of H₂O₂ were added to the samples, which was panned at 10–15 min intervals during the first 4 h of the total 24 h exposure time to maintain contact of the samples with the oxidant. Then 5 mL of acetic acid was added and allowed to react for 2 h at room temperature. The samples of protocol 13 were prepared without a cellulose solving agent for comparison purposes, while the samples of protocol 14 were further treated with a saturated urea solution and the samples of protocol 15 with a Schweizer reagent. The usage of urea was previously reported by Olsen et al. (2020) in combination with thiourea and NaOH to dissolve cellulosic compartments. Instead of this combination used by the authors, 10 mL of a saturated urea solution (Sigma Aldrich, Germany) were added to the samples and stored at -20 °C to allow crystallization. After 40 min, the sample was warmed to room temperature and allowed to react for additional 24 h. For protocol 15, the Schweizer reagent was applied to dissolve cellulosic fractions instead of urea. Due to strong reactions of the copper

solution with H₂O₂ from the previous step, the pre-treated biogenic material was filtered and rinsed with ultrapure water before proceeding. The filtrated solid phase was transferred to another glass container and treated with 5 mL of the Schweizer reagent. After 2 h of exposure time, the Schweizer reagent solution was filtered again, reusing the filters from the previous step to avoid loss of material. The loaded filters were rinsed firstly with ammonia (25%) until colorlessness and secondly with ultrapure water before drying. The Schweizer reagent was prepared from a copper (II) sulfate pentahydrate granule (Sigma-Aldrich, Germany), a detailed description of the preparation procedure can be found in the supplement materials (protocol S1).

After applying the treatment, protocols the resulting samples were filtered, using a glass microfiber filter (Whatman™; 47 mm diameter; 0.7 µm pore size; CatNo. 1825-047) and a vacuum filtration device. The obtained filters were dried at 50 °C for 24 h and weighed with a precision balance (ABT 120-5DM/Kern) after cooling the filter down to determine the weight removal.

In addition to the weight determinations, the efficiency of matrix removal was examined by staining the sample residues with Nile red, which has been used in previous studies to stain and detect microplastic particles (Erni-Cassola et al., 2017; Shim et al., 2016; Tamminga, 2017). Due to the lipophilicity of plastic, the solved dye Nile red adheres to the particle surface, causing it to fluoresce at specific extinction wavelengths (Erni-Cassola et al., 2017). Besides microplastic, some natural lipids were also stained and fluoresced in the same wavelength range, which significantly limited the unambiguous identification of the microplastic particles (Araujo et al., 2018). In this study, Nile red was utilized as an indicator for these natural materials to detect disturbing residues. The fewer particles fluoresce, the more effective the treatment method was and the lower the risk of confusion with potential microplastic particles. For determination of residual fluorescence, the obtained sample filters of each treatment protocol were stained with a 1 µg mL⁻¹ concentrated Nile red solution (Sigma-Aldrich, Germany) solved in methanol (99.9%, Carl Roth, Germany) according to the instructions of Erni-Cassola et al. (2017). The dried stained filters were examined at extinction wavelengths of 460–525 nm under an Axioskop 2 mot plus fluorescence microscope. The microscope from Carl Zeiss (Germany) with 10× optical magnification is equipped with an AxioCam 503 color camera using the AxioVision and ZEN blue software. To compare the background fluorescence between the protocols, images of fluorescent fragment residues and images at a uniform exposure time of 600 ms were acquired for each filter.

2.1.2. Influence of reagents on microplastic degradation

A suitable digestion step for the microplastic determination must not only effectively eliminate biogenic material, but also be gentle to the microplastic particles. To investigate the degree of microplastic degradation caused by the previously used digestion chemicals, microplastic particle size loss, and weight changes were monitored for nine different plastic types in this section. In addition to the most frequently detected plastic types in the environment, such as high-density polyethylene (HDPE, density 955 kg m⁻³, CS Plastik GmbH, Germany), polypropylene (PP, density 0.91 g m⁻³, BASF Novolen® 1101 M), polyethylene terephthalate (PET, density 1.34 g m⁻³, Bühler bottle grade recycled), polystyrene (PS, density 1.05 g m⁻³, BASF 143 E), polyamide (PA, density 1.14 g m⁻³, BASF PA6 EXA® Mid) and polyvinyl chloride (PVC, density 1.56 g m⁻³, WestChemie Rigid-PVC Type 4122) (Andrady, 2011), three less frequently identified types were used as well, such as polyoxymethylene (POM, density 1.42 g m⁻³, DuPont Derlin® 100), polymethylmethacrylate (PMMA, density 1.19 g m⁻³, PLEXIGLAS® 7 N Degussa) and acrylonitrile butadiene styrene copolymer (ABS, density 1.05 g m⁻³, Dow Chemical, Magnum 3404). The acquired granules of each plastic type were crushed separately with a mixer.

To assess the changes in particle size, approximately 10 individual particles of each crushed plastic type were selected using tweezers,

Table 1
 Size, weight, and particle recovery rates for various microplastics after treatment or separation methods. For size and weight recoveries, nine virgin polymer types were tested on the individual chemicals applied in different protocols (Section 2.1.2). All values are given in percent [%] with standard deviation as error range. Significant degradation effects are given in bold. Particle recovery rates were determined for two methods, as described in Section 2.1.3, with virgin microplastics for both methods and beached microplastics for the adsorption separation technique.

Protocol No.	Method	PE	PP	PET	PS	PVC	PA	PMMA	POM	ABS	Mean
Size recovery [%]											
13; 15	HAc (2 h / RT)	100.2 ± 3.4	100.0 ± 3.4	100.4 ± 3.7	100.1 ± 2.9	101.2 ± 4.0	104.5 ± 4.0	99.8 ± 3.7	100.1 ± 6.4	99.9 ± 2.9	100.7 ± 2.3
13; 15	H ₂ O ₂ (24 h / 50 °C)	99.7 ± 3.5	100.0 ± 3.8	100.8 ± 3.4	100.0 ± 3.2	101.0 ± 4.2	96.9 ± 5.7 (a)	101.3 ± 3.7	100.1 ± 5.2	99.9 ± 2.3	100.0 ± 4.0
13; 15	H ₂ O ₂ (48 h / 50 °C)	99.2 ± 3.4	100.7 ± 3.6	100.4 ± 3.9	100.0 ± 3.1	101.5 ± 3.7	54.9 ± 4.6 (2b, 2c)	100.9 ± 4.1	99.5 ± 5.3	100.4 ± 2.5	95.3 ± 21.0
15	NH ₃ (24 h / RT)	100.8 ± 4.3	100.7 ± 2.7	100.0 ± 2.5	100.8 ± 2.3	100.2 ± 3.3	99.7 ± 3.7	100.0 ± 3.6	100.3 ± 3.6	99.8 ± 3.2	100.3 ± 1.6
15	Schw. reagent (2 h / RT)	99.9 ± 3.0	99.5 ± 3.1	99.9 ± 1.9	100.3 ± 3.8	100.4 ± 4.4	100.4 ± 4.0	100.2 ± 3.9	100.0 ± 4.0	99.7 ± 4.6	100.0 ± 1.3
4	KOH (48 h / 50 °C)	100.2 ± 2.1	99.9 ± 3.3	- (5b)	100.2 ± 3.0	99.6 ± 2.5 (2L, 5c)	100.3 ± 4.5	100.8 ± 2.5	99.7 ± 2.4 (1L)	100.1 ± 2.8	89.0 ± 32.4
Weight recovery [%]											
13; 15	HAc (2 h / RT)	100.0 ± 0.6	101.5 ± 1.7	100.0 ± 0.6	99.0 ± 2.0	89.9 ± 1.2	100.8 ± 1.2	100.2 ± 0.6	99.8 ± 0.3	100.8 ± 0.8	99.1 ± 3.4
13; 15	H ₂ O ₂ (24 h / 50 °C) + HAc (2 h / RT)	99.4 ± 1.1	101.7 ± 2.4	100.1 ± 0.3	100.1 ± 1.8	88.7 ± 1.4	101.1 ± 1.3	99.9 ± 0.7	100.9 ± 0.4	100.9 ± 0.7	99.2 ± 3.8
15	Schw. reagent (2 h / RT)	100.0 ± 1.8	101.6 ± 2.2	99.4 ± 0.9	100.5 ± 1.0	100.8 ± 0.8	100.9 ± 1.6	100.4 ± 0.5	99.2 ± 0.6	100.8 ± 1.1	100.4 ± 0.9
Particle recovery [%]											
Density separation											
Adsorption separation											
		98.5 ± 0.3	97.8 ± 0.5	99.1 ± 0.7	98.8 ± 0.8	93.2 ± 4.6	100.3 ± 0.4	98.8 ± 0.9			98.1 ± 2.1
		100.0 ± 0.0	100.0 ± 0.0	99.0 ± 0.8	100.0 ± 0.0	98.7 ± 1.2	88.7 ± 8.6	99.3 ± 0.9			98.0 ± 3.8
		Yellow cap	Blue rope	Transp. tape	Dog toy	Silver foil	Transp. foil				
		98.5 ± 1.7	99.5 ± 0.8	99.7 ± 0.7	96.0 ± 1.5	98.8 ± 1.3	99.2 ± 1.9				98.6 ± 2.1

1, 2, 3, 4, 5 Count of affected particles out of five measured particles.
C, L, D Degree of influence (C: discoloration, L: loss in size D: heavily destroyed).
 - = measurement not possible due to strong decomposition.
 RT = room temperature.
 HAc = acetic acid.

Table 2

Comparison of sampling procedure, microplastic detection method, and resulting microplastic abundances for this study with similar previous studies. Results of microplastic abundances in sediments and water column samples are given in items per 10 g d.w. and items per m³, respectively.

Location	Abundance [items (10 g d.w.) ⁻¹ ; [items m ⁻³]	Sampling procedure	Water depth [m]	Size range [μm]	Digestion agent	Density solution	Identification	Reference
Sediments								
Hong Kong, China	0.49–2.79	Ekman dredge	n.g.	10–5000	H ₂ O ₂	NaCl	FTIR	Tsang et al. (2017)
Vietnam, Southeast Asia	15.42–20.24	PVC tube corer	0.5–5.2	250–5000	H ₂ O ₂	NaCl	FTIR	Strady et al. (2020)
South China Sea	0–9	Multi corer	37–3695	≥10	H ₂ O ₂ + HAc	–	Raman	This study
Pearl River, China	0.80–95.97	Van Veen grab	n.g.	20–5000	KOH	NaCl	FTIR	Lin et al. (2018)
Changjiang Estuary, China	0.20–3.40	Box corer	0–36	47–5000	H ₂ O ₂	NaCl	FTIR	Peng et al. (2017)
Yellow Sea and East China Sea, China	0.60–2.40	Box corer	45–80	60–5000	H ₂ O ₂	NaI	FTIR	Zhang et al. (2019a)
Bohai Sea and Yellow Sea, China	0.72–1.72	Box sampler	12–78	60–5000	H ₂ O ₂	NaCl	FTIR	Zhao et al. (2018)
Bay of Brest, France	0–0.09	Van Veen grab	0–50	87–5000	–	NaCl + ST	Raman	Frère et al. (2017)
Japan, Thailand, Malaysia, South Africa	1.00–19.00	Gravity corer	2–25	300–5000	H ₂ O ₂	NaI	FTIR	Matsuguma et al. (2017)
Arctic deep sea	0.42–65.95	Multi corer	250–5500	<11–5000	Fenton	ZnCl ₂	FTIR	Bergmann et al. (2017)
Arctic Ocean	0–2.00	Gravity and Piston corers	855–4353	≥100	–	ST	FTIR	Kanhai et al. (2019)
Water column samples								
South China Sea	0–0.33	Bongo net (333 μm)	0–200	20–5000	H ₂ O ₂	NaCl	FTIR	Cai et al. (2018)
South China Sea	301–7467	pumping system (44 μm)	surface	20–5000	H ₂ O ₂	NaCl	FTIR	Cai et al. (2018)
South China Sea	0.148–0.842	Neuston net (160 μm)	surface	≤5000	–	–	FTIR	Wang et al. (2019)
Hong Kong, China	0.51–279	Plankton net (153 μm)	surface	10–5000	–	NaCl	FTIR	Tsang et al. (2017)
Xisha Islands, China	200–45,200	Niskin and Plexiglas sampler	1–40	7–4856	–	–	FTIR	Ding et al. (2019)
South China Sea	17–25	Plankton, Multi closing net (500, 100 μm)	0–100	≥10	H ₂ O ₂ + HAc	–	Raman	This study
Pearl River, China	379–7924	5 l water sampler	surface	20–5000	H ₂ O ₂	NaCl	FTIR	Lin et al. (2018)
Northeast Pacific Ocean	0.004–0.190	Neuston, Manta, Bongo net (505 μm)	0–212	≥500	v.s.	–	FTIR	Doyle et al. (2011)
Atlantic Ocean	13–501	Seawater intake	0–250	10–5000	SDS	–	Raman	Enders et al. (2015)
California Monterey Bay	2900–15,000	Remotely operated vehicle (ROV) device	5–1000	100–5000	v.s.	–	Raman	Choy et al. (2019)
Marine Trench	2060–13,510	CTD system	2500–11,000	20–5000	Fenton	–	Raman	Peng et al. (2018)

v.s. = visually selected, n.g. = not given within reference, ST = sodium tungstate, HAc = acetic acid.

placed on a deepened slide, and treated with the respective chemical listed in Table 1. Each selected particle was photographed before and after the treatment under a microscope (Euromex, Holland with cross table and equipped with SWIFTCAM Microscope Digital Camera SC500, 5.1 MP). Chemicals were selected according to the most efficient digestion protocols 13 and 15 identified in Section 2.1.1 (Fig. 1). Rather than testing the effects of the entire protocol on microplastic degradation, the individual chemicals used in the protocols were tested for each plastic type to identify the causative chemical. Due to the frequent use and numerous recommendations for the application of KOH in previous studies (Dehaut et al., 2016; Kühn et al., 2017; Piarulli et al., 2019), the changes in microplastic sizes upon KOH exposure was investigated as well. The microplastic particles of each polymer type were exposed to acetic acid (24%) for 2 h at room temperature, H₂O₂ (30%) for 24 h and 48 h at 50 °C, ammonia (25%) for 24 h and Schweizer reagent for 2 h at room temperature, and KOH (224 g L⁻¹) for 48 h at 50 °C. The length and width of each particle were measured three times at selected positions under the microscope before and after the treatment using the open-source program ImageJ. The size of the particles selected for chemical treatments ranges between 32 and 974 μm (smallest width and largest length, respectively). A microplastic particle is significantly degraded by the chemical treatment if the reduction in length or width is ≥5% (95% confidence interval).

For weight changes, the individual chemicals used in protocols 13 and 15 were also tested on the nine crushed polymer types, but without KOH. Approximately 100 mg of the crushed microplastic powder (size < 2 mm) was weighed into a glass jar and treated with the chemicals

listed in Table 2 in triplicates. The first set was treated with acetic acid (for 2 h at room temperature), for the second set a combination of acetic acid (for 2 h at room temperature) and H₂O₂ (for 24 h at 50 °C) was added, and in the third set, the Schweizer reagent was applied (for 2 h at room temperature). Treated microplastic powders were filtered and rinsed with ultrapure water and in the case of the Schweizer reagent treatment rinsed with ammonia (25%) and ultrapure water instead. The obtained filters were dried and weighed after cooling down. Since some material can be lost during filtration even without treatment, the weight loss caused by filtration alone was also determined in triplicates for each microplastic type. To detect the filtration error, 100 mg of each microplastic type were mixed with 5 mL of ultrapure water, then filtered, dried, and weighed. The filtration error was corrected by adding the mean percentage filtration weight loss to the mean percentage weight recovery of the respective microplastic type. The weight loss of the microplastic due to the chemical treatment becomes significant at ≥5% (95% confidence interval).

To evaluate the potential effects induced by the chemical treatments on the Raman spectra of the polymers, all treated microplastic types, except for PA, were measured before and after the treatment. Due to the black color of PA, Raman measurements were not possible. The Raman measurements were performed using a LabRAM HR 800 Horiba Jobin YVON Raman spectrometer equipped with an Olympus BX41 microscope with variable lenses. The microplastic particles were focused and scanned with a red excitation laser (633 nm, 17 mW, air-cooled HeNe laser) at a 50× magnification, 10 s integration time, and 10 accumulation scans at a wavenumber range of 50–3800 cm⁻¹. The Raman

system was operated by the NGS LabSpec software and the obtained spectra were smoothed, baseline corrected, and assigned using KnowItAll Information System 2020 software equipped with spectra library (WILEY). The polymer spectra were compared by their mutual matching and recovery in the Raman spectra library.

2.1.3. Microplastic recovery rates for two different separation techniques

The protocols 1–15 described in Section 2.1.1 were developed for the elimination of natural biogenic constituents. For samples with high biogenic and sediment contents, a combination of biogenic matrix removal and a density separation is commonly applied. However, the combination can be complex and the intermediate steps difficult to implement without losses or contamination. In this section, a new combinable method with few intermediate steps for the microplastic isolation is introduced. This new approach is based on microplastic adsorption on lipophilic surface and was called adsorption separation in this study. To validate this new adsorption separation technique, the recovery rates were determined and compared with an effective high-density separation solution. Sodium tungstate dihydrate ($\text{Na}_2\text{WO}_4 \cdot 2\text{H}_2\text{O}$) was chosen to prepare a density solution due to its comparatively low toxicity and high density of 1.6 g cm^{-3} in a saturated state, which covers most of the commonly occurring polymer types (Kanhai et al., 2019; Pagter et al., 2018). In both methods, approximately 100 particles each of the virgin reference microplastics PE (average particle diameter of $454 \mu\text{m}$), PP ($501 \mu\text{m}$), PS ($514 \mu\text{m}$), PA ($592 \mu\text{m}$), PVC ($683 \mu\text{m}$), PET ($749 \mu\text{m}$), and PMMA ($548 \mu\text{m}$) were selected and used to determine the recovery rate in triplicates. The particle diameter given is the average particle diameter measured fivefold for all particles applied. To consider possible influences of plastic aging or biofilms on the adsorption properties and associated recovery rates, six different beached and biofouled plastic items from the Baltic Sea beach (Warnemünde, Germany) were also used for the adsorption separation technique (pictures of collected plastics are given in Fig. S1). To identify the polymer type of the collected beached plastic litter, small fractions were analyzed using Raman spectroscopy (used measurement settings are described in Section 2.1.2). To determine the recovery rate for the beached plastics, the plastic items were cut into smaller particles to obtain similar size ranges to the virgin plastic types and were further treated as described above for the virgin microplastic particles. The selected beached plastic items were a yellow cap (PP, diameter of $560 \mu\text{m}$), a blue rope (colored PP, $420 \mu\text{m}$), sticky transparent tape (PP, $820 \mu\text{m}$), a piece of a dog toy (PE, $650 \mu\text{m}$), a silver foil (PP, $1060 \mu\text{m}$), and a transparent foil (PP, $1400 \mu\text{m}$).

For the adsorption separation, a syringe cascade consisting of three syringes (30 mL, Terumo, Japan) was prepared. To obtain uniform surface lipophilicity, the syringes were coated with lubricating oil (Ernst GmbH & Co. KG, Germany) composed of light naphtha (25–50%), propane (20–25%), butane (12.5–20%), and isobutane (12.5–20%) and rinsed with ultrapure water to remove excess oil residues before use. For the recovery rates of the adsorption separation, the counted particles of virgin and beached microplastics were mixed with 20 mL ultrapure water and poured into the cascade in three repetitions. The triple repetition and the use of three consecutive syringes increase the contact possibilities between particles and the lipophilic syringe surface to ensure a maximum adsorption of microplastic particles. After the adsorption, the individual syringes from the cascade were rinsed with ultrapure water to remove non-adsorbed particles. To recover the adsorbed microplastic particles, each syringe was infused three times with a 50°C detergent solution. The obtained solutions containing the desorbed microplastic particles were filtered on a glass microfiber filter (Whatman™; diameter 25 mm; pore size $0.7 \mu\text{m}$; CatNo. 1825-025) and finally analyzed under the microscope by counting the recovered microplastic particles.

For the density separation, the counted particles were transferred to a density separator consisting of a 250 mL threaded glass flask, a brass ball valve ($1/2''$), and a threaded glass tube as an extension (see pictures

in Fig. S2). All parts were attached with Teflon adapters (a plastic which is not considered in the analyses due to its high density). The saturated sodium tungstate solution (1.6 g cm^{-3} , salt from Merck KGaA, Germany) was filled up to half of the upper glass tube and covered with aluminum foil. The solution was stirred for 1 h and then allowed to stand for 24 h to allow particles to float to the surface. Subsequently, the valve was closed and unscrewed from the device to filter the contents on a glass microfiber filter. All recovered particles were counted under the microscope and compared with the initially added particle counts to determine the recovery rates.

The adsorption separation technique offers many advantages compared to density separation. For the adsorption separation, large amounts of chemicals or long sediment settling times are not required. Moreover, with the density solution solely heavier particles were separated, while the use of the adsorption separation guaranteed the removal of non-lipophilic particles, which corresponds to the majority of environmental matrix. Due to these benefits, the adsorption separation was tested on biogenic material in combination with a gentle digestion protocol (described in Section 2.1.1). The digestion step is performed to release microplastics embedded in biogenic material and to prevent clogging in the syringes. In the combined adsorption separation, the digestion step was performed previously, followed by the adsorption separation. For the digestion step, H_2O_2 and acetic acid were added to 0.5 g of the biogenic material in the same manner as described for protocol 13 (Fig. 1), but with a shortened H_2O_2 exposure time of 5 h. After the sample pretreatment, the acidified peroxide solutions were poured into the syringe cascade three times to ensure the adsorption of lipophilic particles. Subsequently, the individual syringes were rinsed with ultrapure water and adsorbed particles were desorbed with the detergent solution as described above for the microplastic recovery rates. After filtration of the obtained solution, the residual weight and fluorescence of the desorbed material were analyzed as described for the protocols given in Fig. 1.

2.2. Field samples

2.2.1. Sampling site and sampling procedure

To examine the applicability of the new adsorption separation technique on natural samples, eight different sediment samples and two plankton net samples were selected from the South China Sea (SCS). The samples were retrieved during the Sonne cruise 269 (SO269) of the German research vessel SONNE 2019 in the framework of the Sino-German project MEGAPOL. The research area in the northern SCS extends in the north-south orientation from the Pearl River estuary near Hong Kong to the deep SCS and is located between Taiwan and Hainan in the east-west orientation (Fig. 2). Samples were collected along a survey perpendicular to the coast of China, which runs along the Pearl River delta crossing the continental slope into the deep SCS.

The study area is influenced by seasonally and inter-annually varying physical forces which affect the transport of the Pearl River freshwater plume. The Pearl River is characterized by its large water volume transport into the SCS and the enormous population density around the river delta with a catchment area of more than $450,000 \text{ km}^2$. Under this condition, the SCS as a focal point in land-ocean interaction offers a unique opportunity to understand how anthropogenic stress acts on the marine environment. Microplastic is one of the major anthropogenic pollutants entering the marine environment especially via rivers (Eerkes-Medrano et al., 2015; Hoellein et al., 2019), making the SCS an excellent study site for microplastic pollution.

For the microplastic investigations, samples taken by a Multi-core vessel and by two different plankton nets were used. Multi-corer was equipped with eight Plexiglas (PMMA) core pipes each with 60 cm height and an inner diameter of 10 cm. The cores applied for microplastic analysis were immediately sliced and stored in PE tubes at 4°C in the dark on board. In the lab, they were freeze-dried for several days at -60°C and 50 mbar. About 10 g of the upper 3 cm of each core

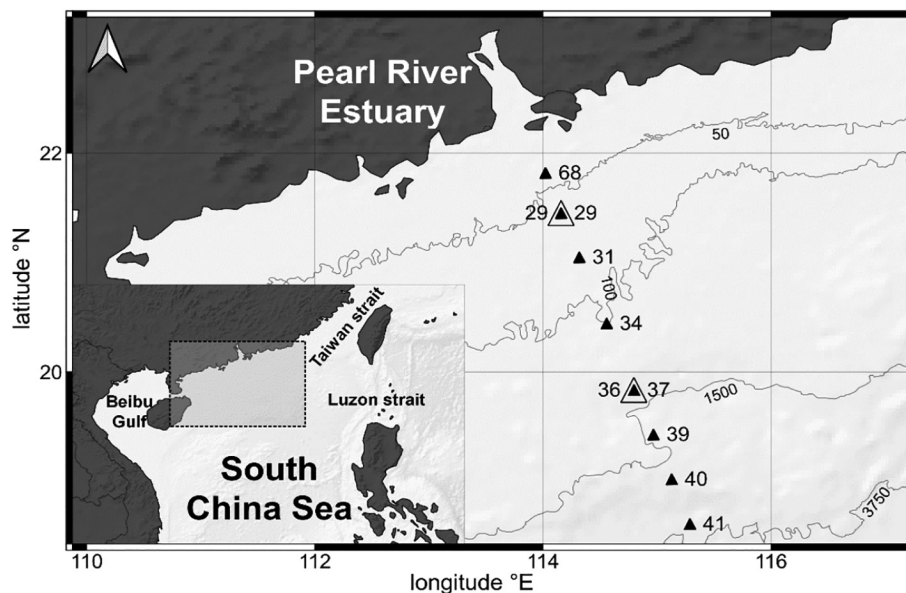


Fig. 2. Sampling stations for microplastic analysis in the South China Sea. The filled triangles symbolize the sediment sampling stations, and the empty triangles indicate the location of the plankton net sampling stations. The Apstein plankton net sample was collected at station SCS 36 and the Multi-closing net sample was collected at station SCS 29.

were taken and stored in a glass vial covered with aluminum foil until analysis. The plankton net samples were taken with a Multi-closing net at station SCS 29 and an Apstein plankton net at station SCS 36. The HYDRO-BIOS Multi-closing net (type MPS Midi Combi, built in 2018) with a mesh size of 100 μm and a square opening of 50 \times 50 cm were vertically hauled at 0.5 m s^{-1} from 50 m water depth to the sea surface. The Apstein plankton net with a mesh size of 500 μm and a ring diameter of 50 cm were also vertically hauled from 100 m to the sea surface at 0.1 m s^{-1} (50 m - surface) or 0.2 m s^{-1} (100–50 m) heave speed. The obtained samples were filled untreated in PE sample bottles and immediately frozen at -20°C . In the home laboratory at IOW, the samples were defrosted, split into two aliquots, freeze-dried, and stored in glass vials covered with aluminum foil.

2.2.2. Microplastic extraction and identification

The collected sediment and net samples with different matrices were separated using the combined adsorption separation technique. A schematic representation of the entire procedure applied including sampling, treatment, adsorption separation, and analysis is illustrated in Fig. 3. For both sample types, pretreatment was performed by adding 20 mL H_2O_2 (30%) to the 10 g sediment sample and the bisected net sample into a beaker. For the reaction, the sample was covered with aluminum foil and incubated for 5 h at 50°C . After the exposure time, 20 mL acetic acid (24%) were added and allowed to react for 2 h at room temperature. For the sediment samples, oversized particles provoking clogging were eliminated by a stainless-steel sieve with 1 mm mesh-size, which was then separately examined for plastic particles (≥ 1 mm) using a SteREO Discovery.V8 stereomicroscope (Carl Zeiss, Germany). The smaller size fraction (< 1 mm) and the net samples were passed through the syringe cascade in triple repetition. Each loaded syringe was rinsed with approximately 30 mL ultrapure water to remove the non-adsorbed sample matrix. The detachment of adsorbed microplastic particles was performed with warm detergent solution as described in Section 2.1.3. The obtained solution with desorbed particles was filtrated using polycarbonate membrane filters (Whatman Nuclepore track-etched Membranes; pore size: 0.4 μm ; diameter: 25 mm) and then rinsed with detergent solutions followed by ultrapure water. The loaded filter was transferred to a slide and covered with a coverslip immediately after filtration to exclude airborne contamination. For the adsorption separation technique, a maximum weight limit of 10 g for sediment samples was set to prevent clogging,

no limit is necessary for aqueous or smaller-sized sample types. Due to the limited sediment sample mass, all corresponding results are reported in the sample scale used in particle numbers (items) or micrograms (μg) per 10 g d.w. of sediment. The microplastic abundances detected in net samples are reported in items per cubic meter (items m^{-3}) or μg per cubic meter ($\mu\text{g m}^{-3}$) for microplastic masses.

Microplastic identification was implemented using the Raman spectrometer and associated software as described in Section 2.1.2, using the same acquisition settings for all samples. The entire filters were manually scanned in transmitted light using a running window method to ensure high visibility even of transparent particles. At a constant objective magnification of 10 \times (window size of 0.7 \times 0.9 mm), the filters were scanned from left to right and from top to bottom using a cross table. Suspicious particles were focused, scanned at a 50 \times magnification, and photographed in each case. The measured particles were confirmed to be microplastic when the matching degree between the measured spectra and the database polymer spectra reached $>80\%$ (also described by Lin et al., 2018). Identified microplastic particles were classified according to their shape into fragments, fibers, or elongated fragments. Particle sizes and volumes were calculated as a function of their length and width (for fibers or elongated fragments) or maximum Feret diameter and particle area (for spherical or irregular shaped fragments). The adoption of the Feret diameter as the particle size has already been described by Imhof et al. (2016) and Anger et al. (2019). For the volume calculations, an ellipsoidal shape was assumed for fragments and a cylindrical shape for elongated fragments or fibers. Using the measured length (maximum axis) and area of the elliptical fragments, the best fit for the width (minimum axis) was determined to calculate an ellipsoidal volume described by Kumar et al. (2010). Finally, using the determined volume and mean polymer type-dependent density (densities were taken from Hidalgo-Ruz et al. (2012)), the plastic mass was calculated and expressed in μg per 10 g d.w. for sediment and in $\mu\text{g per m}^3$ for net samples in this study. Orienting by Feret diameter or fibrous lengths, this method sets the lower detection limit at a size of 10 μm . Accordingly, all measured microplastic particle sizes were assigned in a size range from 10 μm to 1 mm in 10 μm steps.

2.2.3. Contamination control and blank correction

To avoid contamination during the processing, the samples were covered with aluminum foil during and between all steps. All instruments and glasses utilized for the sample separation and storage were

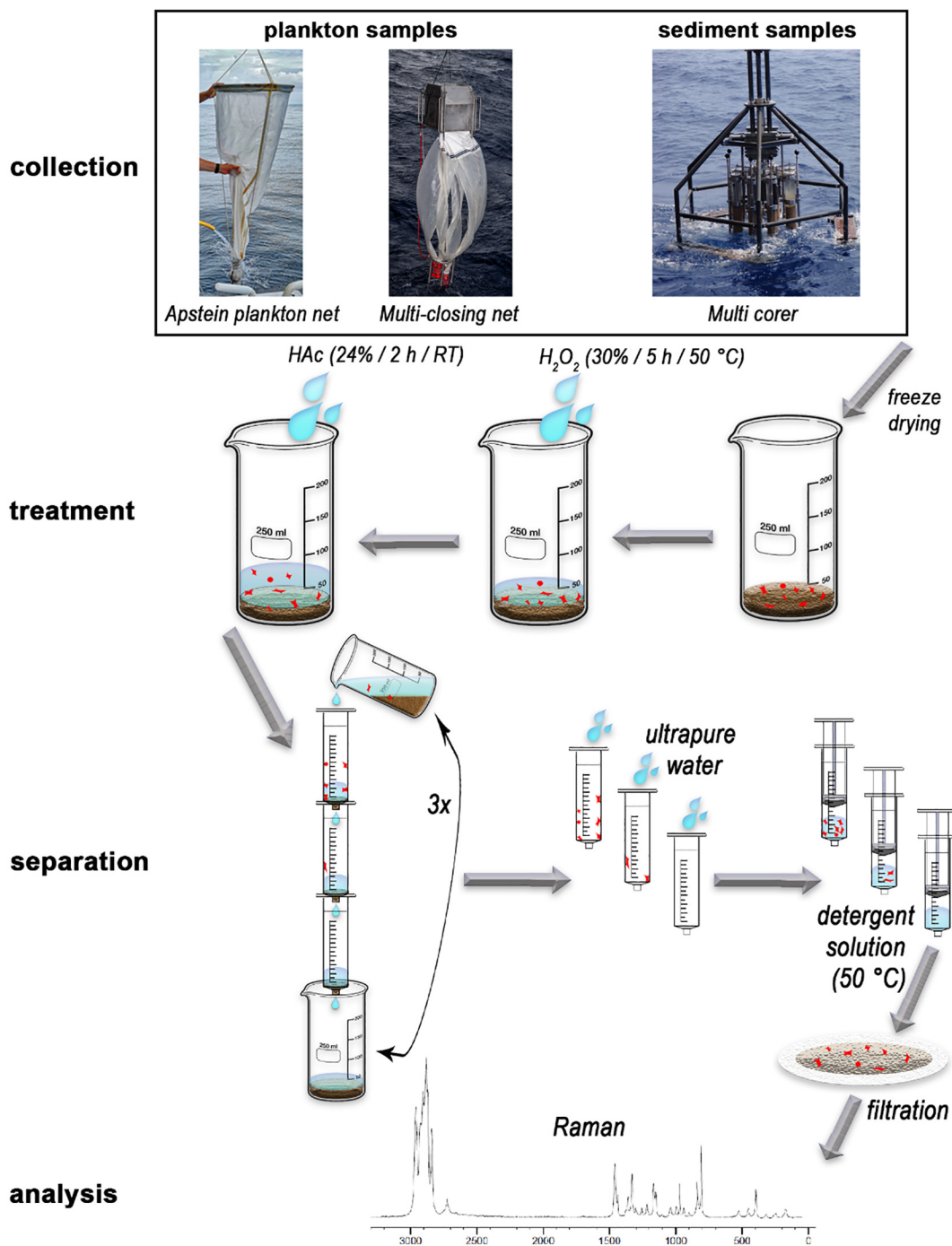


Fig. 3. Scheme of the entire applied process of microplastics detection in marine environmental samples. The method is divided into four steps starting with sample collection by Multi-corer, Multi-closing net, or Apstein plankton net. In the second step, wet samples are freeze-dried and digested by adding H₂O₂ and acetic acid (treatment step). In the separation step, the samples are filled three times into the syringe cascade to allow potential microplastics to adsorb on the surface of the syringes. Sediments and biogenic residues are rinsed out with pre-filtered ultrapure water. Potential adsorbed microplastic particles were desorbed with a warm detergent solution and then filtered. Finally, filters are analyzed by Raman spectroscopy in the last analytical step.

rinsed with prefiltered ultrapure water immediately before use. During the entire working time for the sample treatment procedure, only one person worked in the laboratory, wearing a white cotton lab coat and gloves. All steps in which the sample was briefly in contact with the air were performed under the fume cupboard which was wiped damp with paper towels before and between all steps. Furthermore, all solutions used were filtered (polycarbonate membrane filter with 0.4 µm pore size) and stored in glass bottles until use.

In addition to the contamination prevention, blanks were prepared in all steps and treated at the same time and in the same manner as

the samples to account for possible contamination. The blank samples were prepared without a sample matrix, instead, both digestion chemicals were filled into an empty beaker and further processed as described in Section 2.2.2. If microplastic particles were found on the blank filters, these particles were also determined in their size and mass as described for the sample particles. Finally, the calculated microplastic numbers and masses were corrected by subtracting the respective blank microplastic numbers and masses. In addition, the plastic types used in sampling (PA for net sampling and PMMA for sediment sampling) were excluded from the presented results.

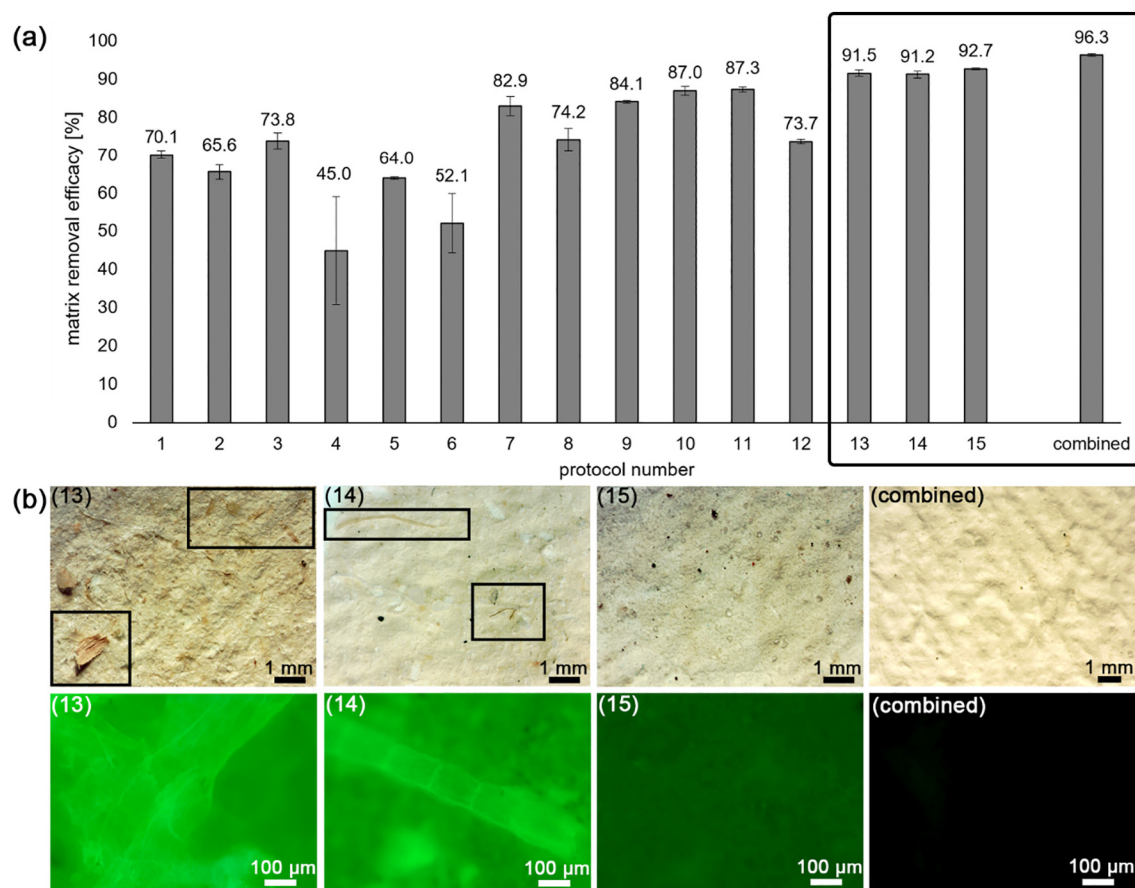


Fig. 4. (a) Resulting percentage digestion efficacies for the investigated digestion protocols 1–15 and the combined adsorption separation technique. The black box frames the four most effective protocols whose microscopic images are illustrated in (b). The top four images show the respective light microscopic images of protocol 13, 14, 15, and the combined adsorption separation (protocol numbers or designation are given in parenthesis). Visible cellulosic residues are framed in black boxes. The lower images demonstrate the related fluorescence micrographs after staining with Nile red at wavelengths of 460–525 nm and a uniform exposure time of 600 ms.

3. Results

3.1. Biogenic matrix removal efficacy

The percentage mass removal efficacies of the biogenic-rich sample achieved for protocols 1–15 ranged from $45.0 \pm 14.1\%$ to $92.7 \pm 0.2\%$. The highest effectivities were observed in the protocols in which several chemicals were used (7–15), while the application of single chemicals such as KOH (protocol 4) exhibited the lowest matrix removal (Fig. 4a). With the different Fenton reagents used in protocol 2 (Fenton acidified with HCl) and 3 (Fenton acidified with acetic acid) a percentage removal of $65.6 \pm 1.9\%$ and $73.8 \pm 2.1\%$, respectively, was achieved. These results demonstrate that replacing a strong acid with a weak acid for the Fenton pH adjustment enables even a higher removal efficacy and prevents the chemical decomposition of plastic to be analyzed. Fenton has been used in several studies as a more efficient and gentle digestion agent compared to H_2O_2 due to the presence of iron as a catalyst (Bergmann et al., 2017; Hurley et al., 2018; Tagg et al., 2017). However, the comparison of the efficacies between H_2O_2 applied in protocol 1 and the Fenton reagents used in protocols 2 and 3, indicates no expected increase in the efficacy (Fig. 4a). To further investigate these initial results of efficacies, the exposure time of both H_2O_2 and the Fenton reagent was shortened for the following protocols 5 and 6, respectively. The evaluation after 7 h exposure time revealed an even lower removal efficiency of $52.1 \pm 7.7\%$ for the Fenton reagent, compared to the mass removal of $64.0 \pm 0.3\%$ achieved with H_2O_2 . Supported by observations during the exposure time it can be assumed that natural iron contents of the samples in combination with the iron originating from the Fenton reagent

cause poorly soluble precipitation, which affected the sample weight after digestion. Accordingly, when using Fenton reagent, the natural sample iron content must be considered and adjusted for each sample type. In this study, H_2O_2 was chosen instead of Fenton reagent for the further process of the digestion protocols to ensure a uniform method for each sample type. In addition, acetic acid continues to be used, as it is a gentle option to dissolve large amounts of calcareous shell material that is not removed by H_2O_2 . Besides H_2O_2 and acetic acid, solutions such as ethanol (protocol 7), detergent (protocol 8), SDS (protocol 9), and ammonia (protocol 10) were used to pre-dissolve biogenic lipids. The use of ammonia proved to be the most effective combination with H_2O_2 and acetic acid with a removal efficacy of $87.0 \pm 1.2\%$ (protocol 10), compared to all previously implemented protocols. As demonstrated by protocol 11, the sequence of the chemical application is not a factor influencing the removal efficiencies, as no significant differences were detected in the resulting digestion efficacies for protocol 11 ($87.3 \pm 0.6\%$) compared to the opposite sequence used in protocol 10 (Fig. 4). In the following protocol 12, another method of activating H_2O_2 by exposure to UV radiation instead of high temperatures or iron catalyst was investigated, but no increased matrix reduction efficiency ($73.7 \pm 0.6\%$) was observed compared to the same treatment previously applied in protocol 11 with a temperature activation. Based on the observation in protocol 12, temperature activation at $50^\circ C$ for H_2O_2 continued to use for the following protocols 13–16. In protocols 13–15, the application of cellulose dissolving substances and panning of the sample were introduced to the matrix removal experiments. The combination of panning and the exposure of H_2O_2 and acetic acid applied in protocol 13 achieved a matrix reduction of $91.5 \pm 0.8\%$. The addition of saturated

urea solution to dissolve poorly soluble cellulose fractions used in protocol 14 reached no further improvement of the removal efficiency ($91.2 \pm 0.9\%$), as illustrated in microscope images in Fig. 4b. Both the light microscope image and the fluorescence microscope image of the filter obtained after the treatment with protocol 14 show remnants of cellulose-containing fragments. These fragments are remnants of algae or wood and must be removed when using the Nile red staining method for microplastic detection to avoid confusion with similar looking fragments. Contrary to this, using the Schweizer reagent in protocol 15 to reduce cellulose-containing substances resulted in slightly higher matrix removal efficiencies of $92.7 \pm 0.2\%$, and solely non-fluorescent particles remained after the treatment (Fig. 4b). These observations were supported by an effectiveness test of the saturated urea solution and the Schweizer reagent with printing paper (details of the performance are given in supplement materials protocol S2). While the Schweizer reagent dissolved $65.9 \pm 1.6\%$ of the used printing paperweight after 1–2 h exposure time, the urea solution reduced the weight only by $1.1 \pm 1.6\%$ after 24 h. Although urea disentangles the paper structure into fine fibers, it does not dissolve them until a liquid state.

3.2. Influence of reagents on microplastic degradation

The resulting percentage recoveries of microplastic weight and size after the chemical treatment are listed in Table 1. Significant changes in the microplastic particle sizes or discolorations were observed after the treatment with H_2O_2 at long exposure times (≥ 24 h) for PA and after 48 h KOH exposure time for PET, PVC, and slightly for POM at $50^\circ C$, respectively. Treatment with KOH destroyed all five PET particles tested, two of five PVC particles lost in size with each PVC particle tested exhibiting discoloration, and one of five POM particles lost in size as well. Due to the severe particle degradation induced by KOH (Table 1) and the least efficacy in reducing the biogenic matrix (Fig. 4), KOH was not investigated further and was discarded for further treatment methods. Further size reductions were recognized for PA after 24 and 48 h of H_2O_2 exposure time, but contrary to expectations, no significant weight loss was observed after the combined treatment of acetic acid

(2 h at room temperature) and H_2O_2 (24 h at $50^\circ C$) (Table 1). This observation indicates that the particle decomposition and modification in the appearance of PA are attributable to particle melting or fractioning, resulting in still filterable particle sizes without weight losses. Instead of PA, PVC was reduced in weight due to the treatment with acetic acid to $89.9 \pm 1.2\%$, while the size recovery of PVC indicates no significant changes ($101.1 \pm 2.9\%$). Considering the calcium additive added during the PVC manufacturing for reinforcement, the weight loss of PVC caused by the acid treatment can be explained by the increased calcium solubility with decreasing pH (pH 2 for a 24% acetic acid solution). This assumption is supported by Raman measurements of treated and untreated PVC particles illustrated in Fig. 5. The characteristic peak intensities of calcium carbonate at 1085 cm^{-1} , 711 cm^{-1} , 281 cm^{-1} , and 154 cm^{-1} , decrease or disappear in the Raman spectra for the treated PVC particle, while typical PVC signals remain present. Despite these changes in calcium carbonate peaks, a comparison of both PVC spectra before and after the treatment still showed a mutual matching of 97%, signifying that the polymer remains intact and measurable. All further measured Raman polymer spectra of PE, PP, PET, PS, POM, PMMA, and ABS remain unchanged after the treatment, with a matching degree $>93\%$. For all remaining chemicals tested, no significant detectable effects on the weight or size recovery of the polymer types were detected (listed in Table 1).

3.3. Microplastic recovery rates for two different separation techniques

The comparison of the investigated density separation with the adsorption separation revealed similarly high recovery rates for both techniques (Table 1). All recovery rates of microplastic particle numbers determined after the density and adsorption separation are listed in Table 1. With the density separation method, an average particle recovery rate of $98.1 \pm 2.1\%$ was achieved, with the lowest recovery for PVC particles at $93.2 \pm 4.6\%$. Despite the same density of the PVC polymer used and the sodium tungstate solution of 1.6 g cm^{-3} , a few particles remained on the vessel bottom. A further reason for a particle recovery rate below 100% especially for PE and PP is the sticking of some fine

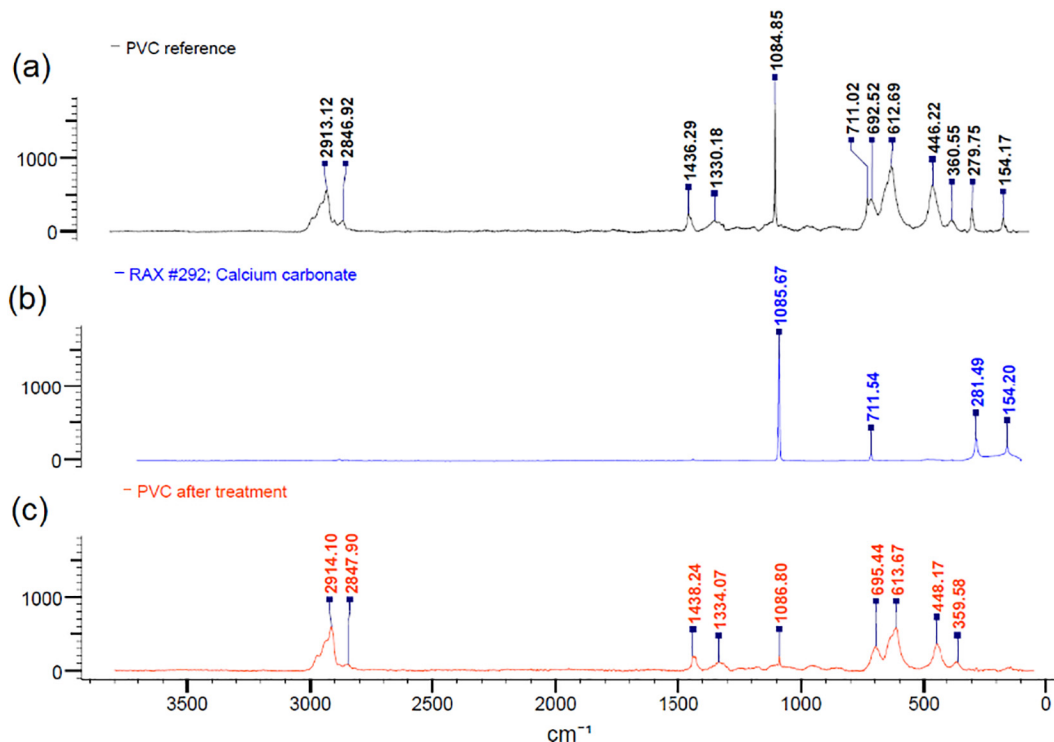


Fig. 5. Comparison of three different Raman spectra: (a) the spectrum of polyvinyl chloride reference material before chemical treatment, (b) calcium carbonate reference spectrum obtained from Raman spectra library, (c) polyvinyl chloride spectrum after the treatment with acetic acid, H_2O_2 , and Schweizer reagent.

particles on the vessel wall not rising to the solutions' surface despite stirring for 1 h and a resting time of 24 h. For the adsorption separation, the lipophilic property of the plastic particles was exploited instead of the density to separate microplastic particles from the surrounding sample matrix. Applying this new adsorption separation technique, an average particle recovery rate of $98.0 \pm 3.8\%$ was achieved, with equal or a higher recovery rates for each polymer type tested compared to the density separation method, except for PA ($88.7 \pm 8.6\%$). In contrast to the other polymer types used, PA absorbed high water amounts (Abts, 2016), which is associated with higher hydrophilicity, lower lipophilicity, and consequently attenuated adsorption strength. Because increased hydrophilicity was also observed for biofouled or degraded particles (Sudhakar et al., 2008; Tu et al., 2020), beached and aged microplastic particles and films were tested for the adsorption separation as well. The selected beached plastic items, consisting of PE and PP, represent the most commonly detected polymer types in the environment (Hidalgo-Ruz et al., 2012). The resulting average particle recovery rate for the tested aged and biofouled microplastic items ($98.6 \pm 2.1\%$) using the adsorption separation is in the same range as these for the virgin polymer types and the density separation method. These results demonstrate that the new adsorption separation technique achieves similar microplastic particle recoveries compared to one of the most effective density separation methods, providing an

option to isolate microplastic particles from different sample matrices in an easier way. Based on these findings, this adsorption separation was combined with a gentle digestion step to reduce sample material for a trouble-free flow through the syringes and to release possible microplastic particles embedded in biogenic material. For this purpose, an exposure time of 5 h for H_2O_2 and 2 h for acetic acid, is already sufficient for the entire chemical treatment. With this final applied combined adsorption separation technique, the highest matrix removal efficiency of $96.3 \pm 0.3\%$ and a fluorescence-free filter compared to any previously performed digestion protocol was achieved (Fig. 4a, b). Due to these methodological advantages of shorter waiting times, gentle chemical treatment, and high recovery rates, the combined adsorption separation method is selected to analyze natural environmental samples for their microplastic content.

3.4. Field samples

Microplastic particles were detected in all analyzed net and sediment samples collected from 10 sampling sites in the South China Sea applying the combined adsorption separation method, except for one sediment sample (Fig. 6). On blank filters, reflecting the contamination during the sample preparation, a maximum of one microplastic particle per filter was found, involving one PET fiber or one PE fragment. In

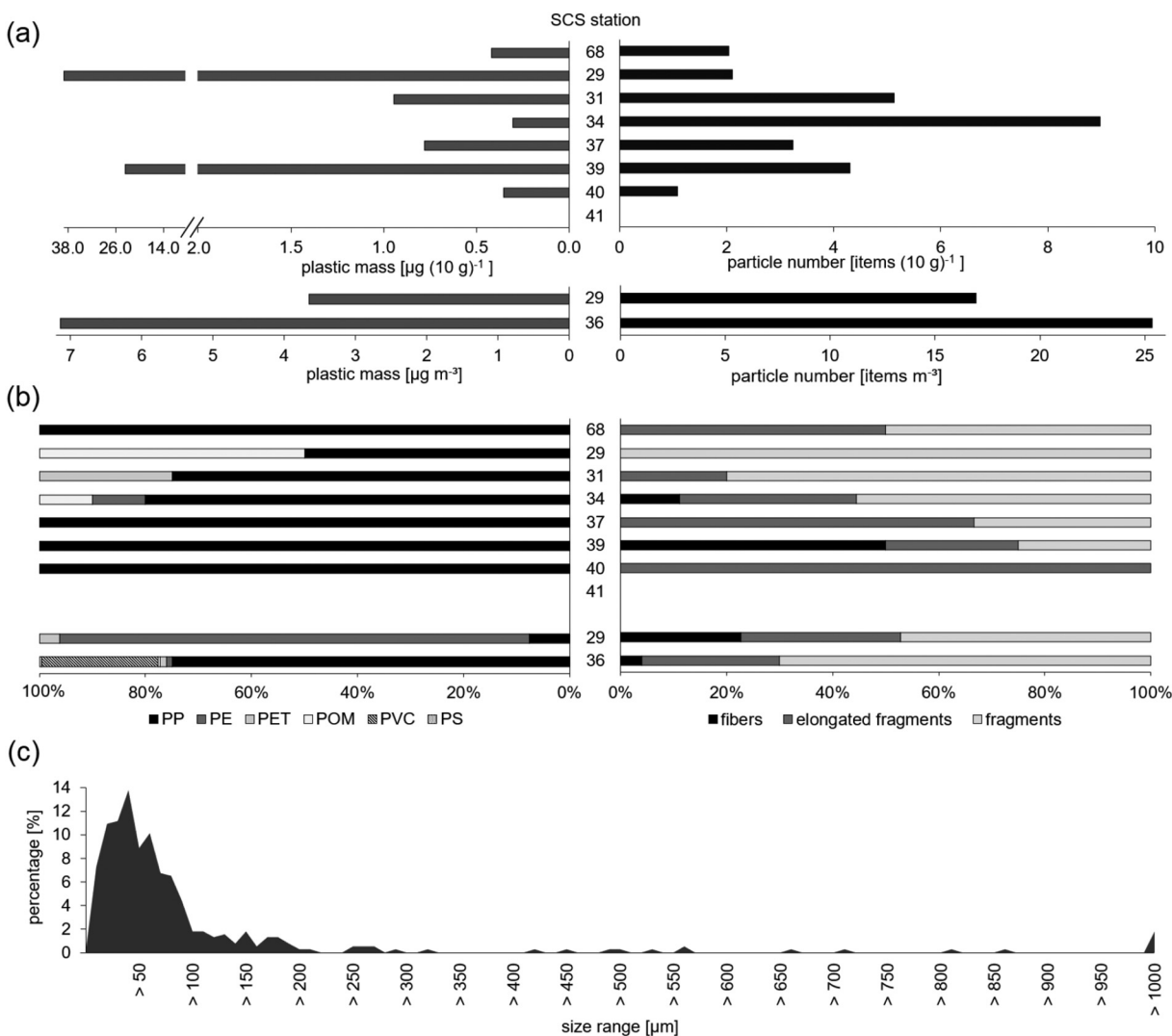


Fig. 6. Abundances, masses, and characteristics of microplastic particles detected in field samples: (a) calculated microplastic mass (left) and respective item number of microplastic particles (right) for the sediments (items or mass per 10 g sediment d.w.) and net samples (items or mass per cubic meter); (b) percentages of polymer types (left) and microplastic shapes (right) for each sampling station; (c) size distribution of all particles identified as microplastic in the field samples in 10 μm steps.

addition, no evidence of contamination was detected during sampling, as no sediment sample contained PMMA (applied for sediment sampling) and no PA (applied for net sampling) was found in the net samples. This results in a blank-corrected number of 0–9 identified microplastic items in 10 g sediment sample mass with a mean number of 3.4 items (10 g d.w.)⁻¹ per sample (Fig. 6a). No microplastics were identified at station SCS 41, which has the greatest distance to land and the Pearl River estuary (Fig. 2). The highest number of microplastics was found at the middle part of the transect at station SCS 34 with 9 items per 10 g d.w. sediment. Further towards the river estuary, at stations SCS 29 and SCS 68, the amount decreased to 2 microplastic items (10 g d.w.)⁻¹. As illustrated in Fig. 6a, considerably more microplastic particles were detected in both plankton net samples. At the sampling station SCS 36, the highest number of 249 items was counted, while at station SCS 29, 106 microplastic items were found in the halved net sample material. This corresponds to a blank-corrected number of 25 and 17 items m⁻³, respectively. Despite a lower number of microplastic items found in sediments than in the net samples, the calculated microplastic mass for the sediments (0–39 µg in 10 g d.w.) was higher than in the determined net samples (3.7–7.1 µg m⁻³) (Fig. 6a). This corresponds to a mean mass of 3.4 µg per identified microplastic item in the sediments and 0.1 µg per item in plankton net samples, which depends on the polymer type characteristic density and their particle sizes. The most frequently counted representative of all microplastic particles was PP (56.9%), which occurred in every sample with the highest proportion of ≥50%, except for the net sampling station SCS 29, where PE was the most prevalent polymer type (88.7%). The proportion of polymer types for the combined counts of all samples analyzed showed that PE predominated (25.6%), followed by PVC (14.4%), and PET (2.1%), while POM (0.8%) and PS (0.3%) accounted for a lower proportion (Fig. 6b).

The morphological characteristics of the verified microplastics were classified as fragments (62.6%), fibers (9.7%), or elongated fragments (27.7%). No spheres or beads were identified as microplastic (Fig. 6b). Colored microplastic suspect particles are difficult to detect by Raman spectroscopy (Dehaut et al., 2019) because the large pigment content leads to a spectral overlay of dyes and polymers, or particle destruction during measurements, leading to inconclusive outcomes. Despite the high probability that blue or red-colored items are microplastic, they were excluded from our results due to their low spectral validity, implying that solely unimpressive white or transparent microplastic particles were considered. For an initial distinction between transparent planktonic silicates and petrochemical microplastics detectable on the sample filter, particle shape assessments were implemented before the Raman measurements. While silicates exhibited a smooth surface, PP and PE particles appeared rather rough, curved, or frayed with an elongated or fragmented surface. Detected PVC items exhibited a decomposed and aged appearance with a rough surface and occurred exclusively in fragmented form. PET occurs exclusively as fibrous microplastic items and was found less frequently in the samples examined, with a proportion of 2.1% (Fig. 6b).

All microplastic items identified in the sediment and net samples examined were identified in the small size fraction of <1 mm. The size distribution of the identified microplastic items <1 mm, illustrated in Fig. 6c, indicates that mainly items <200 µm were found (92.7%). Although 93.0% of all detected microplastic items were collected using nets with mesh sizes of 100 and 500 µm, the percentage of detected microplastics in the size range of 10–80 µm was 68.8%, with a maximum percentage of 40–50 µm (13.8%), followed by 30–40 µm (11.2%).

4. Discussion

4.1. Matrix removal

To our knowledge, this newly presented adsorption separation technique for microplastic isolation from environmental samples has not yet

been validated or applied. The objective was to develop a gentle microplastic separation method for matrix-rich but mass-limited samples with maximum accuracy. In addition, this method aims to provide an easy and quick technique of separation to enable microplastic studies for a wide range of scientific institutions. In previous methods, particularly the combination of density separation with chemical digestion was problematic. Cheap and environmentally friendly density solutions such as NaCl (1.2 g cm⁻³) have been most frequently used (Filgueiras et al., 2019; Peng et al., 2017; Reed et al., 2018; Strady et al., 2020; Zhao et al., 2018), however, the maximum density achievable is too low to include all relevant polymers. PVC and PET (density of approx. 1.4 g cm⁻³) are outside the includable density range but are both frequently found microplastics in the environment (Andrady, 2011). Other commonly used solutions such as sodium iodide, zinc chloride, or sodium polytungstate with higher densities are hazardous or expensive (Stock et al., 2019). Moreover, microplastic recovery rates from decanting the supernatant of the high-density solution alone are still low (Martin et al., 2017). Another challenge is to find a suitable digestion method, that can be performed either before (Cai et al., 2018; Ling et al., 2017; Matsuguma et al., 2017; Strady et al., 2020; Zhang et al., 2019b), during (Tsang et al., 2017; Zhao et al., 2018), after (Bergmann et al., 2017; Zhu et al., 2018) or without a density separation step (Luo et al., 2019; Peng et al., 2018; Zhang et al., 2017). For the density separation, which was performed in this study for comparison purposes, long settling times to remove sediments are required. In combination with biogenic digestion steps, additional long exposure times were required to remove biogenic materials (Fig. 4). Furthermore, density separation is inconvenient to combine with digestion steps, digestion chemicals may react with the density salt, or filtration is required between steps, resulting in losses and contamination. Combined adsorption separation can be performed without long settling or reaction times with improved biogenic matrix removal efficiency (Fig. 4).

In addition to the analyte loss or contamination caused by density separation, the digestion step entailed error sources as well. Several chemicals applied, affect or even dissolve several polymer types (Avio et al., 2015; Castillo et al., 2016; Cole et al., 2014; Dehaut et al., 2016; Enders et al., 2017). Our outcomes supported chemical polymer destruction even for the commonly used digestion agents such as KOH (224 g L⁻¹) and H₂O₂ (30%) after exposure times of ≥24 h at 50 °C or insufficient matrix removal efficiencies for Fenton and KOH (Table 1). The application of KOH destroyed PET, and size changes of PVC and POM were observed. Changes in PET morphology attributed to KOH exposure were also reported by Dehaut et al. (2016). Karami et al. (2017) even realized destructive effects for PVC, PET, and PA, including changes in Raman spectra due to the H₂O₂ treatment. For PA, a decrease in relative Raman peak intensity was also verified (Karami et al., 2017). However, the polymer remains identifiable due to little impact and unchanged peak wavelengths. Conversely, no decreased or increased Raman spectra peak intensities were observed in measurements pre- or post-digestion of PS, PE, and PP (Murray et al., 2011; Zhao et al., 2017). In the present study, each polymer tested was identifiable after 24 h H₂O₂ (30%) and 2 h acetic acid (24%) exposure, signifying that there was no digestion-related impairment in the sample analysis accuracy for the newly developed combined adsorption separation technique. Moreover, for the new adsorption separation technique, no density separation is required and the H₂O₂ exposure time can be minimized to 5 h, which reduces the risk of microplastic degradation.

Besides the influence on the microplastic analyte, the matrix removal efficacy is of great importance for the method validation as well. With the combined adsorption separation method, we achieved a biogenic matrix reduction of 96.3 ± 0.3%, which is slightly higher than 92% reached by Nuelle et al. (2014) or removal of 89% for wash margin sand debris reached by Olsen et al. (2020) after four treatment days. Contrary to that, our resulting effectiveness is not yet as high as that achieved by using enzymes (Cole et al., 2014; Löder et al., 2017).

However, using enzymes for matrix elimination is limited caused by long treatment times (4–16 days), high costs, and an increased risk of contamination due to many intermediate steps. Furthermore, enzymatic digestion steps are solely suitable for biota, and an additional density separation step is required for sediment-containing samples. A completely different approach is the application of ethanol for density separation introduced by Herrera et al. (2018). This method achieves an organic-removal efficacy of 97% but needs a sediment separation step as well and excludes some PS types. Additionally, Herrera et al. utilized particle sizes ranging from 0.5 to 16.50 mm to determine the recovery rate having no comparable significance for microplastic particles smaller than 0.5 mm (Avio et al., 2015; Hengstmann et al., 2018; Quinn et al., 2017; Zhao et al., 2017). To date, few previous microplastic studies have used a consistent validation or detection method (Prata et al., 2019). To compare global values and produce reliable data, either uniform methods or known recovery rates of the applied methods are needed. However, even the determination methods for the microplastic recovery rates differ noticeably in particle sizes, polymer types, and particle quantities used (Castillo et al., 2016; Gewert et al., 2017; Li et al., 2018; Tsang et al., 2017). Usually, solely the recovered number of microplastic particles before and after the treatment is determined for method validation (Avio et al., 2015; Herrera et al., 2018; Munno et al., 2018; Nuelle et al., 2014), providing no information about changes in particle sizes or shapes. Because our results showed that microplastic particles can change significantly in size even without a mass loss (Table 1), determining the polymer mass recovery alone after the chemical treatment is not sufficient as well.

In addition to the chemical influences on particle size, weight, and Raman spectra on various microplastic types and the verification of the method efficacy, the microplastic recovery rates of the new adsorption separation were compared with an effective density separation method. The resulting similarity of both recovery rates of $\geq 98\%$ indicates the reliable applicability for the most virgin as well as aged and biofouled polymer types for the new adsorption separation (Table 1). However, this new technique also provides further potential for improvement. Firstly, a more effective adsorbent could be introduced, since less lipophilic polymer types such as PA (recovery rate of $88.7 \pm 8.6\%$) do not reliably adhere to the cascade surface (Table 1). Secondly, passing large amounts of coarse material through the syringes is problematic, resulting in a limited sediment volume of no more than 10 g. This limitation could be remedied by increase the adsorption surface, minimize the flow rates, and larger the openings. The great potential of this adsorption separation technique is supported by the time and costs saving. While density separation alone requires a few minutes up to six days (Peng et al., 2018) and gentle digestion steps can even take up to 16 days (Löder et al., 2017), the adsorption separation can be performed in approximately 8 h per sample set. Additionally, in this newly presented technique, the remaining matrix was minimized with no detectable influences on small microplastic particles at high microplastic particle recovery rates, making subsequent visual and spectral analysis easier and faster with higher accuracies.

4.2. Field samples

The number of microplastic items detected in the South China Sea seafloor sediment samples in this study is in the same range as those found by Tsang et al. (2017) on the adjacent coast, with 0.5–2.8 items per 10 g dry weight (d.w.) (Table 2). Higher microplastic abundances were found in Pearl River sediments with 0.8–96.0 items (10 g d.w.)⁻¹, which decreased to <2.9 items (10 g d.w.)⁻¹ with shortened sampling site distance to the South China Sea (Lin et al., 2018). Microplastic particle deposition observed by Strady et al. (2020) in seafloor sediments on the coasts of Vietnam was 15.4–20.2 items per 10 g d.w., slightly higher than those reported in this study. The abundance of microplastic in coastal regions and rivers is strongly related to the human population density (Browne et al., 2011; Strady et al., 2020;

Van Cauwenberghe et al., 2015), and is reflected by microplastic detections in seafloor sediments (Lin et al., 2018; Strady et al., 2020; Tsang et al., 2017). This also applies to mangrove and beach sediments, which are directly affected by terrestrial and marine microplastic inputs (Zhou et al., 2020a, 2020b). However, published abundances were similar to our results, except for the higher abundances found in seafloor sediments on the Vietnamese coast and those identified at beaches and mangrove sediments on the Chinese coast with 0.1–57.4 items in 10 g d.w. (Strady et al., 2020; Zhou et al., 2020a). The majority of studies conducted in the SCS found lower than expected microplastic abundances. Whether these results are caused by natural conditions or methodological differences remains uncertain. As listed in Table 2, Lin et al. (2018), Strady et al. (2020), and Tsang et al. (2017) used NaCl for the sediment separation, possibly resulting in underestimation of PVC or PET abundances (Quinn et al., 2017). Additionally, KOH was used by Lin et al. (2018) to digest biogenic materials, which also resulted in PET losses. Furthermore, the microplastic size ranges considered are of great importance. In this study, mainly particles smaller than 250 μm (93.2%) were found, while Strady et al. (2020) included especially items $\geq 250 \mu\text{m}$ in their results. In other Chinese regions within the Yellow Sea and the East China Sea, Zhang et al. (2019a) counted 0.6–2.4 items (10 g d.w.)⁻¹ for a considered particle size range between 60 and 5000 μm . Even this size range would exclude 51.9% of the total microplastic amount reported in this study. Zhao et al. (2018) used the same size range as Zhang et al. do and saturated NaCl for the density separation as Peng et al. (2017). In the study of Bergmann et al. (2017) sediment samples taken from the Arctic deep-sea were separated with a ZnCl_2 density solution and a size range of microplastics between particles smaller than 11 μm and 5000 μm were considered. This approach considered PET and PVC microplastic particles and a similar particle size range as in the present survey. They found microplastic abundances between 0.4 and 66.0 items (10 g d.w.)⁻¹ at 250–5500 m water depth, noticeable more than presented results from the South China Sea.

These comparisons show the importance of a uniform preparation and evaluation method, but the sampling method is also of great importance, which is particularly pronounced for environmental water samples. For the microplastic detection, either bulk water samples or net samples with various mesh sizes were used, which is directly related to the amount of microplastic particles collected (Cai et al., 2018; Desforges et al., 2014; Di Mauro et al., 2017; Hidalgo-Ruz et al., 2012; Lindeque et al., 2020; Nel and Froneman, 2015). In addition to the sampling instruments, sampling depths, considered particle size ranges, and separation methods differ between previous studies, which impedes a dependable comparison and leads to strong variable outcomes of up to seven orders of magnitude (Table 2). Investigations of Pearl River surface water implemented by Lin et al. (2018) revealed that considerably higher abundances were found (379–7924 items m^{-3}) than those measured in the South China Sea in this study (17–25 items m^{-3}). These results may be attributed to the expected higher microplastic abundance in rivers (Luo et al., 2019) or the difference in the sampling procedure. Lin et al. used 5 L sample bottles to scoop the upper water body and filtered the contents with a 20 μm membrane filter, allowing smaller and buoyant particles to be captured. Equally large amounts (301–7467 items m^{-3}) were detected in the South China Sea by Cai et al. (2018). They used a pump-based sampling system that considered particle sizes down to 20 μm as well. In addition to the pump sampling, Cai et al. used a conventional bongo net (333 μm mesh size) for comparison and found 0–0.33 items m^{-3} , which is about 70 times less than the results reported in this study. In contrast, Tsang et al. (2017) reported results in the same order of magnitude as this study with abundances ranging between 0.5 and 279 items m^{-3} in Hong Kong marine waters. They collected surface samples using a plankton net with a comparable mesh size (153 μm) but also used NaCl to remove sediments.

With these initial results presented in this research, we would like to encourage minimizing the methods used for scientific field studies to separate microplastics, but with maximum detection accuracy for the

uniform method used. A homogenized method is essential to achieve global comparability of microplastic abundances (Dehaut et al., 2019).

In this study, a new microplastic separation technique is proposed that is suitable for most sample types, especially for volume- or mass-limited samples and small-sized microplastic items, with a low risk of contamination due to the few and simple processing steps required.

5. Conclusion

Within this study, we developed a commonly applicable, sample-type-independent microplastic separation method with high matrix removal efficiency and high microplastic recovery accuracy. The goal was to reduce the effort required for microplastic detection to enable a realistically performable method for a broader number of institutions. Our outcomes represent a new simple, inexpensive, and rapid method that is particularly suitable for small sample volumes or masses and low analyte abundances. For this method, we used H₂O₂ (30%) as a digestion agent, with the subsequent addition of acetic acid (24%) and an adsorption separation technique implemented by a coated syringes cascade. We achieved an average matrix removal efficacy of 96.25 ± 0.33% with a microplastic particle recovery rate of 98.0 ± 3.8% and a minimized risk of influences by chemical pretreatment, realized through shortened exposure times. Applying this combined adsorption separation technique, the detection by using the Nile red staining method gained in accuracy and subsequent spectral analysis could be accelerated and specified due to lower remaining natural particles. Nevertheless, this new adsorption separation technique offers further opportunities for improvement, especially for a stronger PA adsorption and the separation possibility of sediment sample masses larger than 10 g.

By applying this technique, we already detected comparatively large amounts of small-sized microplastic particles in small volumes of two different marine sample types. However, comparability with previous studies is poor due to the different preparation and sampling methods used in previous studies worldwide.

With this research, we want to emphasize the importance of a uniformly applied microplastic detection technique. More accurate and large-scale studies could present a clearer status of the global microplastic pollution situation, which would be of great benefit for further actions towards environment protection.

CRedit authorship contribution statement

Janika Reineccius: Investigation, analysis, writing draft, writing review & editing. **Jonas Bresien:** Assistance with Raman utilization. **Joanna J. Waniak:** Project leader, funding acquisition, revision of all manuscript versions, project supervision.

Declaration of competing interest

The authors declare that they have no known competing financial interests or personal relationships that could have appeared to influence the work reported in this paper.

Acknowledgements

This study carried out by the Leibniz Institute for Baltic Sea Research Warnemünde, Germany (IOW) is a contribution to the Sino-German MEGAPOL project. MEGAPOL received funding from the Federal Ministry of Education and Research (03F0786A) and SO269-SOCLIS BMBF project (FKZ 03G0269). We thank all scientific and ship crew members of the SO269 cruise. Furthermore, we owe thanks to the inorganic research group of Prof. Dr. Seidel and Prof. Dr. Schulz for the provision of the Raman spectrometer (both University of Rostock, Germany). Finally, we would like to thank Dr. Mischa Schönke (IOW), Andreas Frahm (IOW), Dr. Jassin Petersen (University of Cologne), and

Dr. Ralf Prien (IOW) as well as Anne Köhler (IOW) for sampling and sample preparation support.

Appendix A. Supplementary data

Supplementary data to this article can be found online at <https://doi.org/10.1016/j.scitotenv.2021.147881>.

References

- Abts, G., 2016. *Kunststoff-Wissen für Einsteiger*. 3rd ed. Hanser, Munich.
- Alimba, C.G., Faggio, C., 2019. Microplastics in the marine environment: current trends in environmental pollution and mechanisms of toxicological profile. *Environ. Toxicol. Pharmacol.* 68, 61–74. <https://doi.org/10.1016/j.etap.2019.03.001>.
- Alimi, O.S., Farner Budarz, J., Hernandez, L.M., Tufenkji, N., 2018. Microplastics and nanoplastics in aquatic environments: aggregation, deposition, and enhanced contaminant transport. *Environ. Sci. Technol.* 52, 1704–1724. <https://doi.org/10.1021/acs.est.7b05559>.
- Andrady, A.L., 2011. Microplastics in the marine environment. *Mar. Pollut. Bull.* 62, 1596–1605. <https://doi.org/10.1016/j.marpolbul.2011.05.030>.
- Anger, P.M., Precht, L., Elsner, M., Niessner, R., Ivleva, N.P., 2019. Implementation of an open source algorithm for particle recognition and morphological characterisation for microplastic analysis by means of Raman microspectroscopy. *Anal. Methods* 11, 3483–3489. <https://doi.org/10.1039/c9ay01245a>.
- Araujo, C.F., Nolasco, M.M., Ribeiro, A.M.P., Ribeiro-Claro, P.J.A., 2018. Identification of microplastics using Raman spectroscopy: latest developments and future prospects. *Water Res.* 142, 426–440. <https://doi.org/10.1016/j.watres.2018.05.060>.
- Auta, H.S., Emenike, C.U., Fauziah, S.H., 2017. Distribution and importance of microplastics in the marine environment: A review of the sources, fate, effects, and potential solutions. *Environ. Int.* 102, 165–176. <https://doi.org/10.1016/j.envint.2017.02.013>.
- Avio, C.G., Gorbi, S., Regoli, F., 2015. Experimental development of a new protocol for extraction and characterization of microplastics in fish tissues: first observations in commercial species from Adriatic Sea. *Mar. Environ. Res.* 111, 18–26. <https://doi.org/10.1016/j.marenvres.2015.06.014>.
- Avio, C.G., Pittura, L., d'Errico, G., Abel, S., Amorello, S., Marino, G., Gorbi, S., Regoli, F., 2020. Distribution and characterization of microplastic particles and textile microfibers in Adriatic food webs: general insights for biomonitoring strategies. *Environ. Pollut.* 258, 113766. <https://doi.org/10.1016/j.envpol.2019.113766>.
- Ballent, A., Corcoran, P.L., Madden, O., Helm, P.A., Longstaffe, F.J., 2016. Sources and sinks of microplastics in Canadian Lake Ontario nearshore, tributary and beach sediments. *Mar. Pollut. Bull.* 110, 383–395. <https://doi.org/10.1016/j.marpolbul.2016.06.037>.
- Barnes, D.K.A., Galgani, F., Thompson, R.C., Barlaz, M., 2009. Accumulation and fragmentation of plastic debris in global environments. *Philos. Trans. R. Soc. B Biol. Sci.* 364, 1985–1998. <https://doi.org/10.1098/rstb.2008.0205>.
- Bellas, J., Martínez-Armenttal, J., Martínez-Cámara, A., Besada, V., Martínez-Gómez, C., 2016. Ingestion of microplastics by demersal fish from the Spanish Atlantic and Mediterranean coasts. *Mar. Pollut. Bull.* 109, 55–60. <https://doi.org/10.1016/j.marpolbul.2016.06.026>.
- Bergmann, M., Wirzberger, V., Krumpfen, T., Lorenz, C., Primpke, S., Tekman, M.B., Gerdt, G., 2017. High quantities of microplastic in arctic deep-sea sediments from the HAUSGARTEN observatory. *Environ. Sci. Technol.* 51, 11000–11010. <https://doi.org/10.1021/acs.est.7b03331>.
- Brennecke, D., Duarte, B., Paiva, F., Caçador, I., Canning-Clode, J., 2016. Microplastics as vector for heavy metal contamination from the marine environment. *Estuar. Coast. Shelf Sci.* 178, 189–195. <https://doi.org/10.1016/j.ecss.2015.12.003>.
- Browne, M.A., Crump, P., Niven, S.J., Teuten, E., Tonkin, A., Galloway, T., Thompson, R., 2011. Accumulation of microplastic on shorelines worldwide: sources and sinks. *Environ. Sci. Technol.* 45, 9175–9179. <https://doi.org/10.1021/es201811s>.
- Budimir, S., Setälä, O., Lehtiniemi, M., 2018. Effective and easy to use extraction method shows low numbers of microplastics in offshore planktivorous fish from the northern Baltic Sea. *Mar. Pollut. Bull.* 127, 586–592. <https://doi.org/10.1016/j.marpolbul.2017.12.054>.
- Cai, M., He, H., Liu, M., Li, S., Tang, G., Wang, W., Huang, P., Wei, G., Lin, Y., Chen, B., Hu, J., Cen, Z., 2018. Lost but can't be neglected: huge quantities of small microplastics hide in the South China Sea. *Sci. Total Environ.* 633, 1206–1216. <https://doi.org/10.1016/j.scitotenv.2018.03.197>.
- Carbery, M., O'Connor, W., Palanisami, T., 2018. Trophic transfer of microplastics and mixed contaminants in the marine food web and implications for human health. *Environ. Int.* 115, 400–409. <https://doi.org/10.1016/j.envint.2018.03.007>.
- Castillo, A.B., Al-Maslami, I., Obbard, J.P., 2016. Prevalence of microplastics in the marine waters of Qatar. *Mar. Pollut. Bull.* 111, 260–267. <https://doi.org/10.1016/j.marpolbul.2016.06.108>.
- Choy, C.A., Robison, B.H., Gagne, T.O., Erwin, B., Firl, E., Halden, R.U., Hamilton, J.A., Katija, K., Lisin, S.E., Rolsky, S., C., Van Houtan, K., 2019. The vertical distribution and biological transport of marine microplastics across the epipelagic and mesopelagic water column. *Sci. Rep.* 9, 1–9. <https://doi.org/10.1038/s41598-019-44117-2>.
- Claessens, M., Van Cauwenberghe, L., Vandegehuchte, M.B., Janssen, C.R., 2013. New techniques for the detection of microplastics in sediments and field collected organisms. *Mar. Pollut. Bull.* 70, 227–233. <https://doi.org/10.1016/j.marpolbul.2013.03.009>.
- Cole, M., Webb, H., Lindeque, P.K., Fileman, E.S., Halsband, C., Galloway, T.S., 2014. Isolation of microplastics in biota-rich seawater samples and marine organisms. *Sci. Rep.* 4, 1–8. <https://doi.org/10.1038/srep04528>.

- Coppock, R.L., Cole, M., Lindeque, P.K., Queirós, A.M., Galloway, T.S., 2017. A small-scale, portable method for extracting microplastics from marine sediments. *Environ. Pollut.* 230, 829–837. <https://doi.org/10.1016/j.envpol.2017.07.017>.
- Cózar, A., Echevarria, F., Gonzalez-Gordillo, J.J., Irigoien, X., Ubeda, B., Hernandez-Leon, S., Palma, A.T., Navarro, S., Garcia-de-Lomas, J., Ruiz, A., Fernandez-de-Puelles, M.L., Duarte, C.M., 2014. Plastic debris in the open ocean. *Proc. Natl. Acad. Sci.* 111, 10239–10244. <https://doi.org/10.1073/pnas.1314705111>.
- Crichton, E.M., Noël, M., Gies, E.A., Ross, P.S., 2017. A novel, density-independent and FTIR-compatible approach for the rapid extraction of microplastics from aquatic sediments. *Anal. Methods* 9, 1419–1428. <https://doi.org/10.1039/c6ay02733d>.
- Dehaut, A., Cassone, A.L., Frère, L., Hermabessiere, L., Himber, C., Rinnert, E., Rivière, G., Lambert, C., Soudant, P., Huvet, A., Duflos, G., Paul-Pont, I., 2016. Microplastics in sea-food: benchmark protocol for their extraction and characterization. *Environ. Pollut.* 215, 223–233. <https://doi.org/10.1016/j.envpol.2016.05.018>.
- Dehaut, A., Hermabessiere, L., Duflos, G., 2019. Current frontiers and recommendations for the study of microplastics in seafood. *TrAC - Trends Anal. Chem.* 116, 346–359. <https://doi.org/10.1016/j.trac.2018.11.011>.
- Derraik, J.G.B., 2002. The pollution of the marine environment by plastic debris: a review. *Mar. Pollut. Bull.* 44, 842–852. [https://doi.org/10.1016/S0025-326X\(02\)00220-5](https://doi.org/10.1016/S0025-326X(02)00220-5).
- Desforges, J.P.W., Galbraith, M., Dangerfield, N., Ross, P.S., 2014. Widespread distribution of microplastics in subsurface seawater in the NE Pacific Ocean. *Mar. Pollut. Bull.* 79, 94–99. <https://doi.org/10.1016/j.marpolbul.2013.12.035>.
- Desforges, J.P.W., Galbraith, M., Ross, P.S., 2015. Ingestion of microplastics by zooplankton in the Northeast Pacific Ocean. *Arch. Environ. Contam. Toxicol.* 69, 320–330. <https://doi.org/10.1007/s00244-015-0172-5>.
- Devriese, L.L., van der Meulen, M.D., Maes, T., Bekaert, K., Paul-Pont, I., Frère, L., Robbens, J., Vethaak, A.D., 2015. Microplastic contamination in brown shrimp (*Crangon crangon*, Linnaeus 1758) from coastal waters of the southern North Sea and channel area. *Mar. Pollut. Bull.* 98, 179–187. <https://doi.org/10.1016/j.marpolbul.2015.06.051>.
- Di Mauro, R., Kupchik, M.J., Benfield, M.C., 2017. Abundant plankton-sized microplastic particles in shelf waters of the northern Gulf of Mexico. *Environ. Pollut.* 230, 798–809. <https://doi.org/10.1016/j.envpol.2017.07.030>.
- Ding, J., Jiang, F., Li, J., Wang, Zongxing, Sun, C., Wang, Zhangyi, Fu, L., Ding, N.X., He, C., 2019. Microplastics in the coral reef systems from Xisha Islands of South China Sea. *Environ. Sci. Technol.* 53, 8036–8046. <https://doi.org/10.1021/acs.est.9b01452>.
- Doyle, M.J., Watson, W., Bowlin, N.M., Sheavly, S.B., 2011. Plastic particles in coastal pelagic ecosystems of the Northeast Pacific ocean. *Mar. Environ. Res.* 71, 41–52. <https://doi.org/10.1016/j.marenvres.2010.10.001>.
- Dris, R., Gasperi, J., Mirande, C., Mandin, C., Guerrouache, M., Langlois, V., Tassin, B., 2017. A first overview of textile fibers, including microplastics, in indoor and outdoor environments. *Environ. Pollut.* 221, 453–458. <https://doi.org/10.1016/j.envpol.2016.12.013>.
- Eerkes-Medrano, D., Thompson, R.C., Aldridge, D.C., 2015. Microplastics in freshwater systems: a review of the emerging threats, identification of knowledge gaps and prioritisation of research needs. *Water Res.* 75, 63–82. <https://doi.org/10.1016/j.watres.2015.02.012>.
- Enders, K., Lenz, R., Stedmon, C.A., Nielsen, T.G., 2015. Abundance, size and polymer composition of marine microplastics $\geq 10\mu\text{m}$ in the Atlantic Ocean and their modelled vertical distribution. *Mar. Pollut. Bull.* 100, 70–81. <https://doi.org/10.1016/j.marpolbul.2015.09.027>.
- Enders, K., Lenz, R., Beer, S., Stedmon, C.A., 2017. Extraction of microplastic from biota: recommended acidic digestion destroys common plastic polymers. *ICES J. Mar. Sci.* 74, 326–331. <https://doi.org/10.1093/icesjms/fsw173>.
- Erni-Cassola, G., Gibson, M.I., Thompson, R.C., Christie-Oleza, J.A., 2017. Lost, but found with Nile Red: a novel method for detecting and quantifying small microplastics (1 mm to 20 μm) in environmental samples. *Environ. Sci. Technol.* 51, 13641–13648. <https://doi.org/10.1021/acs.est.7b04512>.
- Filgueiras, A.V., Gago, J., Campillo, J.A., León, V.M., 2019. Microplastic distribution in surface sediments along the Spanish Mediterranean continental shelf. *Environ. Sci. Pollut. Res.* 26, 21264–21273. <https://doi.org/10.1007/s11356-019-05341-5>.
- Frère, L., Paul-Pont, I., Rinnert, E., Petton, S., Jaffré, J., Bihannic, I., Soudant, P., Lambert, C., Huvet, A., 2017. Influence of environmental and anthropogenic factors on the composition, concentration and spatial distribution of microplastics: a case study of the Bay of Brest (Brittany, France). *Environ. Pollut.* 225, 211–222. <https://doi.org/10.1016/j.envpol.2017.03.023>.
- Frias, J.P.G.L., Sobral, P., Ferreira, A.M., 2010. Organic pollutants in microplastics from two beaches of the Portuguese coast. *Mar. Pollut. Bull.* 60, 1988–1992. <https://doi.org/10.1016/j.marpolbul.2010.07.030>.
- Gewert, B., Ogonowski, M., Barth, A., MacLeod, M., 2017. Abundance and composition of near surface microplastics and plastic debris in the Stockholm Archipelago, Baltic Sea. *Mar. Pollut. Bull.* 120, 292–302. <https://doi.org/10.1016/j.marpolbul.2017.04.062>.
- Geyer, R., Jambeck, J.R., Law, K.L., 2017. Production, use, and fate of all plastics ever made. *Sci. Adv.* 3, 25–29. <https://doi.org/10.1126/sciadv.1700782>.
- Gourmelon, G., 2015. Global plastic production rises, recycling lags | Worldwatch Institute. *Worldwatch Inst.* 1–7.
- Graca, B., Beldowska, M., Wrzesień, P., Zgrundo, A., 2014. Styrofoam debris as a potential carrier of mercury within ecosystems. *Environ. Sci. Pollut. Res.* 21, 2263–2271. <https://doi.org/10.1007/s11356-013-2153-4>.
- Hengstmann, E., Tamminga, M., vom Bruch, C., Fischer, E.K., 2018. Microplastic in beach sediments of the isle of Rügen (Baltic Sea) - implementing a novel glass elutriation column. *Mar. Pollut. Bull.* 126, 263–274. <https://doi.org/10.1016/j.marpolbul.2017.11.010>.
- Herrera, A., Garrido-Amador, P., Martínez, I., Samper, M.D., López-Martínez, J., Gómez, M., Packard, T.T., 2018. Novel methodology to isolate microplastics from vegetal-rich samples. *Mar. Pollut. Bull.* 129, 61–69. <https://doi.org/10.1016/j.marpolbul.2018.02.015>.
- Hidalgo-Ruz, V., Gutow, L., Thompson, R.C., Thiel, M., 2012. Microplastics in the marine environment: a review of the methods used for identification and quantification. *Environ. Sci. Technol.* 46, 3060–3075. <https://doi.org/10.1021/es2031505>.
- Hoellein, T.J., Shogren, A.J., Tank, J.L., Risteca, P., Kelly, J.J., 2019. Microplastic deposition velocity in streams follows patterns for naturally occurring allochthonous particles. *Sci. Rep.* 9, 1–11. <https://doi.org/10.1038/s41598-019-40126-3>.
- Hurley, R.R., Lusher, A.L., Olsen, M., Nizzetto, L., 2018. Validation of a method for extracting microplastics from complex, organic-rich, environmental matrices. *Environ. Sci. Technol.* 52, 7409–7417. <https://doi.org/10.1021/acs.est.8b01517>.
- Imhof, H.K., Laforsch, C., Wiesheu, A.C., Schmid, J., Anger, P.M., Niessner, R., Ivleva, N.P., 2016. Pigments and plastic in limnetic ecosystems: a qualitative and quantitative study on microplastics of different size classes. *Water Res.* 98, 64–74. <https://doi.org/10.1016/j.watres.2016.03.015>.
- Kanhai, L.D.K., Officer, R., Lyashevskaya, O., Thompson, R.C., O'Connor, I., 2017. Microplastic abundance, distribution and composition along a latitudinal gradient in the Atlantic Ocean. *Mar. Pollut. Bull.* 115, 307–314. <https://doi.org/10.1016/j.marpolbul.2016.12.025>.
- Kanhai, L.D.K., Johansson, C., Frias, J.P.G.L., Gardfeldt, K., Thompson, R.C., O'Connor, I., 2019. Deep sea sediments of the Arctic Central Basin: a potential sink for microplastics. *Deep. Res. Part I Oceanogr. Res.* 145, 137–142. <https://doi.org/10.1016/j.dsr.2019.03.003>.
- Käppler, A., Fischer, D., Oberbeckmann, S., Schernewski, G., Labrenz, M., Eichhorn, K.J., Voit, B., 2016. Analysis of environmental microplastics by vibrational microspectroscopy: FTIR, Raman or both? *Anal. Bioanal. Chem.* 408, 8377–8391. <https://doi.org/10.1007/s00216-016-9956-3>.
- Karami, A., Golieskardi, A., Choo, C.K., Romano, N., Ho, Y. Bin, Salamatinia, B., 2017. A high-performance protocol for extraction of microplastics in fish. *Sci. Total Environ.* 578, 485–494. <https://doi.org/10.1016/j.scitotenv.2016.10.213>.
- Karlsson, T.M., Vethaak, A.D., Almroth, B.C., Ariese, F., van Velzen, M., Hassellöv, M., Leslie, H.A., 2017. Screening for microplastics in sediment, water, marine invertebrates and fish: method development and microplastic accumulation. *Mar. Pollut. Bull.* 122, 403–408. <https://doi.org/10.1016/j.marpolbul.2017.06.081>.
- Koivunen, J., Heinonen-Tanski, H., 2005. Inactivation of enteric microorganisms with chemical disinfectants, UV irradiation and combined chemical/UV treatments. *Water Res.* 39, 1519–1526. <https://doi.org/10.1016/j.watres.2005.01.021>.
- Kühn, S., van Werven, B., van Oyen, A., Meijboom, A., Bravo Rebolledo, E.L., van Franeker, J.A., 2017. The use of potassium hydroxide (KOH) solution as a suitable approach to isolate plastics ingested by marine organisms. *Mar. Pollut. Bull.* 115, 86–90. <https://doi.org/10.1016/j.marpolbul.2016.11.034>.
- Kumar, R.G., Strom, K.B., Keyvani, A., 2010. Floc properties and settling velocity of San Jacinto estuary mud under variable shear and salinity conditions. *Cont. Shelf Res.* 30, 2067–2081. <https://doi.org/10.1016/j.csr.2010.10.006>.
- Li, J., Zhang, H., Zhang, K., Yang, R., Li, R., Li, Y., 2018. Characterization, source, and retention of microplastic in sandy beaches and mangrove wetlands of the Qinzhou Bay, China. *Mar. Pollut. Bull.* 136, 401–406. <https://doi.org/10.1016/j.marpolbul.2018.09.025>.
- Lin, L., Zuo, L.Z., Peng, J.P., Cai, L.Q., Fok, L., Yan, Y., Li, H.X., Xu, X.R., 2018. Occurrence and distribution of microplastics in an urban river: a case study in the Pearl River along Guangzhou City, China. *Sci. Total Environ.* 644, 375–381. <https://doi.org/10.1016/j.scitotenv.2018.06.327>.
- Lindeque, P.K., Cole, M., Coppock, R.L., Lewis, C.N., Miller, R.Z., Watts, A.J.R., Wilson-McNeal, A., Wright, S.L., Galloway, T.S., 2020. Are we underestimating microplastic abundance in the marine environment? A comparison of microplastic capture with nets of different mesh-size. *Environ. Pollut.* 265, 114721. <https://doi.org/10.1016/j.envpol.2020.114721>.
- Ling, S.D., Sinclair, M., Levi, C.J., Reeves, S.E., Edgar, G.J., 2017. Ubiquity of microplastics in coastal seafloor sediments. *Mar. Pollut. Bull.* 121, 104–110. <https://doi.org/10.1016/j.marpolbul.2017.05.038>.
- Liu, M., Lu, S., Song, Y., Lei, L., Hu, J., Lv, W., Zhou, W., Cao, C., Shi, H., Yang, X., He, D., 2018. Microplastic and mesoplastic pollution in farmland soils in suburbs of Shanghai, China. *Environ. Pollut.* 242, 855–862. <https://doi.org/10.1016/j.envpol.2018.07.051>.
- Löder, M.G.J., Imhof, H.K., Ladehoff, M., Lösche, L.A., Lorenz, C., Mintenig, S., Piehl, S., Primpke, S., Schrank, I., Laforsch, C., Gerdt, G., 2017. Enzymatic purification of microplastics in environmental samples. *Environ. Sci. Technol.* 51, 14283–14292. <https://doi.org/10.1021/acs.est.7b03055>.
- Lots, F.A.E., Behrens, P., Vijver, M.G., Horton, A.A., Bosker, T., 2017. A large-scale investigation of microplastic contamination: abundance and characteristics of microplastics in European beach sediment. *Mar. Pollut. Bull.* 123, 219–226. <https://doi.org/10.1016/j.marpolbul.2017.08.057>.
- Luo, W., Su, L., Craig, N.J., Du, F., Wu, C., Shi, H., 2019. Comparison of microplastic pollution in different water bodies from urban creeks to coastal waters. *Environ. Pollut.* 246, 174–182. <https://doi.org/10.1016/j.envpol.2018.11.081>.
- Martin, J., Lusher, A., Thompson, R.C., Morley, A., 2017. The deposition and accumulation of microplastics in marine sediments and bottom water from the Irish continental shelf. *Sci. Rep.* 7, 1–9. <https://doi.org/10.1038/s41598-017-11079-2>.
- Masura, J., Baker, J., Foster, G., Arthur, C., 2015. Laboratory methods for the analysis of microplastics in the marine environment. *NOAA Mar. Debris Progr. Natl.* 1–39. <https://doi.org/10.1016/j.jjcc.2016.11.011>.
- Matsuguma, Y., Takada, H., Kumata, H., Kanke, H., Sakurai, S., Suzuki, T., Itoh, M., Okazaki, Y., Boonyatumanond, R., Zakaria, M.P., Weerts, S., Newman, B., 2017. Microplastics in sediment cores from Asia and Africa as indicators of temporal trends in plastic pollution. *Arch. Environ. Contam. Toxicol.* 73, 230–239. <https://doi.org/10.1007/s00244-017-0414-9>.
- Mishra, S., Rath, C., Das, A.P., 2019. Marine micro fiber pollution : a review on present status and future challenges. *Mar. Pollut. Bull.* 140, 188–197. <https://doi.org/10.1016/j.marpolbul.2019.01.039>.

- Munno, K., Helm, P.A., Jackson, D.A., Rochman, C., Sims, A., 2018. Impacts of temperature and selected chemical digestion methods on microplastic particles. *Environ. Toxicol. Chem.* 37, 91–98. <https://doi.org/10.1002/etc.3935>.
- Murray, F., Rhys, P., Sea, C., 2011. Plastic contamination in the decapod crustacean *Nephrops norvegicus* (Linnaeus, 1758). *Mar. Pollut. Bull.* 62, 1207–1217. <https://doi.org/10.1016/j.marpolbul.2011.03.032>.
- Nel, H.A., Froneman, P.W., 2015. A quantitative analysis of microplastic pollution along the south-eastern coastline of South Africa. *Mar. Pollut. Bull.* 101, 274–279. <https://doi.org/10.1016/j.marpolbul.2015.09.043>.
- Nelms, S.E., Galloway, T.S., Godley, B.J., Jarvis, D.S., Lindeque, P.K., 2018. Investigating microplastic trophic transfer in marine top predators. *Environ. Pollut.* 238, 999–1007. <https://doi.org/10.1016/j.envpol.2018.02.016>.
- Nuelle, M.T., Dekiff, J.H., Remy, D., Fries, E., 2014. A new analytical approach for monitoring microplastics in marine sediments. *Environ. Pollut.* 184, 161–169. <https://doi.org/10.1016/j.envpol.2013.07.027>.
- Ogata, Y., Takada, H., Mizukawa, K., Hirai, H., Iwasa, S., Endo, S., Mato, Y., Saha, M., Okuda, K., Nakashima, A., Murakami, M., Zurcher, N., Booyatumanondo, R., Zakaria, M.P., Dung, L.Q., Gordon, M., Miguez, C., Suzuki, S., Moore, C., Karapanagioti, H.K., Weerts, S., McClurg, T., Burres, E., Smith, W., Velkenburg, M. Van, Lang, J.S., Lang, R.C., Laursen, D., Danner, B., Stewardson, N., Thompson, R.C., 2009. International Pellet Watch: global monitoring of persistent organic pollutants (POPs) in coastal waters. 1. Initial phase data on PCBs, DDTs, and HCHs. *Mar. Pollut. Bull.* 58, 1437–1446. <https://doi.org/10.1016/j.marpolbul.2009.06.014>.
- Olsen, L.M.B., Knutsen, H., Mahat, S., Wade, E.J., Arp, H.P.H., 2020. Facilitating microplastic quantification through the introduction of a cellulose dissolution step prior to oxidation: proof-of-concept and demonstration using diverse samples from the inner Oslofjord, Norway. *Mar. Environ. Res.* 161, 105080. <https://doi.org/10.1016/j.marenvres.2020.105080>.
- Pagter, E., Frias, J., Nash, R., 2018. Microplastics in Galway Bay: a comparison of sampling and separation methods. *Mar. Pollut. Bull.* 135, 932–940. <https://doi.org/10.1016/j.marpolbul.2018.08.013>.
- Peng, G., Zhu, B., Yang, D., Su, L., Shi, H., Li, D., 2017. Microplastics in sediments of the Changjiang Estuary, China. *Environ. Pollut.* 225, 283–290. <https://doi.org/10.1016/j.envpol.2016.12.064>.
- Peng, X., Chen, M., Chen, S., Dasgupta, S., Xu, H., Ta, K., Du, M., Li, J., Guo, Z., Bai, S., 2018. Microplastics contaminate the deepest part of the world's ocean. *Geochemical Perspect. Lett.* 9, 1–5. <https://doi.org/10.7185/geochemlet.1829>.
- Phuung, N.N., Poirier, L., Lagarde, F., Kamari, A., Zalouk-Vergnoux, A., 2018. Microplastic abundance and characteristics in French Atlantic coastal sediments using a new extraction method. *Environ. Pollut.* 243, 228–237. <https://doi.org/10.1016/j.envpol.2018.08.032>.
- Piarulli, S., Scapiniello, S., Comandini, P., Magnusson, K., Granberg, M., Wong, J.X.W., Sciotto, G., Prati, S., Mazzeo, R., Booth, A.M., Airolidi, L., 2019. Microplastic in wild populations of the omnivorous crab *Carcinus aestuarii*: a review and a regional-scale test of extraction methods, including microfibres. *Environ. Pollut.* 251, 117–127. <https://doi.org/10.1016/j.envpol.2019.04.092>.
- Prata, J.C., da Costa, J.P., Duarte, A.C., Rocha-Santos, T., 2019. Methods for sampling and detection of microplastics in water and sediment: a critical review. *TrAC - Trends Anal. Chem.* 110, 150–159. <https://doi.org/10.1016/j.trac.2018.10.029>.
- Quinn, B., Murphy, F., Ewins, C., 2017. Validation of density separation for the rapid recovery of microplastics from sediment. *Anal. Methods* 9, 1491–1498. <https://doi.org/10.1039/c6ay02542k>.
- Reed, C., 2015. Dawn of the plasticene age. *New Sci.* 225, 28–32. [https://doi.org/10.1016/S0262-4079\(15\)60215-9](https://doi.org/10.1016/S0262-4079(15)60215-9).
- Reed, S., Clark, M., Thompson, R., Hughes, K.A., 2018. Microplastics in marine sediments near Rothera Research Station, Antarctica. *Mar. Pollut. Bull.* 133, 460–463. <https://doi.org/10.1016/j.marpolbul.2018.05.068>.
- Reineccius, J., Appelt, J.S., Hinrichs, T., Kaiser, D., Stern, J., Prien, R.D., Waniek, J.J., 2020. Abundance and characteristics of microfibers detected in sediment trap material from the deep subtropical North Atlantic Ocean. *Sci. Total Environ.* 738, 140354. <https://doi.org/10.1016/j.scitotenv.2020.140354>.
- Rios, L.M., Moore, C., Jones, P.R., 2007. Persistent organic pollutants carried by synthetic polymers in the ocean environment. *Mar. Pollut. Bull.* 54, 1230–1237. <https://doi.org/10.1016/j.marpolbul.2007.03.022>.
- Shim, W.J., Song, Y.K., Hong, S.H., Jang, M., 2016. Identification and quantification of microplastics using Nile Red staining. *Mar. Pollut. Bull.* 113, 469–476. <https://doi.org/10.1016/j.marpolbul.2016.10.049>.
- Stock, F., Kochleus, C., Bansch-Baltruschat, B., Brennholt, N., Reifferscheid, G., 2019. Sampling techniques and preparation methods for microplastic analyses in the aquatic environment – a review. *TrAC - Trends Anal. Chem.* 113, 84–92. <https://doi.org/10.1016/j.trac.2019.01.014>.
- Stolte, A., Forster, S., Gerds, G., Schubert, H., 2015. Microplastic concentrations in beach sediments along the German Baltic coast. *Mar. Pollut. Bull.* 99, 216–229. <https://doi.org/10.1016/j.marpolbul.2015.07.022>.
- Strady, E., Dang, T.H., Dao, T.D., Dinh, H.N., Do, T.T.D., Duong, T.N., Duong, T.T., Hoang, D.A., Kieu-Le, T.C., Le, T.P.Q., Mai, H., Trinh, D.M., Nguyen, Q.H., Tran-Nguyen, Q.A., Tran, Q.V., Truong, T.N.S., Chu, V.H., Vo, V.C., 2020. Baseline assessment of microplastic concentrations in marine and freshwater environments of a developing Southeast Asian country. *Viet Nam. Mar. Pollut. Bull.*, 111870. <https://doi.org/10.1016/j.marpolbul.2020.111870>.
- Sudhakar, M., Doble, M., Murthy, P.S., Venkatesan, R., 2008. Marine microbe-mediated biodegradation of low- and high-density polyethylenes. *Int. Biodeterior. Biodegrad.* 61, 203–213. <https://doi.org/10.1016/j.ibiod.2007.07.011>.
- Suhrhoff, T.J., Scholz-Böttcher, B.M., 2016. Qualitative impact of salinity, UV radiation and turbulence on leaching of organic plastic additives from four common plastics – a lab experiment. *Mar. Pollut. Bull.* 102, 84–94. <https://doi.org/10.1016/j.marpolbul.2015.11.054>.
- Sun, X., Li, Q., Zhu, M., Liang, J., Zheng, S., Zhao, Y., 2017. Ingestion of microplastics by natural zooplankton groups in the northern South China Sea. *Mar. Pollut. Bull.* 115, 217–224. <https://doi.org/10.1016/j.marpolbul.2016.12.004>.
- Tagg, A.S., Harrison, J.P., Ju-Nam, Y., Sapp, M., Bradley, E.L., Sinclair, C.J., Ojeda, J.J., 2017. Fenton's reagent for the rapid and efficient isolation of microplastics from wastewater. *Chem. Commun.* 53, 372–375. <https://doi.org/10.1039/c6cc08798a>.
- Tammings, M., 2017. Nile red staining as a subsidiary method for microplastic Quantification: a comparison of three solvents and factors influencing application reliability. *SDRP J. Earth Sci. Environ. Stud.* 2. <https://doi.org/10.15436/jeses.2.2.1>.
- Teuten, E.L., Saquing, J.M., Knappe, D.R.U., Barlaz, M.A., Jonsson, S., Björn, A., Rowland, S.J., Thompson, R.C., Galloway, T.S., Yamashita, R., Ochi, D., Watanuki, Y., Moore, C., Viet, P.H., Tana, T.S., Prudente, M., Boonyatumanond, R., Zakaria, M.P., Akkhavong, K., Ogata, Y., Hirai, H., Iwasa, S., Mizukawa, K., Hagino, Y., Imamura, A., Saha, M., Takada, H., 2009. Transport and release of chemicals from plastics to the environment and to wildlife. *Philos. Trans. R. Soc. B Biol. Sci.* 364, 2027–2045. <https://doi.org/10.1098/rstb.2008.0284>.
- Tsang, Y.Y., Mak, C.W., Liebich, C., Lam, S.W., Sze, E.T.P., Chan, K.M., 2017. Microplastic pollution in the marine waters and sediments of Hong Kong. *Mar. Pollut. Bull.* 115, 20–28. <https://doi.org/10.1016/j.marpolbul.2016.11.003>.
- Tu, C., Chen, T., Zhou, Q., Liu, Y., Wei, J., Waniek, J.J., Luo, Y., 2020. Biofilm formation and its influences on the properties of microplastics as affected by exposure time and depth in the seawater. *Sci. Total Environ.* 734. <https://doi.org/10.1016/j.scitotenv.2020.139237>.
- Van Cauwenberghe, L., Janssen, C.R., 2014. Microplastics in bivalves cultured for human consumption. *Environ. Pollut.* 193, 65–70. <https://doi.org/10.1016/j.envpol.2014.06.010>.
- Van Cauwenberghe, L., Devriese, L., Galgani, F., Robbins, J., Janssen, C.R., 2015. Microplastics in sediments: a review of techniques, occurrence and effects. *Mar. Environ. Res.* 111, 5–17. <https://doi.org/10.1016/j.marenvres.2015.06.007>.
- Wang, W., Wang, J., 2018. Investigation of microplastics in aquatic environments: an overview of the methods used, from field sampling to laboratory analysis. *TrAC - Trends Anal. Chem.* 108, 195–202. <https://doi.org/10.1016/j.trac.2018.08.026>.
- Wang, T., Zou, X., Li, B., Yao, Y., Zang, Z., Li, Y., Yu, W., Wang, W., 2019. Preliminary study of the source apportionment and diversity of microplastics: taking floating microplastics in the South China Sea as an example. *Environ. Pollut.* 245, 965–974. <https://doi.org/10.1016/j.envpol.2018.10.110>.
- Yu, X., Peng, J., Wang, J., Wang, K., Bao, S., 2016. Occurrence of microplastics in the beach sand of the Chinese inner sea: the Bohai Sea. *Environ. Pollut.* 214, 722–730. <https://doi.org/10.1016/j.envpol.2016.04.080>.
- Zettler, E.R., Mincer, T.J., Amaral-Zettler, L.A., 2013. Life in the “plastisphere”: microbial communities on plastic marine debris. *Environ. Sci. Technol.* 47, 7137–7146. <https://doi.org/10.1021/es401288x>.
- Zhang, K., Su, J., Xiong, X., Wu, X., Wu, C., Liu, J., 2016. Microplastic pollution of lakeshore sediments from remote lakes in Tibet plateau, China. *Environ. Pollut.* 219, 450–455. <https://doi.org/10.1016/j.envpol.2016.05.048>.
- Zhang, W., Zhang, S., Wang, J., Wang, Y., Mu, J., Wang, P., Lin, X., Ma, D., 2017. Microplastic pollution in the surface waters of the Bohai Sea, China. *Environ. Pollut.* 231, 541–548. <https://doi.org/10.1016/j.envpol.2017.08.058>.
- Zhang, H., Zhou, Q., Xie, Z., Zhou, Y., Tu, C., Fu, C., Mi, W., Ebingerhaus, R., Christie, P., Luo, Y., 2018a. Occurrences of organophosphorus esters and phthalates in the microplastics from the coastal beaches in north China. *Sci. Total Environ.* 616–617, 1505–1512. <https://doi.org/10.1016/j.scitotenv.2017.10.163>.
- Zhang, S., Yang, X., Gertsen, H., Peters, P., Salánki, T., Geissen, V., 2018b. A simple method for the extraction and identification of light density microplastics from soil. *Sci. Total Environ.* 616–617, 1056–1065. <https://doi.org/10.1016/j.scitotenv.2017.10.213>.
- Zhang, C., Zhou, H., Cui, Y., Wang, C., Li, Y., Zhang, D., 2019a. Microplastics in offshore sediment in the Yellow Sea and East China Sea, China. *Environ. Pollut.* 244, 827–833. <https://doi.org/10.1016/j.envpol.2018.10.102>.
- Zhang, S., Wang, J., Liu, X., Qu, F., Wang, Xueshan, Wang, Xinrui, Li, Y., Sun, Y., 2019b. Microplastics in the environment: a review of analytical methods, distribution, and biological effects. *TrAC - Trends Anal. Chem.* 111, 62–72. <https://doi.org/10.1016/j.trac.2018.12.002>.
- Zhao, S., Danley, M., Ward, J.E., Li, D., Mincer, T.J., 2017. An approach for extraction, characterization and quantification of microplastic in natural marine snow using Raman microscopy. *Anal. Methods* 9, 1470–1478. <https://doi.org/10.1039/c6ay02302a>.
- Zhao, J., Ran, W., Teng, J., Liu, Y., Liu, H., Yin, X., Cao, R., Wang, Q., 2018. Microplastic pollution in sediments from the Bohai Sea and the Yellow Sea, China. *Sci. Total Environ.* 640–641, 637–645. <https://doi.org/10.1016/j.scitotenv.2018.05.346>.
- Zhou, Q., Tu, C., Fu, C., Li, Y., Zhang, H., Xiong, K., Zhao, X., Li, L., Waniek, J.J., Luo, Y., 2020a. Characteristics and distribution of microplastics in the coastal mangrove sediments of China. *Sci. Total Environ.* 703, 134807. <https://doi.org/10.1016/j.scitotenv.2019.134807>.
- Zhou, Q., Zhang, H., Waniek, J.J., Luo, Y., 2020b. The distribution and characteristics of microplastics in coastal beaches and mangrove wetlands. *Handb. Environ. Chem.* 95, 77–92. https://doi.org/10.1007/698_2020_459.
- Zhu, L., Bai, H., Chen, B., Sun, X., Qu, K., Xia, B., 2018. Microplastic pollution in North Yellow Sea, China: observations on occurrence, distribution and identification. *Sci. Total Environ.* 636, 20–29. <https://doi.org/10.1016/j.scitotenv.2018.04.182>.

Publication II

Full Research Paper, *Environmental Pollution*, 2022

First long-term evidence of microplastic pollution in the deep subtropical Northeast Atlantic

Janika Reineccius & Joanna J. Waniek

Submitted: 3 February 2022; Accepted: 10 April 2022

doi: 10.1016/j.envpol.2022.119302

Abstract No anthropogenic pollutant is more widespread in the aquatic and terrestrial environment than microplastic; however, there are large knowledge gaps regarding its origin, fate, or temporal variations in the oceans. In this study, we analyzed sediment trap material from the deep subtropical Northeast Atlantic (2000 m) in a long-term record (2003–2015) to assess the role of the deep ocean as a potential sink of microplastics. Microplastic particles were identified in all 110 analyzed samples with flux rates of 1.13–3146.81 items day⁻¹ m⁻². Calculated microplastic mass fluxes ranged between 0.10 and 1977.96 µg day⁻¹ m⁻², representing up to 8% of the particle flux. Between years, the composition of the different polymers changed significantly, dominated by polyethylene, whose amount was correlated with the lithogenic input. The correlation between polyethylene and the lithogenic fraction was attributed to an air transport pathway from northeast Africa and surrounding regions. The second most abundant polymer detected in our study was polyvinyl chloride, which is not correlated with lithogenic or biogenic particle flux fractions. Instead, we observed seasonality for polyvinyl chloride with recurring high fluxes in winter before the plankton bloom and significantly lower amounts in summer. Other polymers identified were polypropylene, polyethylene terephthalate, and lower numbers of polystyrene and polymethyl methacrylate. The average microplastic particle size for all samples and polymers was 88.44 ± 113.46 µm, with polyethylene and polyvinyl chloride having the highest proportion of small particles (< 100 µm). Our findings provide first insights into temporal variations of sinking microplastics, which are crucial for understanding the fate of plastic in the oceans.



First long-term evidence of microplastic pollution in the deep subtropical Northeast Atlantic[☆]

Janika Reineccius^{*}, Joanna J. Waniek

Leibniz Institute of Baltic Sea Research, Warnemünde, Seestraße 15, 18119, Rostock, Germany

ARTICLE INFO

Keywords:

Microplastics
Polymer types
Sources
Particle flux
Deep sea
Northeast Atlantic

ABSTRACT

No anthropogenic pollutant is more widespread in the aquatic and terrestrial environment than microplastic; however, there are large knowledge gaps regarding its origin, fate, or temporal variations in the oceans. In this study, we analyzed sediment trap material from the deep subtropical Northeast Atlantic (2000 m) in a long-term record (2003–2015) to assess the role of the deep ocean as a potential sink of microplastics. Microplastic particles were identified in all 110 analyzed samples with flux rates of 1.13–3146.81 items d⁻¹ m⁻². Calculated microplastic mass fluxes ranged between 0.10 and 1977.96 μg d⁻¹ m⁻², representing up to 8% of the particle flux. Between years, the composition of the different polymers changed significantly, dominated by polyethylene, whose amount was correlated with the lithogenic input. The correlation between polyethylene and the lithogenic fraction was attributed to an air transport pathway from northeast Africa and surrounding regions. The second most abundant polymer detected in our study was polyvinyl chloride, which is not correlated with lithogenic or biogenic particle flux fractions. Instead, we observed seasonality for polyvinyl chloride with recurring high fluxes in winter before the plankton bloom and significantly lower amounts in summer. Other polymers identified were polypropylene, polyethylene terephthalate, and lower numbers of polystyrene and polymethyl methacrylate. The average microplastic particle size for all samples and polymers was 88.44 ± 113.46 μm, with polyethylene and polyvinyl chloride having the highest proportion of small particles (<100 μm). Our findings provide first insights into temporal variations of sinking microplastics, which are crucial for understanding the fate of plastic in the oceans.

Author statement

Janika Reineccius: Designed the research content, investigation, analysis, evaluation of the data, writing draft, writing review & editing.

Joanna J. Waniek: Designed the research content, supervised all mooring works and analyses at Kiel 276, secured the funding, provided the idea of microplastic investigations, revised all manuscript drafts and final version.

1. Introduction

Plastic accompanies humans in all aspects of life and lifestyles with high economic importance and has received much attention in recent years due to its ubiquity in the environment (Andrady, 2011; Cole et al., 2011). Depending on the plastic type, it is mainly used as disposable packaging material but is also applied in the building, construction, and

automotive industries (Derraik, 2002). In 2015 alone, global plastic production reached 380 million metric tons (MT) and is still rising, with only about 9% being recycled, 12% incinerated, and 79% disposed of in landfills or accumulating in the natural environment (Geyer et al., 2017). Due to poor waste management, careless waste disposal, industries, or sewage sludge, terrestrial plastic enters the marine environment from land via rivers, atmospheric transport, and beach littering (Auta et al., 2017; Rochman, 2018). It can also be introduced directly via aquaculture, shipping, or fishing (Blumenröder et al., 2017; Chae et al., 2015; Rochman, 2018). Previous estimates indicated that up to 4 MT of plastic enters the oceans every year via rivers alone (Lebreton et al., 2017; Schmidt et al., 2017). Supported by the durability, plastic strongly accumulates in the oceans, causing various harmful effects on the marine ecosystem and human health (Wright and Kelly, 2017). Pollutants such as additives or monomers added during manufacturing, or precursors degradation products, may be released into the surrounding

[☆] This paper has been recommended for acceptance by Maria Cristina Fossi.

^{*} Corresponding author.

E-mail address: janika.reineccius@io-warnemuende.de (J. Reineccius).

water (Gewert et al., 2018). Besides that, microplastics in particular (1 μm –5000 μm in size) offer many attachment sites for lipophilic pollutants, pathogens, and harmful metals that can be transported across the globe adhering to the microplastic surface (Frias et al., 2010; Graca et al., 2014; Zettler et al., 2013). Due to the wide distribution, microplastics can easily be ingested by marine species from all over the world. Mussels are among the most affected species, consuming many microplastics by filtrating large amounts of water (Setälä et al., 2016). Via the food chain, microplastics are transferred to higher trophic levels and can already be verified in the most benthic, pelagic, as well as benthopelagic organisms (Avio et al., 2020; Coyle et al., 2020; Farrell and Nelson, 2013; Setälä et al., 2016). Microplastics that bioaccumulate in the digestive tract, reduce food uptake and survival of various marine animals, or release adsorbed contaminants impairing cellular and molecular functions (Au et al., 2017; Avio et al., 2015a). Due to these multiple dangers, understanding the fate and vertical and horizontal transport pathways of plastics is of great importance.

Currently, previous estimates of global microplastic pollution are based on concentrations determined at the ocean surface, ignoring concentrations in the water column and seabed (Kukulka et al., 2012; Poullain et al., 2019). The buoyancy properties of the most manufactured and commonly used plastic types (Andrady and Neal, 2009) suggest that the majority of plastic exposed to the environment accumulates on the water surface. However, recent investigations have shown that concentrations at the water surface are lower than in the water column and deep sea (Choy et al., 2019; Zhou et al., 2021), especially for millimeter-sized fragments smaller than 1 mm (Bergmann et al., 2017). The presence of microplastics at all depths has already been proven in the deep Arctic Ocean at 2–5569 m depth (Tekman et al., 2020) or the upper North Atlantic Ocean between 0 and 200 m depth (Pabortsava and Lampitt, 2020). This indicates a vertical distribution of microplastic particles through the water column and sinking from the water surface into the abyss even for light plastics with a lower density than oceanic water. The microplastic concentrations in the deep sea are already similar to those found in coastal sediments (Woodall et al., 2014). Once arrived in the deep sea, the lack of solar radiation, low temperatures, and lower oxygen concentrations relative to the atmosphere strongly slow the degradation process, leading to steadily increasing microplastic concentrations in the deep sea (Andrady, 2011). However, the sinking mechanism of microplastic under environmental conditions, especially for lightweight microplastics is not yet fully understood. Previous models have shown that mainly small microplastic particles sink through the water column due to biofouling or aggregation, increasing the microplastic sinking rates up to 81% (Kaiser et al., 2017; Kooi et al., 2017). Consequently, and due to the higher proportion of the small microplastic fraction (Araujo et al., 2018), the vertical distribution of the small fraction is expected to be much broader. However, the small microplastic size fraction (<200 μm) is often neglected in environmental surveys (Coyle et al., 2020) due to limited sampling abilities or high instrumental detection effort, leading to large gaps in the estimated global microplastic pollution.

To determine the exact input of plastic waste into the marine environment and to estimate the rate at which plastic sinks to the deep, measurements of microplastic quantities passing through the water column are necessary (Pabortsava and Lampitt, 2020). Another relevant task is distinguishing between the different polymer types. The enormously broad range of various chemical and physical properties can control the sinking pathway of microplastics (Kaiser et al., 2019, 2017; Kowalski et al., 2016) and thus their retention time in the water column and availability to native fauna.

Here, we provide the first long-term record of microplastic fluxes and compositions from 2003 to 2015 collected with a sediment trap. This trap was deployed at 2000 m depth at the time series station Kiel 276 (water depth 5300 m), moored in the subtropical Northeast Atlantic Ocean (33 °N, 22 °W). Using Raman spectroscopy, we measured microplastic particles down to 10 μm in size and discuss our findings in

the context of measurements in the Atlantic Ocean and predictive models from previous studies. Analyses of sediment trap material allowed us to assess the temporal variability of sinking microplastic within the water column and to define possible mechanisms responsible for microplastic sinking into the deep ocean. By additional analysis of the total sediment trap sample content, potential source regions for the collected material and thus for microplastics were identified.

2. Materials and methods

2.1. Study site and sampling

Sediment traps of the mooring station Kiel 276 were deployed and recovered with the RV POSEIDON and RV Maria S. MERIAN ship as part of eight Atlantic Transect cruises POS297, POS308, POS321, POS349, POS383, MSM18-1, POS459, and POS501 between April 2003 and June 2016. The mooring station is located at 33 °N, 22 °W within the 5300 m deep Madeira Basin at the edge of the North Atlantic Subtropical Gyre and contains a sediment trap at 2000 m depth (Fig. 1). Currents in this region are characterized by velocities of 20–25 cm s^{-1} between the thermocline (270 m) and the Mediterranean outflow (1000 m). Between 1000 and 2600 m depth, the velocities weaken to 5 cm s^{-1} , leading to a theoretical catchment area of about 100 km^2 for this trap (Waniek et al., 2005b). The interannual variability in wind strength at the study site is controlled by the North Atlantic Oscillation (NAO), which additionally influences the North Atlantic Subtropical Gyre, the Azores Current (surface - 2000 m depth), and the Azores Front (240 m depth) (Frazão et al., 2021; Fründt et al., 2013; Fründt and Waniek, 2012; Siedler et al., 2005). The resulting interannual and seasonal propagation of the Azores Front and associated eddy activity leads to temporal variations in the sediment trap's catchment area and affects the mixed layer depth and the related primary production in this area (Fründt and Waniek, 2012; Waniek et al., 2005b).

The primary production in the upper water column, together with the lithogenic particle input via atmospheric transport, constitutes the main content of the particle flux material at 2000 m depth (Brust et al., 2011; Fründt and Waniek, 2012; Waniek et al., 2005a). The biogenic flux, consisting mainly of calcium carbonate (up to 80%) in this part of the subtropical Northeast Atlantic Ocean and is highest in spring related to the water temperature and nutrient availability (Brust et al., 2011; Storz et al., 2009; Waniek et al., 2005b, 2005a). The lithogenic input depends on external sources such as Saharan dust outbreaks, occasionally transporting large amounts of dust to the sediment trap catchment area, which sinks to the deep sea supported by ballast effects (Brust and Waniek, 2010; Pullwer and Waniek, 2020). The lithogenic fraction accounts for 6–13% of the total particle flux and is characterized by a high clay content (Pullwer and Waniek, 2020; Waniek et al., 2005b). Due to the high clay content, the aluminum flux can be used as an indicator for the lithogenic fraction (Pullwer and Waniek, 2020; Waniek et al., 2005a).

The sediment traps used are fiberglass reinforced plastic funnels sealed with epoxide resin (funnel slope of 34°), with a 0.5 m^2 opening and a revolver holding 21 polypropylene sample bottles with 400 cm^3 volume (type S/MT 234, K.U.M., Germany) (Kremling et al., 1996). A hexagonal lattice grid baffle covers the sediment trap funnel to stabilize surrounding currents and reduce washout. This grid baffle is made of resin-sealed special paper to prevent contamination. After cleaning the entire sediment trap and sample bottles, the cleaned bottles were filled with a 4:1 mixture of in situ seawater (collected by Go/Flo sample bottles) and a 5% sodium azide solution with a resulting salinity of 35–38 g L^{-1} to preserve sinking material. On the ship, the loaded and recovered sample bottles were detached from the sediment trap, immediately closed with caps, and stored in the dark at 4–6 °C until laboratory analysis.

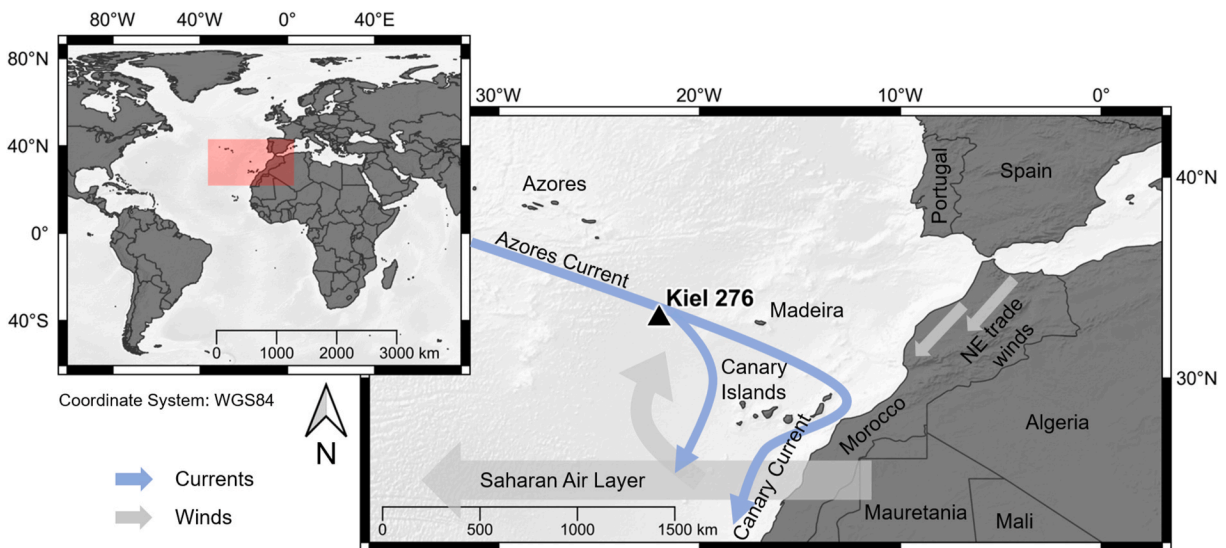


Fig. 1. Sampling location. Position of the long-term mooring station Kiel 276 (33 °N, 22 °W) and the prevailing major currents and winds (adopted from Pullwer and Waniek (2020)).

2.2. Sample preparation and microplastic separation

To determine microplastic particles in sediment traps flux material, the sample bottle content was divided into four equal aliquots using a Churn splitter, and large zooplankton ‘swimmers’ (>1 mm) were removed manually using Teflon tweezers. The liquid sample splits were filled directly into rinsed polypropylene sample bottles, capped, and stored in the dark at 4–6 °C until microplastic analysis. For the microplastic analysis, the sample splits were freeze-dried (-60 °C, 50 mbar) (Rios-Mendoza et al., 2021) and weighted into a beaker (100 mg if available). Freeze-drying is suspected of making microplastic particles brittle, as the temperature is below the glass transition temperature for some polymers in the freeze-drying process, and it has been reported to break cell walls and soil aggregates (Adomat and Grischek, 2021; Thomas et al., 2020). However, cells and other biogenic components contain water inside, which is not the case for plastic particles. To the best of our knowledge, there is no evidence of advanced fragmentation of microplastic particles caused by freeze-drying, but more detailed studies are needed (Adomat and Grischek, 2021; Thomas et al., 2020). After drying, the samples were treated using a previously validated method to separate small microplastic particles from small sample quantities without a loss (Reineccius et al., 2021). This method obtains a digestion step through the incubation with 10 mL hydrogen peroxide (H₂O₂; 30% w/w, for synthesis, Merck KGaA, Germany) for 5 h at 50 °C and 10 mL acetic acid (25% w/w, VWR International, Germany) at room temperature for 2 h. This step was implemented to reduce organic material and shell materials, respectively. The chemical resistance for these chemical concentrations, exposure times, and temperatures were established previously to ensure the integrity of the plastic particles after the treatment processes (Reineccius et al., 2021). The second step comprises the separation step in which the resulting sample solution was passed through a syringe (30 mL, polypropylene, Terumo, Japan) cascade coated with lubricant oil (Ernst GmbH & Co. KG, Germany). This separation method was validated for seven different microplastic particle types (high-density polyethylene, polypropylene, polystyrene, polyvinyl chloride, polyethylene terephthalate, polyamide, and polymethyl methacrylate) for the size range between 182.6 and 1252.8 μm with resulting recovery rates between 88.7 ± 8.6% for polyamide and 100.0 ± 0.0% for polyethylene, polypropylene, and polystyrene. This is a commonly used size range to validate microplastic separation methods and was also used by Catarino et al. (2017) (125–500 μm), Budimir et al. (2018) (100–1000 μm), and Castillo et al. (2016) with strongly differing

sizes between the polymer types (63–4700 μm). Li et al. (2018) and Avio et al. (2015b) used larger microplastic particle sizes ranging between 500 and 5000 μm. Within this adsorption separation step, the lipophilic microplastic particles were trapped on the interior syringe surface while biogenic residues and lithogenic material were removed. Overall, the solution was passed through the cascade three times, and the individual syringes were then rinsed with ultrapure water to remove non-trapped residues. The retained attached microplastic particles on the syringe surface were detached with a 50 °C detergent solution, which was subsequently filtered onto an Anodisc™ filter (Whatman™, 25 mm diameter, 0.2 μm nominal pore size, CatNo. 6809–6022). After sample filtration, the filtration funnel was rinsed with ultrapure water followed by ethanol (30%, Merck KGaA, Germany) to reduce surface tension (Peeken et al., 2018). The sample-loaded filter was then transferred to a glass slide and immediately covered with a coverslip to avoid airborne contamination.

2.3. Raman microscopy

Raman measurements were implemented to identify the molecular composition of potential microplastic particles. For measurements, a LabRAM HR 800 Horiba Jobin YVON Raman spectrometer combined with the system integrated NGS LabSpec software and coupled with an Olympus BX41 microscope with variable lenses and camera was used. Depending on the particle number visible on the filter, either the entire filter, a quarter, or randomly a minimum of 100 filter areas of the filter (corresponding to about 15%) were scanned for possible microplastic particles. The content was subsequently scaled for the entire filter, as suggested by Huppertsberg and Knepper (2018). The filters were manually scanned in transmitted light at an objective magnification of 10 × (window size 0.7 × 0.9 mm) to ensure high visibility for colored and uncolored particles. The minimum particle size reliably detectable by this method was 10 μm. Potential microplastic particles were measured at 50 × magnification with a red laser (633 nm, 17 mW, air-cooled HeNe laser) at 10 s integration time and 10 accumulation scans in the wavenumber range 50–3800 cm⁻¹. In the case of grand assembly of the same plastic type at the filter area, spectra were recorded at lower integration times and accumulation scans for quicker identification by the polymer-specific occurring peaks. Each measured particle was photographed after measurement in transmitted light at 10 × or 50 × magnification depending on their size for subsequent size calculation. Obtained spectra were compared against a spectral library

(WILEY) using the KnowItAll Information System 2020 software. At a matching degree >80% between the measured and polymer spectra from the database, particles were classified as the respective microplastic type. Due to spectral overlay, melting, or interfering fluorescence signals, it is usually impossible to measure dark-colored plastic particles with Raman spectroscopy. However, we could not find any dark-colored particles in our samples, except for some fibers. These fibers were not included in the present results.

2.4. Contamination prevention

The sediment traps were covered and rinsed before and after each deployment to avoid contamination during the sampling procedure. The cleaning procedure for the entire sediment trap includes the bottles, cone, revolver, and connector items and followed the standard treatment procedure for trace element analysis. This treatment comprises an acid treatment with a thorough subsequent rinse with ultrapure water under cleanroom conditions (Kuss and Kremling, 1999). The sample splitting, swimmer removal, and preparation of the fixing solution were carried out under the fume cupboard in a ‘class 100’ cleanroom under positive pressure (Kuss and Kremling, 1999). As reported by Wesch et al. (2017), working under a fume cupboard reduces airborne contamination (average contamination <1 fiber over 0.75–4.75 h) significantly, but blank samples were also prepared and analyzed additionally (see the following section). All following procedures during the digestion steps and the microplastic adsorption separation were performed under the fume cupboard by only one person working in the laboratory wearing a white cotton lab coat and nitrile gloves. Before and between the procedure steps, the working area was wiped damp using white paper towels. The samples were covered with aluminum foil between all treatment steps and for storage. Except for the sediment trap sample bottles and syringes, solely glass containers were used. These glass containers were rinsed thoroughly with ultrapure water immediately before usage. All chemicals and solutions applied for the sample treatment, and the adsorption-desorption processes (H₂O₂, acetic acid, detergent solution, ethanol) were filtered through a glass fiber filter (Whatman™, 47 mm diameter, 0.7 μm nominal pore size, CatNo. 1825–047). Ultrapure water, which was used to prepare the fixing solution and the sample filtration, was filtrated by a system integrated filter device (Millipak®, 47 mm diameter, 0.22 μm nominal pore size).

2.5. Blank test

Despite the elaborate contamination precautions, additional blank samples were prepared and analyzed to eliminate the possibility of airborne contamination. In each sediment trap deployment, one of the 21 sample bottles was not exposed to the marine environment anytime and was used here as a sampling blank (Lundgreen et al., 1997). Contamination by the sediment trap itself can be excluded due to the resin-sealed surface, the use of Teflon (a single Teflon particle was found in one of 110 samples), or metals for every trap component. These sampling blanks were treated and analyzed for the sample series 24, 25, 26, and 29 analogously to the samples. Besides these sampling blanks, method blanks were prepared to distinguish between contamination during treatment in the laboratory and field sampling (Supplementary Tab. S4). Method blanks were prepared simultaneously with a set of 5–10 samples by pouring the digestion chemicals into an empty beaker. Blanks were then treated and analyzed equally to the samples, as described in section 2.2.

2.6. Flux calculations

Prior to calculating the microplastic fluxes, the count of microplastic particles detected on the blank filters was subtracted from the count of microplastic particles identified in the samples. For the microplastic flux Φ_F (items d⁻¹ m⁻²) calculation, the blank-corrected microplastic count n

per sample filter, the sampling duration t , sampling area A , the total sample mass m_{TS} , as well as the used sample mass m_{US} are needed (Reineccius et al., 2020):

$$\Phi_F [\text{items d}^{-1} \text{ m}^{-2}] = \frac{m_{TS}}{m_{US}} \times \frac{n}{t[\text{d}] \times A[\text{m}^2]} \quad (1)$$

The microplastic particle mass required to determine the microplastic mass flux Φ_{MF} (μg d⁻¹ m⁻²) was calculated by multiplying the polymer-specific density (Hidalgo-Ruz et al., 2012) with the particle volume obtained by the two-dimensional (2D) size measurements of the particle images taken by Raman microscopy. For the measurements, the open-source software FIJI-ImageJ 1.53 (Schindelin et al., 2012) was applied using the manually set threshold for pixel brightness for every image to optimize the accuracy for individual particle area measurements (Pabortsava and Lampitt, 2020). Depending on the particle shape, volumes were calculated based on an ellipsoidal (spheres/fragments) or cylindrical shape (elongated particles/fibers) for every microplastic particle. For ellipsoidal-shaped particles, the measured length (maximum axis) and area were used to calculate the best fitting width (minimum axis) according to the method used by Kumar et al. (2010) (used formulas are additionally provided in Supplementary materials ‘Volume calculation’). The same procedure was applied to calculate the mass of microplastics analyzed on the blank filters, which was subtracted from the microplastic mass in the samples before further calculations. The microplastic mass flux was calculated analogously to formula (1) by replacing the blank-corrected microplastic count with the blank-corrected microplastic mass of the respective sample m_{MP} :

$$\Phi_{MF} [\mu\text{g d}^{-1} \text{ m}^{-2}] = \frac{m_{TS}}{m_{US}} \times \frac{m_{MP}}{t[\text{d}] \times A[\text{m}^2]} \quad (2)$$

2.7. Statistical analysis

The statistical evidence used is based on the Neyman-Pearson correlation tests and the nonparametric Mann-Whitney U tests (Pabortsava and Lampitt, 2020). These tests were performed applying the open-source python software (Spyder version 5.0.3) or the statistic program Past (version 4.02). The correlation test was implemented to examine relationships between microplastic (mass) fluxes and element or particle fluxes. Furthermore, correlations with dust in the atmosphere given as the Aerosol Optical Depth (AOD_{550nm}) or precipitation above the water column, particulate organic carbon (POC) concentrations in surface water, or the position of the Azores Front were examined. Significant differences in heavy or light polymer fluxes between the seasons were proven using the Mann-Whitney U test. For this purpose, the respective fluxes were assigned to the spring, summer, fall, or winter months and then compared mutually. A significance level of 5% (α = 0.05) was chosen for both tests.

3. Data availability

All data regarding the microplastic and particle fluxes are attached in the Supplementary materials or are available from the authors upon request. Element and mineral fluxes are available in previous studies (Brust and Waniek, 2010; Pullwer and Waniek, 2020) or upon request from the authors. Additional data about the mooring station Kiel 276 and related ship cruises can be found in the report from Müller and Waniek (2013), downloaded from the public repository PANGAEA (<https://doi.pangaea.de/10.1594/PANGAEA.836,686>) or can be taken from the cruise reports (https://doi.org/10.2312/cr_po459, https://doi.org/10.3289/CR_POS_501). NAO data are freely available at <https://cru.data.uea.ac.uk/cru/data/nao/nao.dat>, updated from Jones et al. (1997).

4. Results

4.1. Temporal variabilities of microplastic fluxes and microplastic mass fluxes

To obtain a time series of microplastic items and masses sinking into the deep sea, we collected and analyzed particle flux material from a 2000 m sediment trap moored at station Kiel 276 in the subtropical northeastern Atlantic Ocean (Pullwer and Waniek, 2020; Waniek et al., 2005b, 2005a). A total of 110 particle flux samples taken between April 2003 and June 2015 were analyzed using Raman microscopy, in which we found microplastic in quantities between 4 and 6816 particles per sample filter. On the blank filters, we found a microplastic particle quantity between 0 and 7 items per filter (0.9 items per filter on average), which mainly consisted of polyethylene and polypropylene, but we also found one polystyrene and one polyethylene terephthalate particle (Tab. S5). After blank correction, this resulted in microplastic fluxes between 1.13 and 3146.81 items $d^{-1} m^{-2}$ sinking into the deep subtropical Atlantic Ocean. The microplastic fluxes show high variability between years and months. The highest microplastic flux signals were observed in May and June 2003 (series 23), in March through June 2004 (series 24), and in September 2010 through April 2011 (series 27) (Fig. 2A). The maximum microplastic mass flux was examined for the sample collected during October 2004 (series 24) with 4754.92 $\mu g d^{-1} m^{-2}$, while the lowest was verified for September to October 2005 (series 25) with 0.10 $\mu g d^{-1} m^{-2}$ (Fig. 2B). Related to the total particle flux of the respective sample, this corresponds to a microplastic mass content of 8.39% or <0.01%, respectively (average $0.45 \pm 1.28\%$). Due to the dependence of the particle mass on the individual particle size and density, the microplastic mass flux was not strictly related to the microplastic flux. This was evident in March through June 2004 (series 24) with a high microplastic flux rate but a relatively low microplastic mass flux, due to dominating small particle sizes.

The resulting average particle size (\pm s.d.) determined for the individual time series ranged between $74.14 \pm 40.53 \mu m$ (May 2011 until July 2013, series 28) to $111.02 \pm 264.25 \mu m$ (May 2007 until December 2008, series 26) (Fig. 3). The average microplastic particle size in all samples was $88.44 \pm 113.46 \mu m$. Assignment of the size ranges to the

individual polymer types showed the most abundant particles in the size fraction <100 μm were detected for polyethylene (78.85%) and polyvinyl chloride (78.45%), followed by polystyrene (72.31%) and polypropylene (63.64%), with a slightly lower contribution to this size range.

Moreover, polyethylene and polyvinyl chloride were the most frequently detected polymers, but polypropylene, polystyrene, polyethylene terephthalate, and polymethyl methacrylate particles were also identified (Fig. 4B and C). Polyamide, polytetrafluoroethylene (Teflon), and the copolymer of polyethylene and polypropylene were found in smaller quantities. Individual polymers, especially polyethylene, polyvinyl chloride, and polystyrene, showed remarkable temporal differences. The highest occurrence of polyethylene was measured in 2003 and 2004, polyvinyl chloride was the dominating polymer type from 2010 to 2011, and polystyrene was mainly found in 2006 and 2007 (Fig. 4A). No linear correlation was determined between the fluxes of the four most abundant polymers (polyethylene, polyvinyl chloride, polypropylene, polystyrene). Instead, strong correlations were found between polyvinyl chloride and polyamide, polyvinyl chloride and polymethyl methacrylate, as well as polyamide and polymethyl methacrylate (Supplementary Tab. S1). For the microplastic mass fluxes, merely polyethylene terephthalate was correlated with polypropylene (Supplementary Tab. S2).

4.2. Seasonality of microplastic fluxes

Intending to determine a potential seasonal pattern in microplastic (mass) fluxes in the deep Atlantic Ocean, the daily flux values between 2003 and 2015 were monthly averaged and compared to the two most important components of the total particle flux, the lithogenic and biogenic flux fraction (Pullwer and Waniek, 2020; Waniek et al., 2005b, 2005a). As the most common microplastic types (polyethylene and polypropylene) are lighter than seawater but were also found in the deep sea (Bergmann et al., 2017), a biogenic ballast effect has to be taken into account as an important deposition process also for microplastics (Auta et al., 2017; Bergmann et al., 2017). Indeed, microplastic fluxes were remarkably lower during the summer months July–August, and highest in April, such as the biogenic flux. However, in the winter months, the

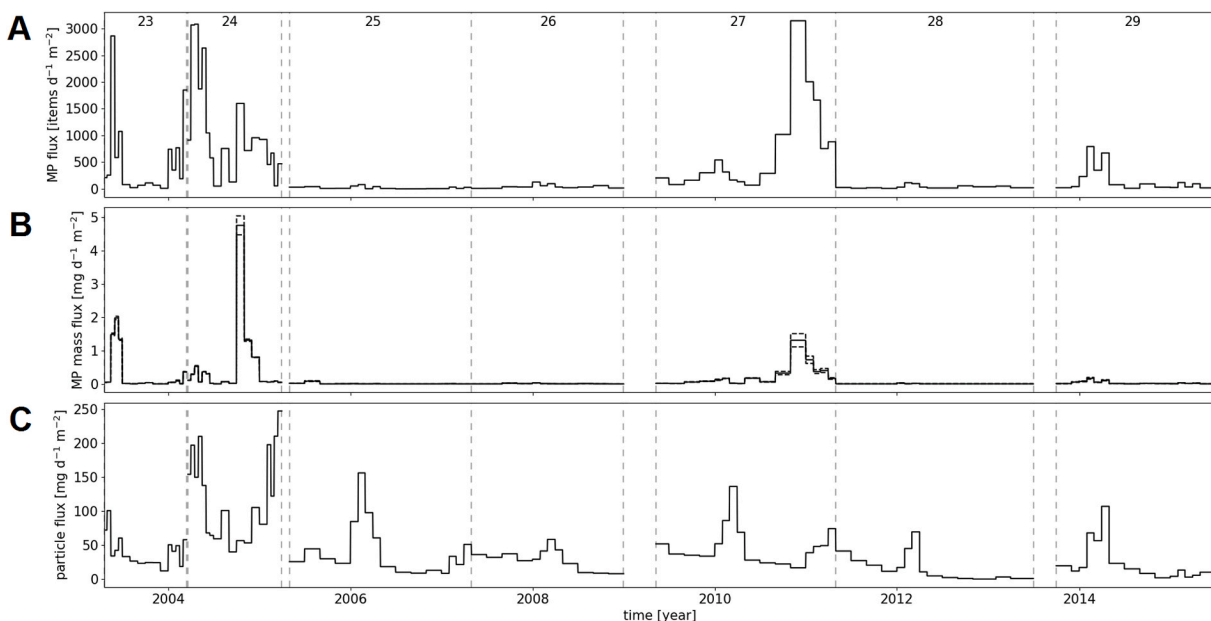


Fig. 2. Microplastic (mass) fluxes at Kiel 276. (A) The black line represents the microplastic flux (items $d^{-1} m^{-2}$), (B) the calculated microplastic mass flux ($mg d^{-1} m^{-2}$) for a sample number of $n = 110$, and (C) shows the total particle flux ($mg d^{-1} m^{-2}$) for comparison. Dashed black lines in (B) illustrate uncertainties resulting from the mass calculations with polymer density ranges. The bar width indicates the sampling time for each sample. Gaps in the fluxes mirror mooring failure or no deployment. Respective series numbers are given at the top and are separated with dashed gray lines. Note that the scale of the y-axis differs between the figures.

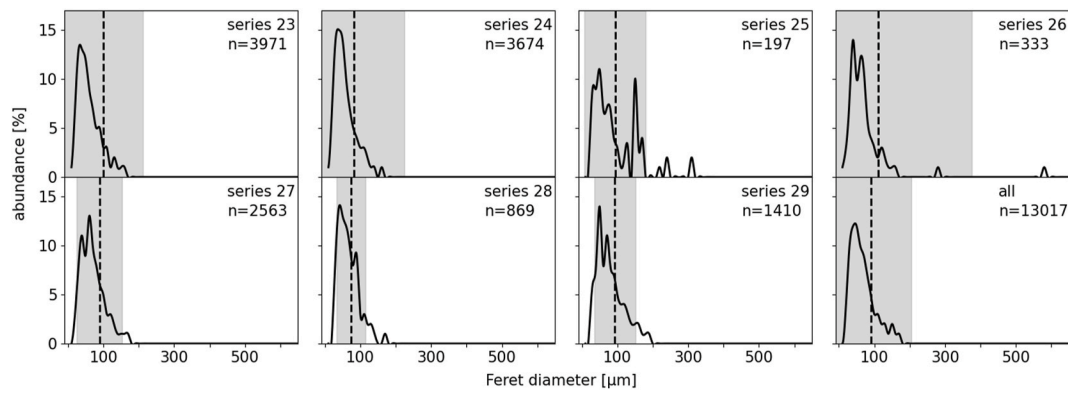


Fig. 3. Size distribution of microplastics. The black line shows the abundance (%) of the respective size (calculated in 10 μm steps) starting at a 10 μm particle diameter for each time series and the sum of all particles detected (all). Dashed line marks the mean size value with \pm s.d. As gray bars, and letter n provides the number of particles measured for the respective time series.

microplastic fluxes and especially the microplastic mass fluxes were higher than expected in relation to the biogenic flux (Fig. 5). Divided into heavy and light polymer types, the high microplastic fluxes during the winter months were largely attributed to the heavy polymers with significantly higher microplastic fluxes in winter (DJF) and lowest during summer months (JJA). This implemented a seasonal dependence for the heavy polymer flux ($n = 73$, Mann-Whitney U test: $W = 401$, $p = 3.49 \times 10^{-3}$, $\alpha = 0.05$) and heavy polymer mass flux ($n = 73$, Mann-Whitney U test: $W = 449$, $p = 1.68 \times 10^{-2}$, $\alpha = 0.05$), but was not observed for the light polymer flux, mainly composed of polyethylene.

Compared to the total particle flux, the polyethylene flux solely was identified to correlate with the lithogenic component ($|r| = 0.60$, $p = 7.76 \times 10^{-12}$), while the correlation with the biogenic component was weaker ($|r| = 0.37$, $p = 8.96 \times 10^{-5}$) (Supplementary Tab. S3). In addition, we observed correlations between other important lithogenic constituents and polyethylene, such as Fe, Mg, Ti, Co, and Zr, while polyvinyl chloride fluxes were correlated with the fluxes of S, As, and Sb (Supplementary Tab. S3). Correlation with atmospheric dust particles (AOD_{550nm}) or precipitation above the water column, particulate organic carbon (POC) concentrations in surface water, or the position of the Azores Front, were not detected neither for heavy polymers nor for the light polymer fraction (Supplementary Tab. S6).

5. Discussion

5.1. Characteristics of microplastic (mass) fluxes

Examination of sediment trap material over a 12-year time interval (2003–2015) demonstrated huge temporal variations in microplastic (mass) fluxes and polymeric composition, while the microplastic size range revealed no significant differences between the polymer types or time intervals. Small microplastic fragments $<100 \mu\text{m}$ (74%) dominated for all sediment trap samples and were more abundant than previously detected in the upper North Atlantic Ocean waters (polyethylene = 68%, polypropylene = 49%, and polystyrene = 67%) (Pabortsava and Lampitt, 2020) but less than for the Arctic Ocean water column (100%) (Tekman et al., 2020). Note that the size detection limits and methodologies were strongly variable between microplastic surveys, making a comparison between those studies challenging.

Overall, we mainly found the plastic polymers polyethylene and polyvinyl chloride, followed by lower quantities of polypropylene, polystyrene, and other less abundantly detected polymers (Fig. 4). The most frequent occurrence of polyethylene corresponds to the global plastic production and disposal (Andrady, 2011; Geyer et al., 2017) as well as the polymers found in the marine environment of the Atlantic Ocean (Enders et al., 2015; Law et al., 2010; Pabortsava and Lampitt, 2020). In more northern regions of the Atlantic Ocean close to the

United Kingdom (Courtene-Jones et al., 2020, 2017; Lindeque et al., 2020) or the Arctic Ocean (Tekman et al., 2020), polyethylene terephthalate or polyamide microplastics were reported as the main component instead of polyethylene. Compared to polymeric compositions previously detected in the upper Atlantic Ocean water column (Enders et al., 2015; Kanhai et al., 2018; Ter Halle et al., 2017) or on beaches (Álvarez-Hernández et al., 2019; Edo et al., 2019), we found remarkably higher polyvinyl chloride and lower polypropylene contents in deep particle flux material.

Consistent with this observation, polyvinyl chloride concentrations are expected to be low in the upper water column due to the higher density of polyvinyl chloride ($\rho = 1.16\text{--}1.58 \text{ g cm}^{-3}$) compared to seawater ($\rho \approx 1.02 \text{ g cm}^{-3}$) (Bergmann et al., 2015; Hidalgo-Ruz et al., 2012). However, due to the high contamination risk during the sampling procedure, polyvinyl chloride was not considered in the analysis for Atlantic Ocean vertical or deep sea surveys in many cases (e.g. Lechthaler et al., 2020; Pabortsava and Lampitt, 2020). Samples of the upper water column (0–240 m depth) in the Atlantic Ocean collected by Enders et al. (2015) in spring 2014 indicated a polyvinyl chloride fraction of 1.8%. In our collected samples, polyvinyl chloride was the dominant component (98%) in 2004. At the water surface (0–20 cm) of the North Atlantic Subtropical Gyre, Ter Halle et al. (2017) attributed 8% of all microplastics found in June 2015 to polyvinyl chloride and 13% polypropylene. We detected 69% polyvinyl chloride and $<1\%$ polypropylene particles for the sampling month May–July of the same year with higher polyvinyl chloride proportions between January and May (83%). One reason for these different vertical polymer compositions could be the density-dependent particle separation due to varying sinking velocities. Another reason might be the horizontal advection of particles within the water column due to the prevailing currents. This results in a longer residence time in the upper water column for polymers lighter than seawater compared to heavier polymers. Another reason for highly variable polymer compositions with increasing water depths (Pabortsava and Lampitt, 2020; Tekman et al., 2020) might be differences in degradation rates and stabilities between the polymer types (Choy et al., 2019; Pabortsava and Lampitt, 2020). Polystyrene and polypropylene are more sensitive to UV radiation and form cracks or flakes faster than polyethylene (Cai et al., 2018; Min et al., 2020; Song et al., 2017). The molecular structure of polyvinyl chloride is considered less resistant than polyethylene, polypropylene, or polystyrene (Min et al., 2020), but added additives during production or the manufactured shape can increase resistance (Chen et al., 2021; Khalil et al., 2013).

Differences in polymer durability and density, and findings of previous surveys resolving the vertical scale, indicate that the composition of microplastics at the water surface is not comparable to that in the deep sea (Pabortsava and Lampitt, 2020; Tekman et al., 2020). To the

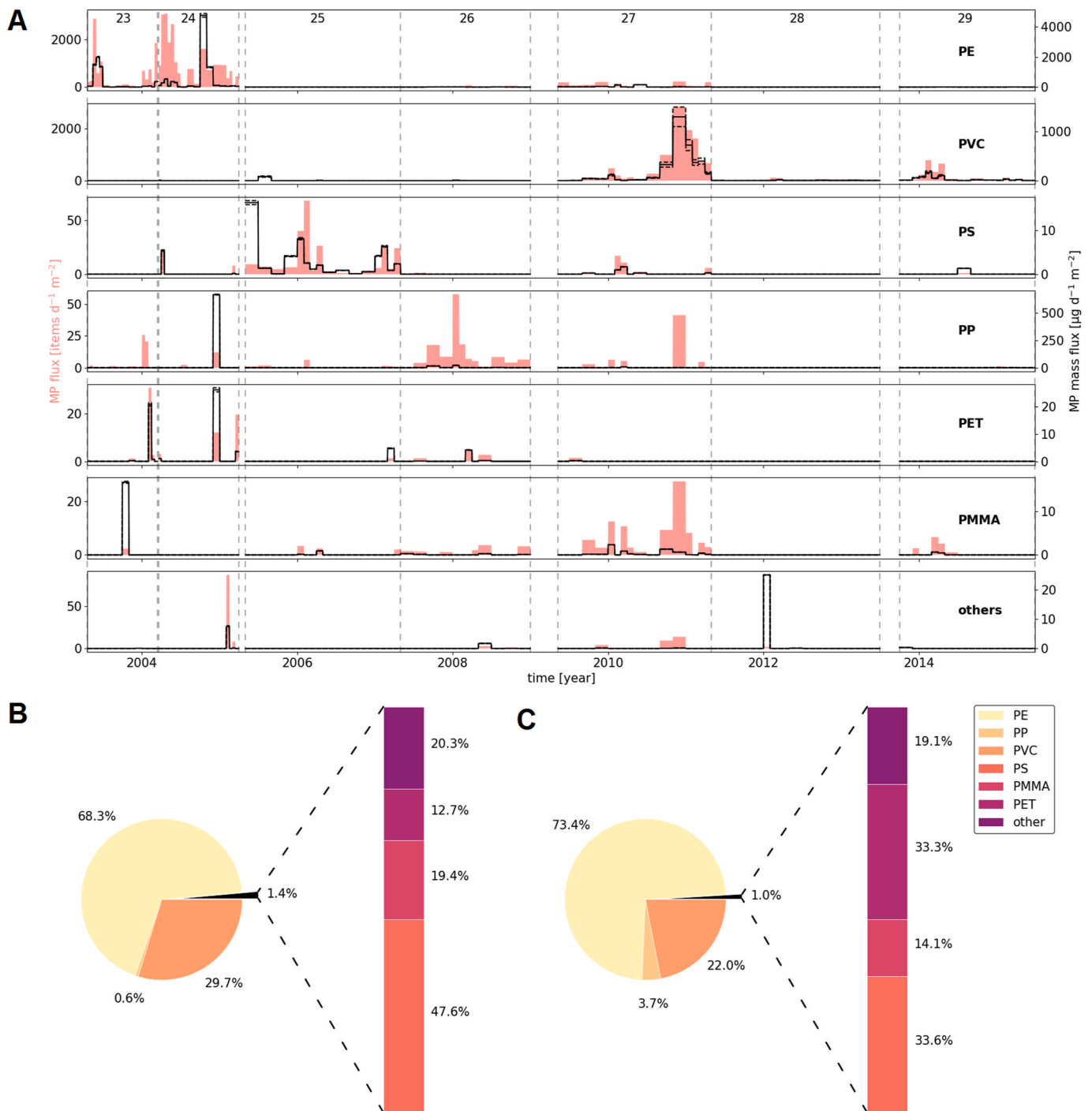


Fig. 4. Distribution of the polymer types. (A) Red bars show the microplastic flux ($\text{items d}^{-1} \text{m}^{-2}$), and black lines illustrate the microplastic mass flux ($\mu\text{g d}^{-1} \text{m}^{-2}$) from $n = 110$ flux material samples for the individual polymers. Dashed black lines illustrate uncertainties from mass calculations with polymer density ranges. The gaps in the fluxes mirror mooring failure or no deployment. Respective series numbers are listed at the top and are separated with dashed gray lines. (B) Percentage (%) of the individual polymers found in the samples of microplastic flux (determined from $n = 110$ samples) and (C) microplastic mass flux ($n = 110$ samples). Stacked bar charts show the proportions of the rarer polymers. PE = polyethylene, PP = polypropylene, PVC = polyvinyl chloride, PET = polyethylene terephthalate, PS = polystyrene, PMMA = polymethylmethacrylate, other = polyamide, polytetrafluoroethylene and copolymers. (For interpretation of the references to color in this figure legend, the reader is referred to the Web version of this article.)

best of our knowledge, no deep sea sediments within 1000 km of our sampling site have been analyzed for microplastics until now. Merely, beach or shallow water sediments were examined for microplastics at the Canary Island and Nigeria in the large size fraction with lower size limits at $90 \mu\text{m}$ (Villanova-Solano et al., 2022) and 1 mm (Álvarez-Hernández et al., 2019; Edo et al., 2019; Fred-Ahmadu et al., 2020). However, as these studies neglect the dominant size fraction of

microplastic (Bergmann et al., 2017; Tekman et al., 2020), a comparison with our results is less meaningful. In contrast to large and heavy items, smaller microplastic particles ($<100 \mu\text{m}$) were found to be dispersed over long horizontal distances or vertically within the mixed layer due to wind-induced mixing and lower sinking velocities (increased retention time) (Kooi et al., 2017; Kowalski et al., 2016; Kukulka et al., 2012; Pabortsava and Lampitt, 2020). Based on our findings, we hypothesize

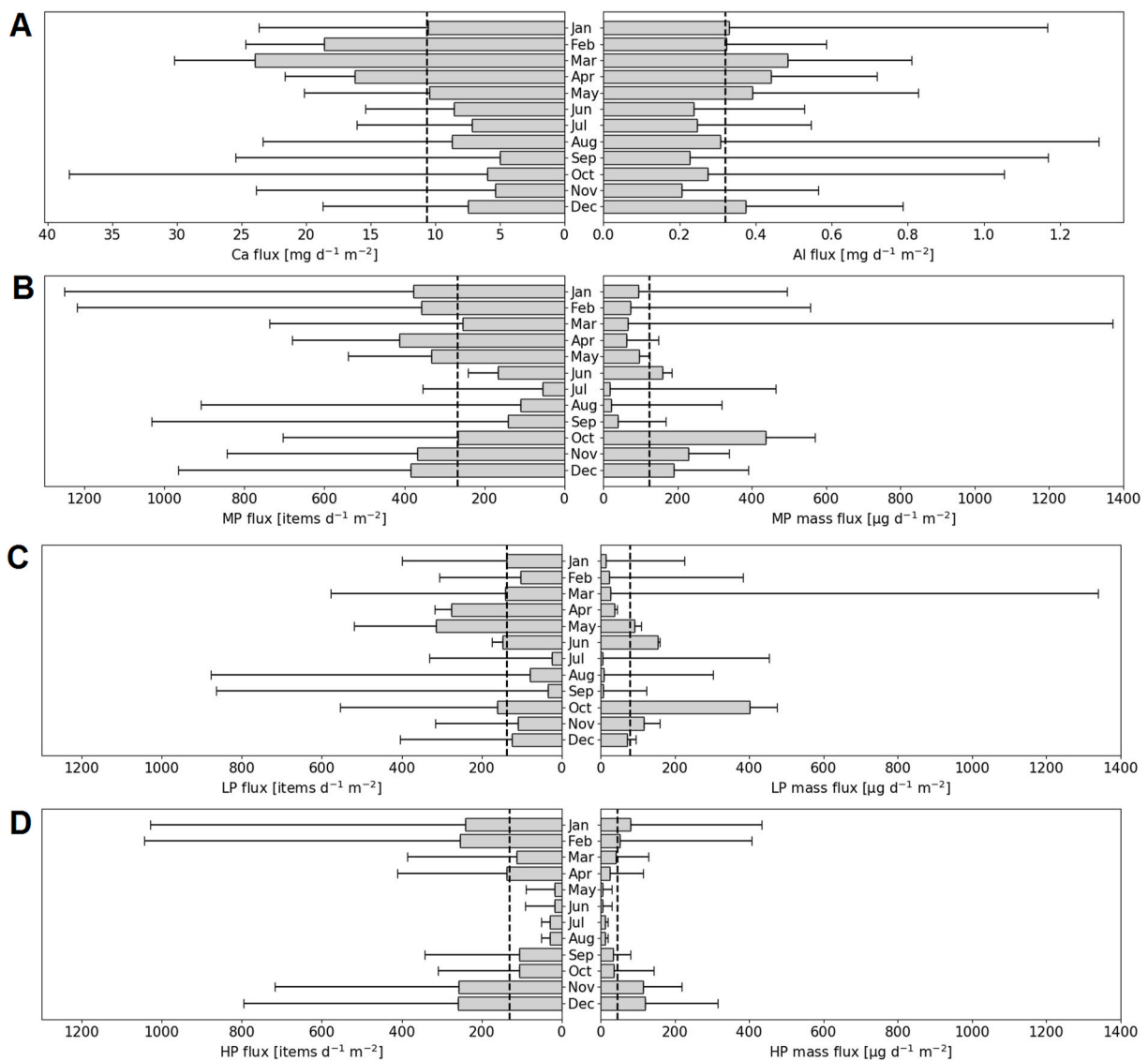


Fig. 5. Seasonality of particle (mass) fluxes. (A) Monthly calcium (Ca) and aluminum (Al) fluxes ($\text{mg d}^{-1} \text{m}^{-2}$) (fluxes taken from a previous study (Pullwer and Waniek, 2020)). (B) Monthly microplastic fluxes and microplastic mass fluxes, as well as monthly fluxes and mass fluxes for the sum of light polymers (LP) ((C); polyethylene, polypropylene, polyethylene/polypropylene) and heavy polymers (HP) ((D); polystyrene, polyethylene terephthalate, polyvinyl chloride, polymethyl methacrylate, polyamide, polytetrafluoroethylene). The dashed line marks the annual mean (mass) fluxes.

high polyvinyl chloride amounts in remote locations like Kiel 276, the Ross Sea in Antarctica (Munari et al., 2017), or the Arctic Central Basin (Kanhai et al., 2018) are attributable to the small particle size, which enables the wide horizontal and vertical transport pathway. We additionally assume that the change of the dominant polymer type entering the sediment trap in certain time intervals could be attributed to different source areas, transport pathways, and sinking mechanisms. Due to the low density of polyethylene ($\rho = 0.92\text{--}0.97 \text{ g cm}^{-3}$) and polypropylene ($\rho = 0.90\text{--}0.91 \text{ g cm}^{-3}$) (Bergmann et al., 2015; Hidalgo-Ruz et al., 2012), sinking is not possible by weight alone. An increase in total particle density is required for low-density microplastics to reach the deep sea, enabled by aggregation or ballasting effects and initiated by incipient biofouling (Kooi et al., 2017; Michels et al., 2018). Polymer types of higher densities do not rely on these processes to sink but can nevertheless be affected by increasing or decreasing total particle density (Kooi et al., 2017).

5.2. Possible source regions of microplastics in the deep northeast Atlantic

The highest amounts of light polymers were detected between April

2003 to March 2005 (series 23 and 24), along with a high biogenic particle flux (Fig. 2), confirming a dependence between primary production and sinking of light polymers. However, we demonstrated that polyethylene flux in 2000 m depth is correlated with the lithogenic rather than expected biogenic particle flux for the investigated time scale (Supplementary Tab. S3). Based on this observation, we assume an airborne input pathway of polyethylene similar to that of lithogenic particles. The polyvinyl chloride flux was not correlated with the lithogenic flux, and no seasonal correspondence with biogenic activity was found (Fig. 5). However, the recurring cycle for heavy polymers with significantly higher concentration in winter and lowest during summer months implements another seasonally occurring dependence. The easterly trade winds (Harmattan) are one explanation for these findings, blowing over Africa and the northeastern Atlantic Ocean. As these winds blow more southerly in winter than in summer, the source region could be changed to a more populated region (south of the Sahel Zone). These prevailing easterly winds are also stronger in winter than in summer (Doherty et al., 2012), which favors the transport of plastic items in the water (sub)surface to the mooring catchment area from neighboring islands (Canary Islands) or mainland. The neighboring

mainland (North and West Africa) is among the 10 regions with the highest concentration of mismanaged plastic waste (Lebreton and Andrady, 2019), and adjacent islands are known for high concentrations of plastic on beaches and coastal waters (Álvarez-Hernández et al., 2019; Edo et al., 2019).

This assumption is highly supported by the rare earth element (REE) concentrations in the lithogenic component of the sediment trap samples (Supplementary Material based on data from Pullwer and Waniek (2020)). The composition of the REE at Kiel 276 was strongly correlated with the REE composition of Gran Canarias soils, especially for samples collected from March 2004 until February 2005, April 2007 to January 2010, and for some samples taken between October 2013 and June 2015. The high polyvinyl chloride fluxes during the winter months may also depend on seasonal processes occurring within the water column. Strong stratification in the surface layer could prevent the sinking of microplastic particles during the summer months (Fig. 5). A deeper mixed layer depth in autumn and winter (Waniek et al., 2005a) could explain the seasonality of the heavier polymers with an increasing flux in November and December. This effect is less pronounced for the low-density polymers due to their lower weight, associated longer residence time in the upper water column, and different source regions.

The exceptionally high fluxes of heavy polymers in winter 2010/2011 (Fig. 5A) cannot be attributed to seasonal fluctuations and are more likely to have been caused by interannual or single events. One reason for the strong interannual variability could be the change in the NAO index, which leads to weaker westerly winds and increased precipitation in North Africa with decreasing index (Pérez et al., 2000; Siedler et al., 2005). More frequent and intense precipitation flush plastic from the land into the sea (Lima et al., 2014) that could subsequently be transported by attenuated westerly winds to the trap's catchment area 600–800 km from land. Contrary to the directly noticeable influence on the atmosphere and the water surface, the effects of the NAO on the oceanic systems are temporally delayed, with fluctuating time lags (Fründt and Waniek, 2012). Combined with additional variability in non-cyclical oceanic meteorological systems (Fründt et al., 2013; Fründt and Waniek, 2012) and numerous ancillary effects, correlations between the NAO index and the microplastic (mass) fluxes are weak, as expected (not shown). Overall, the most plausible reason for the strongly fluctuating fluxes of heavy and light polymers within and between years is the combination of multiple factors. The biogenic activity in the water column, the aerosol input, variable currents, the polymer density, particle shape, and polymer durability can be responsible for the resulting microplastic (mass) flux variations.

To obtain a rough estimate of the microplastic input to the deep ocean for this study period, we scaled our results for the entire Atlantic Ocean area ($81.6 \times 10^{-6} \text{ km}^2$) (Pabortsava and Lampitt, 2020). We calculated a microplastic input of 65.9 MT sinking into the deep Atlantic Ocean between April 2003 and June 2015, corresponding to an annual input of 5.4 MT year^{-1} . These 12 years of microplastic collection are in the same order of magnitude as the plastic accumulation calculated for the entire Atlantic Ocean waters and sediments between 1950 and 2015 (17–47 MT) (Pabortsava and Lampitt, 2020). Within our continuous record, no significant increase in plastic levels was observed in the deep particle flux of the Atlantic Ocean. This also applies to the study of Law et al. (2010), in which no increase in plastic quantities was found for the Atlantic surface over an observation period of 22 years. However, modeling and field studies with time series of 30 and 60 years showed increasing plastic pollution at the ocean surface (Ostle et al., 2019; Wilcox et al., 2020). Note that our scaling should be evaluated with caution, as it was performed based on observations from only one time series station, and detection methods between the studies vary widely. A longer time scale and more sampling sites are needed to confirm or reject the increase in microplastic amounts in the deep sea.

Until now, there is no specific information available about the sinking rates of microplastic particles and limited investigations of deep sea sediments. Potentially, large amounts of marine plastic are

unaccounted for, contributing to a global underestimation of the amount of plastic waste accumulating in the oceans. Within this long-term study, we demonstrate the function of the deep sea in global microplastic pollution between 2003 and 2015 and show that large amounts of microplastic reach the deep sea after crossing the 2000 m deep water column. Due to the ongoing input and the long residence time, microplastic can cause incalculable damage to the marine ecosystem. Therefore, there is a need to clarify knowledge about the resistance time in the water column, the sources, and the fate of microplastic in the complex marine ecosystem to recognize possible harms and provide an early impetus for alternative materials. With these first time series, we are laying the first foundation for determining the deposition rate of microplastics to the deep ocean, but further investigations are needed.

6. Conclusion

This study provides first data of microplastic flux rates and temporal variability of microplastic composition in the deep subtropical Northeast Atlantic. Within the studied period between April 2003 and June 2015, we found mainly polyethylene and polyvinyl chloride in our samples with highest amounts in 2004 and 2010, respectively. Microplastic sizes were dominated by very small, fragmented particles smaller than 100 μm and were not variable between the time series, years, or polymer types. The correlation of the lithogenic flux component in the sediment trap samples with the polyethylene flux could indicate a link between the airborne introduced minerals and the light polymer fraction via similar transport pathways. The observed seasonality of the polyvinyl chloride fluxes with higher abundances in winter months compared to summer months could be attributed to seasonal environmental conditions such as the ocean surface stratification, winds, currents, or precipitation. However, correlations between individual environmental conditions and polyvinyl chloride fluxes were not found. By collecting more microplastic flux samples in the ocean at different depths and study sites, future studies may narrow down the sources and transport pathways of microplastic particles in the marine environment. These initial data, along with future data, can expand the understanding of microplastics in our environment, which is not yet fully understood in terms of fate and transport pathways.

Declaration of competing interest

The authors declare that they have no known competing financial interests or personal relationships that could have appeared to influence the work reported in this paper.

Acknowledgements

We gratefully acknowledge the financial support from the Deutsche Forschungsgemeinschaft (DFG) (WA2175/1–5), which made this long-term study carried out by the Institute for Baltic Sea Research, Germany (IOW), possible. Great thank also goes to the crews, technicians, and scientists for sampling, measuring, and analysis of certain sample parameters on the ship (RV POSEIDON and RV MERIAN) and in the laboratory. We further thank Dr. Judith Stern and Helena Frazão for providing and processing their data for this study. Our special thanks are directed to the inorganic research group of Prof. Dr. Seidel and Prof. Dr. Schulz for the provision and Dr. Jonas Bresien for the support in operating the Raman spectrometer (all University of Rostock, Germany). We finally like to thank Dorian Reineccius (University of Bonn, Germany) to handle the image format for faster particle measurements.

Appendix A. Supplementary data

Supplementary data to this article can be found online at <https://doi.org/10.1016/j.envpol.2022.119302>.

References

- Adomat, Y., Grischek, T., 2021. Sampling and processing methods of microplastics in river sediments - a review. *Sci. Total Environ.* 758, 143691. <https://doi.org/10.1016/j.scitotenv.2020.143691>.
- Álvarez-Hernández, C., Cairós, C., López-Darias, J., Mazzetti, E., Hernández-Sánchez, C., González-Sálamo, J., Hernández-Borges, J., 2019. Microplastic debris in beaches of Tenerife (canary islands, Spain). *Mar. Pollut. Bull.* 146, 26–32. <https://doi.org/10.1016/j.marpolbul.2019.05.064>.
- Andrady, A.L., 2011. Microplastics in the marine environment. *Mar. Pollut. Bull.* 62, 1596–1605. <https://doi.org/10.1016/j.marpolbul.2011.05.030>.
- Andrady, A.L., Neal, M.A., 2009. Applications and societal benefits of plastics. *Philos. Trans. R. Soc. B Biol. Sci.* 364, 1977–1984. <https://doi.org/10.1098/rstb.2008.0304>.
- Araujo, C.F., Nolasco, M.M., Ribeiro, A.M.P., Ribeiro-Claro, P.J.A., 2018. Identification of microplastics using Raman spectroscopy: latest developments and future prospects. *Water Res.* 142, 426–440. <https://doi.org/10.1016/j.watres.2018.05.060>.
- Au, S.Y., Lee, C.M., Weinstein, J.E., van den Hurk, P., Klaine, S.J., 2017. Trophic transfer of microplastics in aquatic ecosystems: identifying critical research needs. *Integrated Environ. Assess. Manag.* 13, 505–509. <https://doi.org/10.1002/ieam.1907>.
- Auta, H.S., Emenike, C.U., Fauziah, S.H., 2017. Distribution and importance of microplastics in the marine environment: a review of the sources, fate, effects, and potential solutions. *Environ. Int.* 102, 165–176. <https://doi.org/10.1016/j.envint.2017.02.013>.
- Avio, C.G., Gorbi, S., Milan, M., Benedetti, M., Fattorini, D., D'Errico, G., Pauletto, M., Bargelloni, L., Regoli, F., 2015a. Pollutants bioavailability and toxicological risk from microplastics to marine mussels. *Environ. Pollut.* 198, 211–222. <https://doi.org/10.1016/j.envpol.2014.12.021>.
- Avio, C.G., Gorbi, S., Regoli, F., 2015b. Experimental development of a new protocol for extraction and characterization of microplastics in fish tissues: first observations in commercial species from Adriatic Sea. *Mar. Environ. Res.* 111, 18–26. <https://doi.org/10.1016/j.marenvres.2015.06.014>.
- Avio, C.G., Pittura, L., d'Errico, G., Abel, S., Amorello, S., Marino, G., Gorbi, S., Regoli, F., 2020. Distribution and characterization of microplastic particles and textile microfibrils in Adriatic food webs: general insights for biomonitoring strategies. *Environ. Pollut.* 258, 113766. <https://doi.org/10.1016/j.envpol.2019.113766>.
- Bergmann, M., Gutow, L., Klages, M., 2015. Marine Anthropogenic Litter, Marine Anthropogenic Litter. Springer Nature. <https://doi.org/10.1007/978-3-319-16510-3>.
- Bergmann, M., Wirzberger, V., Krumpfen, T., Lorenz, C., Primpke, S., Tekman, M.B., Gerdts, G., 2017. High quantities of microplastic in Arctic deep-sea sediments from the HAUSGARTEN observatory. *Environ. Sci. Technol.* 51, 11000–11010. <https://doi.org/10.1021/acs.est.7b03331>.
- Blumenröder, J., Sechet, P., Kakkonen, J.E., Hartl, M.G.J., 2017. Microplastic contamination of intertidal sediments of Scapa Flow, Orkney: a first assessment. *Mar. Pollut. Bull.* 124, 112–120. <https://doi.org/10.1016/j.marpolbul.2017.07.009>.
- Brust, J., Schulz-Bull, D.E., Leipe, T., Chavagnac, V., Waniek, J.J., 2011. Descending particles: from the atmosphere to the deep ocean—A time series study in the subtropical NE Atlantic. *Geophys. Res. Lett.* 38, 1–5. <https://doi.org/10.1029/2010GL045399>.
- Brust, J., Waniek, J.J., 2010. Atmospheric dust contribution to deep-sea particle fluxes in the subtropical Northeast Atlantic. *Deep. Res. Part I Oceanogr. Res. Pap.* 57, 988–998. <https://doi.org/10.1016/j.dsr.2010.04.011>.
- Budimir, S., Setälä, O., Lehtiniemi, M., 2018. Effective and easy to use extraction method shows low numbers of microplastics in offshore planktivorous fish from the northern Baltic Sea. *Mar. Pollut. Bull.* 127, 586–592. <https://doi.org/10.1016/j.marpolbul.2017.12.054>.
- Cai, L., Wang, J., Peng, J., Wu, Z., Tan, X., 2018. Observation of the degradation of three types of plastic pellets exposed to UV irradiation in three different environments. *Sci. Total Environ.* 628–629, 740–747. <https://doi.org/10.1016/j.scitotenv.2018.02.079>.
- Castillo, A.B., Al-Maslami, I., Obbard, J.P., 2016. Prevalence of microplastics in the marine waters of Qatar. *Mar. Pollut. Bull.* 111, 260–267. <https://doi.org/10.1016/j.marpolbul.2016.06.108>.
- Catarino, A.I., Thompson, R., Sanderson, W., Henry, T.B., 2017. DEVELOPMENT AND OPTIMIZATION OF A STANDARD METHOD FOR EXTRACTION OF MICROPLASTICS IN MUSSELS BY ENZYME DIGESTION OF SOFT TISSUES y Institute. *Environ. Toxicol. Chem.* 36, 947–951. <https://doi.org/10.1002/etc.3608>.
- Chae, D.H., Kim, I.S., Kim, S.K., Song, Y.K., Shim, W.J., 2015. Abundance and distribution characteristics of microplastics in surface seawaters of the Incheon/Kyeonggi coastal region. *Arch. Environ. Contam. Toxicol.* 69, 269–278. <https://doi.org/10.1007/s00244-015-0173-4>.
- Chen, Q., Wang, Q., Zhang, C., Zhang, J., Dong, Z., Xu, Q., 2021. Aging simulation of thin-film plastics in different environments to examine the formation of microplastic. *Water Res.* 202, 117462. <https://doi.org/10.1016/j.watres.2021.117462>.
- Choy, C.A., Robison, B.H., Gagne, T.O., Erwin, B., Firl, E., Halden, R.U., Hamilton, J.A., Katija, K., Lisin, S.E., Rolsky, C., Van Houtan, K.S., 2019. The vertical distribution and biological transport of marine microplastics across the epipelagic and mesopelagic water column. *Sci. Rep.* 9, 1–9. <https://doi.org/10.1038/s41598-019-44117-2>.
- Cole, M., Lindeque, P., Halsband, C., Galloway, T.S., 2011. Microplastics as contaminants in the marine environment: a review. *Mar. Pollut. Bull.* 62, 2588–2597. <https://doi.org/10.1016/j.marpolbul.2011.09.025>.
- Courtene-Jones, W., Quinn, B., Ewins, C., Gary, S.F., Narayanaswamy, B.E., 2020. Microplastic accumulation in deep-sea sediments from the Rockall Trough. *Mar. Pollut. Bull.* 154, 111092. <https://doi.org/10.1016/j.marpolbul.2020.111092>.
- Courtene-Jones, W., Quinn, B., Gary, S.F., Mogg, A.O.M., Narayanaswamy, B.E., 2017. Microplastic pollution identified in deep-sea water and ingested by benthic invertebrates in the Rockall Trough, North Atlantic Ocean. *Environ. Pollut.* 231, 271–280. <https://doi.org/10.1016/j.envpol.2017.08.026>.
- Coyle, R., Hardiman, G., Driscoll, K.O., 2020. Microplastics in the marine environment: a review of their sources, distribution processes, uptake and exchange in ecosystems. *Case Stud. Chem. Environ. Eng.* 2, 100010. <https://doi.org/10.1016/j.csee.2020.100010>.
- Derraik, J.G.B., 2002. The pollution of the marine environment by plastic debris: a review. *Mar. Pollut. Bull.* 44, 842–852. [https://doi.org/10.1016/S0025-326X\(02\)00220-5](https://doi.org/10.1016/S0025-326X(02)00220-5).
- Doherty, O.M., Riemer, N., Hameed, S., 2012. Control of Saharan mineral dust transport to Barbados in winter by the intertropical convergence zone over West Africa. *J. Geophys. Res. Atmos.* 117, 1–13. <https://doi.org/10.1029/2012JD017767>.
- Edo, C., Tamayo-Belda, M., Martínez-Campos, S., Martín-Betancor, K., González-Pleiter, M., Pulido-Reyes, G., García-Ruiz, C., Zapata, F., Leganés, F., Fernández-Piñas, F., Rosal, R., 2019. Occurrence and identification of microplastics along a beach in the biosphere reserve of Lanzarote. *Mar. Pollut. Bull.* 143, 220–227. <https://doi.org/10.1016/j.marpolbul.2019.04.061>.
- Enders, K., Lenz, R., Stedmon, C.A., Nielsen, T.G., 2015. Abundance, size and polymer composition of marine microplastics $\geq 10 \mu\text{m}$ in the Atlantic Ocean and their modelled vertical distribution. *Mar. Pollut. Bull.* 100, 70–81. <https://doi.org/10.1016/j.marpolbul.2015.09.027>.
- Farrell, P., Nelson, K., 2013. Trophic level transfer of microplastic: *Mytilus edulis* (L.) to *Carcinus maenas* (L.). *Environ. Pollut.* 177, 1–3. <https://doi.org/10.1016/j.envpol.2013.01.046>.
- Frazaõ, H.C., Prien, R.D., Müller, T.J., Schulz-Bull, D.E., Waniek, J.J., 2021. 30 years of temporal variability of temperature and currents below the main thermocline between 1980–2009 in the subtropical Northeast Atlantic (Kiel 276, 33°N, 22°W). *J. Mar. Syst.* 217, 103517. <https://doi.org/10.1016/j.jmarsys.2021.103517>.
- Fred-Ahmadu, O.H., Ayejuyo, O.O., Benson, N.U., 2020. Microplastics distribution and characterization in epibenthic sediments of tropical Atlantic Ocean, Nigeria. *Reg. Stud. Mar. Sci.* 38, 101365. <https://doi.org/10.1016/j.rmsa.2020.101365>.
- Frias, J.P.G.L., Sobral, P., Ferreira, A.M., 2010. Organic pollutants in microplastics from two beaches of the Portuguese coast. *Mar. Pollut. Bull.* 60, 1988. <https://doi.org/10.1016/j.marpolbul.2010.07.030>, 1992.
- Fründt, B., Müller, T.J., Schulz-Bull, D.E., Waniek, J.J., 2013. Long-term changes in the thermocline of the subtropical Northeast Atlantic (33°N, 22°W). *Prog. Oceanogr.* 116, 246–260. <https://doi.org/10.1016/j.pcean.2013.07.004>.
- Fründt, B., Waniek, J., 2012. Impact of the Azores Front propagation on deep ocean particle flux. *Open Geosci.* 4, 531–544. <https://doi.org/10.2478/s13533-012-0102-2>.
- Gewert, B., Plassmann, M., Sandblom, O., Macleod, M., 2018. Identification of chain scission products released to water by plastic exposed to ultraviolet light. *Environ. Sci. Technol. Lett.* 5, 272–276. <https://doi.org/10.1021/acs.estlett.8b00119>.
- Geyer, R., Jambeck, J.R., Law, K.L., 2017. Production, use, and fate of all plastics ever made. *Sci. Adv.* 3, 25–29. <https://doi.org/10.1126/sciadv.1700782>.
- Graca, B., Beldowska, M., Wrzesień, P., Zgrundo, A., 2014. Styrofoam debris as a potential carrier of mercury within ecosystems. *Environ. Sci. Pollut. Res.* 21, 2263–2271. <https://doi.org/10.1007/s11356-013-2153-4>.
- Hidalgo-Ruz, V., Gutow, L., Thompson, R.C., Thiel, M., 2012. Microplastics in the marine environment: a review of the methods used for identification and quantification. *Environ. Sci. Technol.* 46, 3060–3075. <https://doi.org/10.1021/es2031505>.
- Huppertsberg, S., Knepper, T.P., 2018. Instrumental analysis of microplastics—benefits and challenges. *Anal. Bioanal. Chem.* 410, 6343–6352. <https://doi.org/10.1007/s00216-018-1210-8>.
- Jones, P.D., Jonsson, T., Wheeler, D., 1997. Extension to the North Atlantic Oscillation using early instrumental pressure observations from Gibraltar and south-west Iceland. *Int. J. Climatol.* 17, 1433–1450. [https://doi.org/10.1002/\(sici\)1097-0088\(199711\)17:13<1433::aid-joc203>3.3.co;2-g](https://doi.org/10.1002/(sici)1097-0088(199711)17:13<1433::aid-joc203>3.3.co;2-g).
- Kaiser, D., Estelmann, A., Kowalski, N., Glockzin, M., Waniek, J.J., 2019. Sinking velocity of sub-millimeter microplastic. *Mar. Pollut. Bull.* 139, 214–220. <https://doi.org/10.1016/j.marpolbul.2018.12.035>.
- Kaiser, D., Kowalski, N., Waniek, J.J., 2017. Effects of biofouling on the sinking behavior of microplastics. *Environ. Res. Lett.* 12, 124003. <https://doi.org/10.1088/1748-9326/aa8e8b>.
- Kanhai, L.D.K., Gärdfeldt, K., Lyashevskva, O., Hassellöv, M., Thompson, R.C., O'Connor, I., 2018. Microplastics in sub-surface waters of the Arctic Central Basin. *Mar. Pollut. Bull.* 130, 8–18. <https://doi.org/10.1016/j.marpolbul.2018.03.011>.
- Khalil, H.P.S.A., Tehrani, M.A., Davoudpour, Y., Bhat, A.H., Jawaid, M., Hassan, A., 2013. Natural fiber reinforced poly(vinyl chloride) composites: a review. *J. Reinforc. Plast. Compos.* 32, 330–356. <https://doi.org/10.1177/0731684412458553>.
- Kooi, M., Van Nes, E.H., Scheffer, M., Koelmans, A.A., 2017. Ups and downs in the ocean: effects of biofouling on vertical transport of microplastics. *Environ. Sci. Technol.* 51, 7963–7971. <https://doi.org/10.1021/acs.est.6b04702>.
- Kowalski, N., Reichardt, A.M., Waniek, J.J., 2016. Sinking rates of microplastics and potential implications of their alteration by physical, biological, and chemical factors. *Mar. Pollut. Bull.* 109, 310–319. <https://doi.org/10.1016/j.marpolbul.2016.05.064>.
- Kremling, K., Lentz, U., Zeitzschel, B., Schulz-Bull, D.E.E., Duinker, J.C.C., 1996. New type of time-series sediment trap for the reliable collection of inorganic and organic trace chemical substances. *Rev. Sci. Instrum.* 67, 4360–4363. <https://doi.org/10.1063/1.1147582>.
- Kukulka, T., Proskurrowski, G., Morét-Ferguson, S., Meyer, D.W., Law, K.L., 2012. The effect of wind mixing on the vertical distribution of buoyant plastic debris. *Geophys. Res. Lett.* 39, 1–6. <https://doi.org/10.1029/2012GL051116>.

- Kumar, R.G., Strom, K.B., Keyvani, A., 2010. Floc properties and settling velocity of San Jacinto estuary mud under variable shear and salinity conditions. *Continent. Shelf Res.* 30, 2067–2081. <https://doi.org/10.1016/j.csr.2010.10.006>.
- Kuss, J., Kremling, K., 1999. Particulate trace element fluxes in the deep northeast Atlantic Ocean. *Deep. Res. Part I Oceanogr. Res. Pap.* 46, 149–169. [https://doi.org/10.1016/S0967-0637\(98\)00059-4](https://doi.org/10.1016/S0967-0637(98)00059-4).
- Law, K.L., Morét-Ferguson, S., Maximenko, N.A., Proskurowski, G., Peacock, E.E., Hafner, J., Reddy, C.M., 2010. Plastic accumulation in the North Atlantic subtropical gyre. *Science* 80 (329), 1185–1188. <https://doi.org/10.1126/science.1192321>.
- Lebreton, L., Andrady, A., 2019. Future scenarios of global plastic waste generation and disposal. *Palgrave Commun* 5, 1–11. <https://doi.org/10.1057/s41599-018-0212-7>.
- Lebreton, L.C.M., Van Der Zwet, J., Damsteeg, J.W., Slat, B., Andrady, A., Reisser, J., 2017. River plastic emissions to the world's oceans. *Nat. Commun.* 8, 1–10. <https://doi.org/10.1038/ncomms15611>.
- Lechthaler, S., Schwarzbauer, J., Reicherter, K., Stauch, G., Schüttrumpf, H., 2020. Regional study of microplastics in surface waters and deep sea sediments south of the Algarve Coast. *Reg. Stud. Mar. Sci.* 40, 101488. <https://doi.org/10.1016/j.rsma.2020.101488>.
- Li, J., Zhang, H., Zhang, K., Yang, R., Li, R., Li, Y., 2018. Characterization, source, and retention of microplastic in sandy beaches and mangrove wetlands of the Qin Zhou Bay, China. *Mar. Pollut. Bull.* 136, 401–406. <https://doi.org/10.1016/j.marpolbul.2018.09.025>.
- Lima, A.R.A., Costa, M.F., Barletta, M., 2014. Distribution patterns of microplastics within the plankton of a tropical estuary. *Environ. Res.* 132, 146–155. <https://doi.org/10.1016/j.envres.2014.03.031>.
- Lindeque, P.K., Cole, M., Coppock, R.L., Lewis, C.N., Miller, R.Z., Watts, A.J.R., Wilson-McNeal, A., Wright, S.L., Galloway, T.S., 2020. Are we underestimating microplastic abundance in the marine environment? A comparison of microplastic capture with nets of different mesh-size. *Environ. Pollut.* 265, 114721. <https://doi.org/10.1016/j.envpol.2020.114721>.
- Lundgreen, U., Waniek, J., Schulz-Bull, D.E., Duinker, J.C., 1997. Azide as a tool to evaluate sediment trap behaviour. *Azid als Mittel zur Bewertung des Verhaltens von Sinkstoffallen*. *Dtsch. Hydrogr. Z.* 49, 57–69. <https://doi.org/10.1007/bf02765118>.
- Michels, J., Stippkugel, A., Lenz, M., Wirtz, K., Engel, A., 2018. Rapid aggregation of biofilm-covered microplastics with marine biogenic particles. *Proc. R. Soc. B Biol. Sci.* 285, 20181203. <https://doi.org/10.1098/rspb.2018.1203>.
- Min, K., Cuiffi, J.D., Mathers, R.T., 2020. Ranking environmental degradation trends of plastic marine debris based on physical properties and molecular structure. *Nat. Commun.* 11, 1–11. <https://doi.org/10.1038/s41467-020-14538-z>.
- Müller, T.J., Waniek, J.J., 2013. KIEL276 Time Series Data from Moored Current Meters. Munari, C., Infantini, V., Scoconi, M., Rastelli, E., Corinaldesi, C., Mistri, M., 2017. Microplastics in the sediments of Terra Nova Bay (Ross Sea, Antarctica). *Mar. Pollut. Bull.* 122, 161–165. <https://doi.org/10.1016/j.marpolbul.2017.06.039>.
- Ostle, C., Thompson, R.C., Broughton, D., Gregory, L., Wootton, M., Johns, D.G., 2019. The rise in ocean plastics evidenced from a 60-year time series. *Nat. Commun.* 10, 8–13. <https://doi.org/10.1038/s41467-019-09506-1>.
- Pabortsava, K., Lampitt, R.S., 2020. High concentrations of plastic hidden beneath the surface of the Atlantic Ocean. *Nat. Commun.* 11, 1–12. <https://doi.org/10.1038/s41467-020-17932-9>.
- Peeken, I., Primpke, S., Beyer, B., Gütermann, J., Katlein, C., Krumpfen, T., Bergmann, M., Hehemann, L., Gerdt, G., 2018. Arctic sea ice is an important temporal sink and means of transport for microplastic. *Nat. Commun.* 9, 1–12. <https://doi.org/10.1038/s41467-018-03825-5>.
- Pérez, F.F., Pollard, R.T., Read, J.F., Valencia, V., Cabanas, J.M., Ríos, A.F., 2000. Climatological coupling of the thermohaline decadal changes in central water of the eastern North Atlantic. *Sci. Mar.* 64, 347–353. <https://doi.org/10.3989/scimar.2000.64n3347>.
- Poulain, M., Mercier, M.J., Brach, L., Martignac, M., Routaboul, C., Perez, E., Desjean, M. C., Ter Halle, A., 2019. Small microplastics as a main contributor to plastic mass balance in the north Atlantic subtropical Gyre. *Environ. Sci. Technol.* 53, 1157–1164. <https://doi.org/10.1021/acs.est.8b05458>.
- Pullwer, J., Waniek, J.J., 2020. Particulate trace metal fluxes in the center of an oceanic desert: northeast Atlantic subtropical gyre. *J. Mar. Syst.* 212, 103447. <https://doi.org/10.1016/j.jmarsys.2020.103447>.
- Reineccius, J., Appelt, J.S., Hinrichs, T., Kaiser, D., Stern, J., Prien, R.D., Waniek, J.J., 2020. Abundance and characteristics of microfibers detected in sediment trap material from the deep subtropical North Atlantic Ocean. *Sci. Total Environ.* 738, 140354. <https://doi.org/10.1016/j.scitotenv.2020.140354>.
- Reineccius, J., Bresien, J., Waniek, J.J., 2021. Separation of microplastics from mass-limited samples by an effective adsorption technique. *Sci. Total Environ.* 788, 147881. <https://doi.org/10.1016/j.scitotenv.2021.147881>.
- Rios-Mendoza, L.M., Ontiveros-Cuadras, J.F., Leon-Vargas, D., Ruiz-Fernández, A.C., Rangel-García, M., Pérez-Bernal, L.H., Sanchez-Cabeza, J.A., 2021. Microplastic contamination and fluxes in a touristic area at the SE Gulf of California. *Mar. Pollut. Bull.* 170, 112638. <https://doi.org/10.1016/j.marpolbul.2021.112638>.
- Rochman, B.C.M., 2018. Microplastics research — from sink to source in freshwater systems. *Science* 80 (360), 28–29. <https://doi.org/10.1126/science.aar7734>.
- Schindelin, J., Arganda-Carreras, I., Frise, E., Kaynig, V., Longair, M., Pietzsch, T., Preibisch, S., Rueden, C., Saalfeld, S., Schmid, B., Tinevez, J.Y., White, D.J., Hartenstein, V., Eliceiri, K., Tomancak, P., Cardona, A., 2012. Fiji: an open-source platform for biological-image analysis. *Nat. Methods* 9, 676–682. <https://doi.org/10.1038/nmeth.2019>.
- Schmidt, C., Krauth, T., Wagner, S., 2017. Export of plastic debris by rivers into the sea. *Environ. Sci. Technol.* 51, 12246–12253. <https://doi.org/10.1021/acs.est.7b02368>.
- Setälä, O., Norkko, J., Lehtiniemi, M., 2016. Feeding type affects microplastic ingestion in a coastal invertebrate community. *Mar. Pollut. Bull.* 102, 95–101. <https://doi.org/10.1016/j.marpolbul.2015.11.053>.
- Siedler, G., Armi, L., Müller, T.J., 2005. Meddies and decadal changes at the Azores Front from 1980 to 2000. *Deep. Res. Part II Top. Stud. Oceanogr.* 52, 583–604. <https://doi.org/10.1016/j.dsr2.2004.12.010>.
- Song, Y.K., Hong, S.H., Jang, M., Han, G.M., Jung, S.W., Shim, W.J., 2017. Combined effects of UV exposure duration and mechanical abrasion on microplastic fragmentation by polymer type. *Environ. Sci. Technol.* 51, 4368–4376. <https://doi.org/10.1021/acs.est.6b06155>.
- Storz, D., Schulz, H., Waniek, J.J., Schulz-Bull, D.E., Kučera, M., 2009. Seasonal and interannual variability of the planktic foraminiferal flux in the vicinity of the Azores Current. *Deep. Res. Part I Oceanogr. Res. Pap.* 56, 107–124. <https://doi.org/10.1016/j.dsr.2008.08.009>.
- Tekman, M.B., Wekerle, C., Lorenz, C., Primpke, S., Hasemann, C., Gerdt, G., Bergmann, M., 2020. Tying up loose ends of microplastic pollution in the Arctic: distribution from the sea surface through the water column to deep-sea sediments at the HAUSGARTEN observatory. *Environ. Sci. Technol.* 54, 4079–4090. <https://doi.org/10.1021/acs.est.9b06981>.
- Ter Halle, A., Jeanneau, L., Martignac, M., Jardé, E., Pedrono, B., Brach, L., Gigault, J., 2017. Nanoplastic in the north Atlantic subtropical Gyre. *Environ. Sci. Technol.* 51, 13689–13697. <https://doi.org/10.1021/acs.est.7b03667>.
- Thomas, D., Schütze, B., Heinze, W.M., Steinmetz, Z., 2020. Sample preparation techniques for the analysis of microplastics in soil—a review. *Sustain. Times* 12, 1–28. <https://doi.org/10.3390/su12219074>.
- Villanova-Solano, C., Díaz-Peña, F.J., Hernández-Sánchez, C., González-Sálamo, J., González-Pleiter, M., Vega-Moreno, D., Fernández-Piñas, F., Fraile-Nuez, E., Machín, F., Hernández-Borges, J., 2022. Microplastic pollution in sublittoral coastal sediments of a North Atlantic island: the case of La Palma (Canary Islands, Spain). *Chemosphere* 288, 132530. <https://doi.org/10.1016/j.chemosphere.2021.132530>.
- Waniek, J.J., Schulz-Bull, D.E., Blanz, T., Prien, R.D., Oeschlies, A., Müller, T.J., 2005a. Interannual variability of deep water particle flux in relation to production and lateral sources in the northeast Atlantic. *Deep. Res. Part I Oceanogr. Res. Pap.* 52, 33–50. <https://doi.org/10.1016/j.dsr.2004.08.008>.
- Waniek, J.J., Schulz-Bull, D.E., Kuss, J., Blanz, T., 2005b. Long time series of deep water particle flux in three biogeochemical provinces of the northeast Atlantic. *J. Mar. Syst.* 56, 391–415. <https://doi.org/10.1016/j.jmarsys.2005.03.001>.
- Wesch, C., Elert, A.M., Wörner, M., Braun, U., Klein, R., 2017. Assuring quality in microplastic monitoring : about the value of clean-air devices as essentials for verified data. *Sci. Rep.* 7, 1–8. <https://doi.org/10.1038/s41598-017-05838-4>.
- Wilcox, C., Hardesty, B.D., Law, K.L., 2020. Abundance of floating plastic particles is increasing in the western North Atlantic ocean. *Environ. Sci. Technol.* 54, 790–796. <https://doi.org/10.1021/acs.est.9b04812>.
- Woodall, L.C., Sanchez-Vidal, A., Canals, M., Paterson, G.L.J., Coppock, R., Sleight, V., Calafat, A., Rogers, A.D., Narayanaswamy, B.E., Thompson, R.C., 2014. The deep sea is a major sink for microplastic debris. *R. Soc. Open Sci.* 1, 140317. <https://doi.org/10.1098/rsos.140317>.
- Wright, S.L., Kelly, F.J., 2017. Plastic and human health: a micro issue? *Environ. Sci. Technol.* 51, 6634–6647. <https://doi.org/10.1021/acs.est.7b00423>.
- Zettler, E.R., Mincer, T.J., Amaral-Zettler, L.A., 2013. Life in the “plastisphere”: microbial communities on plastic marine debris. *Environ. Sci. Technol.* 47, 7137–7146. <https://doi.org/10.1021/es401288x>.
- Zhou, Q., Tu, C., Yang, J., Fu, C., Li, Y., Waniek, J.J., 2021. Trapping of microplastics in Halocline and turbidity layers of the semi-enclosed Baltic Sea. *Front. Mar. Sci.* 8, 1–13. <https://doi.org/10.3389/fmars.2021.761566>.

Publication III

Full Research Paper, *Environmental Science and Technology*, 2022

Abiotic long-term simulation of microplastic weathering pathways under different aqueous conditions.

Janika Reineccius, Mischa Schönke, M., Joanna J. Waniek

Submitted: 17 August 2022; Accepted: 20 December 2022

doi: 10.1021/acs.est.2c05746

Microplastics (MPs) are one of the most abundant and widespread anthropogenic pollutants worldwide. In addition to the global spread and threats of plastic to native species by carrying toxic substances, its slow degradation rate and resulting long retention time in the environment constitute a problem that is still poorly understood. In this study, five of the most manufactured plastic types were weathered under simulated beach conditions for 18 months in freshwater, brackish water, and seawater. Those included polyethylene (PE), polypropylene (PP), polystyrene (PS), polyethylene terephthalate (PET), and polyvinyl chloride (PVC). PP was the first polymer type that fragmented after 9 months of weathering and influenced the pH of the surrounding water. Molecular surface changes were detected for all polymers, just after the first week. Hydroxyl bonds were one of the first groups incorporated into the polymers, weakening 2–3 weeks later. Carbonyl groups were also measured early, but with significantly different developments with time between the polymer types. Differences in degradation rates were proven between the water media, with the fastest degradation in seawater compared to brackish water and freshwater for PE and PP. These results are consistent with previous findings on MPs aged under environmental conditions and provide initial long-term observations of MP degradation pathways under simulated environmental conditions. These findings are valuable for assessing the fate and hazards of MPs in aquatic systems.

Abiotic Long-Term Simulation of Microplastic Weathering Pathways under Different Aqueous Conditions

Janika Reineccius,* Mischa Schönke, and Joanna J. Waniek



Cite This: <https://doi.org/10.1021/acs.est.2c05746>



Read Online

ACCESS |



Metrics & More



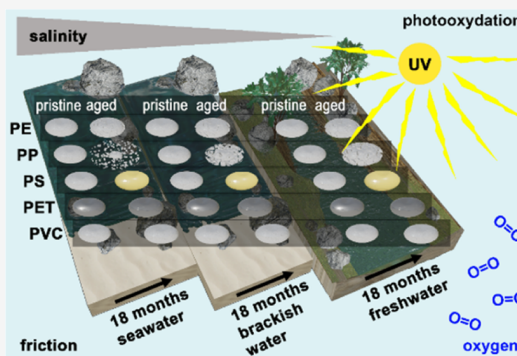
Article Recommendations



Supporting Information

ABSTRACT: Microplastics (MPs) are one of the most abundant and widespread anthropogenic pollutants worldwide. In addition to the global spread and threats of plastic to native species by carrying toxic substances, its slow degradation rate and resulting long retention time in the environment constitute a problem that is still poorly understood. In this study, five of the most manufactured plastic types were weathered under simulated beach conditions for 18 months in freshwater, brackish water, and seawater. Those included polyethylene (PE), polypropylene (PP), polystyrene (PS), polyethylene terephthalate (PET), and polyvinyl chloride (PVC). PP was the first polymer type that fragmented after 9 months of weathering and influenced the pH of the surrounding water. Molecular surface changes were detected for all polymers, just after the first week. Hydroxyl bonds were one of the first groups incorporated into the polymers, weakening 2–3 weeks later. Carbonyl groups were also measured early, but with significantly different developments with time between the polymer types. Differences in degradation rates were proven between the water media, with the fastest degradation in seawater compared to brackish water and freshwater for PE and PP. These results are consistent with previous findings on MPs aged under environmental conditions and provide initial long-term observations of MP degradation pathways under simulated environmental conditions. These findings are valuable for assessing the fate and hazards of MPs in aquatic systems.

KEYWORDS: microplastics, artificial weathering, salinity, seawater, brackish water, freshwater



1. INTRODUCTION

Plastic is ubiquitous in the global aquatic environment, transported around the globe by ocean currents or winds.^{1,2} The slow decomposition rate of plastic combined with increasing plastic production and deposition leads to the accumulation of large quantities of plastic in oceans.^{2,3} Once in the ocean, plastic has various consequences for native species, such as fish^{4–6} or different invertebrates^{7–9} that confuse plastic with their food. After transferring into the marine food web, it also has reached the human diet.^{10,11} Heavily degraded and fragmented plastic provides many attachment sides for lipophilic contaminants, pathogens, and toxic metals that can be transported across the globe attached to the plastic surface. It is suspected that predominantly microplastics (MPs; ≤ 5 mm), with a large surface-to-volume ratio, act as a preferred vector for contaminants.^{12–14} MPs can also release additives or monomers used for manufacturing and generating harmful degradation products under environmental conditions.^{15,16} To assess the numerous dangers MPs pose to the environment, understanding the degradation process is necessary.

Currently, research on the degradation processes and products of MPs is mainly based on theoretical descriptions and is still poorly understood, especially concerning the effects of MPs on the surrounding water.^{15,17–19} The mechanisms

driving the polymer weathering are photo-oxidation, identified as the most contributing degradation pathway,^{17,18} photo-thermal oxidation, mechanical abrasion, hydrolysis, and biodegradation.²⁰ Under beach conditions, the degradation process is expected to occur most rapidly due to available conditions such as solar radiation, mechanical stress from waves and sand, and high-temperature fluctuations at most locations.¹⁸ In addition to environmental conditions, the properties of MPs themselves, including their shape, size, and chemical composition, may also play a substantial role in the degradation rate.^{20–22} Other potential contributors, such as microorganisms or the salinity of the surrounding water, have not yet been fully clarified.^{20,23} For determining the degradation rate of MPs, previous investigations recorded changes in the surface and molecular composition under different environmental conditions.^{18,21,24–27} As the degradation of MPs in the environment can take several decades, the

Received: August 17, 2022

Revised: December 20, 2022

Accepted: December 20, 2022

degradation process of MPs was expedited by using stronger UV radiation with lower wavelengths (<300 nm) than that in natural sunlight that reaches the earth's surface.^{20,28} However, this choice of higher-energy lamps can lead to distortions of the aging process of plastic and the subsequent extrapolation to environmental conditions.^{20,24,28,29} Besides that, these lamps produce high temperatures, further affecting the degradation rate.³⁰

To address these current research needs, a laboratory experiment was conducted to artificially weather MP particles under simulated beach conditions very similar to aqueous environmental conditions. In the frame of this experiment, we monitored the weathering progress of five different polymer types over 18 months by analyzing the surface roughness, contact angles, molecular changes using Raman and FTIR spectroscopy, and the influence of the weathering plastic particles on the pH value of the surrounding water. Understanding the degradation rate of MPs is an important first contribution to assessing future environmental hazards and damage that has already occurred.

2. MATERIALS AND METHODS

2.1. Experimental Setup. **2.1.1. Polymer Types.** MP weathering was simulated in three different water media for the five most common MP types detected in the environment,¹⁹ each exposed to UV radiation and mechanical stress. High-density polyethylene (HDPE), polypropylene (PP), polystyrene (PS), polyethylene terephthalate (PET), and polyvinyl chloride (PVC) pellets were exposed to Warnow River (WW) water, Baltic Sea (BS) water, and South China Sea (SCS) water. More detailed information on the polymer types used for the experiment and an image of the experimental setup are provided in Table 1 and Figure S1, respectively. Based on

Table 1. Overview of Polymer Types Used in the Weathering Experiment Containing Information about the Polymer Provider, Particle Density, and Particle Size Measured under the Microscope Using the Freeware Software ImageJ 1.53o

polymer	provider	density [g m ⁻³]	size [mm]
PE	CS Plastik GmbH, Germany	0.955	3.5–4.5
PP	BASF Novolen 1101 M	0.910	3.5–4.5
PS	BASF 143 E	1.050	3.0–4.0
PET	Bühler bottle-grade recycled	1.340	3.0–3.5
PVC	WestChemie Rigid PVC type 4122	1.560	3.8–4.2

Raman and ATR-FTIR spectroscopy measurements, MP pellets were free of additives, except for PVC with high calcium carbonate (CaCO₃) contents.

2.1.2. Water Media. The SCS water was collected using a seawater intake pump, while for the BS and WW water, a bucket was used. The salinity of the collected water ranged between 2.0 for WW water, 9.0 for BS water, and 27.5 for SCS water. Immediately after collection, the water was filtered through glass microfiber filters (Whatman, diameter 25 mm, pore size 0.7 μm, CAT no. 1825-025) to remove microorganisms and reduce biological activity.

2.1.3. Mechanical Stress. For beach condition simulations, quartz-rich sand from the Baltic Sea coast (beach in Warnemünde) was collected, rinsed with ultrapure water, and placed in the oven at 100 °C for 24 h for drying and

sterilization. One portion of the sand was analyzed for grain size using Mastersizer 3000 with the associated software Mastersizer-v3.72, resulting in an average mode of 585 μm. For the weathering experiment, Erlenmeyer flasks made of borosilicate glass (100 mL, DURAN, Germany) were used, into which 20 g of the dry sand was added, covering the bottom of the flasks. The different water types were divided among the 15 flasks, resulting in five bottles containing 15 mL of the same water media each. Finally, 100 plastic particles were added to each flask, resulting in 15 flasks containing another combination of water and polymer types. The polymer types with a density lower than water (PE and PP) float on the water surface, while the denser particles (PS, PET, and PVC) sink to the sandy substrate covered by water. Subsequently, the flasks were placed on a shaking plate agitating at 130 rpm 24 h a day in circular rotation to exert constant mechanical stress on the plastic particles. During the experiment, neither the heavy nor the light polymer types were buried by the sand but were constantly moved on the sand surface.

2.1.4. Light Irradiation. Three lamps were mounted 18 cm above the shaking plate containing the samples to imitate daylight: one daylight lamp without UV light (OSRAM L 18 W/950 daylight) and two UV lamps with UVA and UVB components (Reptile UVB200 18 W Exo TERRA 24"/60 cm, UV-Index 4.3 at 20 cm distance). The UVB radiation intensity of all installed lamps considering the individual sample distance to the light sources, reached 1.50–1.79 W m⁻². This radiation corresponds to UV-intense latitudes on sunny days as in Indonesia (maximum: 2.17 W m⁻², mean: 1.22 W m⁻²)³¹ but is less than the global radiation under ideal conditions of 4 W m⁻².³² The resulting radiation conditions are similar to natural sunlight and allow extrapolation for arbitrary regions with known sunlight intensities. For borosilicate glass, the transmission of light in the wavelength range between 310 and 2200 nm is negligible and accounts for 25% at 300 nm (clear glass, DURAN product details). Terrestrial sunlight consists of infrared, visible, and UV light with the smallest wavelength at 300 nm (UVB). The UVB content represents about 1.3% of the entire solar spectrum,³³ resulting in a negligible loss of radiation by borosilicate glass. This was also confirmed by measurements of the photon amount, with a mean of 111.4 μE s⁻¹ m⁻² reaching the outer sample flask compared to 110.7 μE s⁻¹ m⁻² passing the flask's bottom glass. The lamp device was covered with aluminum foil to avoid scattering. During the experiment, sample flasks remained uncovered for natural oxygen exchange and were refilled with ultrapure water once a week to compensate for evaporation (~3 mL). The water temperature did not exceed 30 °C (24–27 °C).

2.2. Sampling. After exposure periods of 1, 2, 3, 4, and 6 weeks and 2, 3, 4, 6, 9, 12, 15, and 18 months, five MP pellets were taken from each flask with stainless-steel tweezers, respectively. These MP pellets were then rinsed with ultrapure water, air-dried, and frozen for preservation (–20 °C) until analysis. To exclude effects caused by the freezing process, pristine plastic pellets were treated with the same procedure as a reference. Currently, there is no information on how the present moisture affects the microplastic particle surface during a freezing process, which leads to the formation of tiny crystals and thus can potentially affect polymer fragmentation.³⁴ To avoid this effect to the best possible extent, our samples were dried before freezing.

At the end of the experiment, the 40 remaining pellets in each flask were weighed and compared to 40 pristine MP

pellets to determine the weight changes. The results are reported as the mean and standard deviation (\pm s.d.) calculated from the 40 respective particles. Additionally, the water to which the pellets were exposed was taken by glass pipettes and filtered after the experiment time of 18 months (Whatman Nucleopore Track-Etched Membranes WHA111107, 47 mm diameter, 0.4 μ m pore size). The loaded filters were transferred into a glass Petri dish and air-dried under the fume hood before weighing.

2.3. Surface Structure Analysis. To observe weathering induced changes in particle surfaces, scanning electron microscopy (SEM MERLIN VP Compact from Zeiss, Germany) with Aztec software from Oxford Instruments (Great Britain) with a magnification of 7000 to 30,000 and confocal laser scanning microscopy (LEXT 3D Measuring Laser Microscope OLS4100) with LEXT software at a magnification of 50 were used. For SEM images, particles were coated with carbon for conductivity and claimed in a sample holder to avoid movements during microscopy. The particle surface roughness was derived based on the confocal laser scanning microscopy data. For each polymer type, water media, and exposure time, three different particles (triplicates) were measured at a horizontal resolution of 0.25 μ m resulting in an area of 256 \times 256 μ m (1024 \times 1024 pixels). To investigate roughness changes of particle surfaces, an averaged 2D power spectral density (PSD) was computed, which has proven to be an essential tool to reflect spatial height variations of distinct wavelengths.^{35,36} The entire calculation process of PSD is declared in the Supporting Information (Figure S2). Additionally, to the PSD, the root-mean-square roughness of the surface (S_q) was computed in the time domain. All results of PSD (in μ m⁴) and S_q (in μ m) are reported as a mean with a standard deviation (\pm s.d.) resulting from the triplicate measurements.

2.4. Determination of Functional Groups. Weathering-induced changes at the polymer surface were detected by Raman spectroscopy (LabRAM HR 800 Horiba Jobin YVON coupled with an Olympus BX41 microscope) and attenuated total reflection Fourier transform infrared spectroscopy (ATR-FTIR, ALPHA II Bruker). Detailed information about the measurement procedure is provided in the Supporting Information. The obtained spectra were baseline corrected using the KnowItAll Information System 2020 system. As the spectral intensity may also depend on the particle surface condition, peak intensities were determined in relation to a stable reference peak in the same spectra. These used reference peaks are 2882 (PE), 1463 (PP), 3054 (PS), 1461 (PET), and 1440 cm^{-1} (PVC) for Raman and 2910 (PE), 2920 (PP), 1452 (PS), and 730 cm^{-1} (PET) for ATR-FTIR (assigned in Table S1 in the Supporting Information). As the intensity of each characteristic polymer peak of PVC changed over time in the ATR-FTIR spectra, no reference peak was defined. For this reason, the PVC spectra were normalized using the standard normal variate (SNV) transformation,²⁴ and the individual peak intensities were used instead of the peak ratio for further interpretation of functional groups. The carbonyl index (CI), hydroxyl index (HI), and C=C bond index were calculated using the maximum peak intensities at 1715–1717 cm^{-1} , 3300–3400, and 1600–1680 cm^{-1} of the ATR-FTIR spectra, respectively, relative to the respective reference peak intensity.³⁷ All results are reported as the mean, with the standard deviation (\pm s.d.) calculated from the triplicate

measurements (three different particles with the same water, polymer, and exposure time).

2.5. Determination of Contact Angles and pH. To evaluate the changes in hydrophobicity at the MP surface, the contact angles for all weathered and pristine pellets were measured in triplicates using a binocular microscope (SteREO Discovery.V8, Carl Zeiss, Germany) with a camera (SWIFT-CAM Microscope Digital Camera SC500, 5.1 MP). For the measurements, the defrosted and air-dried pellets were transferred into a glass Petri dish under the microscope, and a 2 μ L droplet of ultrapure water was placed on the pellet using an Eppendorf pipette. After 10 s, a picture was taken to measure the contact angle for curved surfaces as described in previous studies.^{38,39} The contact angles were determined using the open-source image processing program ImageJ v1.53o and were measured four times for each droplet (two times on each side). The corresponding results are given as mean values with standard deviation (\pm s.d.) calculated from the triplicate measurements.

For pH measurement, the water remained after the experiment was filtered (Whatman, diameter 25 mm, pore size 0.7 μ m, CAT no. 1825-025) to separate the aqueous phase from MP fragments generated during the exposure time. The filtrated water and untreated WW, BS, and SCS water were transferred into a glass tube and measured using a pH meter (WTW Series inoLab pH 720).

2.6. Data Analysis and Statistics. T-tests were performed to evaluate peak intensities, contact angles, and surface roughness within the weathering periods. This test was also used to compare pellet weights and filtered particle masses generated during the experiment before and after the weathering experiment to identify potential differences between the water media. To test for relations between the exposure time and the contact angles, surface roughness, or specific peak intensities from the Raman and FTIR spectra, linear and quadratic regressions were implemented. These regressions were carried out using the freeware program Past 3.20 (Hammer, Harper, D.A.T., Ryan, P.D. 2001). The respective curves were assumed to be linear or quadratic with $R^2 \geq 0.50$ and $p \leq 0.05$ for the included variance F test (95% confidence interval). In addition, ANCOVA tests (95% confidence interval) were performed to account for significant differences among the three different water media. The confidence interval of 95% was also used for correlation tests (Pearson), which were implemented with the freeware software Python 5.2.2.

3. RESULTS AND DISCUSSION

3.1. Weight Loss and Surface Roughness. After the total exposure time of 18 months, changes in particle properties were visible for PS and PP pellets in all water types. The PS pellets yellowed visibly after three months, intensifying during the weathering process. Yellowing was also frequently reported for PS in previous studies.^{37,40} The PP pellets became progressively porous, and the water turned visibly milky after nine months, which also intensified during the exposure time. After 18 months, the PP pellet masses differed significantly from the pristine pellet weights (mean weight 26.10 \pm 3.76 mg, $n = 40$) for WW water (mean weight 23.45 \pm 4.10 mg, $n = 40$, $p < 0.05$) and SCS water (mean weight 20.59 \pm 3.78 mg, $n = 40$, $p < 0.05$) but not for BS water (mean weight 24.83 \pm 4.05 mg, $n = 40$, $p > 0.05$). Compared to WW and BS water, the weight loss in SCS water was

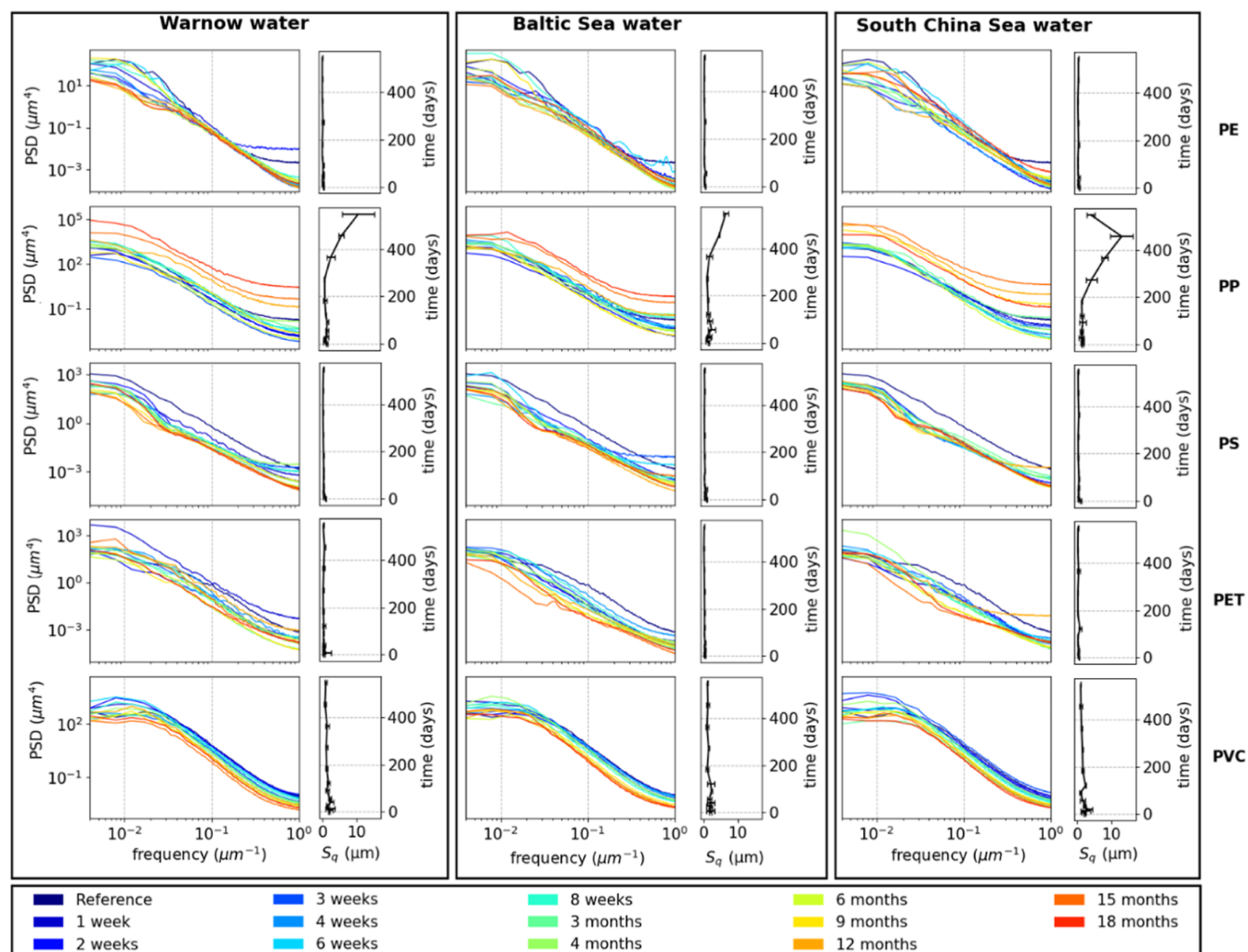


Figure 1. PSD for the weathered and pristine (reference) MP pellets PE, PP, PS, PET, and PVC in color and the respective root-mean-square roughness (S_q) over the exposure time in black for three different water media (Warnow, Baltic Sea, and South China Sea water). Error bars represent the standard deviation (\pm s.d.) resulting from triplicates.

significantly higher. No significant mass changes were found for all other polymer types after the exposure time, except for PVC in WW water (mean weight 46.59 ± 11.84 mg, $n = 40$) compared to the pristine pellets (mean weight 51.69 ± 10.41 mg, $n = 40$, $p < 0.05$). The mass of fragmented plastic particles on the filter broken off during the exposure period confirmed this finding for PP, with the highest fragment mass in SCS water (5135.45 mg L^{-1}), followed by WW (2936.00 mg L^{-1}) and BS water (348.85 mg L^{-1}). This supports the assumption that PP degrades fastest in SCS, followed by WW and BS water. Due to their small size, the largest amount of fragmented PP particles in the water was not possible to measure under the Raman microscope individually but as a mass (particle diameter < 10 μm). SEM images of the PP pellets revealed a high number of broken-out fragments (secondary MP) on the pellet surface after 18 months (Figure S3), varying in size but occurring most frequently in small sizes below 2 μm . A similar observation for the generation of secondary MPs or even nanoplastic formation at the polymer surface had been previously made by Menzel et al.⁴¹ The earlier fragmentation of PP compared to PE is also consistent with previous observations.¹⁸ For other polymer types, no fragments were detected on the pellet surface, and only a few

were found on the filter of the filtered water (0–5 items per filter), with a low weight of this filtered material (≤ 1 mg). The pellet and filter weights for all polymers and water types are available in the Supporting Information Tables S2 and S3, respectively. After sampling the water in which the MP particles were exposed for 18 months, in addition to the fragmented PP pieces floating on the water surface, there were also particles observed floating in the water column and sinking to the bottom of the vial after a short resting period. This implies that the density of the pristine PP pellets (0.91 g m^{-3} , Table 1) increased for the generated fragments during weathering, resulting in PP fragments that exceeded water densities between 1.00 and 1.03 g m^{-3} (depending on salinity). Due to the rapid decay of PP into small (< 2 μm) sinking fragments and the FTIR detection limit of 10 μm , large amounts of PP in the aquatic environment may have been underestimated.

In Figure 1, the surface roughness expressed as the PSD in the frequency range between 4×10^{-3} and 1 μm^{-1} is given for all analyzed polymers and water media over the exposure time. No changes were observed for PE after 18 months. For PP, on the other hand, roughness values increased with increasing exposure time. Initially, fine, long cracks formed on the

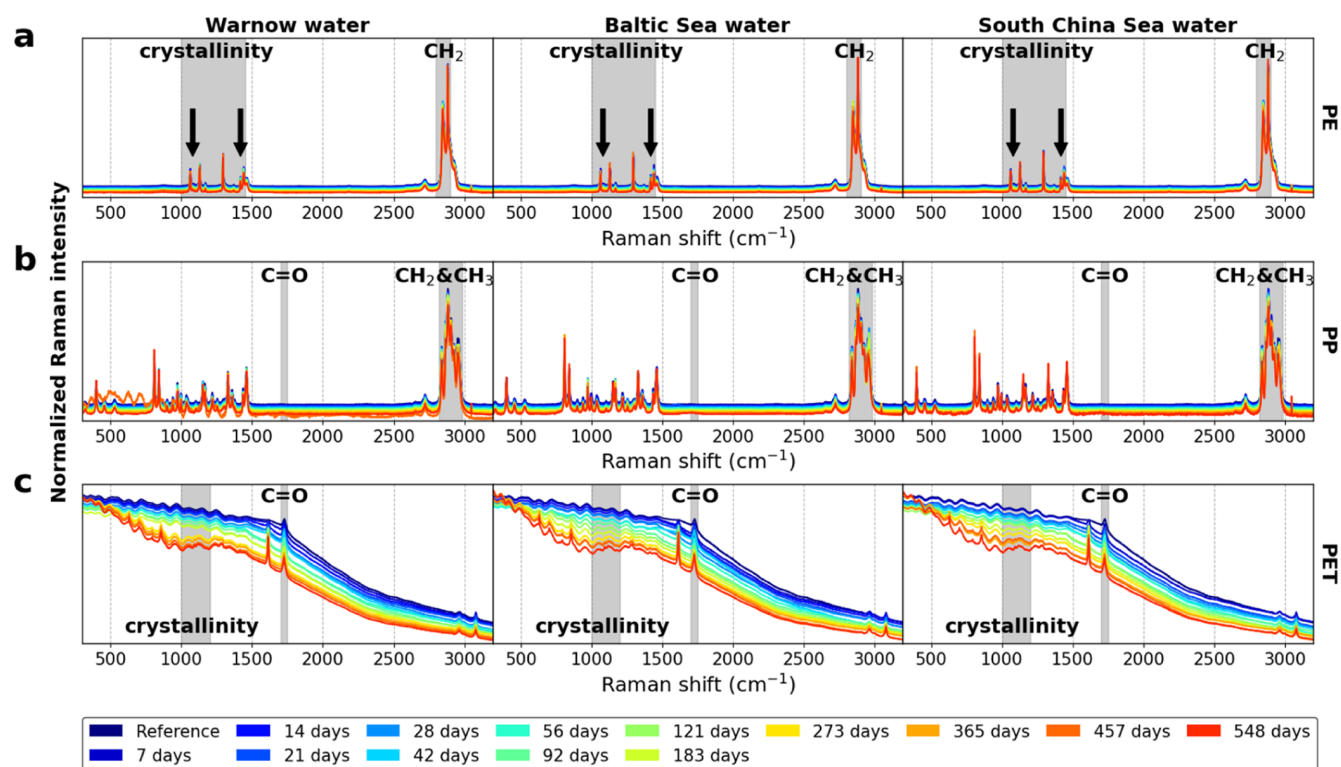


Figure 2. (a) PE, (b) PP, and (c) PET Raman spectra for all analyzed exposure times for Warnow, Baltic Sea, and South China Sea water, with changing peak intensities marked in gray areas.

polymer surface, which widened over time and eventually generated deep holes (Figure S4). Depending on the water media, these processes differ in their temporal occurrence. For PP pellets exposed to BS water, the first cracks were observed after 12 months in combination with small holes $<30 \mu\text{m}$ in their largest diameter. After 15 months, the size of the holes has expanded to about $200 \mu\text{m}$ in length and $50 \mu\text{m}$ in width, achieving the maximum length of $\geq 250 \mu\text{m}$ after 18 months. In WW water, fine cracks, in combination with small flat holes ($2\text{--}3 \mu\text{m}$ in depth) formed earlier after nine months, result in a strongly destroyed and brittle surface by the end of the experiment. Stronger brittleness and elevated surface roughness were recognized for PP exposed to SCS water with a maximum roughness (S_q) after 15 months (Figure 1). After 18 months, roughness decreased in SCS water to a level similar to nine months. Fragmentation of the uppermost weathered polymer layer is likely the cause of the subsequent decrease in the roughness of PP in SCS water after 18 months, as the release of PP fragments into the surrounding water reveals the unweathered and smooth subsurface layer. Combined with the higher weight loss of PP in SCS water, this also suggests a faster fragmentation in saltier water.

The analyzed particles of the three polymer types, PS, PET, and PVC (Figure 1), having a higher density than freshwater or seawater, decreased in their surface roughness with increasing exposure time, indicating a significant surface abrasion by the sand. This was particularly evident for PET and PVC, with numerous artifacts on the particle surface prior to the experiment that disappeared after 18 months of weathering (Figure S4). Although PVC was abraded in all frequencies and all water types very equally, PET was smoothed more irregularly, with the strongest smoothing between 10^{-1} and $9 \times 10^{-1} \mu\text{m}^{-1}$ ($10\text{--}90 \mu\text{m}$) in BS and SCS water. Although the

surface of the PS pellets was already smooth before the experiment started, further smoothing was observed in all water types, with the strongest effect at frequencies between 6×10^{-1} and $9 \times 10^{-1} \mu\text{m}^{-1}$ ($60\text{--}90 \mu\text{m}$). However, no significant differences were identified for PS, PET, or PVC between the three applied water media.

3.2. Changes in Raman Spectra. To demonstrate potential changes in the molecular polymer surface and to verify the identifiability of the plastic pellets during weathering, Raman spectroscopy was applied. Using the Raman spectroscopy, stable and characteristic spectra were obtained for all analyzed polymer types at every exposure time except for the strong fluorescence observed for the grey-colored PET pellets (Figure 2c).

3.2.1. Changes in PE Raman Signals. Starting with PE pellets, no significant changes were determined for the most important identification peaks, such as the C–C stretching vibration peaks at 1060 and 1127 cm^{-1} or the bending vibration of CH_2 at 1293 and 1438 cm^{-1} relative to 2882 cm^{-1} . Contrary to this, the symmetric CH_2 stretching vibration band at 2848 cm^{-1} showed a significant decrease in BS and SCS water (Figure 2a). This relation indicates the translocation of the trans-oriented polymer chains from the noncrystalline to the crystalline phase⁴² and the size of the crystalline phase regions within the polymer.^{42,43} The ratio of the peak intensities at 1418 (CH_2 wagging vibration) and 1080 cm^{-1} (C–C stretching vibration), also signifying the crystalline phases in relation to the amorphous phases of PE,^{43–45} increased over the exposure time for all water types (Figures 2a and S6 in the Supporting Information). We found maximum increasing factors of 1.12, 2.13, and 2.35 for WW (after 15 months), BS (after 15 months), and SCS (after 18 months) water relative to the crystallinity of the pristine pellets,

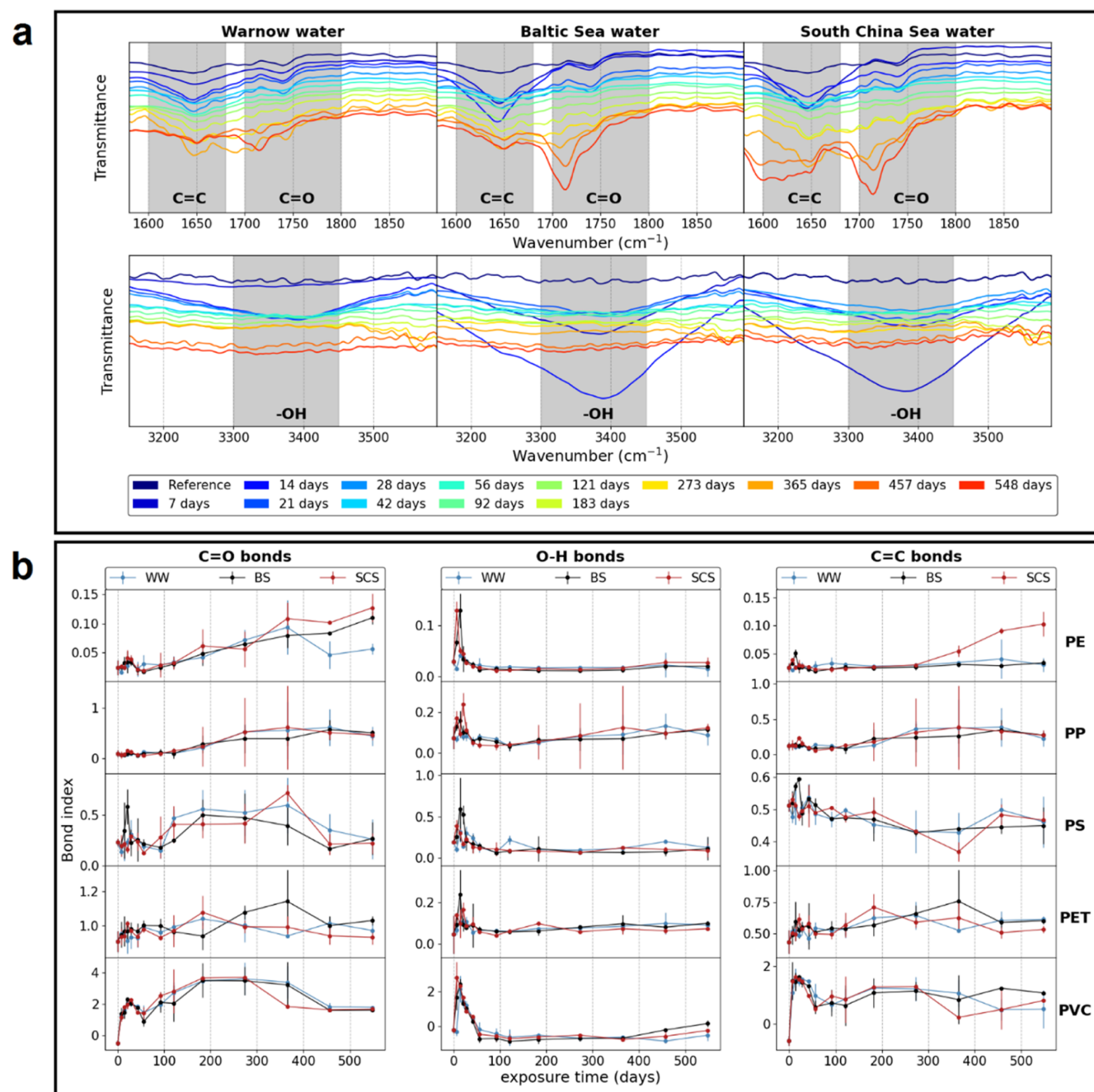


Figure 3. (a) ATR-FTIR spectra of PE in the wavenumber range between 1600 and 1800 cm⁻¹, characteristic for the functional groups C=C (vinyl) and C=O (carbonyl), and between 3300 and 3450 cm⁻¹, indicating -OH (hydroxyl) groups. The visualized spectra were smoothed and normalized using the SNV normalization. (b) Carbonyl (C=O), hydroxyl (O-H), and C=C (vinyl for PE, PP, and PVC and aromatic for PS and PET) bond indices for the five different polymer types (PE, PP, PS, PET, and PVC) and the three water types: Warnow River (WW) water, Baltic Sea (BS) water, and South China Sea (SCS) water. The vertical lines represent the standard deviation (\pm s.d.) resulting from triplicates.

respectively. Additionally, a significantly steeper linear increase for BS [slope: $(6.886 \pm 1.307) \times 10^{-3}$] and SCS [slope: $(7.489 \pm 1.474) \times 10^{-3}$] water compared to WW water [slope: $(2.172 \pm 0.701) \times 10^{-3}$] was verified, suggesting a salinity-dependent increase of crystallinity for PE. The increasing crystallinity combined with the growing sizes of crystalline phases during the experiment may accelerate the embrittlement and accompanying progression of weathering of PE.⁴⁴ Consequently, the crystallinity can be considered an indicator of the weathering degree, but due to the unknown initial crystalline

content of environmentally released PE, this approach was discarded.

3.2.2. Changes in PP Raman Signals. For PP, no increase in crystallinity was observed using the ratio of 809 to 841 cm⁻¹.^{46–48} However, a decrease in the CH, CH₂, and CH₃ stretching vibrations at 2800–3000 cm⁻¹ was recognized (Figures 2b and S7 in the Supporting Information), signifying chain scission within the polymer. A significant reduction in peak intensity was found for all water types at 2839 and 2884 cm⁻¹, SCS water at 2904 cm⁻¹, and WW and SCS water at 2960 cm⁻¹, with the steepest decrease for SCS water for all

water types. Besides that, a very weak new band at 1724 cm^{-1} was detected after nine months in SCS and 12 months in BS water, which significantly increased over the weathering time. This peak, assigned to C=O stretching vibration modes,⁴⁹ increased significantly stronger for SCS water than for BS water. Based on the previously hypothesized degradation pathway of PP with resulting ketones and olefins,¹⁷ weathered PP was expected to increase at 1613 cm^{-1} (C=C bonds)⁴⁹ in its spectra. However, no increasing intensity was recognized with Raman measurements.

3.2.3. Changes in PS Raman Signals. During the experiment, the crystallinity of PS did not increase based on the ratio of peak intensities at 773 and 798 cm^{-1} .⁵⁰ In addition, contrary to previous studies in which PS were weathered with UV radiation, no significant signal decreases or increases were observed for the peaks at 392 , 497 , 526 , 622 (ring deformation mode), 1001 (ring breathing mode), 1286 , or 1511 cm^{-1} .⁵¹

3.2.4. Changes in PET Raman Signals. The interpretation of PET peaks was rather complex due to the strong fluorescence of the gray-colored PET pellets (Figure 2c). However, despite this fluorescence, a significant linear decrease in the peak intensities in 1726 cm^{-1} (C=O stretching vibration⁵²) for WW and BS was observed. Furthermore, a significant linear increase for WW and BS water at 1094 cm^{-1} relative to 1115 cm^{-1} was recognized, which is responsible for the crystallinity of PET⁵³ (Figure S8). The linear regression slopes for the crystallinity ranged between $(8.790 \pm 2.079) \times 10^{-4}$, $(7.008 \pm 1.514) \times 10^{-4}$, and $(6.629 \pm 1.957) \times 10^{-4}$ for WW, BS, and SCS, respectively, with an increasing factor of 1.633 (WW), 1.645 (BS), and 1.635 (SCS) after 18 months compared to the pristine pellets. Under similar weathering conditions, this increase in crystallinity was also observed previously by Oelschlägel et al.⁵⁴ for PET (3%) and PE (4%) analyzed with X-ray diffraction. However, the exposure time of 28 days was much shorter, resulting in increasing factors of 1.125 and 1.073 for PE and PET, respectively. For 28 days of exposure time, we calculated increasing factors of 1.067 for PE and 1.027 for PET weathered in SCS water, showing very similar results to previously reported X-ray measurements of PE and PET weathered in artificial seawater.⁵⁴ These results are consistent with observations by Menzel et al.,⁴¹ with an increasing rate of 1.079 after 28 days for PE exposed to artificial daylight (300–400 nm) after 28 days. However, they used deionized water for their experiments and higher temperatures ($55\text{ }^\circ\text{C}$), making a direct comparison difficult. In contrast to the increasing crystallinity of PE, the evaluation of the linear regression lines for PET revealed no significant differences between water types, indicating that salinity does not affect the degree of weathering of PET.

3.2.5. Changes in PVC Raman Signals. According to previous studies,^{52,55,56} PVC was assumed to have decreasing chlorine (C–Cl) vibration peaks at 635 and 697 cm^{-1} , a declining C–H stretching mode at 2912 cm^{-1} , as well as new peaks at 1510 or 1597 cm^{-1} assigned to a C=C stretching vibration^{56,57} as a result of dehydrochlorination.⁵⁸ However, our results showed no significant linear decrease or increase in peak intensities in Raman spectra over the exposure time.

3.3. Changes in ATR-FTIR Spectra. With a higher oxygen sensitivity of FTIR spectroscopy compared to Raman spectroscopy, changes in oxygen-containing functional groups, such as carbonyl and hydroxyl groups, can be estimated with higher resolution (Figure 3a). In the case of oxygen-free polymer types (PE, PP, PS, and PVC), hydroxyl, carbonyl, and vinyl

groups are formed by weathering processes^{17,24,37,59} and are, therefore, of particular interest in this work.

3.3.1. Changes in PE FTIR Signals. In FTIR spectra of PE, we found a significant linear increase for the ketones peak at 1717 cm^{-1} over the exposure time, which is commonly used to calculate the carbonyl index (CI) as an indication of the weathering degree of plastic.^{26,60–62} This steady increase in CI is also in line with previous studies.^{26,63,64} Results from Brandon et al.³⁷ showed fluctuating CI, which they attributed to the ongoing fragmentation exposing less weathered plastic from the particle interior to the surface. For the PE examination in our study, no fragmentation occurred, but fluctuations in CI were also observed within the first two months, followed by a linear increase (Figure 3b). After 18 months, the lowest CI values for PE were measured for WW water (0.056 ± 0.012) and the highest for SCS water (0.127 ± 0.024) (Figures 3b and S9 in the Supporting Information), suggesting a faster increase in carbonyl functional groups for SCS compared to BS and WW water. A similar dependence on CI was found by Arias-Villamizar et al.⁶⁵ for PE in freshwater compared to seawater after outdoor weathering, revealing that saltier water accelerates weathering. In addition to the CI, an increase in C=C wag vibration intensities, with a strong quadratic fit for BS and SCS water media at 911 cm^{-1} (BS: $R^2 = 0.702$, $p < 0.001$; SCS: $R^2 = 0.771$, $p < 0.001$) and 1640 cm^{-1} for SCS water ($R^2 = 0.867$, $p < 0.001$) was observed. However, no increase in WW water (Figure 3b) was recognized. The hydroxyl index (HI) showed no increase over the total experiment time but increased significantly between the first and third weeks and decreased back to the reference level within the first month (Figure 3b). This intervening appearance of hydroxyl groups indicates an unstable intermediate that continues to react as weathering proceeds. During this first week, the HI was significantly higher for PE weathered in SCS water followed by BS and WW water, implying the fastest generation of hydroxyl groups in SCS water followed by BS and WW water (Figure 3a,b). Based on a three-year roof-top experiment by Brandon et al.,³⁷ weathering PE in seawater under outdoor conditions, the HI ranges between 0 and 0.3 with several increases and decreases during the weathering time. The calculation pathway for the HI was the same as in our study, but we found no variations at exposure periods longer than one month and calculated lower HI values after five months and one year. Additionally, the initial increase within the first month cannot be compared to this previous work due to the lack of available data for this period. In contrast, the hydroxyl peak of highly degraded PE particles collected by Veerasingam et al.⁶⁶ from the coast of Goa, India, was lower, fitting well with our findings after exposure times >1 month.

3.3.2. Changes in PP FTIR Signals. For PP, the CI also increased significantly and linearly for all water types (Figure S10). Although linearity was present, a slight decrease was recognized after 12–15 months, resulting in weaker regression coefficients between 0.362 and 0.619. For SCS, the maximum CI was reached after 12 months with 0.612 ± 0.828 , whereas in WW and BS water, the highest CI was achieved later, after 15 months, with 0.614 ± 0.569 and 0.570 ± 0.195 , respectively. Similar observations were made for the roughness spectra, with fragmentation occurring 3–6 months faster in SCS than in WW or BS water. For HI, there was an early increase in the first 1–2 weeks, decreasing after 4–8 weeks, and increasing very slightly again from the sixth month. This

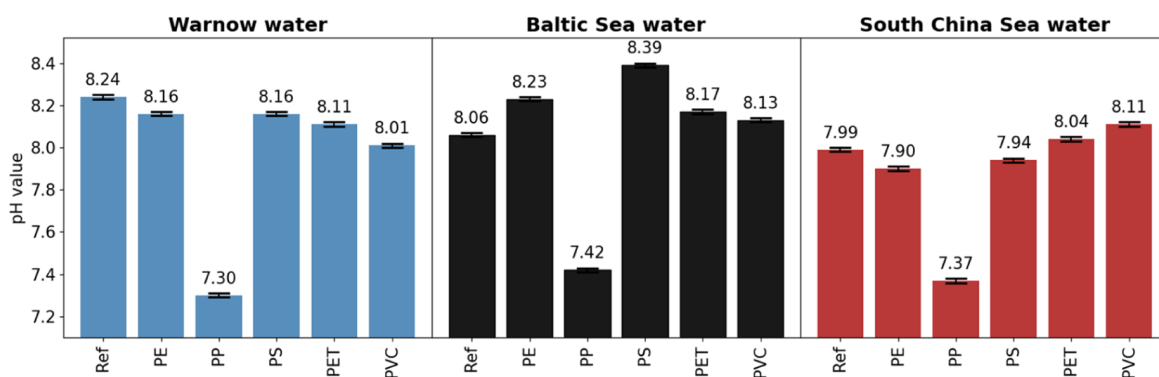


Figure 4. pH values before (ref) and after the exposure time of PE, PP, PS, PET, and PVC in the Warnow, Baltic Sea, and the South China Sea water. The error bars show the potential measurement errors of the pH meter.

indicates the first generation of hydroxyl groups as an intermediate similar to PE, followed by a new generation of hydroxyl groups at newly exposed polymer layers caused by the fragmentation of PP. Brandon et al.³⁷ made a similar observation for HI and CI, except for the initial increase in HI in the first five months due to the lack of data points. Similar to PE, we observed a significantly higher HI for SCS and BS water than WW water for PP after the first week, also suggesting an earlier and more intense degradation pathway in SCS water.

Moreover, a significant linear increase in the C=C peak was seen for all water media, with a weakening increase after nine months (Figure 3b). In contrast to PE, the C=C signal for PP increased much earlier and in parallel with the CI, suggesting a different degradation pathway for both polymer types. Due to the high standard deviation caused by the pellet fragmentation of PP, no significant changes were demonstrated for CI and C=C bands with weathering time between the three water types. As ATR-FTIR spectroscopy probes the near-surface region of the polymer pellet only,⁶⁷ weathering progress cannot be reliably detected after fragmentation.

3.3.3. Changes in PS FTIR Signals. The CI for PS was not linearly or quadratically increasing over the exposure time (Figure S11). Instead, we observed an increase in the first days, which fell back to the initial level until three months, increased again to form a plateau, and fell again after 15 months (Figure 3b). The maximum CI value already occurred after the first three weeks for BS water (0.589 ± 0.174). In WW and SCS water, the maximum CI was reached much later at, 12 months, with 0.600 ± 0.274 and 0.723 ± 0.081 , respectively. A similar development was observed for the aromatic C=C bonds at 1493 cm^{-1} , which was strongly negatively correlated to the aliphatic CH bonds at 2914 cm^{-1} for WW ($|r| = 0.841$, $p < 0.001$) and SCS ($|r| = 0.770$, $p = 0.001$) water. This indicates a significant backbone chain scission with the generation of free aromatic and carbonylic compounds, as suggested by Gewert et al.,¹⁵ but with strong fluctuation. More stable growing CI for PS was examined by Liu et al.,²⁶ but in this research, samples were taken after 5 and 11 months only. Fernández-González et al.⁵⁹ found a first increase followed by a decrease in CI values, explained by the loss of volatile bonds or surface fragmentation. As we did not observe fragmentation at the PS pellet surface, the formation of volatile or soluble compounds is the preferred explanation for these fluctuating peak intensities of carbonyl and CH bonds, which leave the polymer surface once they reach a soluble size.

3.3.4. Changes in PET FTIR Signals. In PET spectra, we also found no significant linear increase or decrease for all potentially changing bands (Table S1). Peak intensities fluctuated strongly during the exposure time, making the regression coefficients low (<0.4), especially for the aromatic C–H (870 cm^{-1}) as well as aromatic and aliphatic C–O bond intensities (1245 and 1100 cm^{-1}) (Figure S12). Such strong fluctuations were also observed by Fernández-González et al.⁵⁹ but with progressive roughness of the polymer surface. In the study by Ioakeimidis et al.,⁶⁸ in which PET bottles were investigated that aged for 1–18 years in the marine environment, decreasing or disappearing intensities were observed in the FTIR spectra for all functional oxygen groups and characteristic aromatic compounds. Such strong effects were not detected within the period of our study.

3.3.5. Changes in PVC FTIR Signals. The PVC spectra changed rapidly and strongly, making identification with ATR-FTIR difficult. In addition, large amounts of additives, commonly used in large quantities for PVC (up to 60%⁶⁹), make the spectra ambiguous due to overlaps. In the current study, the calcium carbonate (CaCO_3) additive in the PVC pellets overlapped the reference spectra at wavenumbers $<1500 \text{ cm}^{-1}$. However, after the first week, the CaCO_3 peaks were weakened or disappeared in the PVC spectra by dissolution. Besides the CaCO_3 peaks, also the C–Cl peak disappeared during the first two weeks, which was visible in the reference spectra at 617 cm^{-1} .

Additionally, the CH bands between 2800 and 3000 cm^{-1} weakened after the first increase and disappeared after three months. However, they reappeared after a total exposure time of nine months, resulting in a strong dependence on a quadratic function for all water types (Figure S13). A similar occurrence was observed for the CI with a negative correlation to the CH groups for WW and SCS water. The CI increased until the fourth week, weakened until the eighth week, grew again until nine months, and decreased for all later measurements. The CH bands at lower wavenumbers (1254 and 1334 cm^{-1}) with the carbon also connected to chlorine developed similarly to the C–Cl (617 cm^{-1}) curve, indicating strong and rapid molecular rearrangement at the PVC surface layer.⁵⁷ It can be assumed that the initial release of chlorine after the first week drives the formation of new carbonyl, polyene, and alkene compounds in the same week. Similar results have been observed previously in high-temperature PVC degradation experiments measured with Raman, in which the evolution of hydrochloric acid was observed as an accelerating weathering

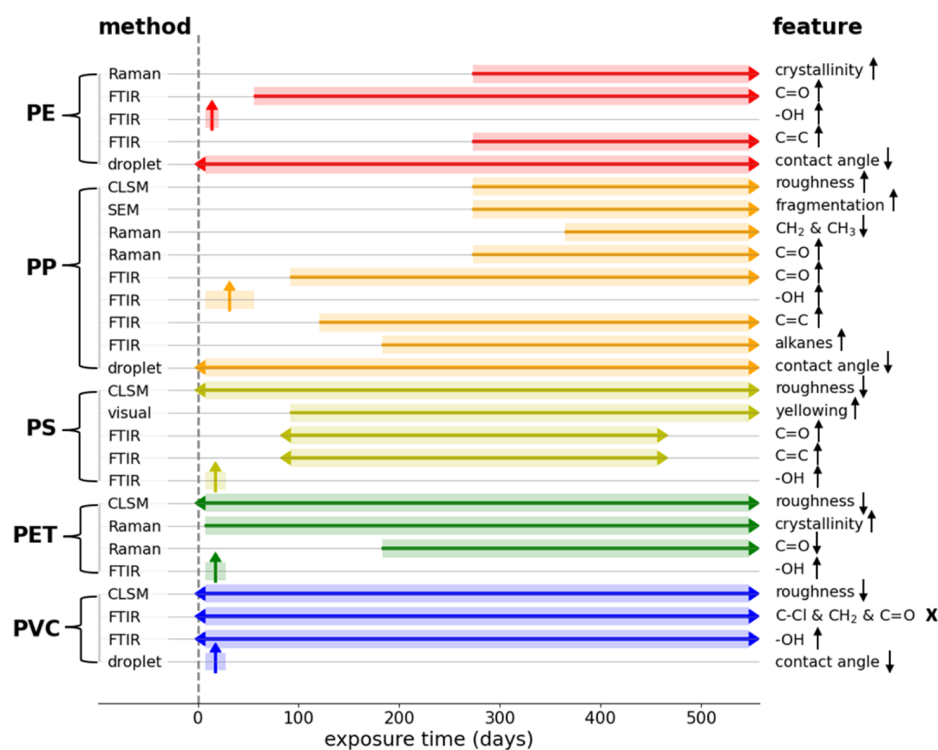


Figure 5. Summary of changing features for the five analyzed polymer types (PE, PP, PS, PET, and PVC). Black arrows signify increasing (↑) or decreasing (↓) changes. Bold X demonstrates that features changed but were not reliably measurable after this change. The colored vertical arrows (↑) amplify a temporal change in this feature, the horizontal double arrow (↔) shows a change that subsequently stabilizes (plateau), and the single horizontal arrow (→) signifies an ongoing change (a linear increase over time).

product.^{55,58,70–72} These observations agree well with the reaction pathway proposed by Wang et al.⁵⁷

3.4. Contact Angles and pH. After an exposure period of 9 to 12 months, the contact angle of PP increased in all water types (Figure S5), with the sharpest increase in SCS and WW water. This late increase was attributed to the strong fragmentation at the polymer surface. Besides that, for PP, PE, and especially for PVC, a sharp decrease was recognized in the first week, going along with increasing hydroxyl bands at the same time (Section 3.3). As the contact angle for these polymers did not increase to this initial level again, but hydroxyl signals disappeared (Figure 3b), the transformation of the polar hydroxyl groups to also polar carbonyl groups of a higher binding energy⁷³ is evident.

Comparing the pH values of the three water media before weathering the plastic pellets and after the experiment, no changes were detected for PE, PS, PET, or PVC (Figure 4). Minor changes in pH were expected due to potential impacts of the sand, air, or ultrapure water to compensate for evaporation. For all water types and polymers, the pH was about eight before and after exposure time, except for PP. PP instead strongly decreased the pH over time in all water media, and a distinct acetic acid odor was perceptible. Acetic acid and other degradation products, such as acetone, have been detected previously,⁶² but the impact on pH has never been considered. Due to the logarithmic dependence of pH, this change signifies a four- to nine-fold increase in H₃O⁺ ions induced by PP compared to untreated water types. Assuming that the formation rate and the release of acidic degradation products remain uniform despite fragmentation, the pH of 1 L of water containing 174 g PP pellets would decrease by one after about one year. However, due to the ongoing

fragmentation, which leads to a higher area-to-volume ratio, an increasing release of degradation products can be assumed.

3.5. Environmental Implications. After weathering MPs under simulated beach conditions, changes were observed for all five polymer types after 18 months (Figure 5). By using different degradation indicators such as the CI, HI, C=C content, roughness, or contact angle, differences in degradation pathways between the polymer types PE, PP, PS, PET, and PVC were also found. We additionally revealed that salinity impacts the degradation rates of the two most frequently manufactured polymer types, PE and PP.¹⁹ These findings indicate that salinity should also be considered in estimates of the weathering degree of MPs collected in the environment. Apart from this, we found further hurdles in determining the weathering degree. Due to fluctuations, the common usage of CI^{26,60–62} may lead to misinterpretations. Based on the linear progression of the CI, the weathering degree can solely be estimated for PE for environmental samples. However, incalculable environmental effects such as biofilms, plastic-degrading microorganisms, or material properties such as additives may also influence weathering progress.

Additionally, the CI has been differently calculated between the studies, using different reference peaks, or integrating an absorbance range instead of specific peaks or peak maxima, hindering the comparison between studies.^{26,37,74} Here, we used the same calculation as Liu et al.,²⁶ conducting an outdoor weathering experiment in Shanghai for 11 months in previously filtered freshwater with additive-free PE spheres, as used in our study. They calculated a CI of 0.02 for PE after 11 months. Considering the average monthly sunshine hours in Shanghai, which range from 5.3 h in January to up to 10.3 h in July, this corresponds to a total irradiation time of 2565 h.

Compared to our experiment, this irradiation time was already reached after 3–4 instead of 11 months with a CI of $0.029\text{--}0.34 \pm 0.013$ for freshwater (WW water). Although, in the current study, artificial weathering simulations of MPs were not absolutely equal to natural conditions, as no temperature or light alterations occurred, and no biofilm formed on the particle surface (observations by SEM images), our results are close to that of the outdoor experiment. This comparison demonstrates the applicability of the weathering simulation experiment implemented here, which allows observation of weathering pathways and associated lifetimes of different polymer types in the environment.

Regarding particle stability, PP was the least stable polymer of all five tested types, which was also observed in previous studies.^{18,28,37} Weathered MPs can release numerous environmentally harmful degradation products,¹⁵ resulting in a significant pH decrease in the case of PP. Considering the current massive plastic pollution in the oceans,^{75,76} these degradation products may contribute to ocean acidification and threaten the marine ecosystem. Another important finding was the generation of PP fragments that are positive, neutral, or negatively buoyant. This observation extends the current knowledge on detecting polymers lighter than seawater on the seafloor.^{77,78} Previous studies assumed that low-density MPs sink through the water column into the deep sea through biological contributions such as biofouling,^{79,80} aggregation,⁸¹ or incorporation into marine snow.^{82,83} However, with this current study, we showed that the advanced abiotic weathering alone could cause the MPs to sink. A further important observation was the size of the generated PP fragments, with the majority below $10\ \mu\text{m}$ in diameter. This particle size is outside the range detectable by currently applied Raman or FTIR spectroscopy methods (minimum size of $10\ \mu\text{m}$), resulting in the majority of secondary PP remaining undetected in the environment.

For determining PVC in environmental samples, we additionally advise avoiding the detection method by ATR-FTIR due to rapid chloride cleavage at the pellet surface after the first week, which restricts the identification success. A similar observation was previously made by Hendrickson et al.⁸⁴ in which PVC measured by pyrolysis-gas chromatography-mass spectrometry (pyr-GC/MS) was identified as PE by ATR-FTIR. This huge potential underestimation of PVC abundances caused by the ATR-FTIR method could explain the low levels of PVC detected in environmental samples compared to the high production rates, as discussed in Reineccius and Waniek.⁸⁵

The recent findings of our experiment contributed to a better understanding of degeneration characteristics for a wide range of MP particle types, which commonly occur in the aquatic environment. Degradation rates provide insight into the actual abundance of MPs in the aquatic environment. Therefore, they may be of great importance for modeling global plastic levels and tracking the fate of MPs in the ocean. However, due to the complexity of this research topic, we could only address the degeneration parameters of salinity and realistic solar radiation. Therefore, further investigations are necessary to consider additional impact factors such as temperature fluctuations and biological processes or degeneration processes of plastic in the absence of solar radiation, like in the deep sea. Finally, a comprehensive understanding of the fate of this popular anthropogenic product may raise awareness

about the use of plastic in everyday life and its potential environmental threats.

■ ASSOCIATED CONTENT

Supporting Information

The Supporting Information is available free of charge at <https://pubs.acs.org/doi/10.1021/acs.est.2c05746>.

Picture of the experimental setup; calculation pathway of the PSD with additional illustration; further details about the Raman and FTIR measuring settings applied for the weathering experiment and the applied reference peaks; weights of the filters containing fragmented MPs generated during the experiment time and respective particle weights before and after the experiment; SEM images of PP after 18 months at 200 and 7000 magnification; particle surface area of PP, PET, and PVC before and after the exposure time in WW, BS, and SCS water; contact angles over the exposure time for PE, PP, PS, PET, and PVC in WW, BS, and SCS water; potential changing ATR-FTIR peaks according to the literature; linear regression graphs for significant changes in Raman peaks for PE, PP, and PET; results for the linear regression of ATR-FTIR peak intensities; and changes in ATR-FTIR peak intensities for PE, PP, PS, PET, and PVC (PDF)

■ AUTHOR INFORMATION

Corresponding Author

Janika Reineccius – Leibniz Institute of Baltic Sea Research, Warnemünde, Rostock 18119, Germany; orcid.org/0000-0002-5253-2979; Email: janika.reineccius@io-warnemuende.de

Authors

Mischa Schönke – Leibniz Institute of Baltic Sea Research, Warnemünde, Rostock 18119, Germany

Joanna J. Waniek – Leibniz Institute of Baltic Sea Research, Warnemünde, Rostock 18119, Germany

Complete contact information is available at: <https://pubs.acs.org/10.1021/acs.est.2c05746>

Funding

This research contributes to the Sino-German MEGAPOL project, which received funding from the Federal Ministry of Education and Research (03F0786A) and the SO269-SOCLIS BMBF project (FKZ 03G0269). Sampling was carried out during the SO269 cruise, while the weathering experiments were implemented at the Leibniz Institute for Baltic Sea Research Warnemünde (IOW) in Germany.

Notes

The authors declare no competing financial interest.

■ ACKNOWLEDGMENTS

We gratefully thank Sascha Pleve (IOW) for taking SEM images; the inorganic research groups of Prof. Dr. Seidel, Prof. Dr. Schulz, and Prof. Dr. Köckerling for provision; and Dr. Jonas Bresien and Florian Schröder for support in operating the Raman and ATR-FTIR spectrometers (all University of Rostock, Germany). We further would like to thank the Institute of Physics of the University of Rostock, especially Chris Rehagen, for support in handling the laser-scanning microscope.

REFERENCES

- (1) Allen, S.; Allen, D.; Baladima, F.; Phoenix, V. R.; Thomas, J. L.; Le Roux, G.; Sonke, J. E. Evidence of Free Tropospheric and Long-Range Transport of Microplastic at Pic Du Midi Observatory. *Nat. Commun.* **2021**, *12*, 1–10.
- (2) Eriksen, M.; Lebreton, L. C. M.; Carson, H. S.; Thiel, M.; Moore, C. J.; Borerro, J. C.; Galgani, F.; Ryan, P. G.; Reisser, J. Plastic Pollution in the World's Oceans: More than 5 Trillion Plastic Pieces Weighing over 250,000 Tons Afloat at Sea. *PLoS One* **2014**, *9*, No. e111913.
- (3) Lebreton, L.; Andrady, A. Future Scenarios of Global Plastic Waste Generation and Disposal. *Palgrave Commun.* **2019**, *5*, 1–11.
- (4) Pereira, J. M.; Rodríguez, Y.; Blasco-Monleon, S.; Porter, A.; Lewis, C.; Pham, C. K. Microplastic in the Stomachs of Open-Ocean and Deep-Sea Fishes of the North-East Atlantic. *Environ. Pollut.* **2020**, *265*, 115060.
- (5) Murphy, F.; Russell, M.; Ewins, C.; Quinn, B. The Uptake of Macroplastic & Microplastic by Demersal & Pelagic Fish in the Northeast Atlantic around Scotland. *Mar. Pollut. Bull.* **2017**, *122*, 353–359.
- (6) Steer, M.; Cole, M.; Thompson, R. C.; Lindeque, P. K. Microplastic Ingestion in Fish Larvae in the Western English Channel. *Environ. Pollut.* **2017**, *226*, 250–259.
- (7) Vandermeersch, G.; Van Cauwenberghe, L.; Janssen, C. R.; Marques, A.; Granby, K.; Fait, G.; Kotterman, M. J. J.; Diogène, J.; Bekaert, K.; Robbens, J.; Devriese, L. A Critical View on Microplastic Quantification in Aquatic Organisms. *Environ. Res.* **2015**, *143*, 46–55.
- (8) Murray, F.; Cowie, P.; Sea, C. Plastic Contamination in the Decapod Crustacean Nephrops Norvegicus (Linnaeus, 1758). *Mar. Pollut. Bull.* **2011**, *62*, 1207–1217.
- (9) Van Cauwenberghe, L.; Janssen, C. R. Microplastics in Bivalves Cultured for Human Consumption. *Environ. Pollut.* **2014**, *193*, 65–70.
- (10) Wright, S. L.; Kelly, F. J. Plastic and Human Health: A Micro Issue? *Environ. Sci. Technol.* **2017**, *51*, 6634–6647.
- (11) Nelms, S. E.; Galloway, T. S.; Godley, B. J.; Jarvis, D. S.; Lindeque, P. K. Investigating Microplastic Trophic Transfer in Marine Top Predators. *Environ. Pollut.* **2018**, *238*, 999–1007.
- (12) Frias, J. P. G. L.; Sobral, P.; Ferreira, A. M. Organic Pollutants in Microplastics from Two Beaches of the Portuguese Coast. *Mar. Pollut. Bull.* **2010**, *60*, 1988–1992.
- (13) Graca, B.; Beldowska, M.; Wrzesień, P.; Zgrundo, A. Styrofoam Debris as a Potential Carrier of Mercury within Ecosystems. *Environ. Sci. Pollut. Res.* **2014**, *21*, 2263–2271.
- (14) Zettler, E. R.; Mincer, T. J.; Amaral-Zettler, L. A. Life in the “Plastisphere”: Microbial Communities on Plastic Marine Debris. *Environ. Sci. Technol.* **2013**, *47*, 7137–7146.
- (15) Gewert, B.; Plassmann, M.; Sandblom, O.; MacLeod, M. Identification of Chain Scission Products Released to Water by Plastic Exposed to Ultraviolet Light. *Environ. Sci. Technol. Lett.* **2018**, *5*, 272–276.
- (16) Sørensen, L.; Groven, A. S.; Hovsbakken, I. A.; Del Puerto, O.; Krause, D. F.; Sarno, A.; Booth, A. M. UV Degradation of Natural and Synthetic Microfibers Causes Fragmentation and Release of Polymer Degradation Products and Chemical Additives. *Sci. Total Environ.* **2021**, *755*, 143170.
- (17) Gewert, B.; Plassmann, M. M.; MacLeod, M. Pathways for Degradation of Plastic Polymers Floating in the Marine Environment. *Environ. Sci. Process. Impacts* **2015**, *17*, 1513–1521.
- (18) Song, Y. K.; Hong, S. H.; Jang, M.; Han, G. M.; Jung, S. W.; Shim, W. J. Combined Effects of UV Exposure Duration and Mechanical Abrasion on Microplastic Fragmentation by Polymer Type. *Environ. Sci. Technol.* **2017**, *51*, 4368–4376.
- (19) Andrady, A. L. Microplastics in the Marine Environment. *Mar. Pollut. Bull.* **2011**, *62*, 1596–1605.
- (20) Alimi, O. S.; Claveau-Mallet, D.; Kurusu, R. S.; Lapointe, M.; Bayen, S.; Tufenkji, N. Weathering Pathways and Protocols for Environmentally Relevant Microplastics and Nanoplastics: What Are We Missing? *J. Hazard. Mater.* **2022**, *423*, 126955.
- (21) ter Halle, A.; Ladirat, L.; Gendre, X.; Goudouneche, D.; Pusineri, C.; Routaboul, C.; Tenailleau, C.; Duployer, B.; Perez, E. Understanding the Fragmentation Pattern of Marine Plastic Debris. *Environ. Sci. Technol.* **2016**, *50*, 5668–5675.
- (22) Min, K.; Cuiffi, J. D.; Mathers, R. T. Ranking Environmental Degradation Trends of Plastic Marine Debris Based on Physical Properties and Molecular Structure. *Nat. Commun.* **2020**, *11*, 1–11.
- (23) Sun, Y.; Yuan, J.; Zhou, T.; Zhao, Y.; Yu, F.; Ma, J. Laboratory Simulation of Microplastics Weathering and Its Adsorption Behaviors in an Aqueous Environment: A Systematic Review. *Environ. Pollut.* **2020**, *265*, 114864.
- (24) Zvekic, M.; Richards, L. C.; Tong, C. C.; Krogh, E. T. Characterizing Photochemical Ageing Processes of Microplastic Materials Using Multivariate Analysis of Infrared Spectra. *Environ. Sci. Process. Impacts* **2022**, *24*, 52–61.
- (25) Luo, H.; Li, Y.; Zhao, Y.; Xiang, Y.; He, D.; Pan, X. Effects of Accelerated Aging on Characteristics, Leaching, and Toxicity of Commercial Lead Chromate Pigmented Microplastics. *Environ. Pollut.* **2020**, *257*, 113475.
- (26) Liu, P.; Qian, L.; Wang, H.; Zhan, X.; Lu, K.; Gu, C.; Gao, S. New Insights into the Aging Behavior of Microplastics Accelerated by Advanced Oxidation Processes. *Environ. Sci. Technol.* **2019**, *53*, 3579–3588.
- (27) Julienne, F.; Delorme, N.; Lagarde, F. From Macroplastics to Microplastics: Role of Water in the Fragmentation of Polyethylene. *Chemosphere* **2019**, *236*, 124409.
- (28) Andrade, J.; Fernández-González, V.; López-Mahía, P.; Muniategui, S. A Low-Cost System to Simulate Environmental Microplastic Weathering. *Mar. Pollut. Bull.* **2019**, *149*, 110663.
- (29) Badji, C.; Beigbeder, J.; Garay, H.; Bergeret, A.; Bénézet, J. C.; Desauziers, V. Correlation between Artificial and Natural Weathering of Hemp Fibers Reinforced Polypropylene Biocomposites. *Polym. Degrad. Stab.* **2018**, *148*, 117–131.
- (30) Müller, A.; Becker, R.; Dorgerloh, U.; Simon, F. G.; Braun, U. The Effect of Polymer Aging on the Uptake of Fuel Aromatics and Ethers by Microplastics. *Environ. Pollut.* **2018**, *240*, 639–646.
- (31) Hamdi, S. Analysis of Ultraviolet Index, Ultraviolet B Insolation, and Sunshine Duration at Bandung in Year 2017. *IOP Conf. Ser. Earth Environ. Sci.* **2019**, *303*, 012018.
- (32) Hölzle, E.; Hönigsman, H. Ultraviolette Strahlung—Quellen, Spektren, Umwelteinflüsse. *J. der Dtsch. Dermatologischen Gesellschaft* **2005**, *3*, 3–10.
- (33) Kadad, I. M.; Kandil, K. M.; Alzanki, T. H. Impact of UVB Solar Radiation on Ambient Temperature for Kuwait Desert Climate. *Smart Grid Renew. Energy* **2020**, *11*, 103–125.
- (34) Bergmann, M.; Wirzberger, V.; Krumpfen, T.; Lorenz, C.; Primpke, S.; Tekman, M. B.; Gerds, G. High Quantities of Microplastic in Arctic Deep-Sea Sediments from the HAUSGARTEN Observatory. *Environ. Sci. Technol.* **2017**, *51*, 11000–11010.
- (35) Panda, S.; Panzade, A.; Sarangi, M.; Roy Chowdhury, S. K. Spectral Approach on Multiscale Roughness Characterization of Nominally Rough Surfaces. *J. Tribol.* **2017**, *139*, 1–10.
- (36) Yang, H.; Baudet, B. A.; Yao, T. Characterization of the Surface Roughness of Sand Particles Using an Advanced Fractal Approach. *Proc. R. Soc. A Math. Phys. Eng. Sci.* **2016**, *472*, 20160524.
- (37) Brandon, J.; Goldstein, M.; Ohman, M. D. Long-Term Aging and Degradation of Microplastic Particles: Comparing in Situ Oceanic and Experimental Weathering Patterns. *Mar. Pollut. Bull.* **2016**, *110*, 299–308.
- (38) Dhar, P.; Khurana, G.; Anilakkad Raman, H.; Jaiswal, V. Superhydrophobic Surface Curvature Dependence of Internal Advection Dynamics within Sessile Droplets. *Langmuir* **2019**, *35*, 2326–2333.
- (39) Guilizzoni, M. Drop Shape Visualization and Contact Angle Measurement on Curved Surfaces. *J. Colloid Interface Sci.* **2011**, *364*, 230–236.

- (40) Kowalski, N.; Reichardt, A. M.; Waniek, J. J. Sinking Rates of Microplastics and Potential Implications of Their Alteration by Physical, Biological, and Chemical Factors. *Mar. Pollut. Bull.* **2016**, *109*, 310–319.
- (41) Menzel, T.; Meides, N.; Mauel, A.; Mansfeld, U.; Kretschmer, W.; Kuhn, M.; Herzig, E. M.; Altstädt, V.; Strohriegel, P.; Senker, J.; Ruckdäschel, H. Degradation of Low-Density Polyethylene to Nanoplastic Particles by Accelerated Weathering. *Sci. Total Environ.* **2022**, *826*, 154035.
- (42) Sagitova, E. A.; Prokhorov, K. A.; Nikolaeva, G. Y.; Pashinin, P. P.; Gerasin, V. A.; Guseva, M. A.; Antipov, E. M. Quantitative Characterization of the Orientation of Macromolecules in Intercalated Nanocomposites of Polyolefins/Layered Silicates by Raman Spectroscopy. *Laser Phys.* **2008**, *18*, 868–881.
- (43) Hiejima, Y.; Kida, T.; Nitta, K. H. In Situ Raman Spectroscopic Observation of Polymer Chains in Semi-Crystalline Polyethylene Solids. *Zeitschrift für Phys. Chemie* **2020**, *235*, 59–79.
- (44) Hiejima, Y.; Kida, T.; Takeda, K.; Igarashi, T.; Nitta, K. he. Microscopic Structural Changes during Photodegradation of Low-Density Polyethylene Detected by Raman Spectroscopy. *Polym. Degrad. Stab.* **2018**, *150*, 67–72.
- (45) Strobl, G. R.; Hagedorn, W. Raman Spectroscopic Method for Determining the Crystallinity of Polyethylene. *AIP Conf. Proc.* **1978**, *16*, 1181–1193.
- (46) Arruebarrena de Báez, M.; Hendra, P. J.; Judkins, M. The Raman Spectra of Oriented Isotactic Polypropylene. *Spectrochim. Acta Part A Mol. Biomol. Spectrosc.* **1995**, *51*, 2117–2124.
- (47) Paradkar, R. P.; Patel, R. M.; Knickerbocker, E.; Doufas, A. Raman Spectroscopy for Spinline Crystallinity Measurements. I. Experimental Studies Rajesh. *J. Appl. Polym. Sci.* **2008**, *109*, 3413–3420.
- (48) Nikolaeva, G. Y.; Sagitova, E. A.; Prokhorov, K. A.; Pashinin, P. P.; Nedorezova, P.; Klyamkina, A. N.; Guseva, M. A.; Gerasin, V. A. Using Raman Spectroscopy to Determine the Structure of Copolymers and Polymer Blends. *J. Phys. Conf. Ser.* **2017**, *826*, 012002.
- (49) Chen, Q.; Wang, Q.; Zhang, C.; Zhang, J.; Dong, Z.; Xu, Q. Aging Simulation of Thin-Film Plastics in Different Environments to Examine the Formation of Microplastic. *Water Res.* **2021**, *202*, 117462.
- (50) Kellar, E. J. C.; Evans, A. M.; Knowles, J.; Galiotis, C.; Andrews, E. H. Raman Vibrational Studies of Syndiotactic Polystyrene. 2. Use of the Fundamental ν_1 Vibrational Mode as a Quantitative Measure of Crystallinity within Isotropic Material. *Macromolecules* **1997**, *30*, 2400–2407.
- (51) Zhang Xiujuan, X.; Li Cuimei, C.; Peng Lixin, L.; Liu Junxian, J.; Wang Guiwen, G. Analysis of Aging Mechanism of Polystyrene Microspheres by Using Single Particle Raman Spectroscopy. *Chinese J. Lasers* **2022**, *49*, 0411002.
- (52) Dong, M.; Zhang, Q.; Xing, X.; Chen, W.; She, Z.; Luo, Z. Raman Spectra and Surface Changes of Microplastics Weathered under Natural Environments. *Sci. Total Environ.* **2020**, *739*, 139990.
- (53) Lin, C. C.; Krommenhoek, P. J.; Watson, S. S.; Gu, X. Depth Profiling of Degradation of Multilayer Photovoltaic Backsheets after Accelerated Laboratory Weathering: Cross-Sectional Raman Imaging. *Sol. Energy Mater. Sol. Cells* **2016**, *144*, 289–299.
- (54) Oelschlägel, K.; Pfeiffer, J.; Potthoff, A. Imitating the Weathering of Microplastics in the Marine Environment *Proceedings of the International Conference on Microplastic Pollution in the Mediterranean Sea*; Springer, 2018; pp 171–179.
- (55) Kaynak, A.; Bartley, J. P.; George, G. A. FT-Raman Spectroscopic Study of the Formation of Polyenes during Thermal Degradation of Poly(Vinyl Chloride) and Poly (N-Vinyl-2-Pyrrolidone) Blends. *J. Macromol. Sci., Pure Appl. Chem.* **2001**, *38*, 1033–1048.
- (56) Kosińska, A.; Jagielski, J.; Wilczopolska, M.; Bieliński, D. M.; Okrasa, M.; Józwiak, I.; Kurpaska, L.; Nowakowska-Langier, K. Study of the Electrical Properties of Ion Irradiated Polymer Materials. *Surf. Coatings Technol.* **2020**, *388*, 125562.
- (57) Wang, C.; Xian, Z.; Jin, X.; Liang, S.; Chen, Z.; Pan, B.; Wu, B.; Ok, Y. S.; Gu, C. Photo-Aging of Polyvinyl Chloride Microplastic in the Presence of Natural Organic Acids. *Water Res.* **2020**, *183*, 116082.
- (58) Kuznetsov, S. M.; Sagitova, E. A.; Prokhorov, K. A.; Nikolaeva, G. Y.; Mendeleev, D. I.; Donfack, P.; Materny, A. Raman Spectroscopic Detection of Polyene-Length Distribution for High-Sensitivity Monitoring of Photo- and Thermal Degradation of Polyvinylchloride. *Spectrochim. Acta Mol. Biomol. Spectrosc.* **2021**, *252*, 119494.
- (59) Fernández-González, V.; Andrade-Garda, J. M.; López-Mahía, P.; Muniategui-Lorenzo, S. Impact of Weathering on the Chemical Identification of Microplastics from Usual Packaging Polymers in the Marine Environment. *Anal. Chim. Acta* **2021**, *1142*, 179–188.
- (60) Miranda, M. N.; Sampaio, M. J.; Tavares, P. B.; Silva, A. M. T.; Pereira, M. F. R. Aging Assessment of Microplastics (LDPE, PET and UPVC) under Urban Environment Stressors. *Sci. Total Environ.* **2021**, *796*, 148914.
- (61) Luo, H.; Zhao, Y.; Li, Y.; Xiang, Y.; He, D.; Pan, X. Aging of Microplastics Affects Their Surface Properties, Thermal Decomposition, Additives Leaching and Interactions in Simulated Fluids. *Sci. Total Environ.* **2020**, *714*, 136862.
- (62) Rouillon, C.; Bussiere, P. O.; Desnoux, E.; Collin, S.; Vial, C.; Therias, S.; Gardette, J. L. Is Carbonyl Index a Quantitative Probe to Monitor Polypropylene Photodegradation? *Polym. Degrad. Stab.* **2016**, *128*, 200–208.
- (63) Cai, L.; Wang, J.; Peng, J.; Wu, Z.; Tan, X. Observation of the Degradation of Three Types of Plastic Pellets Exposed to UV Irradiation in Three Different Environments. *Sci. Total Environ.* **2018**, *628–629*, 740–747.
- (64) Julienne, F.; Lagarde, F.; Delorme, N. Influence of the Crystalline Structure on the Fragmentation of Weathered Polyolefines. *Polym. Degrad. Stab.* **2019**, *170*, 109012.
- (65) Arias-Villamizar, C. A.; Vázquez-Morillas, A. Degradation of conventional and oxodegradable high density polyethylene in tropical aqueous and outdoor environments. *Rev. Int. Contam. Ambient.* **2018**, *34*, 137–147.
- (66) Veerasingam, S.; Saha, M.; Suneel, V.; Vethamony, P.; Rodrigues, A. C.; Bhattacharyya, S.; Naik, B. G. Characteristics, Seasonal Distribution and Surface Degradation Features of Microplastic Pellets along the Goa Coast, India. *Chemosphere* **2016**, *159*, 496–505.
- (67) Käßler, A.; Fischer, D.; Oberbeckmann, S.; Schernewski, G.; Labrenz, M.; Eichhorn, K. J.; Voit, B. Analysis of Environmental Microplastics by Vibrational Microspectroscopy: FTIR, Raman or Both? *Anal. Bioanal. Chem.* **2016**, *408*, 8377–8391.
- (68) Ioakeimidis, C.; Fotopoulou, K. N.; Karapanagioti, H. K.; Geraga, M.; Zeri, C.; Papatheodorou, E.; Galgani, F.; Papatheodorou, G. The Degradation Potential of PET Bottles in the Marine Environment: An ATR-FTIR Based Approach. *Sci. Rep.* **2016**, *6*, 1–8.
- (69) Net, S.; Sempéré, R.; Delmont, A.; Paluselli, A.; Ouddane, B. Occurrence, Fate, Behavior and Ecotoxicological State of Phthalates in Different Environmental Matrices. *Environ. Sci. Technol.* **2015**, *49*, 4019–4035.
- (70) Hillemans, J. P. H. M.; Colemonts, C. M. C. J.; Meier, R. J.; Kip, B. J. An in Situ Raman Spectroscopic Study of the Degradation of PVC. *Polym. Degrad. Stab.* **1993**, *42*, 323–333.
- (71) Veronelli, M.; Mauro, M.; Bresadola, S. Influence of Thermal Dehydrochlorination on the Photooxidation Kinetics of PVC Samples. *Polym. Degrad. Stab.* **1999**, *66*, 349–357.
- (72) Ludwig, V.; Da Costa Ludwig, Z. M.; Rodrigues, M. M.; Anjos, V.; Costa, C. B.; Sant’Anna das Dores, D. R.; da Silva, V. R.; Soares, F. Analysis by Raman and Infrared Spectroscopy Combined with Theoretical Studies on the Identification of Plasticizer in PVC Films. *Vib. Spectrosc.* **2018**, *98*, 134–138.
- (73) Stark, N. M.; Matuana, L. M. Surface Chemistry Changes of Weathered HDPE/Wood-Flour Composites Studied by XPS and FTIR Spectroscopy. *Polym. Degrad. Stab.* **2004**, *86*, 1–9.
- (74) Grause, G.; Chien, M. F.; Inoue, C. Changes during the Weathering of Polyolefins. *Polym. Degrad. Stab.* **2020**, *181*, 109364.

(75) Lebreton, L. C. M.; van der Zwet, J.; Damsteeg, J. W.; Slat, B.; Andrady, A.; Reisser, J. River Plastic Emissions to the World's Oceans. *Nat. Commun.* **2017**, *8*, 1–10.

(76) Geyer, R.; Jambeck, J. R.; Law, K. L. Production, Use, and Fate of All Plastics Ever Made. *Sci. Adv.* **2017**, *3*, 25–29.

(77) Courtene-Jones, W.; Quinn, B.; Ewins, C.; Gary, S. F.; Narayanaswamy, B. E. Microplastic Accumulation in Deep-Sea Sediments from the Rockall Trough. *Mar. Pollut. Bull.* **2020**, *154*, 111092.

(78) Tekman, M. B.; Wekerle, C.; Lorenz, C.; Primpke, S.; Hasemann, C.; Gerdts, G.; Bergmann, M. Tying up Loose Ends of Microplastic Pollution in the Arctic: Distribution from the Sea Surface through the Water Column to Deep-Sea Sediments at the HAUSGARTEN Observatory. *Environ. Sci. Technol.* **2020**, *54*, 4079–4090.

(79) Kaiser, D.; Estelmann, A.; Kowalski, N.; Glockzin, M.; Waniek, J. J. Sinking Velocity of Sub-Millimeter Microplastic. *Mar. Pollut. Bull.* **2019**, *139*, 214–220.

(80) Kooi, M.; Nes, E. H.; Scheffer, M.; Koelmans, A. A. Ups and Downs in the Ocean: Effects of Biofouling on Vertical Transport of Microplastics. *Environ. Sci. Technol.* **2017**, *51*, 7963–7971.

(81) Michels, J.; Stippkugel, A.; Lenz, M.; Wirtz, K.; Engel, A. Rapid Aggregation of Biofilm-Covered Microplastics with Marine Biogenic Particles. *Proc. R. Soc. B Biol. Sci.* **2018**, *285*, 20181203.

(82) Porter, A.; Lyons, B. P.; Galloway, T. S.; Lewis, C. Role of Marine Snows in Microplastic Fate and Bioavailability. *Environ. Sci. Technol.* **2018**, *52*, 7111–7119.

(83) Cole, M.; Lindeque, P. K.; Fileman, E.; Clark, J.; Lewis, C.; Halsband, C.; Galloway, T. S. Microplastics Alter the Properties and Sinking Rates of Zooplankton Faecal Pellets. *Environ. Sci. Technol.* **2016**, *50*, 3239–3246.

(84) Hendrickson, E.; Minor, E. C.; Schreiner, K. Microplastic Abundance and Composition in Western Lake Superior As Determined via Microscopy, Pyr-GC/MS, and FTIR. *Environ. Sci. Technol.* **2018**, *52*, 1787–1796.

(85) Reineccius, J.; Waniek, J. J. First Long-Term Evidence of Microplastic Pollution in the Deep Subtropical Northeast Atlantic. *Environ. Pollut.* **2022**, *305*, 119302.

Recommended by ACS

Are Fish Populations at Risk? Metformin Disrupts Zebrafish Development and Reproductive Processes at Chronic Environmentally Relevant Concentrations

Susana Barros, Teresa Neuparth, *et al.*

DECEMBER 29, 2022

ENVIRONMENTAL SCIENCE & TECHNOLOGY

READ 

Aptamer-Based Glycated Albumin Sensor for Capacitive Spectroscopy

Toshiya Sakata, Shoichi Nishitani, *et al.*

DECEMBER 30, 2022

ANALYTICAL CHEMISTRY

READ 

Wild Bee Exposure to Pesticides in Conservation Grasslands Increases along an Agricultural Gradient: A Tale of Two Sample Types

Michelle L. Hladik, Kelly L. Smalling, *et al.*

DECEMBER 27, 2022

ENVIRONMENTAL SCIENCE & TECHNOLOGY

READ 

The Behavior of Planktonic Copepods Minimizes the Entry of Microplastics in Marine Food Webs

Rocío Rodríguez Torres, Torkel Gissel Nielsen, *et al.*

DECEMBER 22, 2022

ENVIRONMENTAL SCIENCE & TECHNOLOGY

READ 

Get More Suggestions >

Curriculum Vitae

PERSONAL INFORMATION

Name: Janika Melina Reineccius
Birthdate: 08.12.1993
Nationality: German

PROFESSIONAL EXPERIENCES

2019-2023 **PhD student** - Leibniz Institute for Baltic Sea Research Warnemünde - Group of Bio-physical Interactions in Marine Chemistry Department
2018-2019 **Research Assistant** - Leibniz Institute for Baltic Sea Research Warnemünde - Group of Bio-physical Interactions in Marine Chemistry Department
2016 **Research Assistant** - HS Bonn-Rhein-Sieg - Analytical Chemistry Department

EDUCATION

Since 2019 **PhD studies** - Chemistry Department - University of Rostock at the Leibniz-Institute for Baltic Sea Research, Warnemünde Supervision: Prof. Dr. Joanna J. Waniek
2016–2018 **Master of Science** - Chemistry Department - University of Rostock carried out at the Leibniz-Institute for Baltic Sea Research, Warnemünde Supervision: Prof. Dr. Joanna J. Waniek
2013–2016 **Bachelor of Science** - Chemistry Department - HS Bonn-Rhein-Sieg Supervision: Prof. Dr. Steffen Witzleben
Until 2013 **Abitur** - Städtisches Gymnasium Rheinbach

PEER REVIEWED PUBLICATIONS

- 2022** **Reineccius, J.**, Schönke, M., Waniek, J.J. (2022). Abiotic long-term simulation of microplastic weathering pathways under different aqueous conditions. *Environmental Science and Technology*. doi: 10.1021/acs.est.2c05746
- 2022** **Reineccius, J.** & Waniek, J.J. (2022). First long-term evidence of microplastic pollution in the deep subtropical Northeast Atlantic. *Environmental Pollution*. 305, 119302. doi: 10.1016/j.envpol.2022.119302
- 2021** **Reineccius, J.**, Bresien, J., Waniek, J.J. (2021). Separation of microplastics from mass-limited samples by an effective adsorption technique. *Science of the Total Environment*. 788, 147881. doi: 10.1016/j.scitotenv.2021.147881
- 2020** **Reineccius, J.**, Appelt, J.S., Hinrichs, T., Kaiser, D., Stern, J., Prien, R.D., Waniek, J.J. (2020). Abundance and characteristics of microfibers detected in sediment trap material from the deep subtropical North Atlantic Ocean. *Science of the Total Environment*. 738, 140354. doi: 10.1016/j.scitotenv.2020.140354

OTHER PUBLICATIONS

- MSc:** Optimizing methods of microplastic identification in sediment trap material from different study sites of the North Atlantic Ocean (in English)
- BSc:** Untersuchung zur Bildung von kritischen Nebenprodukten bei Einsatz von Ozon in der Trinkwasserdesinfektion (in German)

ORAL PRESENTATIONS

- 2022** **Reineccius, J.**, Schönke, M., Bresien, J., Reineccius, D., Frazão, H.C., Waniek, J.J. (2022). Lost in the deep-sea: Microplastic time series from the deep subtropical Northeast Atlantic (Kiel 276, 33°N, 22°W). *Ocean Science Graduate Student Association*.
- 2021** **Reineccius, J.**, Bresien, J., Reineccius, D., Waniek, J.J. (2021). Microplastic time series from 2003 – 2015 at 2000 m depth of the subtropical northeast Atlantic. *AGU Fall Meeting in New Orleans, LA, 13 - 17 December 2021*.

STUDENT SUPERVISION

- 2023** Heck, Mareike: Mikroplastik im saisonalen Eis der nördlichen Ostsee, Master thesis, Master thesis, University of Rostock, Department of marine Biology, in preparation
- 2021** Heck, Mareike: Oberflächenmorphologie von Mikroplastik entlang eines Tiefengradienten, Südchinesisches Meer, Bachelor thesis, University of Rostock, Department of Biosciences, 43p
- 2021** Zimmermann, Genoveva: Influence of UV, mechanical stress and salinity gradient on ageing of microplastics, Bachelor thesis, University of Rostock, Department of Biosciences, 46p

RESEARCH CRUISES

- 2022/2023** R/V Sonne SO296, Port Hueneme (USA) – Talcahuano (Chile), Pacific. Chief Scientist: Prof. Dr. Detlef Schulz-Bull.
- 2019** R/V Sonne SO269, Singapore – Hong Kong, South China Sea. Chief Scientist: Prof. Dr. Joanna J. Waniek.
- 2019** R/V Elisabeth Mann Borgese (EMB), Baltic Sea. Chief Scientist: Dr. Volker Mohrholz.